Genetically Encoded, Metabolically Autonomous Production of Site-Specifically Clickable Lantibiotics via Methionine Analog Incorporation in Bacteria

By
Harjasmin Mander

A Thesis submitted to the

Faculty of Graduate and Postdoctoral Studies

Of the University of Manitoba

in partial fulfillment of the requirement of the degree of

DOCTOR OF PHILOSOPHY

Department of Chemistry

Faculty of Science

University of Manitoba

Winnipeg, MB, Canada

Copyright © 2026 by Harjasmin Mander

Thesis Outline

ABSTRACT VI

ACKNOWLEDGEMENTS VII

FIGURE LEGEND VIII

TABLES LEGEND XI

APPENDIX FIGURES XII

ABBREVIATIONS XIII

1. INTRODUCTION 1

1.1 Introduction to Genetic Code Expansion 1
1.1.1 Bioorthogonal and Click Chemistry 1
1.1.2 Genetic Code Expansion and Non-Canonical Amino Acids 2
1.1.3 Methionine: A Multifunctional Amino Acid and Its Analogs 5
1.1.0.1 Methionine in Genetic Code and Translation Initiation 5
1.1.0.2 Methionine as a Central Methyl Donor and Metabolic Hub 6
1.1.0.3 Methionine Oxidation, Redox, Homeostasis, and Aging 7
1.1.0.4 Methionine Analogs and Their Utility in Protein Science 8
1.1.0.5 Exploiting Methionine Biosynthesis for ncAA Production 10

AIM OF STUDY 11

2. PART 1: EGFP 12

2.1 Introduction of EGFP 12
2.1.1 Methionine as a Unique Structural and Functional Amino Acid 12
2.1.2 Limitations of Canonical Mutagenesis and the Role of Methionine Analogs 12
2.1.3 EGFP as a Model System to Probe Methionine Side-Chain Chemistry 13
2.2 Results and Discussion 15

2.2.1 Probing the role of Methionine218 for Green Fluorescent Protein stability through side-chain polarity requirements using its non-canonical amino acid analogues 15
2.2.1.1 Quantifying Side Chain Polarities 15
2.2.1.2 The Met218 Microenvironment and Its Role in EGFP Function 16
2.2.1.3 Residues-Specific Incorporation and Methionine Analogs into EGFP 17
2.2.1.4 Side-Chain Polarity Modulates EGFP Fluorescence 19
2.2.1.5 Methionine Analogs Effects on Folding and Refolding Kinetics 20
2.2.1.6 Polarity-Dependent Effects on EGFP Structural Stability 21
2.3 Materials and Methods 23
2.3.1 Cloning 23
2.3.2 Protein Expression and Purification 23
2.3.3 Fluorescence measurements 24
2.3.4 Refolding Experiments 24
2.3.5 Stability analysis 25
2.3.6 HPLC 25
2.3.7 Mass Spectrometric Analysis 25

3. PART 2: NISIN 26

3.1 Introduction to AMR, Lantibiotics and Nisin 26
3.1.1 Introduction to Antimicrobial Resistance and Bacterial Mechanisms of Resistance 26
3.1.2 Antimicrobial Peptides (AMPs) 28
3.1.0.1 Antimicrobial Peptides 28
3.1.0.2 RiPPs and Lanthipeptides 30
3.1.3 Nisin: System, Structure, and Mode of Action 30
3.1.0.3 Nisin Overview and Relevance 30
3.1.0.4 Biosynthetic Gene Cluster 31
3.1.0.5 Key Enzymes for Nisin Biosynthesis and Immunity 32
35
3.1.0.6 Mechanism of Action 35
3.1.4 Resistance to Nisin 38
3.1.0.7 Intrinsic Immunity in produced strains 38
3.1.0.8 Non-producer resistance strategies 39
3.1.5 Challenges with the use of AMPs in clinical settings 41
3.1.6 Engineering approaches to improve the biocompatibility of AMPs 43
3.1.0.9 Chemical Modifications 43
3.1.0.10 Nanocarriers 45
3.1.0.11 Combination Therapies 46
3.1.0.12 Bioengineering Nisin variants 46
3.1.0.13 Genetic Code Expansion as an Enabling Platform 48

3.2 Results and Discussion **51**
3.2.1 Establishment of Nisin wildtype core peptide production in *E. coli* **51**
3.2.1.1 Rationale for Heterologous Expression in E. coli 51
3.2.1.2 Design of Recombinant Expression System 51
3.2.1.3 Optimization of PreNisin Expression Conditions 52
3.2.1.4 Functional Verification by Antimicrobial Assays 54
3.2.1.5 Development of a Multistep Purification Strategy for PreNisin 55
3.2.1.6 Quantification and Sample Preparation Strategies 57
3.2.1.7 Structural Validation by Mass Spectrometry 61
3.2.2 Production and Functional Validation of Nisin Protease (NisP) **64**
3.2.2.1 Design of a Soluble NisP Expression Construct 64
3.2.2.2 Expression of Optimization and Host Selection 64
3.2.2.3 Purification of Active NisP 66
3.2.2.4 Optimization of PreNisin Cleavage 68
3.2.2.5 Verification of Leader Peptide Cleavage 69
3.2.2.6 Mass Spectrometric Confirmation of Mature Nisin 70
3.2.2.7 Chromatographic Resolution of Dehydration and Oxidation States 72
3.2.3 Enhanced non-canonical labelling in Nisin A **75**
3.2.3.1 Conceptual Framework and Experimental Rationale 75
3.2.3.2 Production and validation of Nisin A (M21V) 76
3.2.3.3 SPI-based Incorporation of Methionine Analogs in BU14 81
3.2.4 Enhancement of non-canonical amino acid incorporation with MetG **85**
3.2.4.1 Proof-of Principal Using EGFP 85
3.2.4.1 Application to Nisin A (M21V) 88
3.2.5 Labelling Nisin through *in vivo* azidohomoalanine biosynthesis **93**
3.2.5.1 In vivo Biosynthesis of Azidohomoalanine and in vitro Testing 93
3.2.6 "All-in strain: Development of Modified Nisin A producing cell factory **108**
3.2.7 Outlook: Toward functional conjugates **112**
3.2.7.1 Readiness of azide/alkyne-labelled Nisin for click chemistry 112
3.2.7.2 Transition to dye/probe conjugation and downstream applications 113
3.3 Materials and Methods **117**
3.3.1 Media **117**
3.3.2 Buffers **118**
3.3.3 Plasmids **119**
3.3.4 Strain information **121**
3.3.5 Primers Information **123**
3.3.6 PreNisin Wildtype and Mutant (M21V) Expression **124**
3.3.7 General Nisin Purification Protocol **125**
3.3.8 Nisin Protease Expression and Purification **125**
3.3.9 Nisin Cleavage and Separation **126**
3.3.10 Peptide Precipitation with Trichloroacetic acid **127**

3.3.11 Antimicrobial Assays **127**
3.3.12 Microdilution Assays **127**
3.3.13 Tricine Gels **128**
3.3.14 Expression in BU14, MS51 and MS61 - ncAA labelling via SPI method **128**
3.3.15 *O*-acetylhomoserine sulfhydrylase *in vitro* Assays **129**
3.3.16 Expression in MS89, MS94 and MS105 **129**
3.3.17 Construction of MS89 - Transposition **130**
3.3.18 Plasmid Curing **131**
3.3.19 Colony PCR **131**
3.3.20 Genomic Sequencing **132**
3.3.21 ESI – MS **132**
3.3.22 Click Chemistry Conjugation **133**

4. PART 3: AC6 **134**

4.1 Introduction to Persistent pulmonary hypertension of the newborn and role of AC6 **134**
4.1.1 Persistent Pulmonary Hypertension of the Newborn: Clinical Background 134
4.1.2 cAMP Signaling and Adenylate Cyclases in Vascular Regulation 134
4.1.3 Mammalian Adenylate Cyclase Isoforms and Regulatory Diversity 135
4.1.4 Structural Organization and Regulation of AC6 135
4.1.5 Systemic Roles of AC6 Beyond the Pulmonary Vasculature 136
4.1.6 Nitrosylation of AC6 and Gαs in Hypoxia and PPHN 137
4.1.7 Rationale for Heterologous Expression of AC6 and Gαs 138
4.2 Results and Discussion **139**
4.2.1 Rationale and Design of a Soluble AC6 Expression Construct 139
4.2.2 Expression Screening and Solubility of AC6 in *E. coli* 140
4.2.3 Solubilization, Refolding, and Partial Purification of AC6 141
4.2.4 Expression and Purification of Gαs for Reconstitution Assays 141
4.2.5 HPLC Assays Setup and Nucleotide Separation Controls 142
4.2.6 AC6 Catalytic Activity Depends Strongly on Refolding Conditions 143
Reconstitution Attempts With Activators: Forskolin vs Gαs 145
4.2.7 145
4.2.8 Periplasmic Export Strategy to Improve Folding (pelB ± pTUM4) 147
4.2.9 Domain-Based Strategy: Separate C1 and C2 Domains and Activity Tests 149
4.2.10 Summary and Next Steps 153
4.3 Material and Methods **156**
4.3.1 Media **156**
4.3.2 Buffers **156**
4.3.3 Plasmids **158**

4.3.4 Strain Information 158
4.3.5 Primer Information 159
4.3.6 AC6 Protein Expression and Purification – Flag-Tag peptide 159
4.3.7 Gas Protein Expression and Purification 160
4.3.8 General HPLC Separation Method 161
4.3.9 Bacterial AC6 Assay 161
4.3.10 Improved HPLC Separation Method 162
4.3.11 Periplasmic Expression of AC6, Extraction and Purification 162
4.3.12 Western Blotting of Periplasmic Extracts of AC6 163
4.3.13 Cloning AC6 C1 and C2 164
4.3.14 Expression of C1 and C2 domains 165

5. GENERAL MATERIALS AND METHODS 167

5.1 Materials 167
5.1.1 Antibiotic Stocks 167
5.1.2 Media 167
5.2 Methods 167
5.2.1 Preparation of KCM Competent cells 167
5.2.2 Transformation 168
5.2.3 Standard Gene Expression in *E. coli* 168
5.2.4 Cell Lysis 168
5.2.5 Plasmid DNA Isolation 169
5.2.6 DNA Concentration Measurement 169
5.2.7 Agarose Gel Electrophoresis 169
5.2.8 Sodium Dodecyl Sulfate - Polyacrylamide gel electrophoresis (SDS-PAGE) 169
5.2.9 Gibson Assembly – General 170

6. CONCLUSION AND FUTURE PERSPECTIVES 171

7. REFERENCES 174

8. APPENDIX 187

ABSTRACT

This thesis demonstrates that the successful incorporation of non-canonical amino acids into functional proteins is not determined solely by the chemistry of the amino acid analog, but by a coordinated interplay between chemical compatibility, enzymatic specificity, and cellular context.

Using EGFP as a controlled model system, we show that methionine analog incorporation follows predictable principles based on side-chain polarity and local structural environment, establishing a framework for compatibility between non-canonical residues and protein function. Extending these principles to a complex, post-translationally modified system, we engineered a fully functional *E. coli*-based production platform for the lantibiotic Nisin, enabling site-specific incorporation of clickable methionine analogs. Through metabolic engineering, including MetRS overexpression and genomic integration of azidohomoalanine biosynthesis pathways, we transitioned from external supplementation to an autonomous, genetically encoded system for non-canonical amino acid production and incorporation. This system retains antimicrobial activity while introducing chemical functionality for downstream modification.

Together, these results establish that non-canonical amino acid incorporation is a systems-level problem governed by the balance between translational machinery, metabolic flux, and protein-specific structural tolerance. This work provides both a mechanistic framework for predicting successful incorporation and a scalable platform to produce chemically programmable therapeutic peptides.

ACKNOWLEDGEMENTS

I am deeply grateful to my co-supervisors, Dr. Nediljko Budisa and Dr. John Sorensen, for their exceptional guidance, patience and support throughout these research projects. I also extend my appreciation to my advisory committee members, Dr. Rebecca Davis, Dr. Jörg Stetefeld, and Dr. Prashen Chelikani, for their valuable feedback, insightful questions, and constructive guidance that helped strengthen this research.

I am especially grateful to research associate Hamid Reza Karbalaei-Heidari, who provided invaluable mentorship and patiently answered every question. The Nisin work would not have been possible without his extensive knowledge and generous support. I would also like to thank my lab mates: Michael, April, Huy, Justin, Kathy, April, Harman, Dieu, Dakshina, Marshall, and Alex P. for their friendship and support, which made the laboratory a welcoming environment throughout this journey. I extend my gratitude to the chemistry storeroom staff, Emy the MS technician, and the chemistry office administration for their essential support that enabled me to focus on my research.

I owe my deepest gratitude to my family, who have loved and supported me through every stage of this long journey. To my parents: thank you for raising me with the perseverance and curiosity that carried me through this degree, and for never once doubting I'd get here, even on the days I did. To my sisters: thank you for the phone calls, the pep talks, and for always being in my corner. To Xena, our family dog: thank you for the uncomplicated joy and I truly miss you. Lastly to my husband, above all: thank you for your extraordinary patience and steadiness through every setback, and for celebrating every small win as if it were the biggest one. I could not have done this without you.

FIGURE LEGEND

Figure 1. Techniques for Integrating Non-Canonical Amino Acids into Proteins 5
Figure 2. Methionine and Selected Methionine Analogs Commonly used in Protein Engineering and Genetic Code Expansion. 9
Figure 3. Structural Visualization of EGFP Highlighting Trp57-Met218 Interactions. 14
Figure 4. Determination of sidechain polarity of non-canonical amino acids using HPLC. 16
Figure 5. Structural context of Met218 in EGFP. 17
Figure 6. SDS-PAGE and Mass spectrometric analysis of M218-EGFP and variants with incorporated methionine analogs. 19
Figure 7. Fluorescence Spectral Profiles of EGFP variants. 20
Figure 8. Methionine analogs incorporation effect on Fluorescence Recovery Kinetics of EGFP. 21
Figure 9. Structural stability analysis of EGFP variants using fluorescence intensity measurement in the presence of various concentration of Gdm-HCl. 22
Figure 10. Drivers and mechanisms of antimicrobial multidrug resistance. 27
Figure 11. Classification and Key Features of Antimicrobial Peptides (AMPs). 29
Figure 12. Scheme of Nisin Biosynthesis, Regulation and Immunity. 35
Figure 13. Proposed membrane-disruption mechanisms of antimicrobial peptides (AMPs). 36
Figure 14. Dual mode of action of Nisin mediated by Lipid II interaction. 38
Figure 15. Major limitations associated with antimicrobial peptides (AMPs). 43
Figure 16. Strategies to enhance antimicrobial peptide (AMP) stability, activity, and delivery. 50
Figure 17. Scheme of the Nisin Expression system and antimicrobial susceptibility assay for confirmation of Nisin expression in bacterial strain. 52
Figure 18. Antimicrobial Assays and Tricine-SDS-PAGE of purified PreNisin after recombinant expression in *E. coli*. 55
Figure 19. Antimicrobial Assays and Tricine-SDS-PAGE of PreNisin purified with size exclusion chromatography (A) 57
Figure 20. Scheme of the Trichloroacetic Acid Precipitation Method and 96-well plate Antimicrobial Assay. 59
Figure 21. Antimicrobial activity retention testing of trichloroacetic acid precipitated Nisin WT and the Nisin standard. 60
Figure 22. ESI-MS spectrum of purified wildtype PreNisin recombinantly produced in *E. coli*. (A) 61

Figure 23. Evaluation of Nisin Protease Expression in *E. coli* BL21(DE3) and BL21-AI Cells at Different Temperatures. 65
Figure 24. Expression Test of Nisin Protease in *E. coli* BL21(DE3) with different expression durations. 66
Figure 25. SDS-PAGE Analysis of Nisin Protease Purification Using Affinity and Ion Exchange Chromatography Techniques. 67
Figure 26. Determination of Optimal Conditions for Nisin Protease Cleavage 70
Figure 27. ESI-MS spectrum of purified wildtype nisin, recombinantly synthesized in Escherichia coli, following incubation with NisP. 71
Figure 28. Mass Spectrometric Analysis of Peptide Modification States. 73
Figure 29. Flowchart illustrating the purification of the Nisin peptide before and after cleavage. 74
Figure 30. Methionine substitution strategy for site-specific labeling of nisin. 76
Figure 31. ESI-MS spectrum of purified PreNisin (M21V) recombinantly produced in *E. coli*. 78
Figure 32. ESI-MS spectrum of purified Nisin-M21V, recombinantly synthesized in *Escherichia coli*, following incubation with NisP. 79
Figure 33. LC-ESI-MS Analysis showcasing separation of varying dehydrated and oxidized species of Nisin-M21V. 81
Figure 34. Expression scheme for non-canonical amino acid incorporation into Nisin. (A) 82
Figure 35. Comparison of Nisin M21V Expression upon Methionine or non-canonical amino acid incorporation in BU14. 83
Figure 36. MetRS Overexpression Strains and ncAA Incorporation Protocol. 86
Figure 37. EGFP Expression and Azidohomoalanine Incorporation in MetRS-overexpressing strains. 88
Figure 38. Comparative expression of ncAA-labelled Nisin M21V in MetRS-enriched strains 90
Figure 39. ESI-MS Analysis of Nisin-M21V-Aha produced with MetRS-enriched strain MS51. 91
Figure 40. Engineering of direct sulfhydrylation pathway in E. coli methionine metabolism for azidohomoalanine biosynthesis. 94
Figure 41. Enzymatic production of L-azidohomoalanine with MetY enzyme (OAHSS) 95
Figure 42. Visualization of Genomic Integrations and Expression Scheme for Azidohomoalanine Biosynthetic Strain 97
Figure 43. Comparative Expression and Mass Spectrometry Analysis of EGFP with azidohomoalanine biosynthetic strains. 98

Figure 44. Comparative Expression and Mass Spectrometry Analysis of Nisin M21V with azidohomoalanine biosynthetic strain. 100
Figure 45. Agarose Gel Verification of Multi-Site Genomic Integration in Strains MS88 and MS89. 102
Figure 46. Visualization of Genomic Integrations for multifunctional strain MS94 103
Figure 47. Optimization of Nisin M21V Expression in MS94 Using Various Culture Media. 104
Figure 48. Analysis of Nisin-M21V Modification Profiles and Extent of Dehydration in Engineered MS94 strain. 106
Figure 49. Visualization of Genomic Integrations for 'ALL-IN" strain MS105. 109
Figure 50. Comparative functional expression of Nisin -M21V-Aha from Plasmid-Based vs Chromosomally Integrated *nisABC* Genes..... 111
Figure 51. Copper-catalyzed azide-alkyne cycloaddition of Aha and Dansyl Alkyne Dye. 114
Figure 52. Mass spectrometric Confirmation of Bioorthogonal Click Chemistry Between Azidohomoalanine-labeled Nisin and Dansyl Alkyne. 115
Figure 53. Modulation of cAMP/PKA Signalling Pathway by G-protein Coupled Receptors and Regulation of Vasodilation by Nitric Oxide. 138
Figure 54. Expression and solubility of truncated AC6 in E. coli strains and at different temperatures (SDS-PAGE)...... 140
Figure 55. Multi-step Purification of Gαs Analysed by SDS-PAGE. 142
Figure 56. 142
Figure 57. AC6 activity depends on refolding conditions as measured with HPLC. ... 144
Figure 58. Activation of refolded AC6 by forskolin and Gαs (HPLC). 146
Figure 59. Periplasmic expression of AC6 using pelB signal peptide ± pTUM4 (SDS-PAGE and Western blot) 149
Figure 60. Mapping and expression of AC6 cytosolic domains. 150
Figure 61. HPLC separation of adenine nucleotides and adenosine standards. 151
Figure 62. Activity assays of isolated AC6 C1 and C2 domains (HPLC). 152

TABLES LEGEND

Table 1. Determination of the molecular masses and charged species of wildtype-PreNisin (-Met) by ESI-MS. 62
Table 2. Evaluation of Buffer Conditions to Identify the Optimal Buffer for Nisin Protease Cleavage Reaction 68
Table 3. Determination of the molecular masses and charged species of wildtype-Nisin by ESI-MS. 72
Table 4. Determination of the molecular masses and charged PreNisin-M21V (-Met) by ESI-MS. 79
Table 5. Determination of the molecular masses and charges for Nisin-M21V by ESI-MS.. 80
Table 7. Composition and Conditions for pET29b Backbone PCR Reaction. 165
Table 6. Composition and Conditions for C1 and C1 Domain PCR Reaction. 165

APPENDIX FIGURES

Appendix Figure 1. Agar well diffusion assay of antimicrobial activity under varying induction conditions. 190
Appendix Figure 2.IEX purification of nisin. 190
Appendix Figure 3.Nisin WT LC-MS Analysis at the Proteomics Centre List. 191
Appendix Figure 4. Nisin M21V LC-MS Analysis at the Proteomics Centre List. 192
Appendix Figure 5. MS51 New Junction Evidence Summary after Breseq Analysis. .. 193
Appendix Figure 6. MS61 New Junction Evidence Summary after Breseq Analysis. .. 194
Appendix Figure 7. MS39 New Junction Evidence Summary after Breseq Analysis. .. 195
Appendix Figure 8. ESI-MS analysis of azidohomoalanine labelled Nisin M21V expressed in BU14 and MS51. 195
Appendix Figure 9. Cloning of MetY into pQE80L for expression. 196
Appendix Figure 10. SDS-PAGE analysis of MetY Expression and purification. 196
Appendix Figure 11. MS94 New Junction Evidence Summary after Breseq Analysis. 197
Appendix Figure 12. Ninhydrin strain thin-layer chromatography of MetY-catalyzed synthesis of Aha. 197
Appendix Figure 13. MS105 New Junction Evidence Summary after Breseq Analysis. 198
Appendix Figure 14. HPLC-monitored click reaction kinetics between azidohomoalanine and dansyl alkyne. 199
Appendix Figure 15. Effect of Promoter Architecture of *nisBC* Genes on the Yield of Functionally Modified Nisin as Measured by Antimicrobial Activity. 199
Appendix Figure 16. Gαs expression trials in various E. coli strains. 200
Appendix Figure 17. HPLC Peak Integration data for AC6 Assays Following Protein Refolding. 201
Appendix Figure 18. HPLC Peak Integration data for AC6 Assays with Various Activators. 201
Appendix Figure 19. Metabolic Pathway for the Enzymatic Breakdown of ATP to Inosine. 202
Appendix Figure 20. Cloning of C1a and C1b Domains into pET29b for Expression. .. 202

Abbreviations

aaRS	aminoacyl-tRNA synthetases
ABC	ATP-binding cassette
AC6	Adenylate cyclase 6
ACN	Acetonitrile
Aha	Azidohomoalanine
AKI	acute kidney injury
Amp	Ampicillin
AMPs	Antimicrobial Peptides
AMR	Antimicrobial Resistance
Apr	Apramycin
ATP	adenosine triphosphate
ATCC	American type culture collection
AUA	Mitochondrial methionine codon
B. pertussis	*Bordetella pertussis*
BCA	Bicinchoninic acid
BSA	Bovine Serum Albumin
BTTAA	2-(4-((Bis((1-(*tert*-butyl)-1*H*-1,2,3-triazol-4-yl)methyl)amino)methyl)-1*H*-1,2,3-triazol-1-yl)acetic acid
C. difficile	*Clostridium difficile*
C. glutamicum	*Corynebacterium glutamicum*

cAMP	cyclic adenosine monophosphate
CAMPs	cationic antimicrobial peptides
CAST	Crispr-associated transposition
CFTR	Cystic fibrosis transmembrane conductance regulator
Cm	Chloramphenicol
COGS	cost of goods sold
CRP	cAMP receptor protein
crRNA	*CRISPR RNA*
CuAAC	Copper-catalyzed azide-alkyne cycloaddition
CyaA	adenylate cyclase toxin
Degrees Celsius	°C
Dha	2,3-didhydroalanine
Dhb	2,3-dihydrobutyrine
DMCT	demeclocycline hydrochloride
DPG	diphosphatidylglycerol
DSPG	1,2-distearoyl-sn-glycero-3-phospho-(1'-rac-glycerol)
DTT	Dithiothreitol
E. coli	*Escherichia coli*
EDTA	Ethylenediaminetetraacetic acid
EGFP	Enhanced Green Fluorescent Protein
ESI-MS	Electrospray Ionization – Mass Spectrometry
Eth	Ethionine

fMET	N-formylmethionine
FRET	Fluorescence resonance energy transfer
Fsk	Forskolin
GCE	genetic code expansion
GCPR	G-protein coupled receptor
GDP	Gross Domestic Product
GFP	Green fluorescent protein
GlcNAc	N-acetylglucosamine
HEK	Human Embryonic Kidney
HIC	Hydrophobic interaction chromatography
Hpg	Homopropargylglycine
HPLC	High performance liquid chromatography
HSAT	homoserine acetyltransferase
IBMX	3-isobutyl-1-methylxanthine
IEX	Ion Exchange
Ile	Isoleucine
IMAC	Immobilized metal affinity chromatography
IPTG	isopropyl-b-D-thiogalactoside
Kan	Kanamycin
L. lactis	*Lactococcus lactis*
L. monocytogenes	*Listeria monocytogenes*
Lan	Lanthionine

LB	Luria Bertani
LE	Left End
LPS	Lipopolysaccharides
MAPs	multiple-antigen peptides
MbPylRS).	*Methanosarcina barkeri pyrrolysyl-tRNA synthetases*
MDR	Multidrug resistant
MeLan	(methyl-)lanthionine
Met	Methionine
MetA	homoserine succinyl transferase
MetE	cobalamin-independent methionine synthase
MetH	cobalamin-dependent methionine synthase
MetO	Methionine sulfoxide
MetRS	Methionyl-tRNA synthetase
MjTyrRS	*Methanocaldococcus jannaschii* tyrosyl-tRNA synthetase
MmPylRS	*Methanosarcina mazei pyrrolysyl-tRNA synthetases*
Mox	Methoxinine
Msr	Methionine sulfoxide reductase
MSRA	Methicillin-resistant *Staphylococcus aureus*
MurNAc	N-acetylmuramic acid
ncAA	Non-canonical amino acid
NisB	Nisin Dehydratase
NisC	Nisin Cyclase

NisP	Nisin Protease
Nle	Norleucine
NMM	New minimal media
Nsr	Nisin resistance operon
o-pair	Orthogonal aminoacyl-tRNA synthetase:tRNA pair
OAHS	*O*-acetyl-*L*-homoserine
OAHSS	*O*-acetylhomoserine sulfhydrylase
OASS	*O*-acetylserine sulfhydrylase
OD_{600}	Optical density at 600nm
OmpT	outer membrane protease
P. aeruginosa	*Pseudomonas aeruginosa*
PAM	protospacer adjacent motif
PBP	Penicillin-binding protein
PBS	Phosphate buffered saline
PEG	polyethylene glycol
PLGA	poly (lactide-co-glycolic acid)
PPHN	persistent pulmonary hypertension of the newborn
PTM	post-translational modification
R&D	research and development
RE	Right End
RiPPs	Ribosomal synthesized and post translationally modified
ROS	Reactive Oxygen Species

S. aureus	*Staphylococcus aureus*
SAH	S-adenosylhomocysteine
SAM	S-adenosylmethionine
SCS	stop-codon suppression
SDS-PAGE	Sodium Dodecyl Sulfate–Polyacrylamide Gel Electrophoresis
SEC	Size exclusion chromatography
Sem	Selenomethionine
SPAAC	Strain-promoted azide-alkyne cycloaddition
SPI	Selective Pressure Incorporation
Suc	Sucrose
TBAHS	Tetrabutylammonium hydrogen sulfate
TBTA	Tris((1-benzyl-4-triazolyl)methyl)amine
TCA	trichloroacetic acid
TCS	two component systems
THPTA	Tris(3-hydroxypropyltriazolylmethyl)amine
TFA	Trifluoroacetic acid
TLC	Thin Layer Chromatography
TM	Transmembrane domains
TOF	Time of Flight
TRIS	tris(hydroxymethyl)aminomethane
tRNA	Transfer RNA

Trp	Tryptophan
TSD	Target Site Duplication
UDP	uridine diphphophate
Val	Valine
VRE	vancomycin-resistant *Enterococci*
WASH	Water, sanitization, hygiene
WHO	World Health Organization
WT	Wildtype

1. Introduction

1.1 Introduction to Genetic Code Expansion

1.1.1 Bioorthogonal and Click Chemistry

Biorthogonal chemistry, a term coined by Carolyn Bertozzi in 2003, refers to selective chemical reactions that proceed without interfering with biological systems. In 2003, Barry Sharpless introduced the concept of "click chemistry", which encompasses biologically compatible reactions that yield high amounts of regiospecific products.[1] These reactions are feasible in aqueous environments, exhibit rapid kinetics, and seldom generate toxic by-products, allowing them to be performed on cell surfaces, within the cytoplasm, and throughout the body.

A quintessential click reaction is the copper-catalyzed azide-alkyne cycloaddition (CuAAC). It evolved from the copper-catalyzed azide-alkyne cycloaddition (CuAAC) is a prominent click reaction, originating from the azide-alkyne Huisgen 1,3-dipolar cycloaddition developed by Rolf Huisgen. This reaction involves the interaction of an azide and a terminal alkyne to produce a disubstituted triazole. It is characterized by its highly exothermic nature and a significant activation barrier, resulting in a slow and non-regioselective process.[2] The reaction could not be performed under physiological conditions and necessitated elevated temperatures exceeding 100 degrees Celsius, resulting in a mixture of 1,4-triazole and 1,5-triazole regioisomers. These challenges were addressed through the application of a copper catalyst, as reported by Sharpless and Meldal. This reaction was highly regioselective producing only the 1,4-regioisomers and much faster (10^7) in comparison to the uncatalyzed version. The copper (I) species can be regenerated with the use of the reducing agent sodium ascorbate. The Cu^{1+} species serves as the most appropriate catalyst due to its capacity to engage the terminal alkyne in both sigma and pi interactions. However, it is thermodynamically unstable and readily oxidizes to the catalytically inactive Cu^{2+} form. In

aqueous conditions, Cu^{1+} is generated in situ by employing Cu(II) salts, such as copper sulphate pentahydrate, along with the reducing agent sodium ascorbate and water as a base in the reaction. However, copper's cytotoxicity present a significant challenge for *in vivo* applications.[3] Elevated copper levels are harmful to cells due to their increased redox activity, which results in the generation of highly reactive hydroxyl radicals that damage all biological molecules. Furthermore, copper exhibits a strong affinity for thiols, allowing it to bind to cysteine residues and disrupt redox-sensitive proteins.[3,4] The significant disadvantage of copper-catalyzed reactions in *in vivo* systems has prompted extensive research to mitigate this issue, including the development of copper-stabilizing ligands. Examples of these include Tris(3-hydroxypropyltriazolylmethyl)amine (THPTA), 2-(4-((Bis((1-(*tert*-butyl)-1*H*-1,2,3-triazol-4-yl)methyl)amino)methyl)-1*H*-1,2,3-triazol-1-yl)acetic acid (BTTAA) and Tris((1-benzyl-4-triazolyl)methyl)amine (TBTA).[2] These ligands can form heterocyclic chelates with Cu(I), enhancing reaction rates while maintaining the metal in its reduced state. They also prevent copper from engaging in interactions that could lead to its degradation by surrounding the Cu(I) centre and eliminating free binding sites for destabilizing interactions. The tertiary amino group[5] serves as a necessary base during reactions in organic solvents. Furthermore, the copper's reactivity with biomolecules is reduced, resulting in fewer reactive oxygen species.[6] Further examples to mitigate the cytotoxicity of copper involve the application of strain-promoted click reactions (strain-promoted azide-alkyne cycloaddition (SPAAC)). These reactions utilize electron-deficient alkynes, such as cyclooctyne, and proceed due to the release of ring strain. However, incorporating these moieties into proteins and synthesizing them presents challenges. Bertozzi was awarded a Nobel Prize for her development of these reactions and has investigated their application in bioorthogonal chemistry. [2]

1.1.2 Genetic Code Expansion and Non-Canonical Amino Acids

The introduction of click reactive handles into proteins is possible due the development of the field of synthetic biology. This field is relatively new, introduced first in the 1980s where it was used to describe genetically engineered bacteria made using recombinant DNA

technology.[7] Synthetic biology involves constructing new biological pathways, organisms, and redesigning existing natural systems for new purposes.[7]

Novel organic functional groups with click handles can be introduced into biological systems using non-canonical amino acids (ncAAs). These are amino acids outside the 20 canonical amino acids and not assigned a triplet codon. These amino acids are introduced into the system by hijacking the translational machinery and the use of the expanded genetic code. A diverse array of non-canonical amino acids, available through synthesis or purchase from suppliers, can be employed to impart novel properties to proteins. These include fluorinated analogs, which modify electronegativity and enhance protease resistance; alkylated amino acids, which alter hydrophobicity; and click-reactive amino acids, featuring handles such as alkynes, azides, and alkenes for use in click chemistry.

The expansion of the genetic code is facilitated by the inherent promiscuity of aminoacyl-tRNA synthetases (aaRS). These enzymes are uniquely responsible for the implementation of the genetic code. They perform the esterification reaction on transfer RNA (tRNA) molecules, thereby loading them with their corresponding amino acids. This enzyme possesses two distinct binding sites: one for ATP binding and another for specific interactions with amino acids. The recognition mechanism for each amino acid varies among different aminoacyl-tRNA synthetases, contributing to their low error rate during translation. Although the recognition of each amino acid by aaRSs is distinct, the fundamental mechanisms and reactions involved are consistent. Additionally, these enzymes possess a post-transfer editing domain containing an amino acid tRNA ligase and AA-tRNA deacylase. The double sieve model posits that the catalytic site functions as a “coarse” sieve, filtering out larger amino acids, while the editing site acts as a “fine” sieve capable of hydrolysis. The pocket of this editing site is smaller than that of the cognate amino acid. Additionally, this site is responsible for de-acylating any amino acid that successfully passes through the first site. Evidence supporting the existence of this site is observed in ten aminoacyl-tRNA synthetases from both classes. Pre-editing transfer takes place after the formation of aminoacyl-AMP, prior to its transfer to tRNA, whereas post-transfer editing occurs after the amino acid has been charged onto the tRNA. Despite these highly regarded

editing mechanisms, there exists a world of non-canonical amino acids that surpass such mechanisms.[8] There are various methods that exist for the incorporation of non-canonical amino acids into proteins: such as the selective pressure incorporation (SPI) method and stop-codon suppression (SCS) method.

SPI utilizes auxotrophic bacterial strains and requires the ncAA to be an isostructural analog of the depleted canonical amino acid (e.g, methionine). The endogenous aaRS mischarges the analog, leading to residue -specific replacement at all sites of that amino acid. This method requires a proper expression system, control over fermentation conditions, and selective pressure for amino acid replacement, which can be achieved through auxotrophy. This methodology involves the cultivation of bacteria harboring the target plasmid within a minimal medium. The expression of the gene of interest is regulated by an inducible promoter (e.g., IPTG), which remains repressed until the bacteria enter an arrested growth phase. This cessation of growth is triggered by the depletion of a limiting amino acid (ie. Methionine). After the arrested phase is reached, the media is supplemented with the non-canonical amino acid, and the target protein expression is induced. In this approach, the amino acids utilized are isostructural analogs of the canonical ones being substituted, thus only the endogenous aminoacyl-tRNA synthetase (aaRS):tRNA pair is required. This technique enables “residue-specific” labelling, and in cases where multiple residues are present, non-deleterious mutations are introduced through site-directed mutagenesis.

Although prediction software can identify non-essential residues suitable for replacement, experimental data may reveal that mutations of these residues can lead to a decrease in protein stability, function, and other critical properties. In instances where site-specific labelling is necessary, the stop codon suppression method proves advantageous. This approach employs an orthogonal aminoacyl-tRNA synthetase:tRNA pair (o-pair) that remains non-disruptive to the host cell’s machinery. This pair is primarily engineered to recognize the amber stop codon via codon reassignment. Site-specific incorporation of engineered stop codons allows for precise control over amino acid replacement. Furthermore, these orthogonal pairs can be designed to incorporate larger and more chemically complex non-canonical amino acids through libraries developed via directed

evolution and computational methods. Although this approach offers significant advantages, it typically results in lower yields, and the design of orthogonal pairs can be challenging, sometimes lacking in specificity.[9]

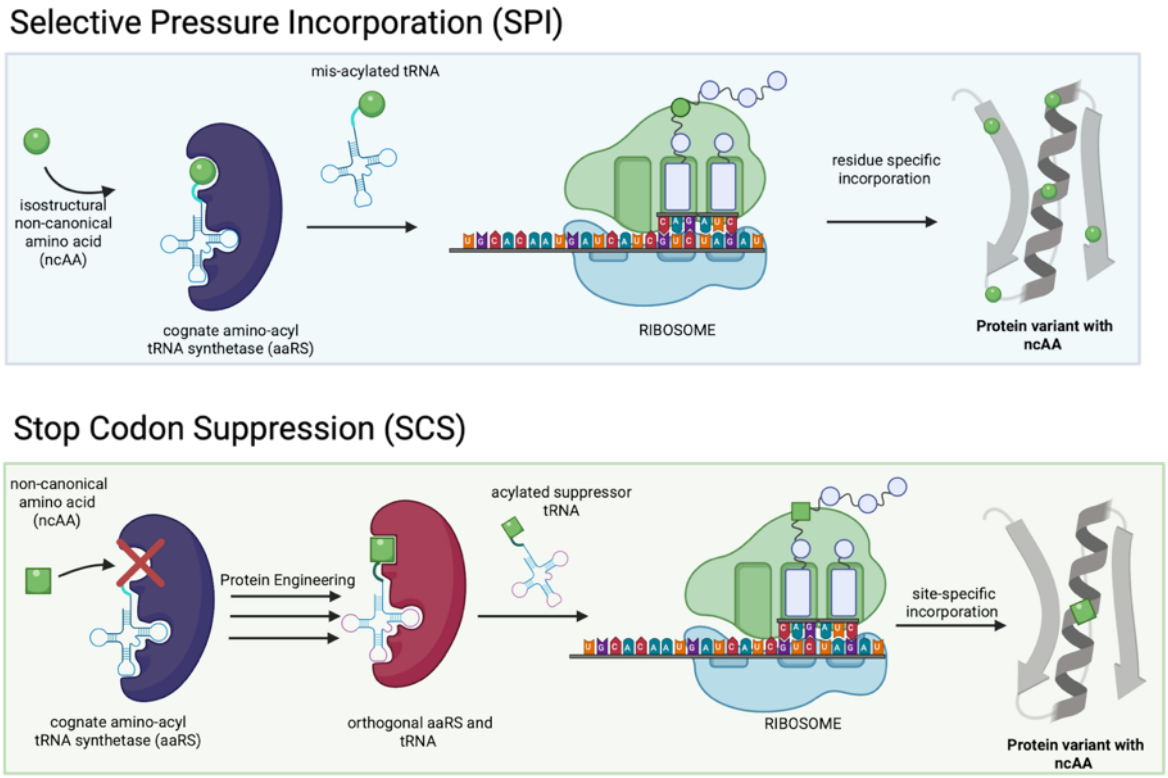


Figure 1. Techniques for Integrating Non-Canonical Amino Acids into Proteins (Top) Selective Pressure Incorporation Method: This technique employs an auxotrophic strain to replace a natural amino acid. An isostructural amino acid is charged onto the corresponding aminoacyl-tRNA synthetase (aaRS), producing a misacylated tRNA. The ribosome then incorporates this non-canonical amino acid into the protein at the site of the natural amino acid, achieving residue-specific incorporation. **(Bottom) Stop Codon Suppression (SCS) Method:** This approach allows for the incorporation of larger or non-isostructural non-canonical amino acids into proteins. By engineering an orthogonal aaRS and tRNA pair, the unique amino acid is loaded onto a suppressor tRNA. The mRNA transcript is altered to contain a premature stop codon, which is recognized by the suppressor tRNA, enabling site-specific labelling. Created with Biorender

1.1.3 Methionine: A Multifunctional Amino Acid and Its Analogs

1.1.0.1 Methionine in Genetic Code and Translation Initiation

While there are useful non-canonical amino acids corresponding to each natural amino acid, this thesis emphasizes methionine and its analogs. Methionine, although less

prevalent than other amino acids, is essential for cellular functions. Its roles encompass contributions to the genetic code and evolutionary processes, metabolic functions, and structural or protective roles within protein architecture. These include serving as an initiator for protein biosynthesis, a crucial methyl donor in biological systems and aiding to maintain cellular oxidation balance.[10,11] Methionine serves as the start codon for initiation of protein synthesis in eukaryotes while in prokaryotes (along with the mitochondria and chloroplasts), N-formylmethionine (fMet) serves the same purpose.[11,12] The formyl group is added to the free alpha-amino groups of Met-tRNA (fMet) by the methionyl-tRNA-formyltransferase. The formyl group does not remain persistently and is removed by the peptide deformylase.[12] The hydrophobic characteristic of methionine is considered essential for the formation of the preinitiation complex, facilitating the interaction between the charged initiator tRNA and initiation factor eIF2.[11]

1.1.0.2 Methionine as a Central Methyl Donor and Metabolic Hub

Methionine functions as universal methyl donor in the form of S-adenosylmethionine (SAM). This cofactor plays crucial roles in gene regulation through DNA and protein methylation, particularly histone proteins. It also functions to methylate RNA, influencing its stability, splicing, and translation. After transfer of the methyl group to the substrate, the resulting molecule of S-adenosylhomocysteine (SAH) is further broken down into homocysteine and adenosine by SAH hydrolase. The homocysteine is either recycled to form methionine by methionine synthase or is directed into the transsulfuration pathway where is first converted to cystathionine and further into cysteine. SAM plays important physiological roles in epigenetic regulation, maintaining cellular redox balance through its contribution to glutathione synthesis, and in neurotransmitter synthesis, such as the methylation of norepinephrine and serotonin. In addition, sustaining the balance between SAM and SAH is crucial as low SAM/SAH ratio has been linked to conditions like cancer and neurodegenerative diseases and a decrease in methylation capacity upon cellular aging.[13]

1.1.0.3 Methionine Oxidation, Redox, Homeostasis, and Aging

Methionine is an aliphatic and hydrophobic amino acid that participates in hydrogen bonding and hydrophobic interactions to help maintain protein structure. Additionally, it is prone to oxidation, undergoing reversible oxidation and reductions similarly to cysteine, and plays an important role as a cellular antioxidant.[14] Methionine forms methionine sulfoxide (metO) with the addition of oxygen to its sulfur atom and further oxidation leads to the formation of methionine sulfone. Methionine sulfoxide can be reduced to methionine by the methionine sulfoxide reductase (Msr) enzymes. These enzymes are stereospecific in that MsrA catalyzes the reduction of *S*-MetO while MsrB reduces *R*-MetO and are crucial for maintaining oxidative balance.[10,14,15] Exposed methionine residues on protein surfaces are the most susceptible to oxidation, while buried methionine residues are less prone to oxidation and may be vital to protein stability. These residues may act as lightning rods, protecting the more buried residues from oxidation and ensuring proper protein folding and stability.[10,14] Alpha-2-macroglobulin exemplifies this, with each subunit containing eight methionine residues that can be oxidized without compromising activity. Many examples of methionine residues acting as bodyguards against reactive oxygen species (ROS) are known to exist in nature. In the mitochondria, an additional methionine codon (AUA) is present, leading to a significant increase in the overall methionine content from 3% to 6%. This increase is crucial for antioxidant effects, protecting the organelle from the ROS produced during the respiratory chain reaction.[10] The aging process is often associated with increased oxidation while the antioxidant capabilities of cells decrease. Methionine sulfoxide reductases and methionine oxidation may also play roles in aging and various diseases. It has been previously shown that MsrA expression decreases with age in rats, even in organs where it is generally high, such as the liver, kidneys, and brain. In *Drosophila* flies, it was shown that MsrA hyperexpression led to an almost doubling of the maximum lifespan,[16] highlighting the importance of these proteins. Reports have shown that with age, in human collagen methionine sulfoxide accumulation increases and have also shown that methionine oxidation in dopamine receptor signalling in mice was linked to abnormal dopamine regulation and locomotor activity. Additionally, it was observed that the

expression of the MsrA protein decreased in the brains of Alzheimer patients, despite having similar mRNA levels as control brains without the diagnosis. Altogether these finding show the importance of maintaining the methionine oxidation balance for protein stability and functions.[15]

1.1.0.4 Methionine Analogs and Their Utility in Protein Science

A large repertoire of non-canonical amino acids are present in literature that can be incorporated in the place of methionine such as norleucine (Nle), selenomethionine (Sem), Methoxinine (Mox), ethionine (Eth), azidohomoalanine (Aha), homopropargylglycine (Hpg), homocysteine, etc. While they are isostructural analogs of methionine, these amino acids have a range of chemical properties (electronegativity, click reactive groups, varying polarities) that are useful in protein science. For example, the insertion of selenomethionine into proteins was useful in X-ray crystallography for solving the phase problem.[17] Azidohomoalanine and Homopropargylglycine contain the azide and alkyne groups that can participate in the CuAAC reaction and insertion of these ncAAs into protein allows for chemical modifications without disruption to biochemical metabolism. Lastly, Norluecine and Methoxinine: amino acids with opposing polarities can be used to study the effect on polarities and single atom replacement in protein structure. While most of these amino acids do not interfere with the methionine cellular pathways, ethionine is one exception and can be highly toxic to the cell. Met is an important methyl donor in the form of S-adenylyl methionine and the replacement with ethionine can disrupt this functionality resulting in detrimental effects to the cell metabolism.[13]

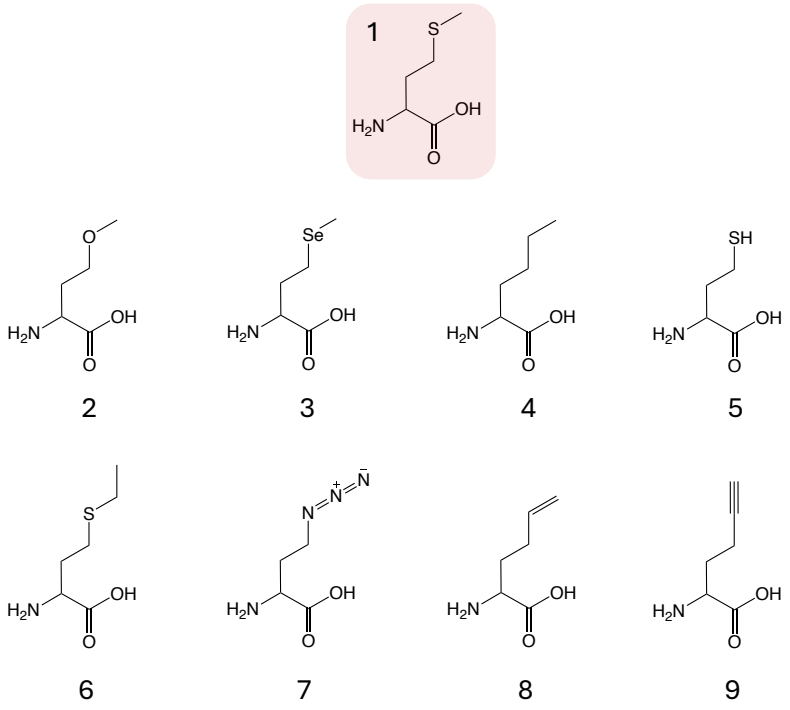


Figure 2. Methionine and Selected Methionine Analogs Commonly used in Protein Engineering and Genetic Code Expansion. (1) Methionine [Met] (2) Methoxinine [Mox] (3) Selenomethionine [Sem] (4) Norleucine [Nle] (5) Homocysteine [HCys] (6) Ethionine [Eth] (7) Azidohomoalanine [Aha] (8) *S*-allylhomocysteine [Shac] (9) Homopropargylglycine [Hpg]

Methionine (Met), an essential amino acid for protein synthesis, is not highly abundant in bacterial proteins. Its biosynthesis is tightly regulated, with intracellular concentrations in *Escherichia coli* (*E. coli*) approximately 0.15 mM.[18] There are a few biosynthetic pathways for methionine production in bacteria, referred to as transsulfurylation or direct sulfurylation. These pathways differ in their source of sulphur and the process used to attach it. For example, bacteria like *E. coli* use trans-sulfuration pathways, while bacteria like *Corynebacterium glutamicum* (*C. glutamicum*) use the direct pathway.[19] Both pathways convert *L*-homoserine, which is made from aspartate in several steps, into *L*-homocysteine. These pathways in bacteria are not mutually exclusive, as numerous species possess both, providing metabolic flexibility. In *E. coli*, homoserine is converted to *O*-succinyl-L-homoserine using the homoserine succinyl transferase (metA) and this is further converted to *L,L*-Cystathionine through the enzyme Cystathionine-γ-synthase and lastly the Cystathionine-β-lyase produces *L*-homocysteine. The alternative pathway uses only two

enzymes with homoserine acetyltransferase (HSAT) converting *L*-homoserine to *O*-acetyl-*L*-homoserine and *O*-acetylhomoserine sulfhydrylase (OAHSS) to convert the *O*-acetyl-*L*-homoserine to *L*-homocysteine. The final steps of these pathways are analogous, involving the conversion of *L*-homocysteine to methionine through either the cobalamin-dependent methionine synthase (MetH) or the cobalamin-independent methionine synthase (MetE). The methyltransferase encoded synthase catalyzes the transfer of a methyl group from 5-methyltetrahydrofolate to homocysteine, requiring the vitamin B12 cofactor for its function. The MetE encoded synthase can carry out the same function in the absence of cobalamin with 5-methyltetrahydrofolate serving as the methyl donor. [20]

1.1.0.5 Exploiting Methionine Biosynthesis for ncAA Production

In the direct pathway, the OAHSS enzyme is known to be promiscuous and can take other nucleophiles such as azides, cyanides, etc., in addition to its natural substrate of organic sulfide.[21] This pathway can be hijacked to produce a variety of amino acids with interesting chemical functionalities not readily found in nature. The synthesis of *L*-azidohomoalanine can be achieved by incorporating sodium azide[22], whereas the addition of allyl-mercaptan results in the formation of *S*-allyl-homocysteine.[23] By utilizing the pathway, a variety of non-canonical amino acids can be produced *in vivo*, eliminating the need to purchase these highly expensive ncAAs.

AIM OF STUDY

The objective of this study is to engineer functional, non-native proteins in *E. coli*, addressing two distinct but related challenges in recombinant protein production: site-specific chemical diversification through non-canonical amino acid incorporation (Parts 1 and 2), and heterologous expression of a structurally complex, multi-domain eukaryotic enzyme (Part 3). Utilizing the selective pressure method, various methionine analogs were incorporated into the proteins of interest in Parts 1 and 2. Furthermore, the genomic integration of enzymes for azidohomoalanine biosynthesis facilitated the *in vivo* production of the non-canonical amino acid, thereby eliminating the necessity for external supplementation.

Part 1 focused on using enhanced green fluorescent protein (EGFP) as the model protein. The incorporation of various methionine analogues enabled the investigation of its physiochemical properties and facilitated testing of different strains generated through genomic integration.

Part 2 focused on a highly studied antimicrobial peptide called nisin, produced by the lactic acid bacterium *Lactococcus lactis* (*L. lactis*). An expression system was produced to synthesize the Nisin peptide and the Nisin protease for the processing of the leader peptide. The integration of clickable amino acids like azidohomoalanine and homopropargylglycine, along with copper-catalyzed azide-alkyne cycloaddition, enables the development of novel antibiotics that function as multifunctional drugs. Due to the low yields of non-canonical amino acid (ncAA)-labelled peptides, systems were developed to enhance production, and a cell factory was established for the *in vivo* biosynthesis of the non-canonical amino acid.

Part 3 shifts focus to studying the adenylate cyclase 6 (AC6) Gαs protein and their roles in persistent pulmonary hypertension of the newborn (PPHN). Expression systems were developed to produce these proteins heterologously in *E. coli*. While the goal was to introduce clickable non-canonical amino acids into these proteins, heterologous expression in *E.coli* yielded a significant challenge.

2. Part 1: EGFP

2.1 Introduction of EGFP

2.1.1 Methionine as a Unique Structural and Functional Amino Acid

The amino acids methionine (Met), thought to be two of the latest additions to the genetic code is among the more complex proteinogenic amino acids with the greatest metabolic cost.[24] Methionine and tryptophan (Trp) are the only amino acids with a single codon, breaking the code's degeneracy[25] and the rarest with an abundance in proteins of 1.4% for Trp and 2% for Met (in comparison, leucine has an abundance of 9.1% in proteins).[26,27] Met is universal start signal[28] in protein translation and universal methyl group donor in life in form of S-adenosyl-L -methionine.[13]

Beyond its central roles in metabolism and translation, Met as a nonpolar, aliphatic amino acid is involved in protein folding, and stability through hydrophobic interactions and hydrogen bonding. Aliphatic, nonpolar and moderately hydrophobic thioester side chain of Met shows no strict preferences for protein interiors or surfaces. Its linear non-branched hydrophobic side-chain can easily fit into hydrophobic interiors of proteins whereas upon solvent (i.e., environment) exposure it is prone to oxidation and participate in radical scavenging thereby contributing to cellular redox homeostasis.[29]

2.1.2 Limitations of Canonical Mutagenesis and the Role of Methionine Analogs

Met contributes to protein stability, often via interactions with an aromatic side chain.[30] Indeed, the methionine aromatic motif plays a unique role in stabilizing protein structure via sulphur-Pi interaction that have recently been identified as prevalent and important stabilizing interactions in 1/3 of all known protein structures.[31] While sulfur – aromatic interactions are longer (5-7 Å) than salt bridges (<4 Å), both types of interaction have comparable energies.[32]

Attempts to precisely parameterize these interactions by traditional site-directed mutagenesis are limited as follows. Within the standard amino acid repertoire of the genetic

code, similar substitutions of canonical amino acids such as Threonine/Valine or Cysteine/Selenocysteine are possible. However, there are no such possibilities for S-methyl thioether as the most similar aliphatic hydrophobic amino acids leucine (Leu) and isoleucine (Ile) have branched and rigid hydrocarbon side chains that are not fully isosteric to the Met.

A more refined approach is the use of ncAAs that enable non-disruptive, isosteric substitutions. Already in 1950s Yoshida, Cohen and co-workers used Selenomethionine[33] (Sem), Norleucine[34] (Nle) and Ethionine[35] (Eth) as potential substrates for *in vivo* protein biosynthesis. Over the past 20 years, the successful incorporation of oxo-analog of Met, Methoxinine (Mox)[36], and its chemically distinct but sterically similar counterparts azidohomoalanine (Aha) and homopropargylglycine (Hpg) has been reported.[37] These analogs are sterically almost indistinguishable from the Met side chain, but have different polarities and chemical reactivity, making them powerful probes for structure-function studies.

The amino acid property called polarity requirement[38] is a measure that indicates whether an amino acid side chain is hydrophobic (i.e. the extent of hydrophobicity), based on empirical parameters such as chromatographic mobility[39] in a given environment or partitioning to polar/nonpolar solvents.[40] Kubyshkin[41] recently measured the lipophilicity of Nle, Sem, Mox, Aha, and Eth experimentally and constructed lipophilicity tables using methyl esters of N-acetylamino acids in partitioning experiments between octan-1-ol and water.[42] The obtained lipophilicity indices (i.e., logP) values reflect the actual polarity of the side chain since the influence of the polarity of the backbone is eliminated in these measurements by chemical protection of amino and carboxyl groups. In addition, high-resolution structures of proteins containing some of these amino acids are available in the PDB.

2.1.3 EGFP as a Model System to Probe Methionine Side-Chain Chemistry

It was postulated that the green fluorescent protein (GFP) with typical β-barrel structure from marine organism *Aequorea victoria* owes its structural stability and functional integrity

among others to specific sulphur-aromatic interaction between Met218-Trp57[43] which is crucial for protein folding and stability and is involved in fluorescence resonance energy transfer (FRET) to the chromophore. The characteristic fluorescence is only possible if the chromophore is protected from quenching by water via a properly folded protein matrix consisting of a B-barrel structure that isolates the interior of the protein from the aqueous medium.[44]

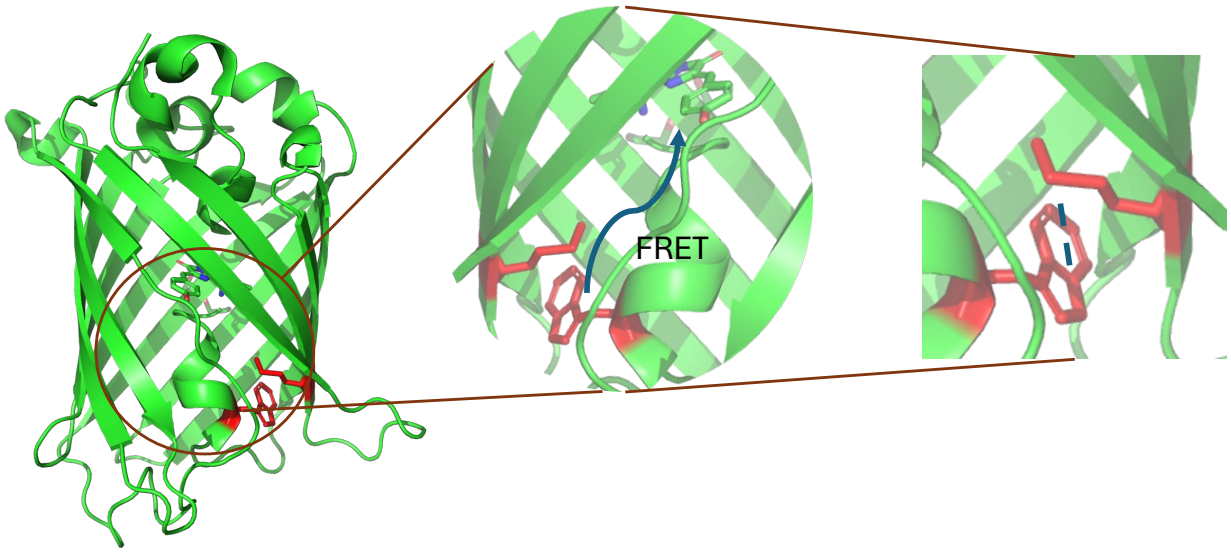


Figure 3. Structural Visualization of EGFP Highlighting Trp57-Met218 Interactions. Overall structure of EGFP (left), shown in green with its characteristic β-barrel architecture. The region of interest is expanded (center), showing the proximity of Trp57 and Met218 (highlighted in red) to the chromophore, at a FRET distance. A magnified view (right) reveals a sulfur–π interaction between the methionine sulfur of Met218 and the aromatic ring of Trp57, illustrating a stabilizing non-covalent interaction within the barrel that contributes to the local structural environment. Structural representation based on the crystallographic structure of EGFP (PDB ID: 4EUL).

To investigate the specific role of Met218 in this process, we selected the Enhanced Green Fluorescent Protein (EGFP), which is a Phe64Leu/Ser65Thr variant derived from the original GFP. The Met218 was systematically replaced with analogs (Fig. 1) using a method known as selective pressure insertion (SPI). Using simple spectroscopic studies combined with SPI method[9] and computer-guided modeling, it is possible to quantify the role of the polarity of the Met218 side chain in stability and functional properties of EGFP and to gain valuable mechanistic insights.

2.2 Results and Discussion

2.2.1 Probing the role of Methionine218 for Green Fluorescent Protein stability through side-chain polarity requirements using its non-canonical amino acid analogues

2.2.1.1 Quantifying Side Chain Polarities

As a quantification of side chain polarity, the methionine analogs were analyzed by high performance liquid performance (HPLC). These analogs were derivatized accordingly to protocol mentioned elsewhere[41] to remove effects of the backbone that may result on separation due to the zwitterionic nature of amino acids. Based on the data presented in the **Figure 4**, norleucine stands out as the most hydrophobic amino acid analog in the series. Its highly non-polar side chain gives it the highest LogP value, a measure of hydrophobicity. In contrast, the substitution of sulfur with the highly electronegative oxygen atom in Methoxinine (Mox) results in a dramatic change in polarity. This makes Mox the most polar methionine analog, as evidenced by its significantly different retention time compared to its counterparts. Interestingly, homopropargylglycine and azidohomoalanine, despite their distinct chemical structures, exhibit very similar retention times—8.3 and 7.9 minutes, respectively, suggesting their overall polarity is quite similar. The addition of a single methyl group to methionine to form ethionine significantly alters its polarity, as indicated by a notable change in its retention time. Finally, selenomethionine is the closest chemical relative to methionine among the analogs studied. This is reflected in their very similar retention times, with only a 0.9-minute difference. The small difference in retention time is likely due to the slight difference in atomic mass and electronegativity between selenium and sulfur. Overall, the general trends seen on this analysis match well with hydrophobicity scales previously mentioned.[41]

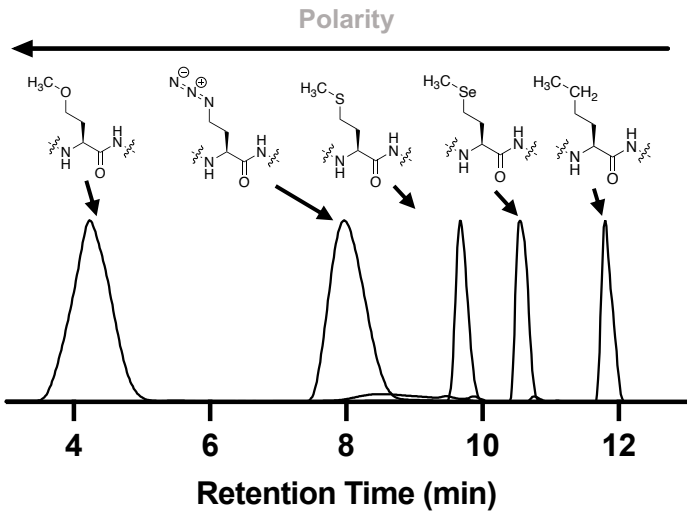


Figure 4. Determination of sidechain polarity of non-canonical amino acids using HPLC. The retention times of various methionine analogs are shown: Norleucine (11.8), Selenomethionine (10.6), Methionine (9.7), Azidohomoalanine (7.9) and Methoxine (4.2). Samples were separated based on side chain polarity using a gradient from 10 to 90% Acetonitrile in Water (0.075%) TFA on a C18 column from XBridge™ on a Waters HPLC system. The amino acids were detected with the Waters 2996 Photodiode Array UV detector with a 215 nm wavelength corresponding to amide bond absorption.

2.2.1.2 The Met218 Microenvironment and Its Role in EGFP Function

Prior to any experimental work, structural analysis of EGFP using LipPlot and Pymol provides robust insight into the microenvironment surrounding the Trp57-Met218 interaction which may be influenced upon non-canonical amino acid incorporation. Using LigPlot, the hydrophobic interactions with the side chain of methionine were mapped. Based on these calculations, various surrounding residues such as Leu64 and Valine61 (Valine) interact with the Cε of Met218 while Trp57 interacts hydrophobically with Cβ of Met218. Additional interactions with other residues that interact with the methionine backbone are shown in **Figure 5**. The use of Pymol helps to determine additional hydrophobic interactions with the side chain of Met218. This plot showcases that Trp57 and Val61 interact with the methionine sulfur atom and Phe46 interacts with Cε of Met 218. Earlier reports express that Trp57 participates in fluorescence resonance energy transfer to the chromophore.[43] Due to this phenomenon, upon excitation of the tryptophan residue, chromophore emission is observed. For FRET to occur, various criteria such as stated must be met: the donor and acceptor molecules must be within 10 to 100 Å, there must be overlap between the

absorption spectra of the acceptor and emission spectra of the donor and lastly their transition dipoles must be approximately parallel.[45] These requirements are fulfilled with Trp and the chromophore which are approximately 25 Å apart. [43]

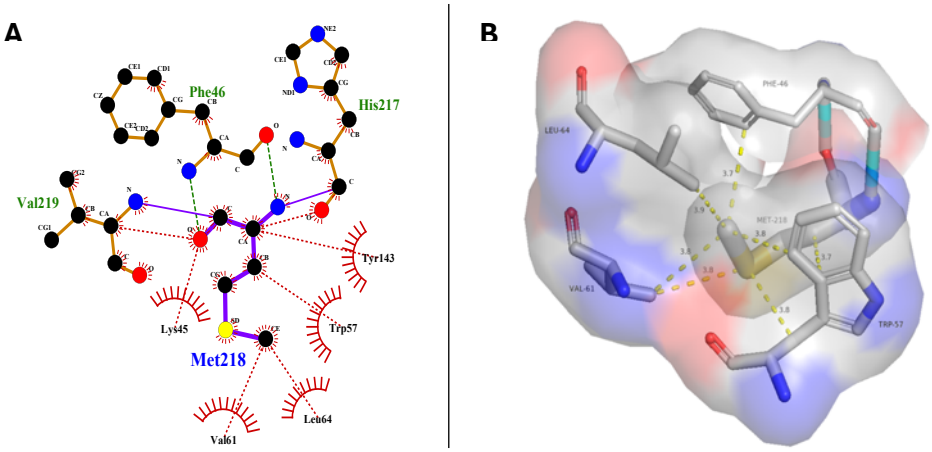


Figure 5. Structural context of Met218 in EGFP. LigPlot and PyMOL analysis of the Trp57–Met218 interaction and surrounding hydrophobic network (Val61, Leu64, Phe46). Trp57 is positioned to participate in fluorescence resonance energy transfer (FRET) with the chromophore, highlighting the functional importance of Met218 in chromophore shielding and fluorescence stability.

2.2.1.3 Residues-Specific Incorporation and Methionine Analogs into EGFP

The selective pressure incorporation method was used for the incorporation of the methionine analogs. This method involves using the cognate amino acyl tRNA synthetase of methionine to incorporate analogs in the place of the met codon within the mRNA sequence. This method is possible due to the promiscuity of the natural aaRS. The SPI method requires an auxotrophic strain of methionine, a defined medium and the analogs to be structurally resembling the amino acid to be replaced.[9] Since it is a residue specific, not site-specific method, the non-essential methionine residues were mutated to other natural amino acids using site-directed mutagenesis to avoid their incorporation effect on folding properties of the protein. The His-tagged EGFP protein variants were expressed in a Met-auxotrophic *E. coli* strain with the addition of the various analogs in the culture medium at the time of induction in varying concentrations (2.5 mM to 5mM). The expression of the incorporated variants resulted in a green cell pellet that was fluorescent under UV light, apart from Mox

which was detrimental to EGFP resulting in the complete loss of colour and fluorescence. The proteins were isolated from the soluble fraction (**Figure 6**) and purified using a combination of immobilized metal affinity chromatography (IMAC), anionic exchange chromatography and hydrophobic interaction chromatography (HIC). These purified proteins were subjected to Electrospray Ionization – Mass Spectrometry (ESI-MS) analysis to confirm mutations of methionine residues in EGFP and successful incorporation of varying analogs. The wildtype (WT)-EGFP sample calculated mass after chromophore formation is 27746.3 Da which corresponds well to the observed mass ($[M_{obs} + H]^+$ = *27744.2 Da)*. To isolate the effects of the Trp57:Met218 interaction four methionine residues were mutated (M79L, M89L, M154T and M234K) and these changes were confirmed with the help of ESI-MS measurements. The calculated mass for the M218-EGFP ($[M_{calc} + H]^+$ = *27677.14 Da)* corresponds well to the observed mass on seen on the ESI-MS profile in green (**Figure 6**). The SeMet-EGFP sample presented two prominent peaks. 27590.6 Da and 27768.7 Da. The first mass peak ($[M_{obs} + H]^+$ = 27590.6 Da) indicates cleavage of Met 1 along with along with incorporation of SeMet-EGFP at Met218 where the selenium atom is oxidized and the second mass ($[M_{obs} + H]^+$ = 27768.7 Da) corresponding to the incorporation of SeMet-EGFP in both Met1 and Met218 (**Figure 6**) The ESI-MS profiles of Aha-EGFP ($[M_{obs} + H]^+$ = 27664.7 Da, $[M_{calc} + H]^+$ = 27667.17 Da) and Nle-EGFP ([*Mobs* $+H]^+$ = 27639.1 Da, $[M_{calc} + H]^+$ = 27641.23.9 Da) all coincide with full incorporation of each analog into Met1 and Met218. An interesting finding from the ESI-MS spectra of Mox-EGFP, it is observed that partial Mox incorporation is achieved at the expense of successful chromophore formation ($[M_{obs} + H]^+$ = mass: 27660.2, $[M_{calc} + H]^+$ = 27661.2 for single incorporated and ($[M_{calc} + H]^+$ = 27645.18 for double incorporation). The methoxinine amino acid can be incorporated into either Met1 or Met218 but based on the results and loss of chromophore formation, it is most likely incorporated into the Met218.

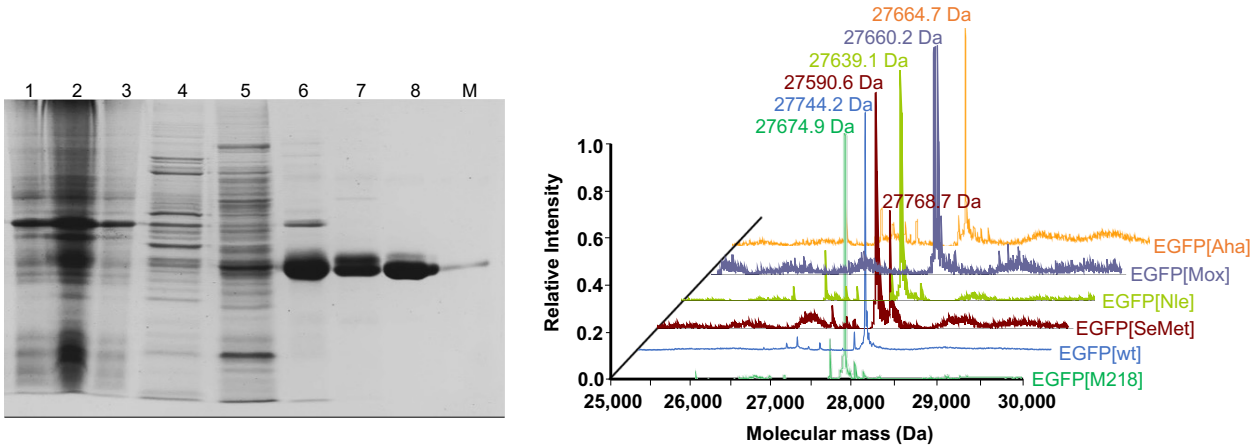
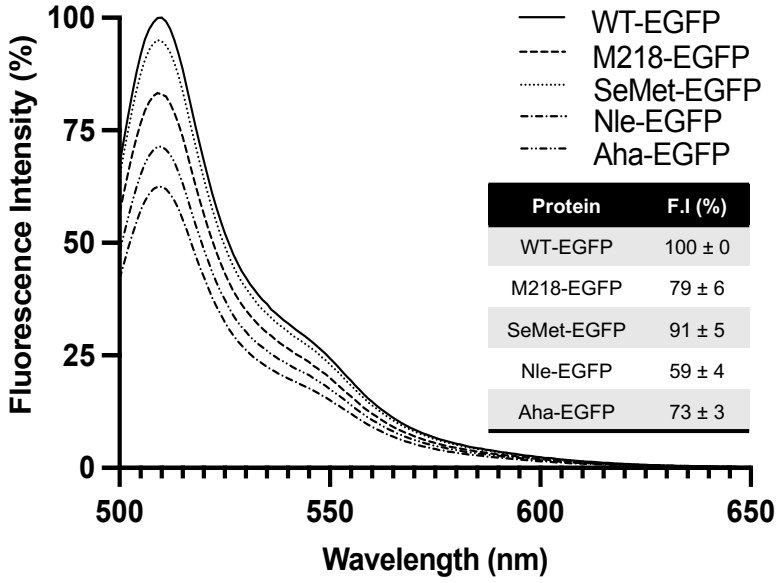


Figure 6. SDS-PAGE and Mass spectrometric analysis of M218-EGFP and variants with incorporated methionine analogs. (Left) SDS-PAGE analysis of EGFP (wt) across purification steps. Lanes: 1–3 (non-induced, induced soluble fraction, induced insoluble fraction), 4–6 (IMAC flow-through, wash, elution), 7 (IEX elution), 8 (HIC elution), and 9 (marker, purified EGFP). **(Right)** Deconvoluted ESI-MS spectra of His_6-tagged EGFP variants: M218-EGFP (27674.9 Da), SeMet-EGFP (27768.7 Da), Mox-EGFP (27660.2 Da), Nle-EGFP (27639.1 Da), Aha-EGFP (27664.7 Da), and WT-EGFP (27744.2 Da). Observed masses correspond predominantly to species containing two methionine substitutions at positions Met1 and Met218, except for Mox-EGFP.

2.2.1.4 Side-Chain Polarity Modulates EGFP Fluorescence

In addition, the fluorescence profiles upon excitation of the chromophore at 488 nm can provide further spectral information on what effects incorporation has on the chromophore. The mutation of the methionine residues (aside from Met1 and Met218) in EGFP drastically impacts the fluorescence of EGFP as fluorescence intensity is reduced to 79% in comparison to the WT-EGFP. The fluorescence is partially recovered with the introduction of SeMet at position 218 as fluorescence intensity increased to 91% in comparison to M218-EGFP. It can be speculated that SeMet incorporation increases the fluorescence intensity due to increased hydrophobic interaction with the surrounding residues leading to the creation of a larger hydrophobic barrier that protects the chromophore from the surrounding aqueous environment. The incorporation of azidohomoalanine further affected the fluorescence with a decrease in relative fluorescence intensity to 73%. The Nle-EGFP variant has the lowest relative fluorescence intensity (59%) in comparison all other variants and with the incorporation of Mox the fluorescence was completely diminished. Based on these

results, it shows that side chains changes at either end of the polarity scale were the most detrimental to the enhanced green fluorescent protein's fluorescence intensity.

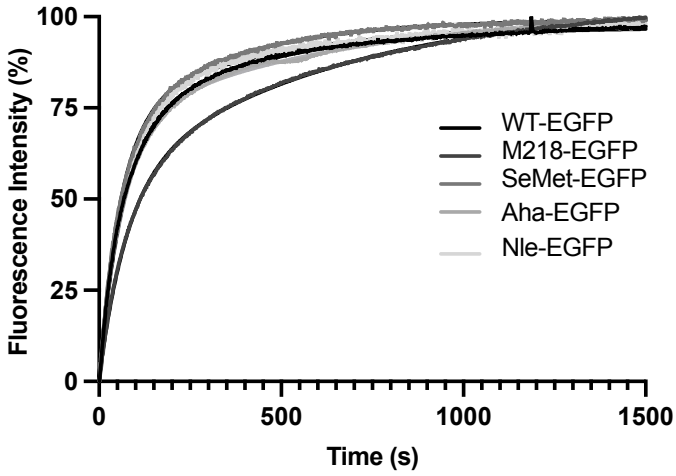


Protein	F.I (%)
WT-EGFP	100 ± 0
M218-EGFP	79 ± 6
SeMet-EGFP	91 ± 5
Nle-EGFP	59 ± 4
Aha-EGFP	73 ± 3

Figure 7. Fluorescence Spectral Profiles of EGFP variants. Fluorescence emission spectra were measured using a HORIBA fluorometer upon chromophore excitation at 488 nm and emission scanned from 500 to 700 nm with a slit size of 2.5 nm. Protein concentration was kept constant at 0.6 μM in PBS buffer. The fluorescence intensity relative to wt-EGFP was based on fluorescence intensity at λ_{max} for each variant. F.I. – Fluorescence Intensity. FI represented as Mean ± SD (n=2).

2.2.1.5 Methionine Analogs Effects on Folding and Refolding Kinetics

The refolding was monitored for at least one hour by measuring chromophore emission at 509 nm. The refolding kinetics show that SeMet-EGFP displays an initial fast rate of 1.9 s^{-1} and slow rate of 0.33 s^{-1} which are superior in comparison to the rates of wildtype-EGFP: 1.6 s^{-1} and 0.3 s^{-1} respectively. M218-EGFP refolding kinetics showcase an initial fast rate of 1.3 s^{-1} and 0.17 s^{-1} as the slow rate, both slower than SeMet-EGFP and WT-EGFP. Nle-EGFP and Aha-EGFP has similar initial rate of 1.5 s^{-1} and differing slow rates of 0.22 and 0.15 s^{-1}, respectively. It is interesting to note that M218 – EGFP refolding kinetics were comparatively slower in comparison to the variants (**Figure 8**)



Protein	K_{fast} ($x10^{-2}$ s^{-1})	K_{slow} ($x10^{-3}$ s^{-1})
WT-EGFP	1.65 ± 0.14	2.77 ± 0.60
M218-EGFP	1.31 ± 0.09	1.65 ± 0.05
SeMet-EGFP	2.2 ± 0.38	4.1 ± 0.5
Nle-EGFP	1.47 ± 0.05	2.17 ± 0.11
Aha-EGFP	1.48 ± 0.01	1.51 ± 0.04

Figure 8. Methionine analogs incorporation effect on Fluorescence Recovery Kinetics of EGFP. The proteins were denatured in the PBS + 5mM DTT containing 8 M Urea and heated at 95°C for 5 minutes to fully denature protein. For refolding, proteins were diluted 100x into buffer without urea. The sample was excited at 488 nm and fluorescence recovery was monitored with the emission at 509 nm. Protein refolding for all proteins starts with a fast initial phase and then a slower refolding phase. Data represented as Mean ± SD (n=2)

2.2.1.6 Polarity-Dependent Effects on EGFP Structural Stability

Effect of various concentrations of guanidinium hydrochloride as a denaturant on EGFP variants structure revealed that WT-EGFP has the most favourable stability with QC_{50} of 2.44 M after 30 min incubation at 37 °C in pH 7.4 which is the concentration of Gdm-HCL causes 50% chromophore fluorescence quench. As can be seen in Fig. 6, comparison of QC50 showed that Aha-EGFP variant is the second stable variant (QC50: 2.0) followed by Met218-EGFP (1.88 M), SeMet-EGFP (1.82 M) and Nle-EGFP as the lowest stable variant (QC50: 1.68 M). Faster refolding kinetics do not necessarily correlate with maximal thermodynamic

stability, suggesting distinct contributions of side-chain polarity to folding pathways versus final state stabilization. These findings suggest that methionine side-chain polarity fine-tunes protein stability and folding kinetics in a context-dependent manner, with implications extending beyond EGFP to other sulfur-rich protein architectures.

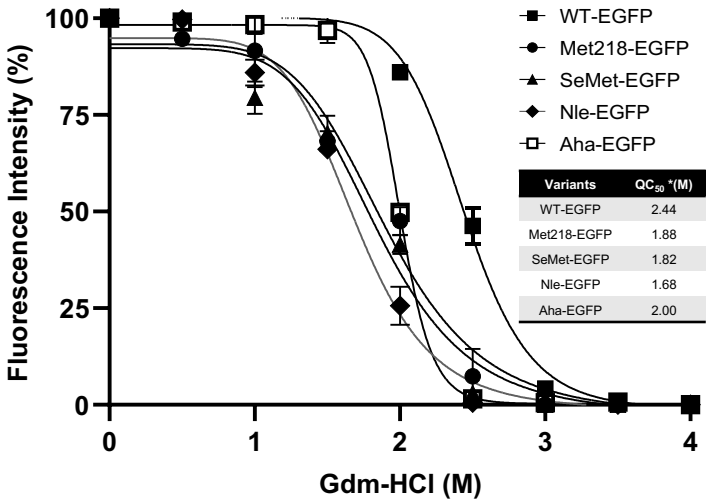


Figure 9. Structural stability analysis of EGFP variants using fluorescence intensity measurement in the presence of various concentration of Gdm-HCl. The WT-EGFP, Met218-EGFP, and EGFP variants samples were diluted appropriately by 100 mM potassium phosphate, 50 mM NaCl, pH 7.4, containing 0-4.0 M Gdm-HCl. The samples were prepared in 96 well microplate and the fluorescence intensities were measured at 530 nm when after 30 min incubation at 37 °C.

Across these experiments, EGFP methionine analog variants were characterized in duplicate (n = 2) for fluorescence, refolding kinetics, and stability measurements, reflecting the limited quantities of purified protein obtainable per analog under selective pressure incorporation. Differences reported between variants, including QC50 values and refolding rates, should therefore be interpreted as consistent trends across two independent protein preparations showcasing preliminary trends.

2.3 Materials and Methods

2.3.1 Cloning

To isolate the effects of the Trp57:Met218 interaction, four residues were mutated as follows: M79L, M89L, M154T and M234K. The mutations were carried out using the GeneArt® Site-Directed Mutagenesis PLUS System from Invitrogen™ (Thermo Fisher) and protocols therein. The primers used for mutagenesis were: forward1: 5'CACAACGTCTATATC ACCGCCGACAAGCAGAAG, reverse 1: 5' CTTCTGCTTGTCGGCGGTGATATAGACGTTGTG, forward 2: 5' GGGATCACTCTCGGCAAAGACGAGCTGTACAAGC, reverse 2: 5' GCTTGTACAGCTCGTCTTTGCCGAGAGTGATCCC, forward3: 5'GCTACCCCGACCACCTGAAG CAGCACGACTTCTTCAAGTCCGCCCTGCCCGAAGGCTACG and reverse 3: 5'CGTA GCCTTCGGGCAGGGCGGACTTGAAGAAGTCGTGCTGCTTCAGGTGGTCGGGGTAGC.

The mutated plasmid was isolated with Thermo Scientific™ GeneJET Plasmid Miniprep Kit. The mutations were confirmed with DNA sequencing and the mutated plasmid was transformed into the methionine auxotrophic cell; BU14 (E. coli B C> F- dcm ompT hsdS(rB-mB-) gal metλ (DE3 [lacI lacUV5-T7 gene 1 ind1 sam7 nin5]) for protein expression.

2.3.2 Protein Expression and Purification

From an overnight culture, EGFP (wt) was expressed in Luria-Bertani (LB) broth using 0.5 mM IPTG overnight at 30°C. To incorporate the methionine analogs, the proteins were expressed in new minimal media (NMM). The overnight culture was inoculated in NMM containing a limiting concentration of methionine. Upon the depletion of methionine, the cultures were supplemented with varying concentrations of each Met analog and protein expression was induced with 0.5mM IPTG and cultured overnight at 30°C. The cells were centrifuged at 17,000 xg for 15 minutes and the cell pellet was resuspended in HisTag binding buffer (50mM sodium phosphate, 300mM sodium chloride, pH 8.0) and lysed with sonication. Protein purification was conducted using the HisTrap™ column from GE Healthcare© and the protein

was eluted with a high concentration of imidazole. Further purification was conducted with a HiTrap™ FF Q column from GE Healthcare© and lastly a polishing step was conducted using either HiScreen™ Capto™ Butyl Impres Column or HiLoad™ Superdex 16/600 column. The purified proteins were dialyzed into phosphate buffered saline (PBS) for subsequent measurements.

2.3.3 Fluorescence measurements

The native and refolded protein fluorescence measurements were carried out using a Horiba PTI Quanta Master Fluorometer with FelixGX software and a PMT Detector. A Hellma UV/VIS Quartz Glass 10 mm Quartz Cell was used for measurements. Protein samples were excited at 488 nm and an emission scan was taken from 500 to 700 with a slit size of 2.5 nm. Protein concentration was kept constant at 0.6 µM in PBS buffer.

2.3.4 Refolding Experiments

Due to the high stability of EGFP, harsh denaturation conditions were applied for full denaturation of this protein and its variants. Denaturation of purified EGFP and the methionine analogs incorporated variants were conducted in PBS containing 8M Urea and 5mM DTT for 5 minutes at 95°C. These samples were renatured at room temperature by a 100-fold dilution into PBS + 5mM DTT buffer (-Urea). Protein refolding was monitored using the “Time-based” function on the fluorometer and it was monitored by fluorescence recovery at 509 nm. The measurements were taken at 1 second intervals for 1 hour with a slit size of 2.5 nm and an excitation wavelength of 488 nm was used. The data was imported into GraphPad prism and normalized before plotting. The data was fitted using exponential equations within the GraphPad Prism software.

2.3.5 Stability analysis

To study the structural stability of different EGFP variants, the protein samples were prepared in 50 mM potassium phosphate, 100 mM NaCl, pH 7.4 containing 0- 4.0 M Gdn-HCL. 4 µL of each EGFP variants were mixed with 96 µL buffer in a 96 well microplate and incubated at 37°C for 30 min. The fluorescence intensity was measured at 530 nm after excitation at 480 nm. 10s vibrational mixing with 2 mm amplitude was conducted before measurement using TECAN microplate reader.

2.3.6 HPLC

The methionine analogs were derivatized for measurements as stated elsewhere.[19] The derivatization was conducted to remove effects of the backbone upon measurement. Approximately 2-4 mg of each compound was dissolved in a mixture of 50% water and 50% acetonitrile. The solvents were HPLC grade purchased from Sigma and filtered through a 0.45µm filter. The compounds were run on a Waters 2695 HPLC system with a Waters 2996 Photodiode Array UV detector. The column specifications are as stated: XBridge™ C18 5µM 4.6 x 150.0 mm. The methionine analogs were separated using a gradient from 10% - 90% acetonitrile in water containing 0.075% TFA. A wavelength of 215nm was used to detect the compound as this corresponds to the wavelength of amide bond absorption.

2.3.7 Mass Spectrometric Analysis

The incorporation of methionine analogs into EGFP was confirmed with Electrospray ionization time of flight mass spectrometry (ESI-TOF-MS). The measurements were conducted with a Bruker compact™ mass spectrometer. The samples were purified and dialyzed into 10mM ammonium acetate for measurements. The filtered samples were directly infused by autosampler with Bruker Elute SP System at the flow rate of 0.3 ml/min and a gradient with Acetonitrile was used. The data was deconvoluted using Maximum Entropy software from Bruker.

3. Part 2: Nisin

3.1 Introduction to AMR, Lantibiotics and Nisin

3.1.1 Introduction to Antimicrobial Resistance and Bacterial Mechanisms of Resistance

Antimicrobial resistance (AMR) is an emerging global threat to humans, and the World Health Organization (WHO) predicts that by 2050 is likely to become the leading cause of death. This phenomenon occurs when organisms no longer respond to medicines, increasing the risk of spread, severe illness and even death. Based on reports by the WHO, AMR was the 3rd largest cause of death in 2019 worldwide, resulting in 4.95 million deaths[46] and additionally this rising death toll is associated with burdening economic costs. Predictions have indicated that AMR may cause up to $1 trillion USD additional healthcare costs by 2050 and by 2030 may result in $1-3.4 trillion USD gross domestic product (GDP) losses per year.[47] A further cause for concern is the sharp decline in the creation of new antimicrobials each year, accompanied by rising discovery costs and limited profitability. Antimicrobial drug development is a financially challenging endeavor, with an estimated cost of up to $1.1 billion before commercialization and an additional $350 million for post-approval expenses.[48] This is made worse by the fact that profits often only reach around $46 million[49], highlighting the urgent need for new innovations and technologies to reduce these significant costs.

While there are multiple drivers of antimicrobial resistance, the leading cause is the increased consumption and misuse of antimicrobials in humans and animal husbandry. In the agriculture industry, antibiotics are commonly used for treating or preventing disease in animals meant for consumption, but their food sources can be contaminated with antibiotics of full therapeutic potential.[50,51] Additionally, the lack of access to water, sanitization, and hygiene (WASH),[47] on top of poor disease control in hospitals with bacterial infection outbreaks can further lead to the spread of multidrug resistant (MDR) bacteria. While bacterial resistance is commonly found in nature (ie. Intrinsic resistance), acquired resistance attained by competent bacteria through modes of horizontal gene transfer poses

a larger threat to world health.[51] Common mechanism associated with intrinsic resistance include natural efflux pumps and reduction in membrane permeability. Acquired resistance occurs through bacteria acquiring mutations (due to deletions/substitutions or stressors such as starvation, UV radiation and chemicals) that affect genes that code for drug transporters and target drug modifying enzymes leading to decreases in drug effectiveness. [52,53]

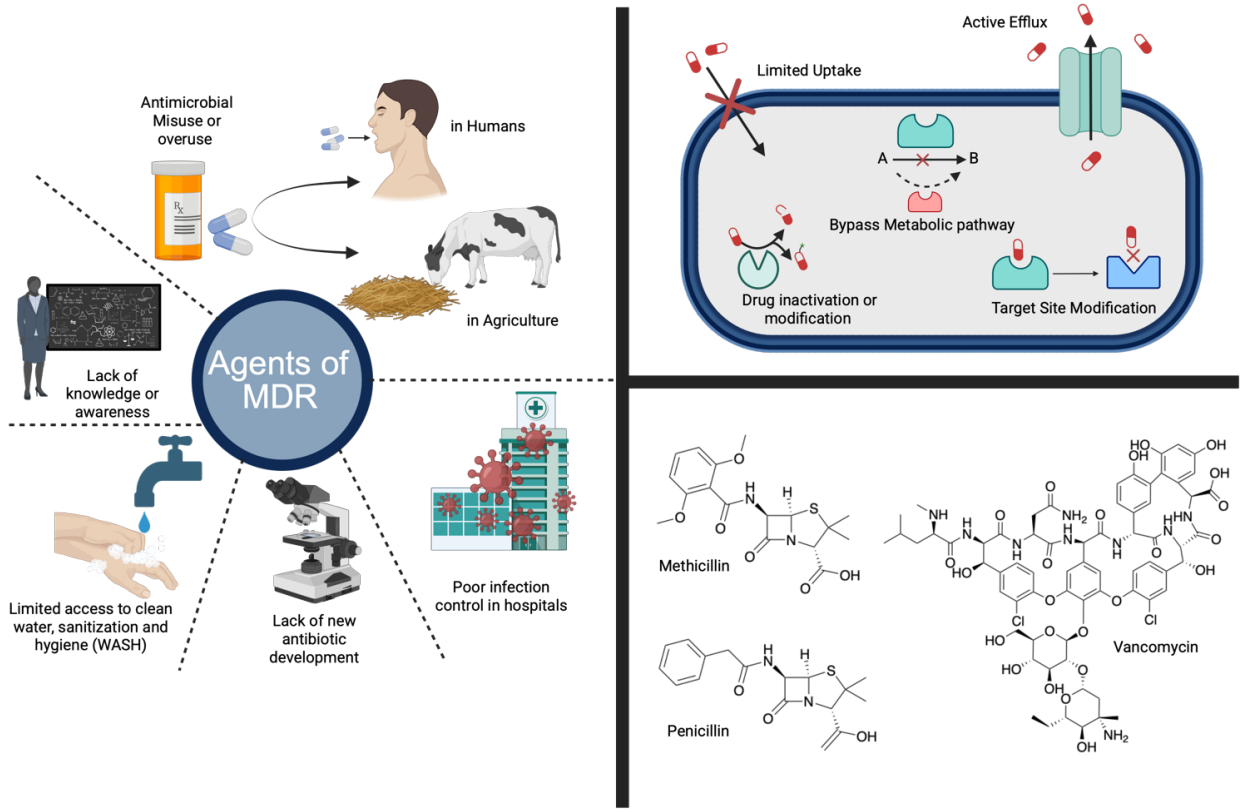


Figure 10. Drivers and mechanisms of antimicrobial multidrug resistance. **Left:** Major agents contributing to the emergence and spread of MDR across human, animal, and environmental interfaces. Antimicrobial misuse and overuse in humans and animals are the most common causes of multidrug resistance, and the lack of new antibiotic development does not meet the demand for new antimicrobials against these pathogens. **Right-Top:** Representative cellular mechanisms underlying MDR. Bacteria can limit the uptake of a drug through reduction of porins or express transporter proteins for active drug reflux. Additional mechanisms such as modification of target proteins, drug inactivation or modification are modes in which bacteria acquire resistance. **Right-Bottom:** Common Antibiotics with high multidrug resistance rates.[49] Created with Biorender

With traditional antibiotics, resistance bacteria soon emerge by obtaining one or more of the main mechanisms of antimicrobial resistance: limitation of drug intake, modification of drug targets, inactivation of the drug and active drug efflux. To limit the uptake of a drug bacteria can change the structure of porin channels or gram-negative bacteria have the

Lipopolysaccharides (LPS) layer which acts as a natural defence mechanism against permeabilization of harmful substances. In the literature, various examples exist of bacteria that modify target biomolecules to render a drug ineffective.[52] For instance, Methicillin-resistant *Staphylococcus aureus* (MRSA) acquires the *mecA* gene, which encodes a modified penicillin-binding protein (PBP) with decreased or completely diminished binding capacity, conferring resistance against β-lactam drugs[54]. Similarly, the acquisition of *van* gene clusters by vancomycin-resistant *Enterococci* (VRE) causes changes in peptidoglycan precursors.[53] The drug can be inactivated by the bacteria through either drug degradation or chemical modifications. A highly famous example of drug inactivation is the production of β-lactamase enzymes that inactivate the β-lactam antibiotics by hydrolyzing the β-lactam ring structure, obstructing their ability to bind their target PBPs. Various β-lactamase inhibitors have been developed that are given in combination with β-lactam antibiotics to combat this problem. Lastly, bacteria contain natural active drug efflux pumps, for example ATP-binding cassette (ABC) transporters to help remove any harmful substances (ie. Antibiotics). The swift rise of bacterial resistance highlights a critical need to develop new antimicrobials that are less susceptible to resistance. Antimicrobial peptides, as an alternative class of antimicrobials, may offer a promising solution.[52,53]

3.1.2 Antimicrobial Peptides (AMPs)

3.1.0.1 Antimicrobial Peptides

Antimicrobial peptides (AMPs) are small but powerful molecules found in a wide range of living things, from mammals and insects to plants and microbes. These short peptides, typically 5 to 100 amino acids long, are crucial for a variety of biological functions, often acting as a first line of defense against pathogens.[55] For bacteria, these peptides are essential tools for survival, giving them a competitive edge in the fight for nutrients. In the more complex world of eukaryotes, they have evolved to serve many different purposes—acting as immune regulators in mammals and a primary defense against pathogens in plants.[56] Although their name might suggest a narrow function, antimicrobial peptides (AMPs) possess remarkable versatility. They have a broad range of activity, not only targeting Gram-positive and Gram-negative bacteria but also fighting off viruses, fungi, parasites, and

protozoa, with some peptides even demonstrating anti-cancer effects.[55] Structurally, antimicrobial peptides are composed of cationic and hydrophobic amino acids, which gives them their characteristic amphiphilic nature. This structure allows them to first engage in electrostatic interactions with the negatively charged phospholipid heads and then embed themselves within the membrane via their hydrophobic regions. Resistance to antimicrobial peptides is far less common than with traditional antibiotics. This is attributed to their broad-spectrum activity, more complex modes of action that directly disrupt cell membranes and higher pathogen killing efficiency (lower bactericidal concentrations)[55,57]. The inherent thermal stability and adequate water solubility of these peptides makes them attractive targets for the development of next-generation antimicrobials, particularly in the fight against multidrug resistance[57].

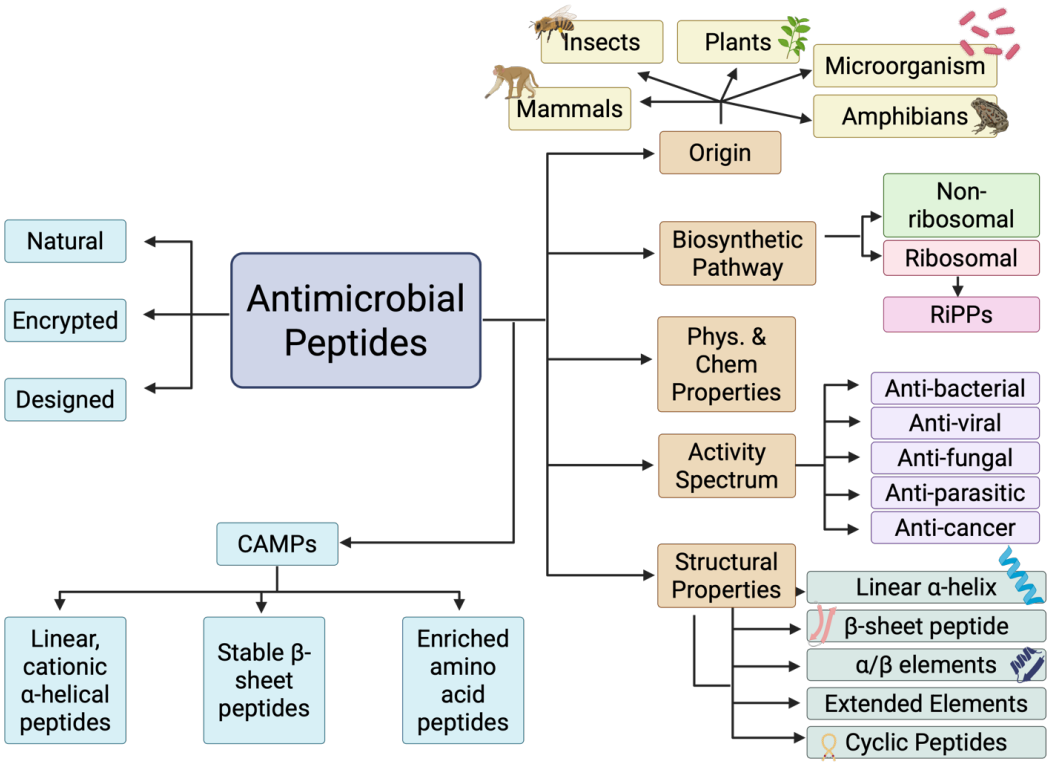


Figure 11. Classification and Key Features of Antimicrobial Peptides (AMPs). AMPs originate from natural, encrypted, or rationally designed sequences and are found across diverse taxa including microorganisms, plants, insects, mammals, and amphibians. They are produced through ribosomal (including RiPPs) or non-ribosomal biosynthetic pathways and exhibit broad bioactivity spectra such as antibacterial, antiviral, antifungal, antiparasitic, and anticancer activity. Structurally, AMPs are commonly grouped into α-helical, β-sheet, α/β, extended, and cyclic peptides, with cationic antimicrobial peptides (CAMPs) representing a major functional class. Created with Biorender

3.1.0.2 RiPPs and Lanthipeptides

Ribosomal synthesized and post translationally modified peptides (RiPPs) are a highly diverse class of natural products with ranging bioactivities. Their biosynthesis generally starts with a precursor peptide and the enzymes that modify this peptide are generally co-localized in the genome[58]. Within this class of antimicrobials, the largest and most notable subgroup is the lanthipeptides, which are characterized by distinctive lanthionine (Lan) or (methyl-)lanthionine ((Me)Lan) rings. While lanthipeptides have diverse bioactivities, lantibiotics are a specific subbranch that exhibits potent antimicrobial activity.

These peptides are synthesized as precursors containing a N-terminal leader peptide that contains important recognition elements for the post-translational modification enzymes, and the C-terminal core peptide that undergoes various post-translational modifications. There is a wide array of modifications such as halogenation of tryptophan residues exists but there are two universal modifications present in all lanthipeptides. The dehydration of serine and threonine residues to form 2,3-didehydroalanine (Dha) and 2,3-dihydrobutyrine (Dhb) respectively are a characteristic signature of lanthipeptides. The coupling of these modified residues to nearby cysteines results in the formation of the lanthionine rings, which gives these peptides their high biological stability and rigid structural conformity. Lanthipeptides can be further broken down into classes based on the modification machinery present in the system. The first class of lanthipeptides are contain two modification enzymes: LanB and LanC for dehydration and cyclization respectively, while the second class contains a single enzyme; LanM for both these reactions. The class 3 lanthipeptides are modified by LanKC; a bifunctional enzyme with 3 catalytic domains: lysase, Ser/Thr-kinase domain and a cyclase domain. The last class contains the modification enzyme LanL containing similar domains to LanKC, but its cyclase domain bears more similarity to the zinc dependent LanC from class 1.[59]

3.1.3 Nisin: System, Structure, and Mode of Action

3.1.0.3 Nisin Overview and Relevance

The best-known natural example of a lanthipeptide is Nisin, a lantibiotic made by the bacterium *Lactococcus lactis*. Nisin has been used as a food preservative for almost 50

years and bacteria have developed very little resistance to this peptide. While it was first discovered in 1928 in fermented milk cultures, it wasn't until 1969 that it was approved by the FDA for use in food as a preservative.[60] It exhibits potent antimicrobial activity against Gram-positive bacteria by binding lipid II, thereby inhibiting cell wall biosynthesis and inducing membrane pore formation. This dual mechanism contributes to its remarkably low rate of resistance development and long-standing safety record in food preservation. Nisin is synthesized as a precursor peptide that undergoes extensive post-translational modifications to yield the mature bioactive compound. These modifications, along with peptide regulation, secretion, and self-immunity, are encoded within a dedicated biosynthetic gene cluster, making nisin a well-characterized model for studying lantibiotic biosynthesis and engineering novel antimicrobial peptides.

3.1.0.4 Biosynthetic Gene Cluster

The Nisin biosynthetic gene cluster contains 11 genes involved in precursor peptide biosynthesis, post-translational modification, transport, extracellular processing, regulation, and immunity. This gene cluster consists of the genes: nisABC, nisT, nisP, nisRK and nisIFEG. Central to this system is the nisA gene, which encodes the 57-amino acid precursor peptide consisting of a N-terminal leader peptide and a 34-amino acid core peptide. The leader peptide plays crucial roles in directing Nisin to the post-translational modification (PTM) machinery, acting as a mechanism to protect its producer strain from the active peptide and as signal sequence for membrane transport after which is it cleaved by the extracellular protease. The core peptide is the portion that undergoes dehydration and cyclization reactions, ultimately giving rise to the characteristic lanthionine rings essential for Nisin's biological activity. The nisBC genes encodes for the posttranslational machinery, while the nisT and nisP encodes for the transportation and processing machinery. In addition to the biosynthetic genes, the cluster contains the regulatory genes (nisR and nisK) and immunity genes (nisI and nisFEG), which together ensure tight control of nisin production and protection of the producing strain. Collectively, these genes form the Nisin biosynthetic cassette responsible for the synthesis, maturation, secretion and regulation and self-resistance.

3.1.0.5 Key Enzymes for Nisin Biosynthesis and Immunity

NisB – Nisin Dehydratase

The Nisin dehydratase (NisB) is encoded by the *nisB* gene and ensure the proper dehydration of serine residues to produce 2,3-didhydroalanine and the dehydration of threonine residues to 2,3-dihydrobutyrine. The Nisin dehydratase is a 117kDa dimer protein containing a bifurcated cleft-like structure in its centre. Its N-terminal region is comprised of the glutamylation domain (~700 residues) and the C-terminal domain contains the elimination domain (~300 residues). In addition to these two domains, additional domains for glutamyl-tRNA interaction and a region for binding Nisin have been also identified.[61] Various key residues have been identified in this structure and mutational studies have shown their effect on Nisin maturation such as improper dehydration to lack of secretion.[62] The first step of dehydration mechanism involves the hydroxyl groups of serine and threonine getting glutamylated using the cognate $tRNA^{Glu}$ as the glutamyl-donor. The published crystal structure showcases the importance of the FLND box in the Nisin leader peptide as a recognition point and binding motif for the NisB enzyme. The Nisin leader peptide interacts with a twisted beta-strand thus forming a four-stranded anti-parallel beta sheet with residues Leu166-Asn175 in NisB. The Phe18 within the Nisin FNLD box binds within a hydrophobic cage consisting of these residues in NisB: Val176, Val198, Tyr202, Leu209, and Tyr213.[62] The last step of the reaction involves the elimination of the glutamyl group resulting in the formation of dehydrated residues previously mentioned.

NisC – Nisin Cyclase

The *nisC* gene encodes the Nisin cyclase (NisC) enzyme responsible for the formation of the thioether bonds between the dehydrated residues and cysteines to produce the distinctive lanthionine rings. This protein contains a toroid core with 6 helices each, an SH2-like domain and a Zn^{2+} ion coordinated by conserved cysteine residues (Cys284 and Cys 330) and a histidine residue (His331). A proposed mechanism showcases potential for zinc to function

as a docking site for the cysteine residues of Nisin which causes the displacement of water from the zinc ion and further the sulfur atom on cysteine is deprotonated. This deprotonation serves as an essential step that can accelerate the further 1, 4-Michael addition reaction that follows to form the lanthionine rings. The zinc atom may also play a crucial role in the helping to orientate the thiolate for a nucleophilic attack. It was shown that the His212 and Asp 141 residues in NisC were also essential for activity maintenance and mutations to these residues can cause hinderance in its activity to form correct ring structures.[63]

NisT- Nisin Transporter

After the dehydration and cyclization steps, the fully modified preNisin peptide is transported across the membrane by the ABC transporter encoded by the *nisT* gene. This transporter consists of two domains: the transmembrane domain forming the channel for PreNisin translocation and the nucleotide binding domain responsible for the binding/hydrolysis of ATP which provides the energy for the translocation process.[64,65] The Nisin transporter is considered to be a half-transporter containing only two out the four modules commonly seen in ABC transporters[64] thus requires homodimer formation for proper functioning.[64,65] Interestingly, this transporter can transport fully modified to completely unmodified peptides.[65]

NisP – Nisin Protease

The fully modified PreNisin peptide is transported outside the cell where it meets this subtilisin-like protease encoded by the *nisP* gene, named the Nisin Protease (NisP). This extracellular protease cleaves the leader peptide to produce the mature and active Nisin. It is a serine protease containing the catalytic triad: Asp259, His306, and Ser512, and is synthesized as a pre-pro-enzyme of 682 residues. It contains a N-terminal Sec-signal (for secretion across the cytoplasmic membrane), a C-terminal membrane spanning domain containing the Gram-positive cell-wall anchor consensus motif – LPxTG- motif. This motif is

recognized by sortase and NisP is anchored to the membrane surface. The propeptide sequence ends at Arg195, which is where the NisP proteases undergoes self-cleavage at the -VSPR- site to produce the mature protease (459 amino acids long). While many other subtilisin-like proteases that contains calcium binding sites, the Nisin protease does not contain these calcium chelation sites.[66] The Nisin protease recognises the -G**ASPR/**IT- site[67]; like its own cleavage site, contained within the Nisin precursor and cleaves Prenisin between Arg-1 and Ile1 to release the mature nisin. While it was previously accepted that the lanthionine rings in Nisin were crucial for NisP activity, newer studies have shown that while they are not essential for cleavage, they may play a role in forming the correct interactions with the protease and help to position the substrate within the active site.

NisRK – Nisin Regulation

In addition to these biosynthesis genes, there are regulatory genes encoded by *nisR* and *nisK* under the control of a constitutive promoter. Due to this, these genes are expressed independent of Nisin biosynthesis. The *nisK* gene encodes a sensor histidine kinase while a response regulator is encoded by *nisR*. This NisK protein is known to have stringent substrate specificity and is activated only upon the binding of mature Nisin/Prenisin while there is little to no effect upon binding of unmatured Nisin and other lantibiotics. The NisK protein is localized to the cytoplasmic membrane and upon binding of mature Nisin, it undergoes autophosphorylation on a conserved histidine residue in the C-terminal cytoplasmic “transmitter” domain. Further, this phosphoryl group is transferred to a conserved aspartic acid residue in the NisR protein.[68] This protein acts as a transcriptional activator that binds to the promoter regions of nisABCTPK and nisFEG thus inducing the expression of genes required for Nisin synthesis and immunity. (**Figure 12**)

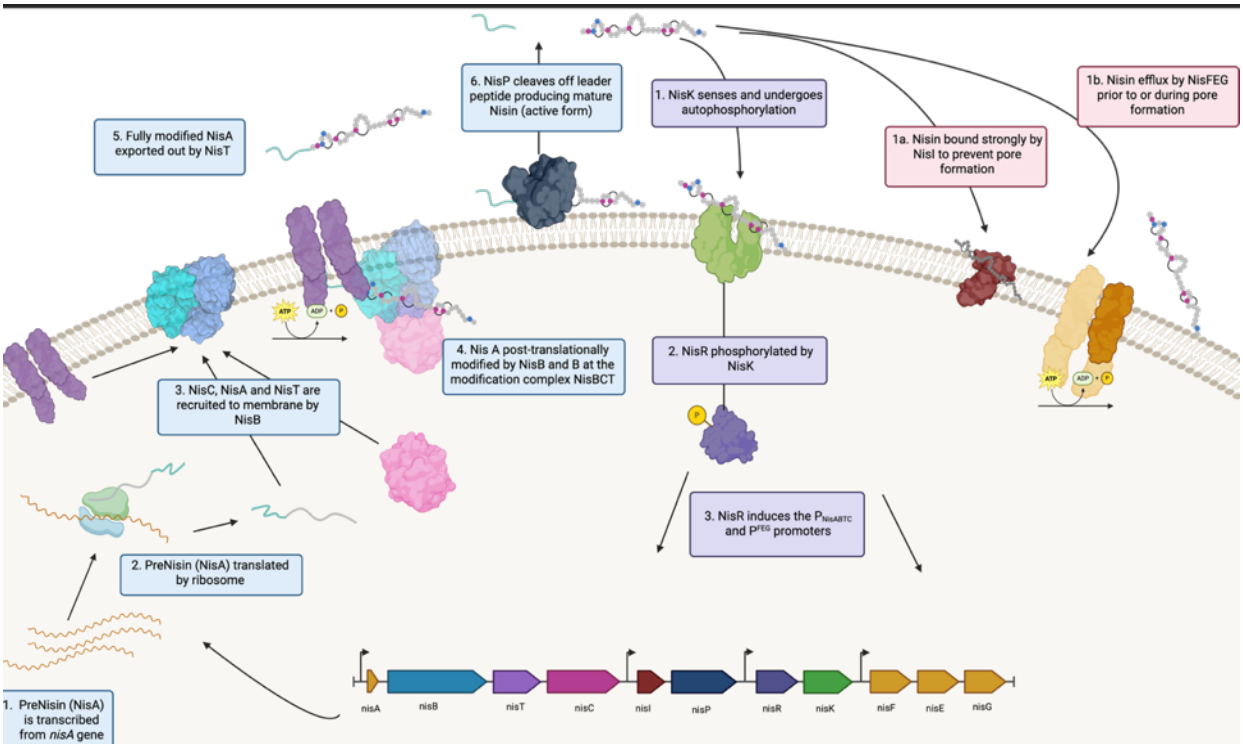


Figure 12. Scheme of Nisin Biosynthesis, Regulation and Immunity. Nisin is synthesized as the unmodified precursor made up of the leader and core peptide. This precursor undergoes processing by the dehydratase NisB and cyclase NisC. The modified precursor is transported outside the cell by the transporter NisT, where the leader peptide gets cleaved by the Nisin Protease NisP, producing the mature active Nisin. The immunity system is comprised of lipoprotein NisI and the ABC transporter NisFEG. Nisin expression is regulation by the two-component signal TCS composed of a sensor kinase NisK and the response regulator NisR which goes onto active the nisin promoter. Adapted from Field et al. Created with Biorender

3.1.0.6 Mechanism of Action

The mechanism of action of antimicrobial peptides can mainly be divided into two categories: membrane disruption and intracellular disruption. The hydrophobic and cationic nature of these peptides allows them to insert into and disrupt biological membranes through three proposed models. In the barrel-stave model, peptides vertically insert membranes forming barrel-shaped aggregates that create pores, causing leakage of intracellular components. The toroidal model involves vertical embedding with pore formation through AMP-lipid head association, disrupting bilayers where both lipids and AMPs form the pore. In the carpet model, AMPs spread across the membrane until reaching critical concentration, causing membrane collapse in a detergent-like manner.[69,70] Some antimicrobial peptides can translocate across membranes and interfere with intracellular

processes including protein synthesis, enzyme activity, and nucleic acid synthesis. They can disrupt protein folding by blocking chaperone entry and inhibit cell division through DNA replication interference. In addition to their antimicrobial functions, AMPs also have immunomodulatory effects such as the human defensins which can modulate the host's immune response through recruitment of immune cells to the infection site, phagocytosis enhancement, etc.[56]

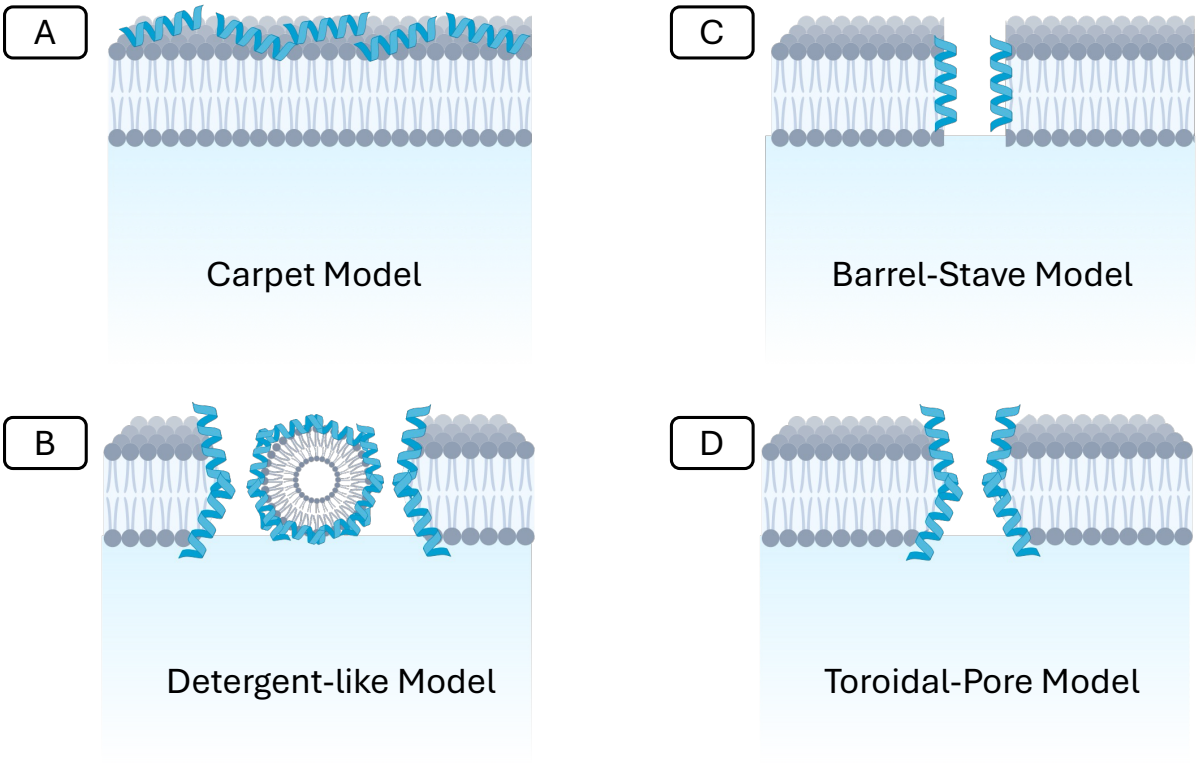


Figure 13. Proposed membrane-disruption mechanisms of antimicrobial peptides (AMPs). Schematic illustration of the major models describing AMP interactions with bacterial membranes: (A) Carpet model, where peptides accumulate on the membrane surface and cause membrane destabilization; (B) Detergent-like model, where peptides solubilize the membrane into micelle-like structures; (C) Barrel-stave model, where peptides insert and oligomerize to form transmembrane pores; and (D) Toroidal-pore model, where peptides induce curved pores lined by both peptides and lipid head groups. Created with Biorender

Nisin exhibits broad-spectrum activity against Gram-positive bacteria through a dual mechanism involving pore formation and cell wall synthesis inhibition. Central to Nisin's activity is Lipid II, an essential cell wall biosynthesis precursor. Lipid II synthesis begins in the cytoplasm with uridine diphosphate (UDP)-N-acetylmuramic acid (MurNAc)

pentapeptide linking to the undecaprenyl (C_{55}) phosphate[58] molecule via a pyrophosphate linkage to form Lipid I. The pentapeptide ((typically L-Ala-D-γ-Glu-L-Lys-D-Ala-D-Ala)[71,72] is attached to the MurNAc at the 3' carbon.[72,73] Subsequently, UDP-activated N-acetylglucosamine (GlcNAc) is added to Lipid I to complete Lipid II assembly. Lastly, the Lipid II molecule is transported across the membrane into the extracellular domain where it undergoes polymerization to build the peptidoglycan cell wall.[71,72,74] Lipid II acts as a docking molecule for Nisin and the activity of Nisin increases 2-fold in the presence of lipid II.[75]

The N-terminal rings of Nisin; rings A and B, bind to the pyrophosphate cage around the lipid II headgroup[73,76] and the flexible hinge region allows the C-terminus to insert itself into the membrane to form the pores. Structures published in 2004[71] reveal that the N-terminal backbone amides coordinate the pyrophosphate moiety of lipid II via intermolecular hydrogen bonds forming a cage like structure when N-terminus of nisin folds back onto the first two lanthionine rings. While the pyrophosphate moiety is the primary binding site, the MurNAc unit is critical for pore formation and the pentapeptide plays a role in stabilizing the Nisin-lipid II pore complex.[73] These Lipid II-Nisin complexes accumulate to assemble pores with a stoichiometry of 2:1 of Nisin to Lipid II[73] and lipid II is crucial for maximum pore formation. These pores cause the efflux of vital intracellular components, dissipation of the membrane potential, eventually leading to cell death.[76] In addition, Nisin causes segregation of Lipid II resulting in the inhibition of the peptidoglycan production cycle by preventing the cross-linking of the peptidoglycan chains.[75] The production of these chains is crucial for cell wall biosynthesis and inhibition of this process further harms the bacteria as their robust cell wall cannot be formed making them more susceptible to environmental stressors and lysis. This dual mode of action is one of the reasons that resistance to Nisin is rare despite its continuous use in the food industry.[77] While lipid II interaction is important for vancomycin activity, bacteria with the *vanA*-type gene cluster evade vancomycin by substituting the terminal D-Ala-D-Ala in the pentapeptide of their Lipid II with D-Ala-D-Lac.[78] Unlike vancomycin, nisin remains fully effective against *vanA*-type resistant bacteria because it binds to a different part of the Lipid II molecule.[71] Overall, bacteria do not readily

develop resistance against lantibiotics as Lipid II is unique to bacteria and highly important for bacterial integrity and growth.

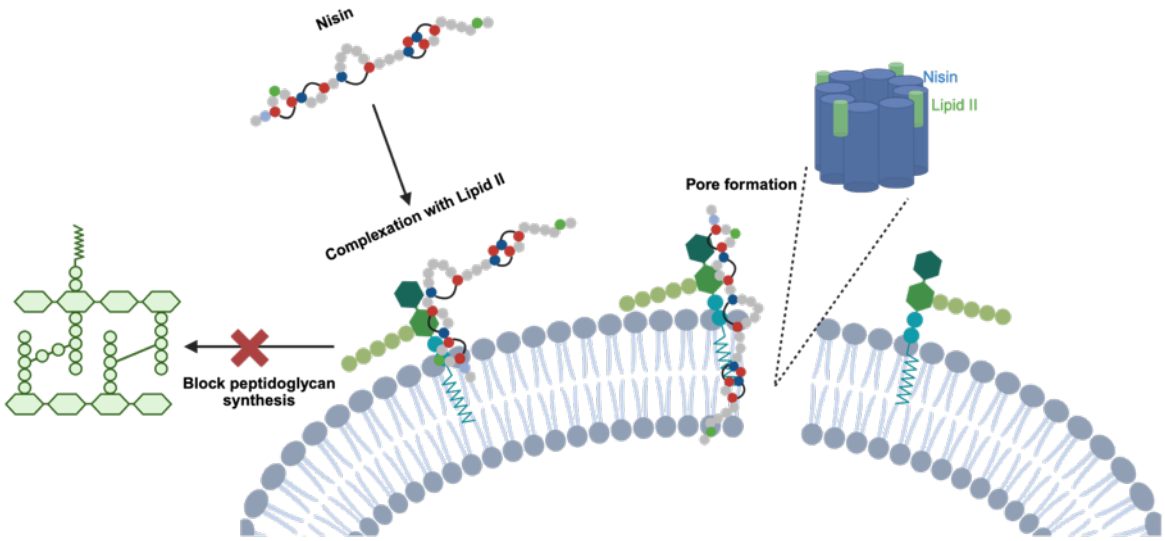


Figure 14. Dual mode of action of Nisin mediated by Lipid II interaction. The N-terminal rings of the lantibiotic Nisin interact with the pyrophosphate group of the cell wall precursor, Lipid II, anchoring Nisin to the bacterial membrane. Subsequently, the C-terminal domain (rings D and E) inserts into the membrane leading to pore formation, causing detrimental effects to the targeted bacterium. The Lipid II-Nisin complexes assemble into pores with a stoichiometry of 2:1 of Nisin to Lipid II. Additionally, the sequestering of Lipid II blocks its participation peptidoglycan synthesis. Created with Biorender

3.1.4 Resistance to Nisin

3.1.0.7 Intrinsic Immunity in produced strains

Nisin-producing *Lactococcus lactis* strains contain immunity genes that protect the host from nisin's antimicrobial activity. These immunity genes include *nisI* and *nisFEG*, which encode a lipoprotein and an ATP-binding cassette (ABC) transporter, respectively. The NisI protein contains a signal sequence for membrane transport that is cleaved after secretion, followed by a lipidation site at the first cysteine residue. The mature, lipid-anchored protein localizes to the outer portion of the cytoplasmic membrane and provides immunity through two mechanisms: sequestering nisin to protect the bacteria and inducing cell clustering that prevents nisin from reaching Lipid II. This process is reversible when nisin concentrations fall below inhibitory concentration 50% IC_{50} values.[79]

The *nisFEG* genes encode an ABC transporter localized in the cellular membrane that expels nisin prior to pore formation.[80] This transporter comprises the nucleotide binding domain NisF, which utilizes adenosine triphosphate (ATP) hydrolysis for energy, and heterodimeric transmembrane domains NisE (26 kDa integral membrane protein) and NisG (24 kDa protein). Each transmembrane domain contains six transmembrane (TM) helices forming the nisin expulsion channel. The complete complex stoichiometry is $NisF_2EG$, representing a crucial component of the host's immunity system. NisFEG acts cooperatively with NisI, with NisI inhibiting pore formation while NisFEG expels nisin from the membrane before pore formation can occur.[81]

3.1.0.8 Non-producer resistance strategies

While lantibiotic resistance emergence is significantly less common than with other antibiotic classes, limited cases have been documented recently. Various bacterial species have developed resistance strategies analogous to *L. lactis* intrinsic immunity, including membrane property alterations and active efflux mechanisms. Bacteria employ multiple strategies to overcome nisin activity, including altering membrane rigidity, surface charge, permeability, and thickness, or modifying lipoteichoic acids in the cell wall. Additional mechanisms include producing nisin-specific proteases, activating two-component stress response systems, and employing ABC transporters for active nisin efflux.

Listeria monocytogenes demonstrates comparatively higher nisin resistance than other Gram-positive pathogens[82] by reducing diphosphatidylglycerol (DPG) membrane content[83], thereby decreasing net negative membrane charge and hindering positively charged nisin insertion. [84] Resistant strains also lower their C15:C17 fatty acid ratio, increasing membrane rigidity and reducing susceptibility to nisin membrane insertion.[85] Various *Streptococcus* species modify membrane properties to confer nisin resistance. *Streptococcus bovis* alters cell surface properties including reduced hydrophobicity, increased lipoteichoic acid content that can be further modified to enhance resistance, and increased net positive charge.[84] *Streptococcus thermophilus* thickens its cell wall in response to nisin exposure as

shown by Garde et al.[86] *Staphylococcus aureus (S. aureus)* modifies lipoteichoic acid in the membrane, resulting in higher net positive charge that hinders nisin binding ability.[84] It was reported[87] that in *Clostridium difficile (C. difficile)*, cationic antimicrobial peptides (CAMPs) induce the transcription of the *dlt* operon, which results in the addition of *D*-alanine to teichoic acids of the cell wall by the encoded proteins. This D-alanine addition increases net positive charge on the bacterial cell surface, decreasing electrostatic interactions between CAMPs and their target cells.

Beyond membrane modifications, various bacteria contain two-component systems (TCS) and ABC transporters capable of sensing environmental nisin and subsequently expelling it from the cell. *L. monocytogenes* confers resistance through a complex TCS/ABC transporter system consisting of VirSR TCS/VirAB and the ABC transporter AnrAB.[82] Although VirAB is classified as an ABC transporter, it does not perform the typical function of this family of transporters.[82,88] Instead, it is responsible for sensing antimicrobials and activates the intramembrane-sensing histidine kinase VirS, which phosphorylates response regulator VirR. This response regulator binds to the VirR consensus sequence in the promoter region of *anrAB* and induces the expression of the ABC transporter AnrAB[88] which is responsible the transportation of the antimicrobials out of the cell.[82,84] Similarly, *Staphylococcus aureus* contains a similar highly complex system TCS/ABC transporter system: VraDE-BraSR-BraDE system[89]. This system includes two ABC transporters: BraDE for sensing and signal transduction to BraSR and VraDE for bacitracin and Nisin removal[82,89,90]. BraSR activation leads to BraS-dependent phosphorylation of BraR which activates the *braDE* and *vraDE* operons. [90] Randall et al[91] reported that acquired resistance to Nisin in *S. aureus* is resultant of mutations in BraS (or NsaS) which ultimately leads to higher levels of BraDE/VraDE expression. *Clostridium difficile* utilizes the Cpr (cationic antimicrobial peptide resistance) system to confer resistance to a range of lantibiotics including Nisin. This intricate system is comprised of three core proteins—CprA (a nucleotide-binding domain) and the two transmembrane domains, CprB and CprC—as well as a histidine kinase and a response regulator. [80,84]

Streptococcus agalactiae emplys a unique nisin resistance operon (nsr) encoding an intricate defence system. This operon contains genes for a two-component system, NsrRK, and an ABC-transporter, NsrFP. The system's distinctiveness stems from the inclusion of a gene for a membrane-associated serine protease, designated as the nisin resistance protein (NSR). While nisin is intrinsically resistant to proteolytic cleavage due to lanthionine rings causing steric hindrance within protease active sites, NSR cleaves the peptide at the C-terminus between MeLan28 in ring E and Ser29. This produces a shortened nisin (residues 1-28) with up to 100-fold reduced activity and loses its pore formation efficiency. However, through the mutation of Serine at position 29 to proline resulted in 20x fold decrease in activity against various NSR producing strains while retaining activity against Nisin.[92] These resistance mechanisms pose a threat to the development of nisin and other lantibiotics for therapeutic use.

3.1.5 Challenges with the use of AMPs in clinical settings

While antimicrobial peptides offer great promise as agents to combat multi-drug-resistant bacteria, several innate drawbacks limit their clinical application. Although many AMPs demonstrate broad-spectrum activity and potent efficacy against various pathogens, their activities are often limited to *in vitro* studies, with *in vivo* studies showcasing significantly weaker antimicrobial activity.[93]

This diminished efficacy results from microenvironmental alterations including pH shifts, elevated ionic strength, and the presence of blood components that inhibit AMP activity. Within the bloodstream, proteins like serum albumin bind to peptides, sequestering them and reducing antimicrobial properties. Additionally, AMPs are highly susceptible to proteolytic degradation, and under physiological conditions, their bactericidal activity may be compromised due to loss of electrostatic interactions with cell membranes in saline environments.[56,93]

Clinical translation often fails to meet expectations. For example, Omiganan, a synthetic indolicidin analogue, showed activity against *S. aureus* for treating moderate atopic

dermatitis, but clinical symptoms in patients did not improve.[94] Such conditions make it difficult to accurately predict outcome in clinical settings. Administration strategies are severely limited by these inherent properties. Oral administration is restricted by proteolytic degradation in the digestive tract and poor intestinal mucosa penetration due to high polarity and molecular weight, resulting in low oral bioavailability.[56,69,93,95] Intravenous administration is problematic due to short half-lives from rapid proteolytic degradation, renal and hepatic clearance, and potential systemic toxicity.[69,96] While AMPs generally display low toxicity, hemolytic and cytotoxic effects can occur, potentially triggering chronic inflammatory diseases due to low selectivity. Their cationic nature enables interaction with negative ions on erythrocyte surfaces, causing oligomer formation that destroys cells (hemolytic activity).[97] Despite clinical utility, Polymyxins and vancomycin are frequently associated with nephrotoxicity significantly limiting their application.[98,99] Notably, Polymyxin use is restricted by acute kidney injury (AKI) incidence in 50–60% of patients.[100] Due to these limitations, clinical AMP use is restricted to topical applications, where they remain vulnerable to proteolytic enzyme degradation. Although resistance emergence is less common than with conventional antimicrobials, it remains a noteworthy concern.

Economic barriers further hinder clinical development. Limited manufacturers can produce peptides at commercial scales, resulting in high cost of goods sold (COGS) compared to small molecules. Production costs for peptides (~5000 Da) can be 10-fold higher than small molecules (~500 Da)[96], with costs increasing with peptide length and complexity. Recombinant production technologies require extensive research and development (R&D) phases while restricting modifications[96] that may be circumvented by the incorporation of non-natural amino acid building blocks. Finally, financial viability is burdened by high clinical trial costs and inconsistent *in vitro-in vivo* efficacy correlations.[93]

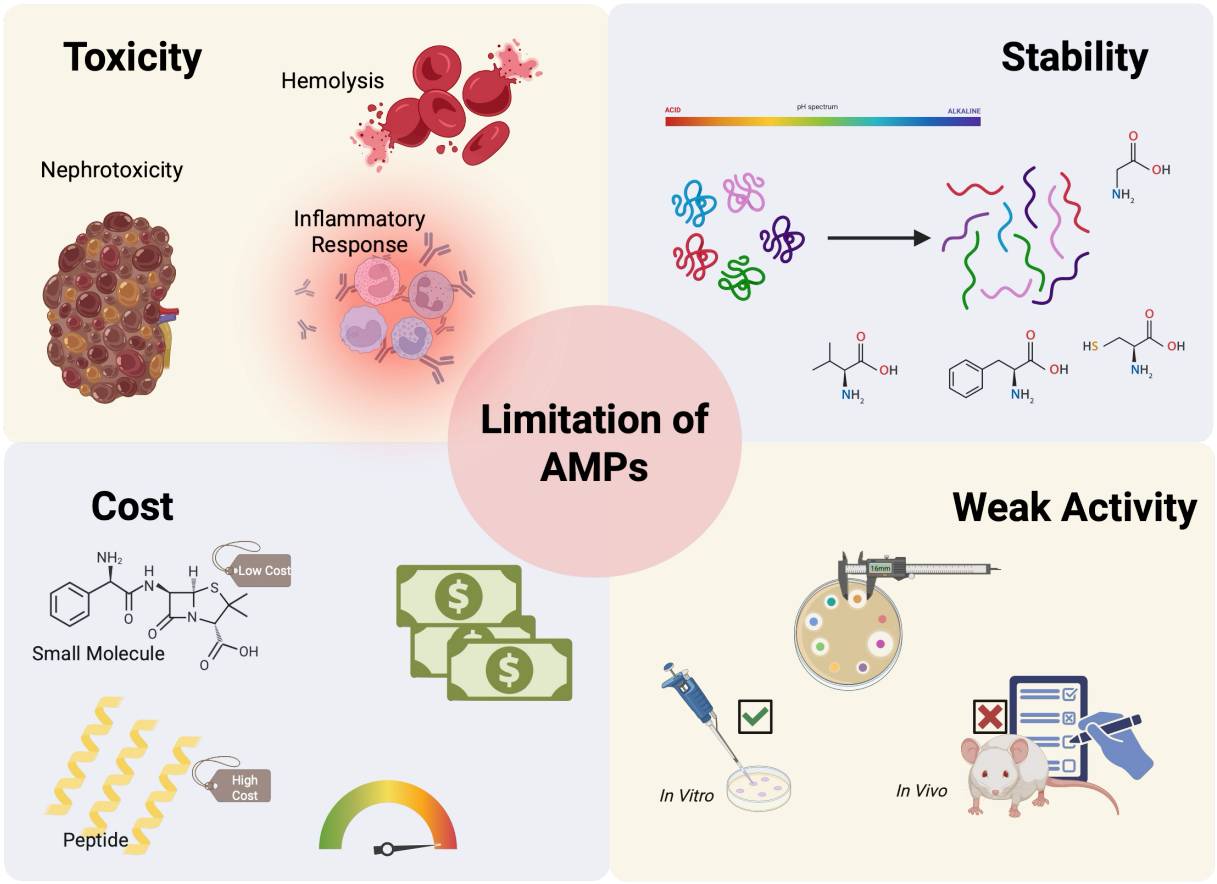


Figure 15. Major limitations associated with antimicrobial peptides (AMPs). Overview of key challenges limiting the clinical translation of AMPs, including toxicity (e.g., hemolysis, nephrotoxicity, and inflammatory responses), poor stability due to proteolytic degradation and environmental conditions, high production cost relative to small-molecule antibiotics, and reduced efficacy *in vivo* despite promising *in vitro* activity. These limitations highlight important barriers that must be addressed to enable the therapeutic development of AMPs. Created with Biorender

3.1.6 Engineering approaches to improve the biocompatibility of AMPs

Multiple strategies have been developed to improve the pharmacokinetic properties, stability, and resistance to proteolytic degradation of antimicrobial peptides, thereby enhancing their viability as agents for tackling multi-drug resistance. These strategies include chemical modifications, drug conjugates, nanocarriers, and modifications introduced using genetic code expansion.

3.1.0.9 Chemical Modifications

Chemical modifications such as terminal acetylation/amidation, cyclization, peptidomimetics, and D-amino acid substitution are widely employed to enhance peptide

stability, reduce proteolytic degradation, and minimize toxicity.[56,70,93] D-amino acid substitution improves resistance to endogenous proteases and decreases immune recognition, thereby enhancing biocompatibility and *in vivo* stability while often broadening antibacterial activity against Gram-positive bacteria.[56] For example, BMAP28, a bovine myeloid peptide, when modified to D-BMAP28 through L-to-D amino acid replacement, effectively preserved both antimicrobial and immunomodulatory properties.[101] Similarly, substitution of cationic residues with L-ornithine improves proteolytic resistance, with poly-L-ornithine peptides exhibiting potent antimicrobial and anti-biofilm activities against *Pseudomonas aeruginosa (P. aeruginosa)*.[102] Hydrophobicity strongly influences AMP toxicity; substituting highly hydrophobic residues such as tryptophan and phenylalanine with less hydrophobic amino acids reduces hemolytic activity.[93] Conversely, terminal tagging with tryptophan or β-naphthylalanine improves salt and serum stability.

Cyclization strategies, including disulfide bonding, head-to-tail cyclization, and side-chain cross-linking, increase serum stability, reduce hemolysis, and limit protease accessibility through steric hindrance.[56,70,93,102] Branched antimicrobial peptides, such as multiple-antigen peptides (MAPs), similarly enhance resistance to plasma and serum proteases, extending peptide half-life.[99] Terminal modifications further enhance peptide performance. C-terminal amidation increases structural stability and antimicrobial activity, while N-terminal acetylation[70] increases helicity, preventing enzyme degradation[103] and protecting against aminopeptidases[70,93] activity. However, N-acetylation removes the positive charge on the peptide N-terminus, potentially reducing membrane binding due to weaker electrostatic interactions with negatively charged lipid head groups.[93] Strategies such as polyethylene glycol (PEG) attachment (PEGylation) and lipidation improve peptide biocompatibility and pharmacokinetic properties. PEG attachment improves solubility and peptide flexibility while retaining PEG's non-toxic and non-immunogenic properties.[99] Lipidation involves attaching fatty acid chains to N-terminal amines or lysine residues [99,104], increasing hydrophobicity, membrane interaction, and proteolytic resistance, although excessive hydrophobicity may increase toxicity.[99]

Peptidomimetics represent an effective approach for improving peptide stability, bioavailability, and permeability. Peptoids, where side chains attach to backbone nitrogen rather than α-carbon, exhibit strong resistance to proteolytic degradation, with cyclization further enhancing stability.[56]

3.1.0.10 Nanocarriers

Delivery systems have been extensively explored to improve stability, reduce toxicity, and extend antimicrobial peptide half-life.[93] These platforms include inorganic materials, polymers, and surfactant- or lipid-based carriers. Inorganic nanocarriers such as titanium, quantum dots, mesoporous silica, graphene, and carbon-based materials offer advantages through large surface areas for AMP absorption and prevention of peptide self-aggregation.

Gold nanoparticles are highly biocompatible and improve therapeutic efficacy through controlled release kinetics, enhancing metabolic and chemical stability.[99] Gold-aptamer conjugated nanoparticles effectively deliver AMPs to bacterial cells, while silver nanoparticles enhance delivery to fungal cells.[105] Mesoporous nanoparticles provide well-defined pore structures allowing efficient peptide encapsulation.[96] Nisin conjugation to graphene oxide nanotubes enhances antimicrobial activity against methicillin-resistant *Staphylococcus aureus* (MRSA).[106]

Lipid and surfactant-based systems, including micelles and liposomes, improve physical and chemical stability, prolong circulation time, enhance biocompatibility, and reduce toxicity to healthy cells[103,105] while enabling targeted delivery to infection sites.[105] For instance, nisin encapsulation within 1,2-distearoyl-sn-glycero-3-phosphocholine (DSPC)/1,2-distearoyl-sn-glycero-3-phospho-(1'-rac-glycerol) (DSPG) liposomes protects the peptide under extreme pH and temperature conditions.[56,107] Polymer-based systems including chitosan, dextran, polyethylene glycol (PEG), and poly(lactide-co-glycolic acid) (PLGA) are extensively used due to tunable physiochemical properties and biomedical application versatility.[103] Self-assembling AMPs can form liposome-like nanostructures improving stability and enzymatic degradation resistance.[103]

3.1.0.11 Combination Therapies

The development of drug conjugates and combination therapies has further enhanced the pharmaceutical potential and bioactivity of AMPs. One effective approach involves creating hybrid peptides by combining two distinct AMPs, often resulting in improved antimicrobial potency and reduced cytotoxicity. For example, the BMAP-27/OP-145 hybrid demonstrated broad-spectrum activity against multidrug-resistant bacteria with reduced toxicity to eukaryotic cells[108], while the PA2–GNU7 hybrid displayed enhanced activity against *P. aeruginosa*.[109] The combination of AMPs with conventional antibiotics has shown significant clinical potential by overcoming antibiotic resistance limitations.[103] For instance, combining colistin with salicylamine improves treatment efficacy against multidrug-resistant (MDR) Gram-negative bacteria by enhancing membrane permeability. Additionally, combinations of the tetracycline antibiotic demeclocycline hydrochloride (DMCT) and the AMP SAAP-148 show utility against MDR *Pseudomonas aeruginosa* PAO1 and *P. aeruginosa* American Type Culture Collection (ATCC) 27853.[93] Drug combinations with polymyxins, such as with carbapenems or rifampicin, suppress polymyxin resistance development. The combination of polymyxin with gramicidin and neomycin seen in Neosporin® reduces resistance development and cytotoxic effects.[110]

AMP conjugation with other molecules can enhance stability, selectivity, and antimicrobial activity. Peptides can be linked to membrane-binding or cell-penetrating peptides to improve activity against Gram-negative bacteria, or conjugated with molecules such as fatty acids, anticancer drugs, antibodies, and photosensitizers to introduce new functional properties. Notably, photosensitizer conjugates eliminate resistant bacteria through reactive oxygen species generation upon light activation, while antibody conjugates provide target selectivity, minimizing off-target and cytotoxic effects.[103]

3.1.0.12 Bioengineering Nisin variants

While the modifications above address lanthipeptide incompatibility with biological systems, bioengineering offers additional modification scope. Mutagenesis of various amino acids in nisin has expanded the existing variant pool, with several notable examples.

At the N-terminus, replacing isoleucine at position 1 with aromatic amino acids such as tryptophan and phenylalanine resulted in greater antimicrobial activity but may interfere with nisin protease cleavage.[111] The first two rings (A and B) are crucial for Lipid II interactions, with early mutagenesis attempts (S3T) dramatically reducing activity. However, less drastic changes such as I4V increased antimicrobial and anti-biofilm activity against *Staphylococcus pseudintermedius* and showed activity against *S. aureus* when used with antibiotics.[112] Ring B variants are less likely to increase activity and generally do not produce effective mutants. A promising ring C variant, nisin M17Q, demonstrated high efficacy against *Staphylococcus epidermidis* biofilm formation, outperforming wild-type Nisin.[111] The hinge region, a 3-amino acid linker crucial for conformational flexibility and pore formation activity,[111] shows direct activity relationship with length mutations. Shortening the hinge by one amino acid sharply decreased activity, while extending it by two amino acids improved efficacy against many target strains, particularly indicator strains with thicker membranes.[113] Mutations to C-terminal rings (D and E) and the C-terminal tail have been investigated. Nisin mutants lacking rings D and E or just ring E show higher resistance to cleavage by nisin resistance protease, highlighting these rings' importance for protease recognition.[114] Later studies confirmed that C-terminal rings coordinate enzyme to the cleavage point (Ser29)[115] and ensures substrate specificity. Mutational studies revealed S29P and C28P mutations retained decent antimicrobial activity while inhibiting resistance protease cleavage.[111,115]

Another strategy involves creating hybrid peptides to increase nisin's potency or broaden its activity spectrum. One study synthesized a hybrid peptide featuring two Lipid II binding motifs, constructed using nisin's N-terminal segment (amino acids 1–22) and haloduracin's C-terminal segment. One peptide (TL19) showed 64-fold higher activity against *Enterococcus faecium*, though pore-forming activity was diminished.[116] Other studies found that conjugating this nisin fragment (amino acids 1–22) with small insect defense peptide variants produced molecules with substantial activity against Gram-negative pathogens and increased resistance to nisin resistance proteins.[116] Oncocin conjugation to nisin's C-terminal tail increases nisin's ability to penetrate Gram-negative bacterial outer membranes.

An alternative strategy for outer membrane disruption involves using ethylenediaminetetraacetic acid (EDTA) in combination with the therapeutic agent.[111]

To improve peptide stability, nisin-peptoid hybrids containing the nisin Lipid II targeting domain show increased *in vivo* stability, increased chemical diversity, and considerable activity against resistant strains like MRSA.[117]

3.1.0.13 Genetic Code Expansion as an Enabling Platform

In addition to mutagenesis and diverse post-translational modifications already present in lantibiotics, genetic code expansion (GCE) can further expand the toolbox by enabling site-specific incorporation of chemical handles that facilitate directed, orthogonal modifications and conjugation. Through non-canonical amino acid (ncAA) introduction, chemical diversity scope increases as moieties such as azides, alkynes, olefins, and hydrazones can be inserted. The insertion of ncAAs such as azidohomoalanine and homopropargylglycine enables copper(I)-catalyzed azide-alkyne cycloaddition for chemical modifications. These reactions are uniquely bioorthogonal as they do not interfere with biological processes and can be conducted under mild conditions, with examples in mammalian systems.

Various methods can be used for ncAA incorporation. The simplest is selective pressure incorporation (SPI), which utilizes auxotrophic microbial strains and natural promiscuity of cognate aminoacyl-tRNA synthetases (aaRS).[9,118] The auxotrophic strain is grown in minimal media depleted of the amino acid being replaced. The non-canonical amino acid is incorporated in place of the canonical amino acid by natural aaRS in a residue-specific manner. For example, azidohomoalanine and homopropargylglycine incorporation utilizes methionine auxotrophic strains, with these amino acids incorporated by cognate methionyl-tRNA synthetase (MetRS). A downside is that the non-canonical amino acid incorporates into all residues of the replaced amino acid and is limited to isosteric analogs.

To circumvent these limitations, stop-codon suppression has proven useful. Crucial to this method is introducing in-frame stop codons at target locations within the peptide or protein through mutagenesis where the ncAA will be introduced. These engineered stop codons are

read by specified orthogonal aminoacyl-tRNA-synthetase:tRNA pairs (o-pairs) that can be engineered to incorporate a large repertoire of non-canonical amino acids. Commonly used pairs are based on *Methanocaldococcus jannaschii* tyrosyl-tRNA synthetase (MjTyrRS) and *Methanosarcina mazei/barkeri* pyrrolysyl-tRNA synthetases (MmPylRS or MbPylRS).[118] This method has downsides including low expression yields and early termination of protein synthesis due to stop codons.

Using such methods for ncAA incorporation, nisin properties such as stability, specificity, half-life, and bioavailability can be significantly improved. Through clickable amino acid introduction into nisin, various drug conjugates can be produced to increase activity against Gram-negative bacteria. Literature provides examples of successful conjugation reactions where an azide-containing N-terminal nisin fragment (amino acids 1–12) was combined with an alkyne-containing vancomycin derivative, resulting in a hybrid molecule with significantly higher activity than the starting compounds.[116]

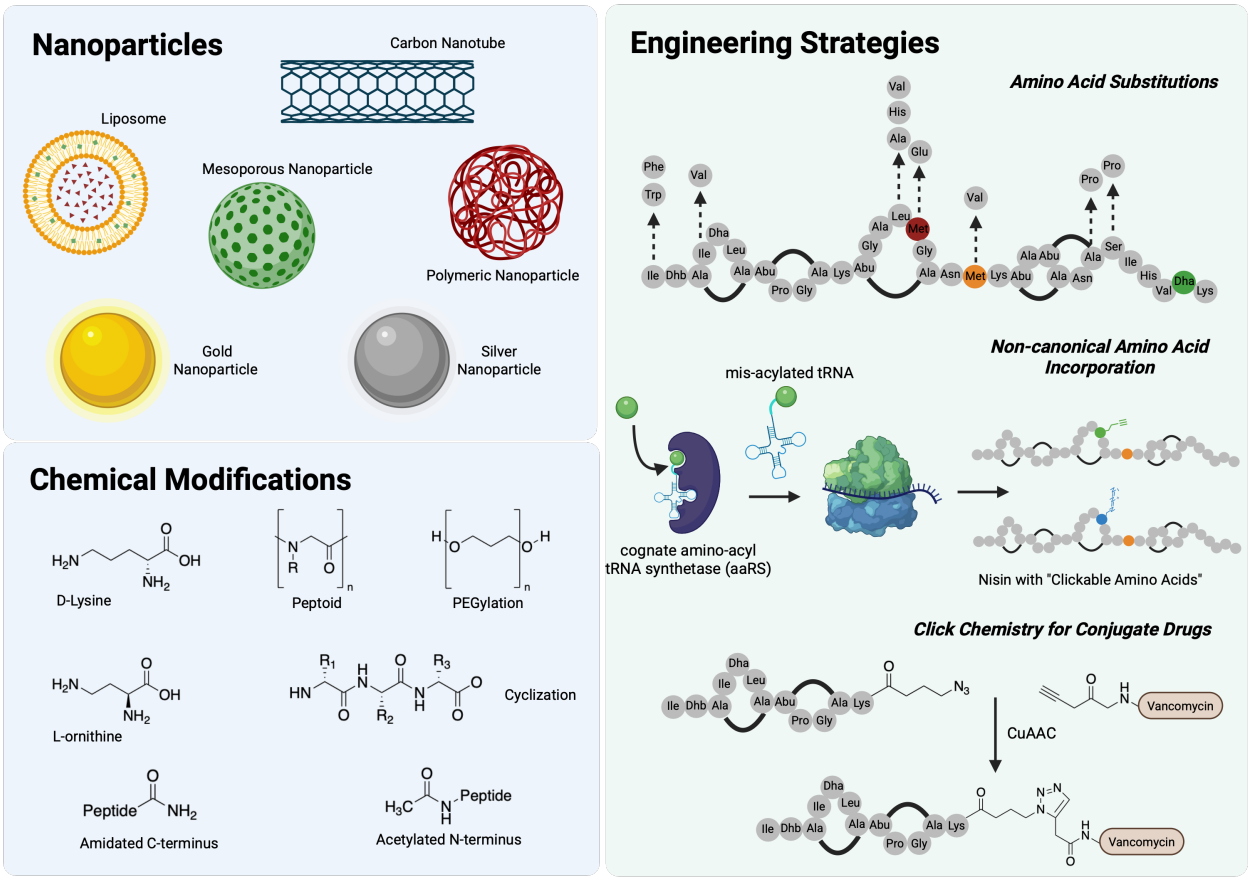


Figure 16. Strategies to enhance antimicrobial peptide (AMP) stability, activity, and delivery. Overview of approaches used to improve the therapeutic potential of AMPs, including nanoparticle-based delivery systems (e.g., liposomes, mesoporous, polymeric, carbon nanotube, and metallic nanoparticles), chemical modifications (e.g., D-amino acid substitution, PEGylation, cyclization, and terminal modifications), and protein engineering strategies such as amino acid substitutions and incorporation of non-canonical amino acids. Bioorthogonal click chemistry further enables the conjugation of AMPs to other therapeutics to generate hybrid molecules with enhanced pharmacological properties. Created with Biorender

3.2 Results and Discussion

3.2.1 Establishment of Nisin wildtype core peptide production in *E. coli*

3.2.1.1 Rationale for Heterologous Expression in E. coli

The expression of Nisin in literature and in industry is mainly conducted in its host organism; *Lactococcus lactis*. However, for the purposes of our experiments, optimizing the expression of Nisin in *E. coli* would be useful for numerous reasons. Expression in the native host is not cost-effective due to the fastidious nature of *Lactococcus lactis* thus requiring complex growth requirements. Due to this, its expression media is highly expensive, especially in large scale productions. Using a recombinant expression system with *E. coli* offers a more cost-effective option and is highly tunable for any requirements. A wide variety of *E. coli* strains for multiple purposes are available and due to the extensive study of its genome, it is easy to genetically manipulate.

3.2.1.2 Design of Recombinant Expression System

In general, many proteins can be expressed in this host with high expression levels in soluble form. Furthermore, the selective pressure incorporation method and the stop codon suppression method have been established in *E. coli*, bypassing the need for engineering to make the organism suitable for such needs. The expression of lanthipeptides in *E coli* has been previously established in literature[119] and by previous lab members. The Nisin biosynthesis cassette contains over 10 genes, but only three are essential for expression within *Escherichia coli*. These include the *nisA* gene, which encodes the Nisin precursor peptide, and the *nisBC* genes, which express the essential modification machinery for dehydration and cyclization. The Nisin expression plasmid (pET-3a_NisA) with ampicillin (Amp) resistance and the modification machinery plasmid (pRSFDuet-1_NisBC) with kanamycin (Kan) resistance were obtained from Dr. Nediljko Budisa's Lab in Berlin. The Nisin gene N-terminus was previously modified to contain a His6-tag and a small linker

(MGSSHHHHHH) for easier purification. The expression of Nisin was confirmed using both ESI-MS and antimicrobial assays.

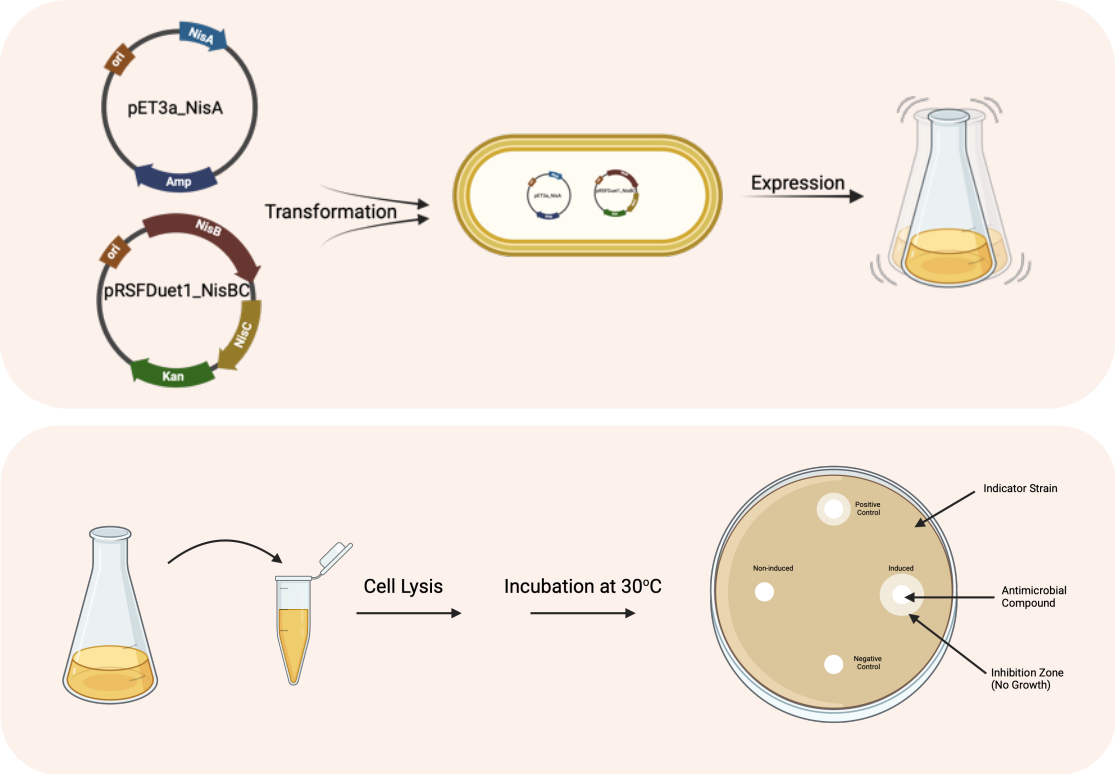


Figure 17. Scheme of the Nisin Expression system and antimicrobial susceptibility assay for confirmation of Nisin expression in bacterial strain. Top: To express the PreNisin peptide, the plasmids pET3a_NisA (for precursor Nisin) and for the modification enzymes; NisB (dehydratase) with NisC(cyclase) are co-transformed into E. coli BL21 and expressed in a rich medium. Bottom: After overnight expression, 1 ml of the culture is pelleted, normalized relative to cell density and lysed. These cell samples are added to wells on an agar plate containing L. lactis NZ9000 (with pNGnisPT plasmid for Nisin protease expression). After diffusion, the plate is incubated overnight at 30°C. Growth inhibition zones will then become visible, indicating the presence of Nisin's antimicrobial activity. Created with Biorender

3.2.1.3 Optimization of PreNisin Expression Conditions

The established antimicrobial assays provided a robust and reliable methodology for the preliminary verification of Nisin production. Building upon established agar diffusion assays, this method was developed as a simple but effective tool for assessing antimicrobial activity during later experimental stages. The assay involves introducing the antimicrobial compounds into wells on an agar plate and incubating them overnight at the required

temperature. The following day, if an antimicrobial compound is present, then inhibition zones are observed (areas where no bacterial cell growth is present). While this assay is only qualitative and does not provide a minimum inhibitory concentration, it is useful for determining nisin expression and comparing expression levels in various conditions. This can be done by measuring the size of the halos with fixed concentrations or conditions. For conducting these assays, a special indicator strain; the gram-positive *L. lactis* NZ9000 (pNGNisPT), was obtained from the Dr. Oscar Kuipers lab. While *Lactococcus lactis* has innate immunity to Nisin, this strain is Nisin-sensitive due to the removal of the immunity genes (*nisIFEG*). In addition, this strain contains the pNGNisPT plasmid that encodes the Nisin transporter and protease that is secreted by the cell and anchored to the membrane. The Nisin protease can cleave the leader peptide from PreNisin to produce the fully active peptide with antimicrobial activity. Since protease is already present, PreNisin samples can be measured without further processing. These aspects make this strain quite useful for testing Nisin expression in our samples.

Briefly, for these assays, an overnight culture of *L. lactis* NZ9000 pNGNisPT (OD_{600} = 0.6) is mixed with GM17 media (M17 media supplemented with glucose) containing an agar concentration of 0.7%. Once the agar hardens, wells are created with the larger end of a sterilized Pasteur pipette, and samples are added to each well. The use of soft agar facilitates the easy diffusion of the strain and sample. The plasmid (pNGNisPT) in this strain requires 5 µg/ml chloramphenicol (cm) which is added prior to the media being poured into the plate. Since this strain is relatively sensitive to higher concentrations of chloramphenicol, a positive control concentration of 400 µg/ml Cm is used. The sample buffer serves as the negative control in these experiments. For initial tests for Nisin wildtype expression, the NisA and NisBC plasmids were transformed into KCM component BL21 (DE3) cells. To achieve the best expression conditions, various media and expression times were tested. Expression was carried out in Luria Bertani (LB) medium and the autoinduction ZYP-5052 medium, where induction with isopropyl-b-D-thiogalactoside (IPTG) is not required. In addition, expression times of 6 hours and overnight were tested simultaneously. Briefly, an overnight culture of BL21 (with pET3a_NisA and pRSFDuet-1

NisBC) is inoculated into either LB or ZYP-5052 media. After the culture reaches an OD_{600} = 0.8-1.2, the LB media was induced with 1mM IPTG and incubated at 28°C for expression. Samples of 1 ml were collected from each media prior to induction, 6 hours after induction and after overnight induction. These samples were centrifuged at high speeds and kept at -20°C until required for antimicrobial assays. For conducting the assays, the samples were all normalized to OD_{600} = 1, lysed with lysis buffer (See

Buffers) and assays were carried out according to protocols in section **Material and Methods.**

3.2.1.4 Functional Verification by Antimicrobial Assays

Based on the results (**Appendix Figure 1)** the highest expression was seen in the LB medium at 6 hours after induction, while in the ZYP-5052 medium, it was observed after overnight incubation. A reduction in peptide expression was observed following overnight incubation in LB media, which may be attributed to degradation of the peptide. The optimal Nisin expression occurred in ZYP-5052; therefore, this medium was selected for all subsequent wild-type and mutant expression studies. Development of a Nisin purification strategy was necessary for subsequent experiments, such as verifying leader peptide cleavage and the incorporation of non-canonical amino acids. In previous work, the peptide was partially purified, but for downstream applications, a high purity of Nisin is required. For such purposes, purifications protocols were estabiashed using the wild-type Nisin. Initial purification was conducted using Ni^{2+}-immobilized metal-ion affinity chromatography (IMAC) as described in **Materials and Methods**. After protein expression, the pelleted cells were resuspended in lysis buffer and subject to sonication. After a centrifugation step, the lysate was loaded onto the column for purification. (**Materials and Methods**) For initial analysis purposes, 1 ml fractions were collected using the elution step to track Nisin elution. These fractions were analyzed via a Tricine Sodium dodecyl sulfate–polyacrylamide gel electrophoresis (SDS-PAGE) gel and antimicrobial assays in parallel. The antimicrobial assays showcase (**Figure 18**) elution of Nisin well after elution fraction 11. On the Tricine-

SDS-PAGE gel, a band at ~10kDa corresponds the Nisin precursor peptide. Due to the semi-circular nature of Nisin, the peptide may travel slower than expected on the SDS-PAGE gel. Even with only very faint Nisin bands visible on the gel for fractions 1 and 11+, the antimicrobial assays successfully confirmed Nisin's presence. This demonstrates the high sensitivity of the assay for determining Nisin in samples. Furthermore, based on the IMAC fractions seen on the gel, there are still may other proteins present thus further purification steps are required.

3.2.1.5 Development of a Multistep Purification Strategy for PreNisin

Downstream protein purification strategies include ion exchange chromatography and size exclusion chromatography. Ion exchange (IEX) chromatography separates proteins based on their net charge using a charged resin that binds the protein. Proteins are eluted from the

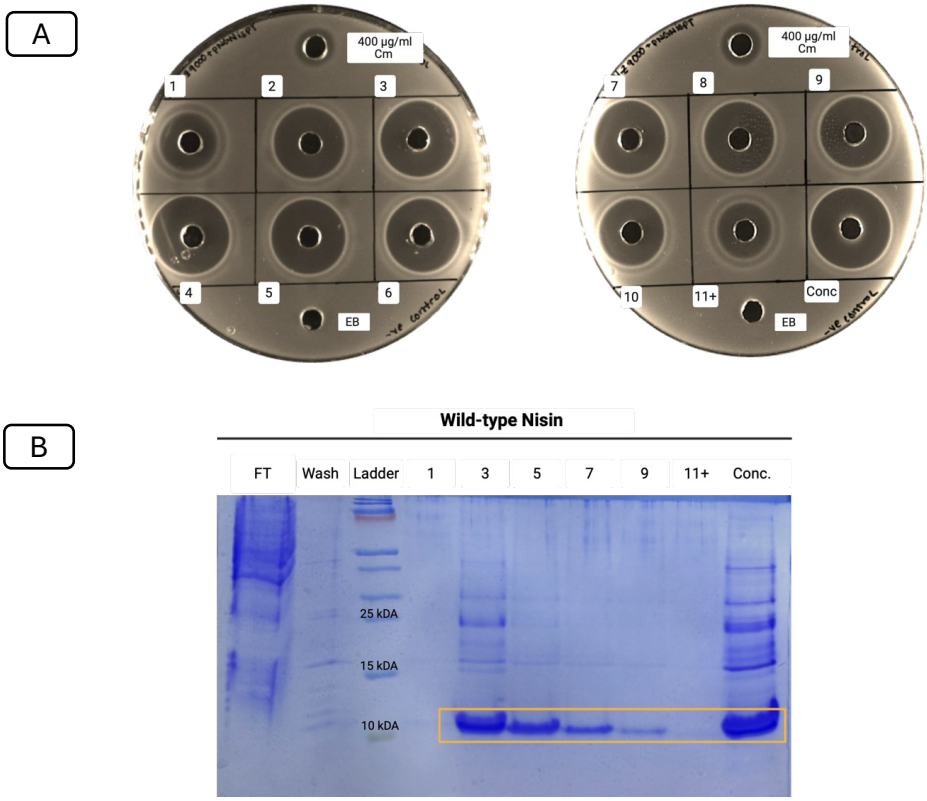


Figure 18. Antimicrobial Assays and Tricine-SDS-PAGE of purified PreNisin after recombinant expression in *E. coli*. (A) Antimicrobial activity of IMAC elution fractions 1-11+ against indicator strain. Chloramphenicol (400 µg/mL) served as positive control. Conc: Fractions after protein concentration, EB: elution buffer. **(B)** Tricine SDS-PAGE gel showcasing PreNisin IMAC elution fractions (indicated with numbers), flow-through (FT) and wash fractions. Boxed in yellow indicate PreNisin bands at expected molecular weight of 7299 Da. Ladder: PageRuler™ Prestained Protein Ladder, 10 to 180 kDa.

resin by either increasing the ionic strength of the buffer or altering the pH. These changes alter the interactions between the proteins and the resin, causing the protein to be released. The two common types of resin are anion exchange, which contains a positive charge and binds negatively charged proteins, and cation exchange, which contains a negative charge and binds positively charged proteins. Based on the overall charge of ~ +7.0 of the Nisin precursor peptide at pH=6.0, a cation exchange column was selected. Previously published protocols[120] were adapted and modified to purify using this method. Protein preparation included pooling IMAC purified fractions and concentration using an Amicon device followed by stepwise dialysis into the ion exchange start buffer. The samples were loaded onto the column and purified using a gradient with increasing salt concentration. While purification with ion exchange chromatography aided to further purify the protein, many impurities were still present in the sample (**Appendix Figure 2**). Based on the chromatograph, PreNisin elutes at ~300mM NaCl concentration and the antimicrobial assay results prove that PreNisin is not lost during the purification process. Interestingly, fraction F5 contains high antimicrobial activity while on the gel, the Nisin band at ~10kDa is not detected. The band at ~ 15kDa may corresponds to Nisin and may be a partially modified form (with fewer dehydrations events) causing it to migrate differently on the gel.

Purification with ion exchange chromatography left many impurities in the sample thus size exclusion chromatography (SEC) was explored as an option. This method separates proteins based on their molecular weight. Various resins exist on the market, each with different pore sizes and compositions. These resins contain small pores that allow smaller molecular weight proteins to enter and spend more time within the column. As a result, with size exclusion chromatography, larger proteins (which bypass the pores) are eluted first, followed by smaller molecular weight proteins that elute towards the end. In this method, the protein preparation involves concentrating the sample to very low volumes (<1 ml) and then loading it directly onto the column. The column acts as a means for buffer exchange thus proving

quite useful for PreNisin purification. The sample purified using SEC was much higher in purity compared to the IEX fractions.

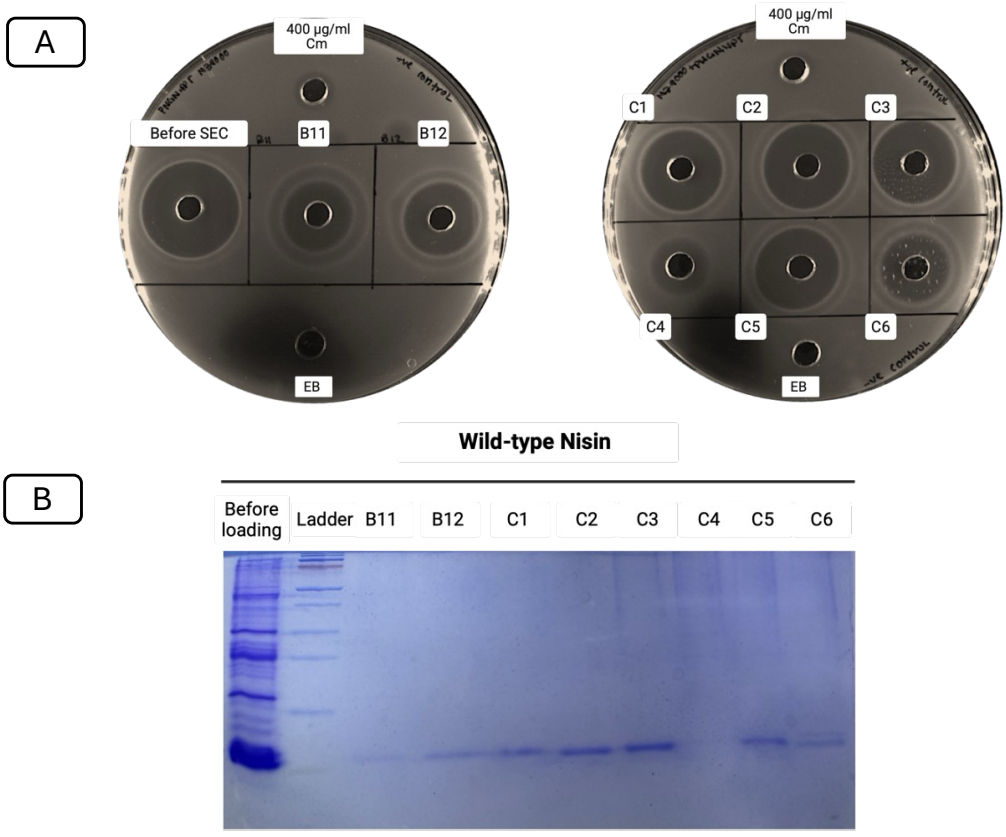


Figure 19. Antimicrobial Assays and Tricine-SDS-PAGE of PreNisin purified with size exclusion chromatography (A) Antimicrobial susceptibility assay of SEC elution fractions B11-C6 of wild-type PreNisin. Purification was carried out in 50mM Phosphate, 300mM NaCl, pH 7.5. 400 µg/mL Cm served positive antimicrobial control compound. Before SEC: Loaded sample prior to run, EB: elution buffer. **(B)** Tricine SDS-PAGE gel showcasing PreNisin SEC elution fractions (indicated with 96 well plate numbers). PreNisin bands present at expected molecular weight of 7299 Da. Ladder: PageRuler™ Prestained Protein Ladder, 10 to 180 kDa.

3.2.1.6 Quantification and Sample Preparation Strategies

Highly purified proteins samples enable concertation determination and mass spectrometry analysis. Conventionally, protein concentration is typically measured using either spectroscopic methods or a colorimetric assay. Spectroscopically, the concentration is determined using Beer's Law and the protein's unique extinction coefficient (ϵ) and by measuring the absorbance at 280 nm. Alternatively, colorimetric assays, such as Bradford and Bicinchoninic acid (BCA) assay, can aid to determine the concentration. However, since

PreNisin lacks tryptophan residues and doesn't react well with the Bradford reagent, these methods are ineffective for determining its concentration. The BCA assay, however, produces a signal in the presence of PreNisin, making it the assay of choice. This assay works by the protein reducing copper (II) to copper (I) and the reduced copper forms a purple complex with the BCA reagent with measurements are taken at 562 nm. It is a highly sensitive assay which allows for the measurement of low protein concentrations. PreNisin contains a limited number of peptide bonds that react with copper, so an enhanced protocol with a working range of 5 to 250 µg/ml was used. To determine the unknown Nisin concentration, a calibration curve was first created using Bovine Serum Albumin (BSA). While this assay was useful for determining PreNisin concentration, large samples volumes were required and due to the complexation with copper, the sample could not be recovered. An alternative option was quantifying PreNisin production by measuring peptide weight. This option and downstream application such as HPLC or MS analysis, require the buffer and interfering salts to be removed from the peptide sample. Dialysis is typically used, but this option becomes unviable once the peptide is cleaved in later steps. In literature, trichloroacetic acid (TCA) precipitation is routinely used to precipitate nisin from the media solution, removing any interfering compounds. This method was therefore explored to not only remove interfering substances but also to produce a Nisin powder that could be weighed. The TCA precipitates proteins by disrupting the hydrogen bonds holding water molecules around them, causing them to become insoluble and precipitate out of solution. While there are multiple published procedures, the final optimized procedure is shown in **Figure 20**. The peptide is precipitated with TCA, and the resulting protein pellet is washed multiple times with ice-cold acetone to remove TCA and any further contaminants. First, the method was tested with a Nisin standard obtained from Sigma. After precipitation, the peptide was redissolved in buffer, and an antimicrobial assay was used to determine the retention of Nisin's antimicrobial activity. The method is outlined in **Figure 20** (and detailed in **Materials and Methods**)where the redissolved sample is subsequently diluted across each well in GM17 media. The Nisin-sensitive bacteria were added to wells and incubated overnight at 30^{O}C with minimal shaking. The optical density was measured the following day using a plate

reader. This method also allows for the approximate determination of Nisin concentration when compared to commercially purchased Nisin control samples. This method is used after the cleavage of the leader peptide, as discussed in the following section. PreNisin samples rely on the protease produced by the indicator *L. lactis* strain, whose processing may not be effective in this experimental set up.

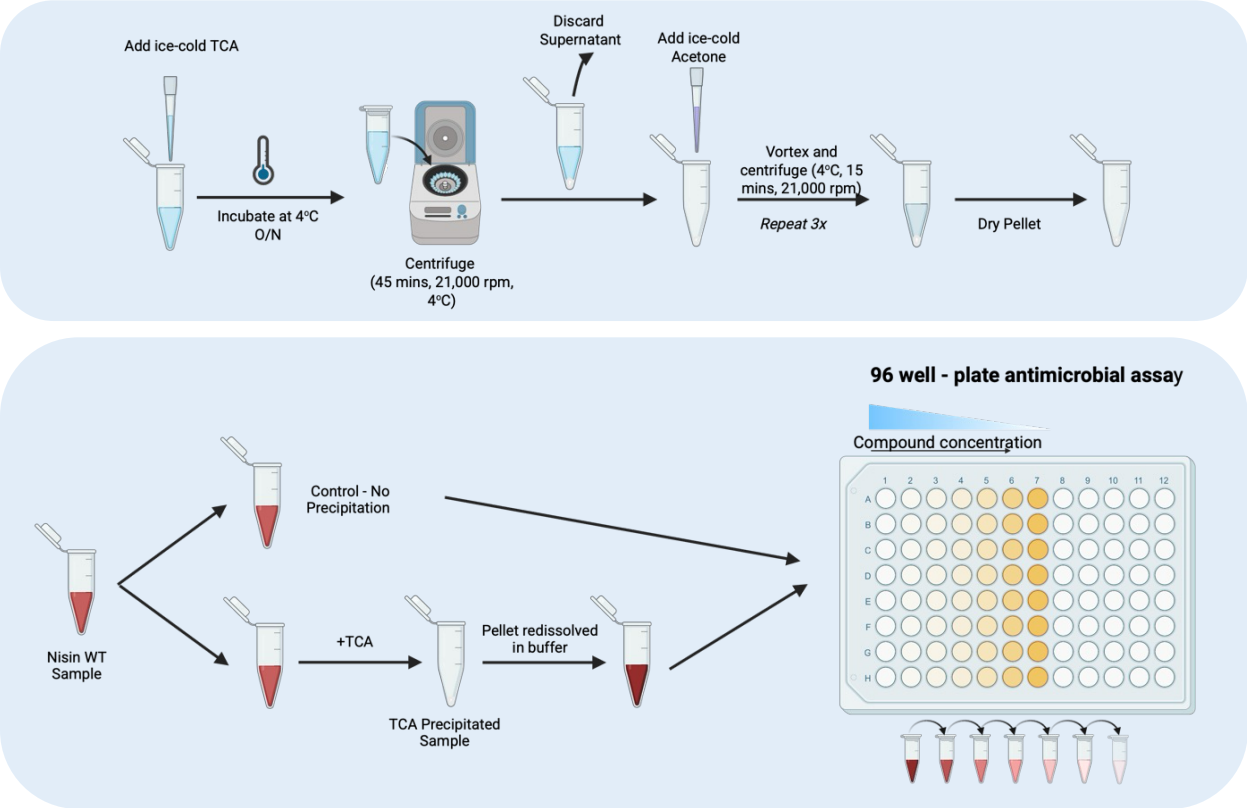


Figure 20. Scheme of the Trichloroacetic Acid Precipitation Method and 96-well plate Antimicrobial Assay. Top: Scheme outlining the TCA precipitation method for proteins. The protein is precipitated with ice-cold TCA overnight. The resulting pellet is washed multiple times with ice-cold acetone to remove residual TCA and dried for acetone removal. **Bottom:** Scheme showcasing determination of antimicrobial activity of TCA-precipitated peptides. The samples are redissolved in buffer and diluted across a 96-well plate containing GM17 media and the *Lactococcus lactis* indicator strain NZ9000. Plate is incubated at 30°C overnight with minimal shaking and optical density measured with a plate reader the following day. Created with Biorender

To test the protocol's efficiency, recombinantly produced Nisin samples were precipitated in either 10% or 20% TCA, as these concentrations are commonly used in literature. During each test, a commercially purchased Nisin sample was run as a positive control for antimicrobial activity. Each run also included a bacterial growth control (without any

antimicrobial compound) and a sterility control (containing only GM17 media with no bacterial inoculation). The bacterial growth control grew to an approximate optical density of 0.89 while the sterility control had no growth in comparison. (**Figure 21**) The commercial nisin control product demonstrated growth inhibition until a concentration of 0.7 µg/ml. A slight growth was observed in the 0.35 µg/ml well. When comparing the samples precipitated with 10% or 20% TCA, we observed similar levels of efficiency. Both treatments showed growth in sample 3 for the control sample (non-TCA-treated Nisin). Since the TCA-treated Nisin sample was twice as concentrated as the non-treated control sample, and the wells are two times diluted across, we observe the growth of the control Nisin sample in one well earlier. These results demonstrate that Nisin activity is preserved after treatment with trichloroacetic acid, making this method effective for removing buffer and salt impurities.

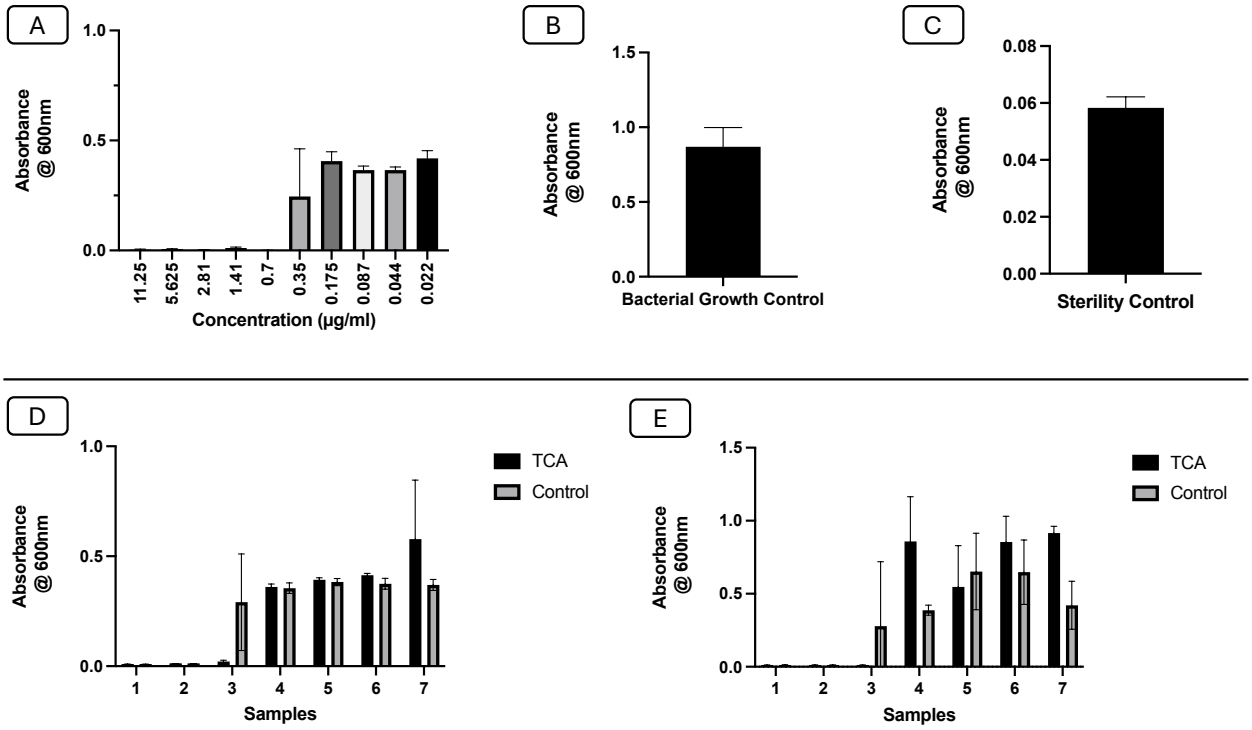


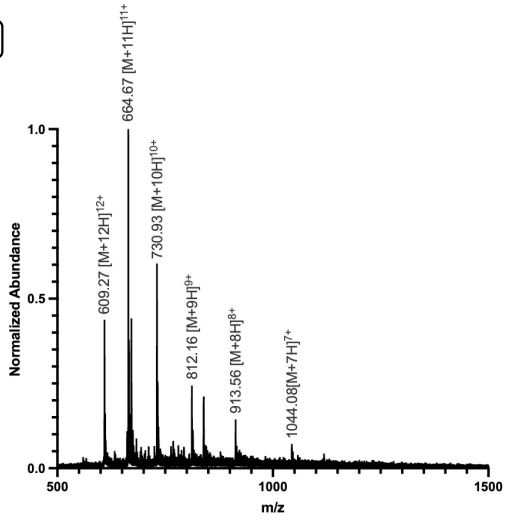
Figure 21. Antimicrobial activity retention testing of trichloroacetic acid precipitated Nisin WT and the Nisin standard. The TCA-precipitated samples were diluted 2x across the wells in GM17 media. Lactococcus lactis strain NZ9000 was normalized to OD_{600}=0.125 and added to each well. The 96-well plate was incubated at 30C with minimal shaking overnight. The OD600 measurements of the plate were taken with a Tecan plate reader instrument. **(A)** Nisin Standard purchased from Sigma was made to as listed on the x-axis and serially diluted across the wells (n=2). **(B)** Bacterial Growth Control containing only *L. lactis* NZ900 strain with no antimicrobial compound. **(C)** Sterility control containing only GM17 media with no bacterial inoculation. **(D)** Bacterial growth inhibition comparison of 10% TCA precipitated sample with Nisin control sample (n=3). **(E)** Comparison of bacterial growth inhibition of the Nisin Control and 20% TCA precipitated sample (n=3).

After treating the samples with TCA, any buffer or salt impurities were removed, allowing for further analysis. Additionally, PreNisin could be purified by removing interfering substances using the chloroform-methanol precipitation method.[121] These methods were used interchangeably especially in the case of the non-cleaved peptide.

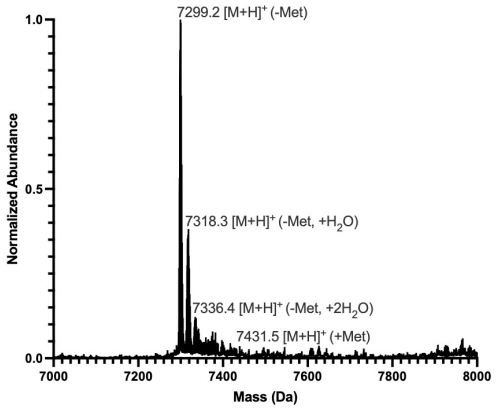
3.2.1.7 Structural Validation by Mass Spectrometry

To determine the correct formation of lanthionine bridges and complete dehydration of the appropriate residues, mass analysis was conducted for the samples. Since the dehydration of serine and threonine results in the loss of a water molecule for each event, the mass difference is easily observed using mass spectrometry. In total, complete modification results in the loss of 8 total water molecules (-18.001 Da for each water molecule).

A



B



C

Species	Expected	Observed
Nisin (+Met)	7431.56	7431.5
Nisin (- Met)	7300.52	7299.2

D

MGSSHHHHHHSQDPMSTKDFNLDLVSVSKKDSGASPR*ITSISLCTPGCKTGALMGCNMKTATCHCSIHVSK(Stop) Nisin (+ Met)

GSSHHHHHHSQDPMSTKDFNLDLVSVSKKDSGASPR*ITSISLCTPGCKTGALMGCNMKTATCHCSIHVSK(Stop) Nisin (- Met)

Figure 22. ESI-MS spectrum of purified wildtype PreNisin recombinantly produced in *E. coli*. (A) MS chromatogram of wildtype PreNisin showcasing fragmentation pattern for 7299.2 Da peak **(B)** Deconvoluted ESI-MS Spectrum of wildtype Nisin showcasing various dehydrated variants. The calculated masses for wildtype PreNisin (-Met) was $[M_{calc}+H]^+$ = 7300.52 Da, $[M_{calc}+H]^+ + H_2O$ = 7318.53 Da, $[M_{calc}+H]^+ + 2H_2O$= 7336.54 Da and the observed mass $[M+H]^+$ = 7299.2 Da, $[M+H]^+ + H_2O$ = 7318.3 Da and $[M+H]^+ + 2H_2O$ = 7336.4 Da. Additionally a peak related to wildtype Nisin (+Met) was also observed $[M+H]^+$ = 7431.5 Da while the calculated was $[M_{calc}+H]^+$ is 7431.56 Da. **(C)** Observed and calculated masses for Nisin wildtype with and without initiator methionine. **(D)** Amino acid sequence of the precursor peptide nisA with (+Met) and without (-Met) the initiating Met in the leader sequence. Leader sequence carrying an N-terminal His-tag.

The redissolved Nisin sample or dialyzed samples were analyzed by LC-MS-ESI-TOF using a Bruker ESI-Quadrupole Time-of-Flight Mass Spectrometer System. With this method, proteins can be observed with multiple-charged ions. These charges seen are dependent on the protein molecular weight and the number of protonatable amino acids (lysine, arginine, and histidine). The ESI-MS analysis shows that recombinantly expressed peptide contains a mixture of various dehydrated forms. Based on the spectrum, the highest abundant peak corresponds to the fully modified WT-PreNisin ($[M_{obs}+H]^+$ = 7299.2 Da), which is close to the expected mass of this version ($[M_{calc}+H]^+$ = 7300.56 Da). The initiator methionine in most cases is cleaved which is a common occurrence with protein expression in *E. coli*. Since glycine is the second residue in the sequence, it increases the likelihood of this N-terminal cleavage occurring.[12] For the fully modified peptide, various charge states from z = +7 to +12 were detected. For instance, a peak at 1044.08 Da corresponds to the 7-fold charged species $[M+7H]^{7+}$ while a peak at 609.27 corresponds to the 12-fold charged species $[M+12H]^{12+}$. A comprehensive list of all observed and calculated peaks is shown in **Table 1**. The curve of these peaks showcases a bell like curve which indicates the relative intensity of each charged species. In addition, a small peak corresponding to the fully modified wildtype PreNisin with starting methionine ($[M_{obs}+H]^+ = 7431.5$) was detected.

Table 1. Determination of the molecular masses and charged species of wildtype-PreNisin (-Met) by ESI-MS.

Species	Calculated Mass (Da)	Observed Mass (Da)
$[M+7H]^{7+}$	1043.94	1044.08
$[M+8H]^{8+}$	913.57	913.56
$[M+9H]^{9+}$	812.18	812.16
$[M+10H]^{10+}$	731.06	730.93
$[M+11H]^{11+}$	664.69	664.67
$[M+12H]^{12+}$	609.38	609.27

The recombinant expression of this peptide in *E. coli* produces a variety of dehydrated species, in addition to the fully modified peptide. Partially modified forms are also detected after analysis with mass spectrometry. The peptide lacking one dehydration is observed ($[M_{obs} + H]^+ = 7318.3$) and this species mostly likes corresponds to the lack of dehydration of serine 33.[122] Additionally, PreNisin lacking two dehydrations was observed ($[M_{obs} + H]^+ = 7318.3$) which could be lack of dehydrations to threonine 2 and serine 5 which do not participate in lanthionine bridge formation. However, this lack of dehydration could be associated with residues participating in lanthionine ring formation, which results in ring breakage. All taken together, the ESI-MS results showcase proper expression of the fully modified wildtype precursor Nisin. This further confirms the successful establishment of expression and purification protocols that do not disturb the Nisin structure. In particular, the purification protocols can be used for modified Nisin and non-canonical amino acid incorporated Nisin in further experiments.

3.2.2 Production and Functional Validation of Nisin Protease (NisP)

3.2.2.1 Design of a Soluble NisP Expression Construct

The previous section discusses the production of the Nisin precursor, which lacks bioactivity and requires cleavage of the leader peptide to become active. Further downstream applications require the cleaved form of Nisin, so this section focuses on the Nisin protease that carries out this reaction. The host strain *Lactococcus lactis* contains an extracellular protease which cleaves the leader peptide from the precursor to produce the active form. As previously stated, the protease is produced in an inactive form containing a signal peptide, membrane-spanning domain, pro-peptide, and active protease domain. It is anchored to the membrane by sortase and undergoes autoproteolysis upon protein folding. The membrane anchored protease may be difficult to express in the soluble form in *E. coli* thus an intracellular version is required. From the pNGNisPT plasmid, a soluble form of the protein was cloned into the pQE80L vector (resultant plasmid = pQE80L_NisP). This form lacks the signal peptide and membrane-spanning domain but includes a linker and a C-terminal HisTag for purification purposes. This soluble form of the protease was used for all further experimentation for Nisin precursor peptide processing.

3.2.2.2 Expression of Optimization and Host Selection

Budisa group members previously worked only with PreNisin, so protocols for expressing and purifying the Nisin protease were not established. Expression of a protease in *E. coli* can be harmful due to its proteolytic activity. Therefore, expression was tested in BL21 (DE3) and BL21-AI™ strains. BL21-AI™ strains are useful for applications involving strict regulation and strong expression of toxic proteins using T7 promoter-based systems. This strain is a derivative of BL21 that lacks the Ion protease and is deficient in the outer membrane protease OmpT. It also lacks two key proteases that protect the heterologously expressed protein from degradation. The T7 TNA polymerase in this strain is under the control of an

arabinose-inducible promoter system, allowing for finer control of protein expression. The plasmid containing the soluble protein was transformed into both strains. Various expression temperatures and times were tested in LB media. From an overnight culture, the bacterium was inoculated into LB and grown until OD600= 0.8-1.2. After the proper optical density was reached, the protein was induced with IPTG and expressed either at 30 or 37oC degrees overnight for the initial tests.

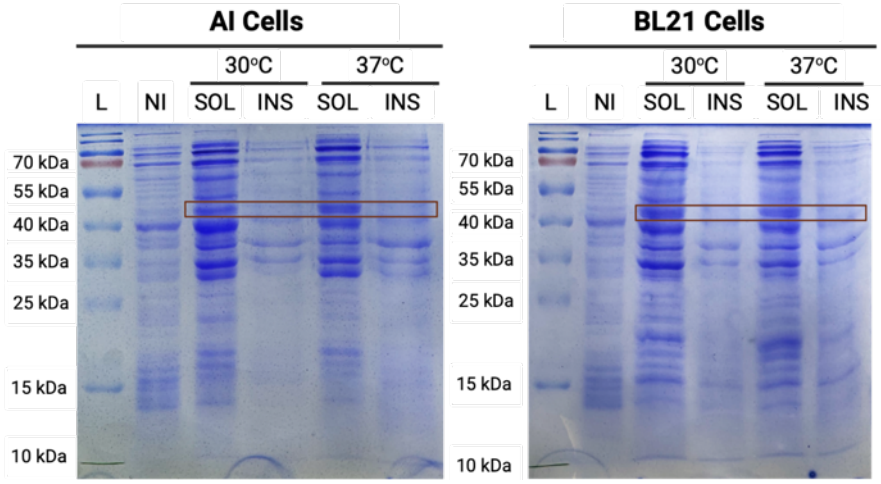


Figure 23. Evaluation of Nisin Protease Expression in *E. coli* BL21(DE3) and BL21-AI Cells at Different Temperatures. On each the gel, the NI = non-induced, SOL= soluble and INS = insoluble fractions are shown. **Left:** SDS-PAGE of Nisin protease expression in AI cells at 30°C and 37°C. The red box highlights the expression of the protease at ~43 kDA and protein mainly expressed in soluble fractions. **Right:** SDS-PAGE of Nisin protease expression in BL21 *E. coli* cells at 30°C and 37°C. The protein expression higher in BL21 cells as seen in red box around ~43kDA.

Nisin protease was successfully expressed under all tested conditions. The inactive form, with the propeptide attached, has a molecular weight of 61.6 kDa, while the active form, which cleaves the propeptide during folding, has a molecular weight of 42.8 kDa. A prominent band between 40 to 55 kDa on the expression gel indicates active protease production, confirming correct processing in *E. coli*. The BL21 strain exhibited higher expression levels compared to other strains, with minimal differences in expression temperatures. Soluble protein expression was successful, with little protein detected in insoluble fractions. The BL21 strain was selected for its higher protein yield, and an expression temperature of 37°C was chosen for further experiments. Due to potential

overnight protein degradation and increased cellular toxicity, various expression times were tested with BL21 cells.

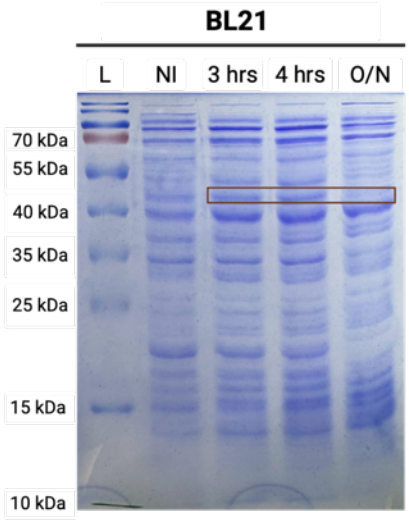


Figure 24. Expression Test of Nisin Protease in *E. coli* BL21(DE3) with different expression durations. SDS-PAGE of Nisin protease showcasing the non-induced and soluble fractions after various expression times. Expression conducted in *E. coli* BL21(DE3) cells at 37°C with the expression times listed. Highlighted in the red box is the Nisin protease at ~43 kDa with highest expression seen between 3 to 4 hours after induction.

Protein expression was tested over varying induction times by expressing the protein at a smaller scale in LB media and sampling at different times post-induction. Cell pellets were lysed via sonication, and soluble fractions were analyzed on SDS-PAGE to assess expression differences. Optimal protein production was observed between 3 and 4 hours, with 3.5 hours selected as the ideal expression time.

3.2.2.3 Purification of Active NisP

To maintain the previously attained high purity of the Nisin peptide, the Nisin protease must achieve comparable purity. Purification conditions were optimized based on established protocols.[67] Initial purification was conducted using Ni^{2+}-immobilized metal-ion affinity chromatography, as outlined in section **Materials and Methods.** The cell pellet was lysed on ice using sonication, followed by centrifugation to remove insoluble materials. The soluble fraction was loaded onto a HiTRAP HP affinity column and purified with an ÄKTA start™

chromatography system using high salt buffers for binding, wash, and elution. SDS-PAGE analysis showed a distinct band in the elution lane corresponding to Nisin proteose (40-55 kDa). Despite multiple elution and wash steps, impurities remained in the final fraction, necessitating an additional purification step with a different technique.

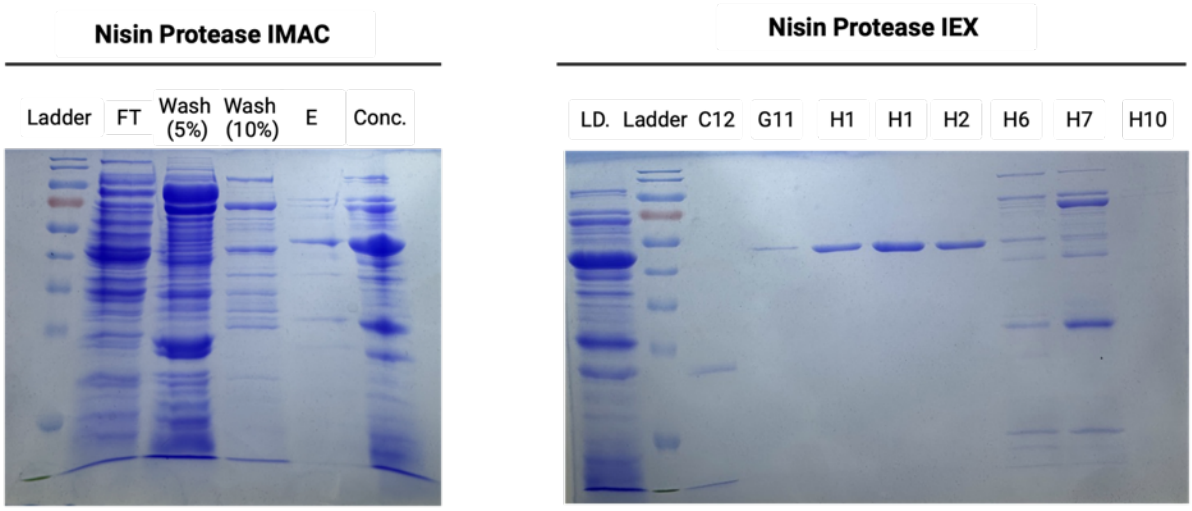


Figure 25. SDS-PAGE Analysis of Nisin Protease Purification Using Affinity and Ion Exchange Chromatography Techniques. Left: SDS-PAGE of Nisin protease purified using Nickel affinity chromatography. Buffer A: 50mM phosphate, 500 mM NaCl pH 7.5 and Buffer B: 50 mM phosphate, 500mM NaCl, 250mM Imidazole, pH 7.5. Wash steps conducted with 5% buffer B and then 10% buffer. E = elution fraction, Conc. = Elution fraction concentrated, Ladder: PageRuler™ Prestained Protein Ladder, 10 to 180 kDa. **Right:** Nisin Protease purification with ion exchange chromatography with step wise gradient from 50mM phosphate pH 7.5 to 50mM phosphate, 1M NaCl pH 7.5 Fractions collected in 96 well plate and fractions tested labelled with well location. L.D = Loading samplex

Ion exchange chromatography was employed to purify Nisin protease, which has an isoelectric point of 6.01, using anion exchange. The protein was gradually dialyzed into the IEX start buffer to reduce salt concentrations and prevent precipitation. Despite some post-dialysis precipitate, it contained other impurities, leaving the target protein intact. Initial trials used a linear gradient to determine the elution salt concentration, followed by an optimized stepwise gradient for purification. Fractions with a 280 nm peak were analyzed by SDS-PAGE, revealing the protein eluted at ~300 mM salt. SDS-PAGE confirmed high purity

across fractions, validating the method's effectiveness. The optimization procedure for Nisin protease production was successfully completed.

3.2.2.4 Optimization of PreNisin Cleavage

While the SDS-PAGE confirms the presence of active protease, further tests were required to demonstrate its activity against Nisin. Since optimized protocols had not been developed, appropriate conditions for the cleavage reaction had to be determined. Various conditions (buffers, pH, divalent ions, temperature) were tested to determine the most optimal parameters for the cleavage reaction. (**Table 2**)

Table 2. Evaluation of Buffer Conditions to Identify the Optimal Buffer for Nisin Protease Cleavage Reaction

Condition	Buffer	Additive
1	50mM Phosphate	-
2	50mM Phosphate	300mM NaCl
3	100mM Tris	-
4	100mM Tris	300mM NaCl
5	100mM Tris	5mM $CaCl_2$
	Buffer	**Temperature**
6	Optimal Buffer conditions	4°C
7		Room Temperature
8		37°C

Concentrations of 50mM phosphate with 100mM TRIS buffers were compared. Typically, buffers include additives such as salts to enhance buffer capacity and facilitate protein solubility, as well as divalent cations that serve as cofactors in enzymatic reactions. Additives such as 300mM NaCl and 5mM $CaCl_2$ were tested for the Nisin protease cleavage reaction. NisP, a member of the subtilase family of serine proteases, is hypothesized to possess a calcium binding site crucial for protease stability and activity. According to previous research[67], the optimal buffer for the cleavage reaction is 100mM Tris with 5mM $CaCl_2$. The buffer pH was maintained at 6, optimal for Nisin and the protease. Protease was purified via ion exchange, pooled, and buffer-exchanged using an Amicon centrifugal device. After exchange, 0.4 µM protease was added to 250 µL of PreNisin (adjusted to 0.1

absorbance at 280 nm) to reach a final protease concentration of 0.036 µM. PreNisin buffer was also exchanged before the cleavage reaction. Samples were incubated at 37°C overnight and analyzed using antimicrobial assays to assess protease efficiency in each buffer. The indicator strain Lactococcus lactis NZ9000, lacking nisIFEG immunity genes and the pNGNisPT plasmid, was used to detect Nisin activity, indicating functional protease cleavage of PreNisin.

3.2.2.5 Verification of Leader Peptide Cleavage

After analyzing the antimicrobial assays, the best buffer was 50 mM phosphate with 300 mM NaCl. In contrast, the phosphate buffer without salt was the worst condition for the cleavage reaction. Similarly, the addition of calcium did not increase the efficiency of the reaction indicating it was not crucial for activity. Upon further literature analysis, based on the published crystal structure, there are no residues present that correspond to calcium chelation sites. Additionally, residues that may be involved in calcium chelation are in a linear conformation, preventing the formation of a metal-ion coordination system. The combined results explain why adding calcium does not affect the reaction and makes it slightly less efficient. Based on these results, the chosen buffer was the phosphate buffer with salt, which also matched the initial conditions of the proteins before buffer exchange. This chosen buffer was used for further tests to determine the optimal temperature for the cleavage reaction. The temperatures tested were 37°C, room temperature, and 4°C. The reactions were set up in a similar fashion to previous tests. The antimicrobial assays indicated comparable outcomes across all tested temperatures. Nevertheless, 37°C was selected for these reactions due to its prior use in the literature.[67] Additionally, on the antimicrobial assays shown in **Figure 26**, only halo are observed after incubation with NisP, showcasing this strain is not able to cleave Nisin on its own.

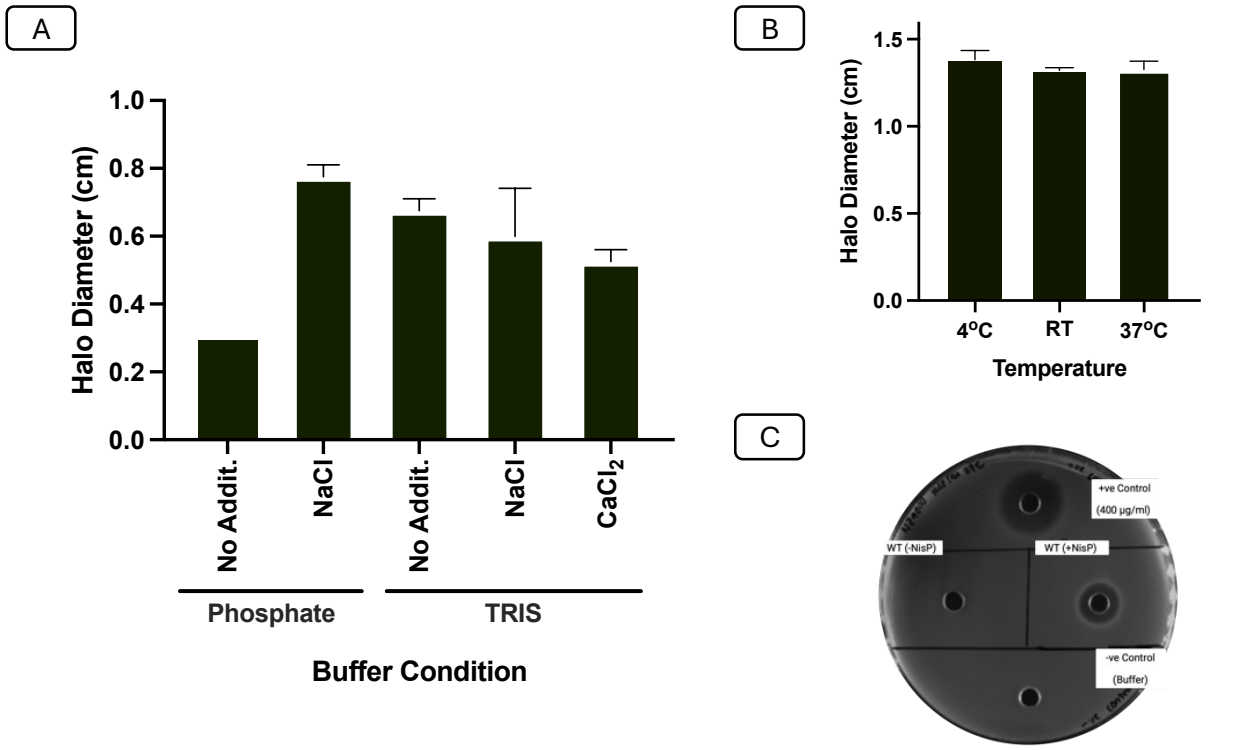
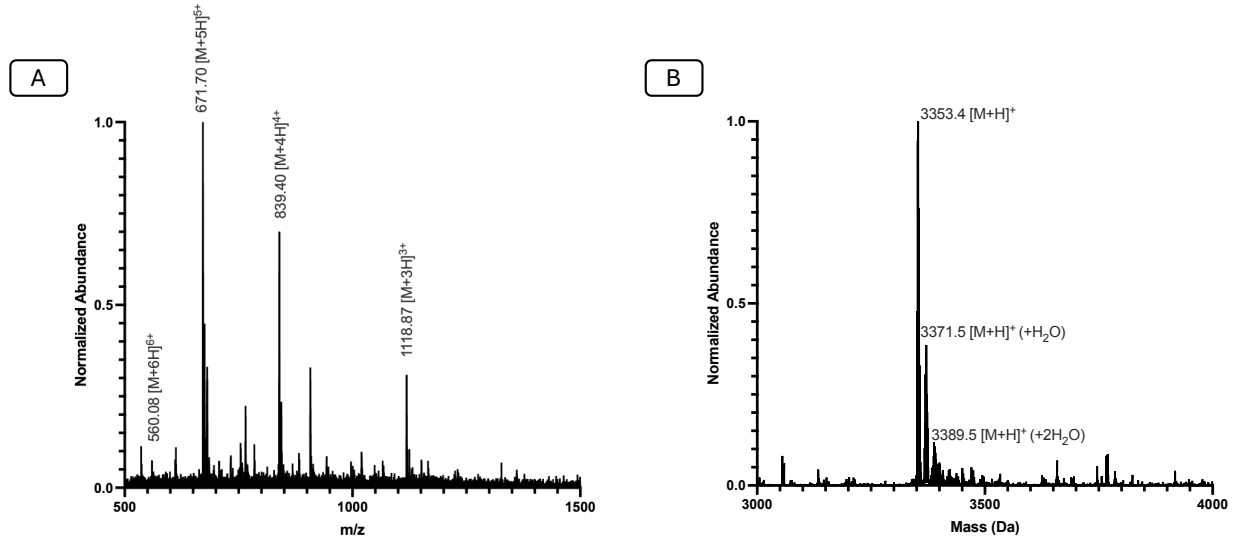


Figure 26. Determination of Optimal Conditions for Nisin Protease Cleavage Assays carried out using *L. lactis* NZ9000 and conducted at 37°C with overnight incubation. **(A)** Identification of Ideal Buffer Parameters for the Nisin Protease Cleavage Reaction. Final concentration of Protease = 0.036 µM and PreNisin concentration adjusted to 0.1 @ 280nm. The optimal condition was determined to be 50mm Phosphate with 300mM NaCl (n=2). **(B)** Determining the optimal temperature for the Nisin protease cleavage reaction. The temperature of the cleavage reaction was irrelevant, as all temperatures yielded similar results (n=2) **(C)** Antimicrobial assays demonstrating the activation of PreNisin through cleavage by Nisin Protease. In the absence of NisP addition, no inhibition halo is observed. Following activation with NisP, a halo is evident, signifying the successful cleavage of the leader peptide.

3.2.2.6 Mass Spectrometric Confirmation of Mature Nisin

Following the selection of optimal conditions, the cleaved Nisin sample underwent analysis via mass spectrometry to further verify the successful cleavage of the leader peptide from the core. The samples for mass spectrometry analysis were prepared using chloroform-methanol precipitation, a technique that facilitates the precipitation of biological molecules while maintaining the solubility of interfering substances such as salts and detergents. To precipitate the proteins and remove contaminants, a volume ratio of 1:1:4:3 of aqueous protein sample:chloroform:methanol:water is used. The supernatant is decanted, and subsequent methanol wash steps are employed to guarantee the thorough elimination of

interfering contaminants. The samples are resolubilized in 80% Water (0.1% Formic acid): 20% ACN mixture.[121]



C

Species	Expected	Observed
Nisin (+Met)	3354.07	3353.4

Figure 27. ESI-MS spectrum of purified wildtype nisin, recombinantly synthesized in Escherichia coli, following incubation with NisP. (A) MS chromatogram of wildtype Nisin showcasing fragmentation pattern for 3353.4 Da peak (B) Deconvoluted ESI-MS Spectrum of wildtype Nisin showcasing various dehydrated. The calculated masses for wildtype Nisin was $[M_{calc}+H]^+$ = 3353.07 Da, $[M_{calc}+H]^+ + H_2O$ = 3372.08 Da, $[M_{calc}+H]^+ + 2H_2O$= 3390.09 Da and the observed mass $[M+H]^+$ = 3353.4 Da, $[M+H]^+ + H_2O$ = 3371.5 Da and $[M+H]^+ + 2H_2O$ = 3389.5 Da. **(C)** Observed and calculated masses for Nisin wildtype.

Based on the ESI-MS analysis, various dehydrated forms of the core peptide are observed. The main peak observed corresponds to the fully modified form of Nisin ($[M_{obs}+H]^+ = 3353.4$) which well aligns with the expected mass of ($[M_{obs}+H]^+ = 3354.07$). In this fully modified configuration, a range of charged states from z = +3 to +6 was detected. Notably, the peak at 671.70 Da represents the 5-fold charged species $[M+5H]^{5+}$, which exhibits the highest abundance. Additionally, the second most abundant peak at 839.40 Da corresponds to the 4-fold charged state $[M+4H]^{4+}$. A full list of observed and expected ion is seen in **Table 3**. The expression of this protein in *E. coli* results in incomplete dehydration as a peptide lacking one dehydration is observed ($[M_{obs}+H]^+ = 3371.5$) which may correspond to lack of dehydration at serine 33. An additional peak related to the lack of two dehydration steps is also observed ($[M_{obs}+H]^+ = 3389.5$) however the location of the lacking second dehydration

is not as clear. Overall, these results showcase proper formation of the lanthionine rings and correct processing by the Nisin protease. Furthermore, the proper functioning of the Nisin protease is confirmed because Nisin was cleaved in the correct position, and no off target cleavage was observed.

Table 3. Determination of the molecular masses and charged species of wildtype-Nisin by ESI-MS.

Species	Calculated Mass (Da)	Observed Mass (Da)
$[M+3H]^{3+}$	1119.03	1118.87
$[M+4H]^{4+}$	839.53	839.40
$[M+5H]^{5+}$	671.82	671.70
$[M+6H]^{6+}$	560.02	560.08

3.2.2.7 Chromatographic Resolution of Dehydration and Oxidation States

Further analysis of the Nisin wildtype core peptide at the Proteomics Centre demonstrates that liquid chromatography can effectively separate the different dehydrated and oxidized forms of this peptide. An inverse correlation between molecular mass and chromatographic retention times are observed (**Figure 28**). As the number of dehydration events increases from 3 to 8, there is a consistent decrease in the total mass of the peptide, corresponding to the loss of water molecules during the formation of the dehydrated amino acids. The transition from the hydrated serine and threonine to an unsaturated dehydro-residues increases the hydrophobic character of the core peptide. This is evidenced by the shift in elution time from approximately 15.2 minutes (3 dehydrations) to over 18.0 minutes (8 dehydrations), indicating a strong affinity for the non-polar stationary phase in the HPLC column. Unlike, oxidation appears to be a stochastic modification that occurs independently of the peptide's dehydration state. The oxidative events likely represent the formation of the methionine sulfoxides. In general, the higher oxidation of a particular dehydrated state elutes prior to the unoxidized version. The observed heterogeneity highlights the challenges in achieving uniform enzymatic processing during *in vitro* or heterologous biosynthesis. Ultimately, this mass distribution confirms that the degree of

dehydration is the primary determinant of the peptide's physicochemical properties and chromatographic behavior.

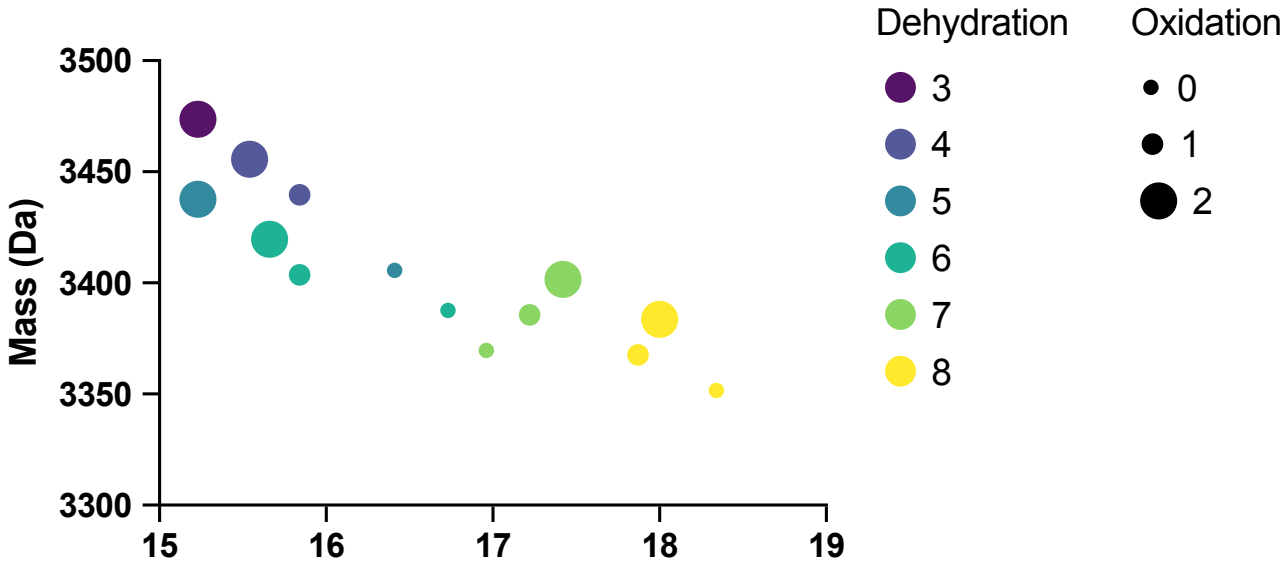


Figure 28. Mass Spectrometric Analysis of Peptide Modification States. Plot illustrates the distribution of peptides species based on their observed mass (Da) and chromatographic retention time (mins). The colour of the bubble indicates the number of dehydration events, ranging from 3 (purple) to 8 (yellow). Increased dehydration correlates with decreased mass and increased retention time. The bubble size represents the oxidation state ranging from 0 (no methionine oxidation) to 2 (both residues oxidized). Dehydration results in enhancing the interaction with the stationary phase, resulting in later elution times.

These two sections describe the strategies for the expression and purification of the wildtype Nisin and the Nisin protease. Furthermore, the conditions for the cleavage reaction were optimized to ultimately obtain the core peptide, the mature and active form. Following incubation with the protease, the sample undergoes an additional purification step utilizing a Nickel affinity column, as depicted in **Figure 29**. This procedure is designed to separate the leader peptide from the core peptide, while simultaneously eliminating the Nisin protease. The leader and protease retain the 6xHis tag, allowing them to bind to the column, whereas the desired core peptide elutes through the column in the flow through fraction. In the event of any residual uncleaved peptide, it can be dialyzed into a buffer devoid of imidazole and re-incubated with the protease.

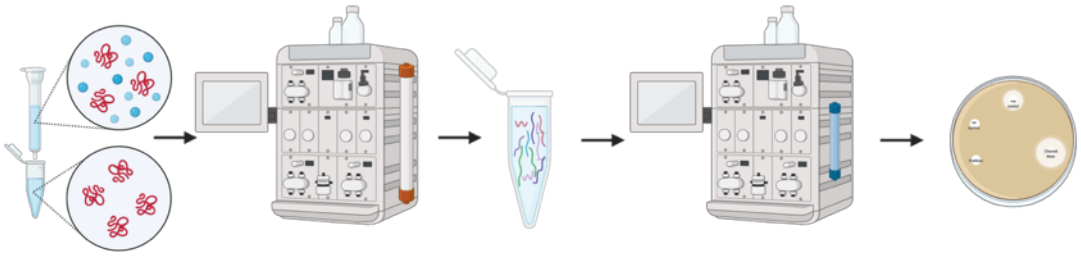


Figure 29. Flowchart illustrating the purification of the Nisin peptide before and after cleavage. Initially, the peptide is purified using affinity chromatography, followed by size exclusion chromatography, to ensure a highly pure precursor. After incubation with the Nisin protease, cleavage occurs. The protease and leader peptide are then removed from the core peptide through a second affinity chromatography step. The purified mature peptide is analyzed using antimicrobial assays to assess its activity. Created with Biorender

3.2.3 Enhanced non-canonical labelling in Nisin A

3.2.3.1 Conceptual Framework and Experimental Rationale

Previous sections established the protocols for production of the wildtype and its protease to produce the final and active form. Further experimentation centers around the incorporation of non-canonical amino acids into Nisin to increase functionality. The introduction of ncAAs, particularly those containing bioorthogonal “clickable” functional groups, enables the installation of unique chemical handles that facilitate downstream conjugation reactions and the generation of modified peptide derivatives. Nisin exhibits potent antimicrobial activity against Gram-positive bacteria but has limited efficacy against Gram-negative species. By incorporating bioorthogonal click handles, nisin can be chemically conjugated to other molecules, such as antibiotics targeting Gram-negative bacteria, enabling the development of hybrid agents with an expanded antimicrobial spectrum. Additionally, these functional groups allow the attachment of fluorescent probes for visualization and mechanistic studies.

For the incorporation of non-canonical amino acids, there are two methods available such as the selective pressure incorporation method and stop codon suppression method. (**Figure 1**). In this study, the SPI approach was selected due to its simplicity and efficiency for global amino acid replacement without requiring engineered orthogonal tRNA/synthetase systems. SPI exploits the native aminoacyl-tRNA synthetase machinery by charging endogenous tRNAs with ncAA analogs under amino acid-limited conditions, enabling the replacement of a canonical amino acid throughout the peptide sequence. In this study, the focus is placed on methionine analogs such as homopropargylglycine and azidohomoalanine containing the click reactive groups, alkyne and azide respectively. Since these amino acids are isostructural analogs of methionine, they can be incorporated by the selective pressure incorporation method.

To further improve labeling specificity and peptide performance, the M21V hinge mutant of nisin was designed. Substitution of methionine at position 21 with valine removes an internal methionine residue, creating a single remaining methionine site for ncAA incorporation, thereby enabling controlled, site-selective labeling. Additionally, this modification has been reported to improve antimicrobial activity and enhance oxidative stability, as methionine residues are susceptible to oxidation. Collectively, this strategy enables the generation of functionalized nisin variants with enhanced chemical versatility and improved biochemical properties. In addition to this, methionyl tRNA synthetase enrichment was explored as a strategy to improve the incorporation efficiency and yield of labeled variants.

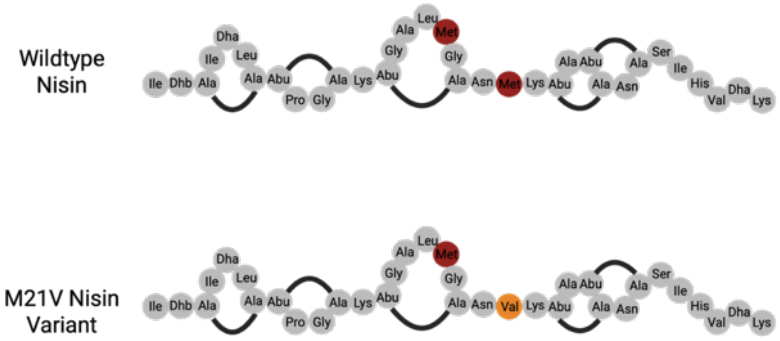


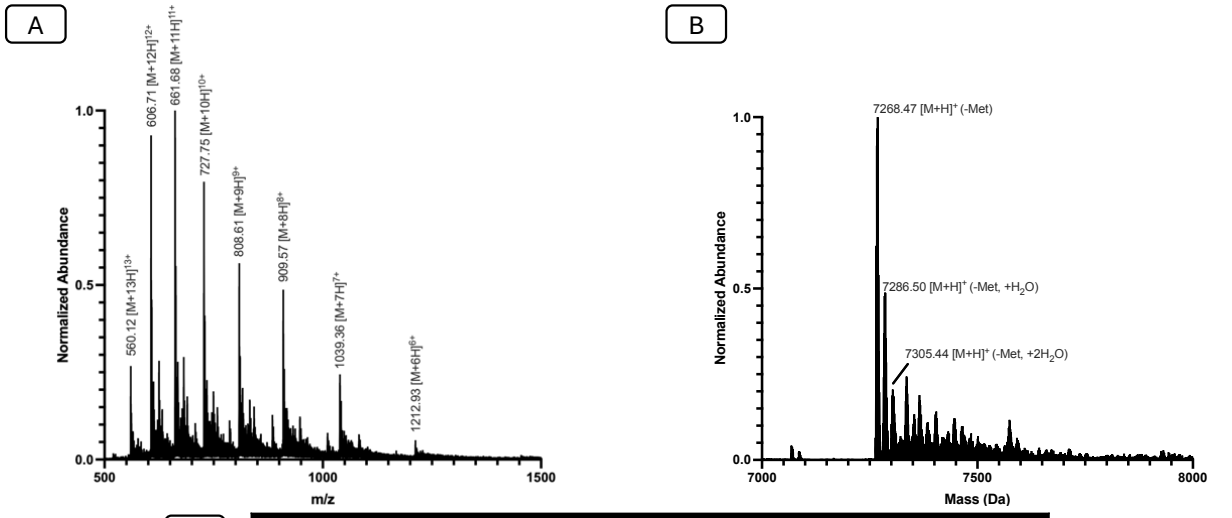
Figure 30. Methionine substitution strategy for site-specific labeling of nisin. Comparison of wild type nisin (top) and the M21V hinge mutant (bottom). The M21V mutation (valine highlighted in orange) removes an internal methionine, leaving a single methionine residue (red) available for selective incorporation of methionine analogs for site-specific functionalization. Created with Biorender

3.2.3.2 Production and validation of Nisin A (M21V)

Previous literature has vastly explored various mutants of Nisin with the hopes of increasing its selectivity and activity. A significant variant produced is the hinge variant of M21V, where mutagenesis replaces one methionine residue valine, resulting in a single methionine within the core peptide. This variant is shown to have enhanced activity against a variety of target strains in comparison to the wildtype and a few examples are listed below. Minimal enhancement was observed when tested against strains like *Lactococcus lactis* and *Streptococcus agalactiae*. However, increased efficacy was noted against several other pathogenic strains. It was shown to have enhanced anti-biofilm activity against

Staphylococcus when used alone or in combination with antibiotics and additionally in combination with plant essential oils, it could inhibit gram-negative bacteria such as *Cronobacter sakazkii* and *E. coli* O157:H7.[112] When tested against the MSRA strain (*Staphylococcus aureus* ST528), the M21V variant displayed 100% increase in specific activity thus making it a better alternative for biomedical applications compared to the wildtype. *Listeria monocytogenes* is a harmful food pathogen and the M21V variant was shown to have also 100% increase in activity against *L. monocytogenes* strains 10403S and EGDe.[123] Due to its higher activity against this pathogen, the M21V variant may provide a better alternative for food bio-preservation applications where the wildtype Nisin is highly used. This mutant was created in the lab using site directed mutagenesis where Met21 was replaced with the valine codon. The mutagenesis was confirmed through genome sequencing. Using similar protocols established in previous sections for the production and purification of Nisin, the M21V variant was produced. After purification, Nisin M21V was precipitated using TCA precipitation and confirmed by mass spectrometry. On the instrument, both the variant PreNisin **(Figure 31)**and core peptide **(Figure 32)** samples were run to confirm proper production of both species.

The LC-ESI-MS analysis of the PreNisin (M21V) showcases multiple peaks corresponding to varying dehydrated variants. Based on the obtained deconvoluted spectrum, the most prevalent peak relates to the fully modified M21V-PreNisin [M_{obs} *+H]*$^{+}$ *= 7268.47)* which is highly similar to the expected mass of this version ([M_{calc} *+H]*$^{+}$ *= 7268.54)*. This variant lacks the starting methionine which is commonly cleaved in *E. coli* during protein expression. Comparably to the wildtype Nisin, more states are observed for the variant ranging from z = +6 to +13. For example, the highest peak at 661.68 corresponds to the 11-fold charged species *[M+11H]*$^{11+}$ and a full list of the expected and observed peptides are shown in **Table 4**. The observed mass difference of ~31 Da between the Nisin wildtype and Nisin-M21V confirms the successful mutagenesis of Met21 to valine. Similarly to the wildtype, the recombinant expression results in various forms of the dehydrated peptide. As observed on the spectrum, the single mis-dehydrated peptide ([M_{obs} *+H]*$^{+}$ *= 7286.5*) is relatively abundant,



C

Species	Expected	Observed
Nisin M21V (+Met)	7399.53	Not observed
Nisin M21V (- Met)	7268.54	7268.47

D

MGSSHHHHHHSQDPMSTKDFNLDLVSVSKKDSGASPR*ITSISLCTPGCKTGALMGCNVKTATCHCSIHVSK(Stop) Nisin M21V (+ Met)

GSSHHHHHHSQDPMSTKDFNLDLVSVSKKDSGASPR*ITSISLCTPGCKTGALMGCNVKTATCHCSIHVSK(Stop) Nisin M21V (- Met)

Figure 31. ESI-MS spectrum of purified PreNisin (M21V) recombinantly produced in *E. coli*. (A) MS chromatogram of PreNisin (M21V) showcasing fragmentation pattern for 7268.47 Da peak **(B)** Deconvoluted ESI-MS Spectrum of PreNisin (M21V) showcasing various dehydrated variants. The calculated masses for wildtype PreNisin-M21V (-Met) was $[M_{calc}+H]^+$ = 7286.56 Da, $[M_{calc}+H]^+ + H_2O$ = 7304.57 Da, $[M_{calc}+H]^+ + 2H_2O$= 7322.58 Da and the observed mass $[M+H]^+$ =7268.47, $[M+H]^+ + H_2O$ = 7286.50 Da and $[M+H]^+ + 2H_2O$ = 7305.44 Da. **(C)** Observed and calculated masses for PreNisin (M21V) with and without initiator methionine. **(D)** Amino acid sequence of the precursor peptide nisA-M21V with (+Met) and without (-Met) the initiating Met in the leader sequence. Leader sequence carrying an N-terminal His-tag and valine mutation shown in light green.

with only 50% less abundance in comparison to the fully dehydrated peptide. In contrast, the peptide variant lacking 2 dehydrations ($[M_{obs}+H]^+ = 7305.44$) makes up a smaller portion of the peptides in the mixture. In the Nisin-M21V samples, there were no peptides observed with the starting methionine intact thus full processing of the initiating methionine occurs. While there are multiple impurities present, these do not correspond to any calculated masses of varying dehydrated forms of this peptide and may be peptides that could not be separated during the size exclusion chromatography step. Overall, these results confirm the successful recombinant production of the PreNisin-M21V variant in *E. coli*.

Table 4. Determination of the molecular masses and charged PreNisin-M21V (-Met) by ESI-MS.

Species	Calculated Mass (Da)	Observed Mass (Da)
$[M+6H]^{6+}$	1212.43	1212.93
$[M+7H]^{7+}$	1039.37	1039.36
$[M+8H]^{8+}$	909.58	909.57
$[M+9H]^{9+}$	808.62	808.61
$[M+10H]^{10+}$	727.86	727.75
$[M+11H]^{11+}$	661.78	661.68
$[M+12H]^{12+}$	606.72	606.71
$[M+13H]^{13+}$	560.13	560.12

The successful synthesis of active Nisin necessitates processing by the Nisin protease to cleave the leader peptide. Like the wildtype Nisin, this variant undergoes cleavage by the Nisin protease to yield the final active form. The leader peptide and protease are separated from the core peptide using affinity chromatography, as previously described. Although antimicrobial assays can verify the correct cleavage of this peptide, confirmation requires mass spectrometry analysis.

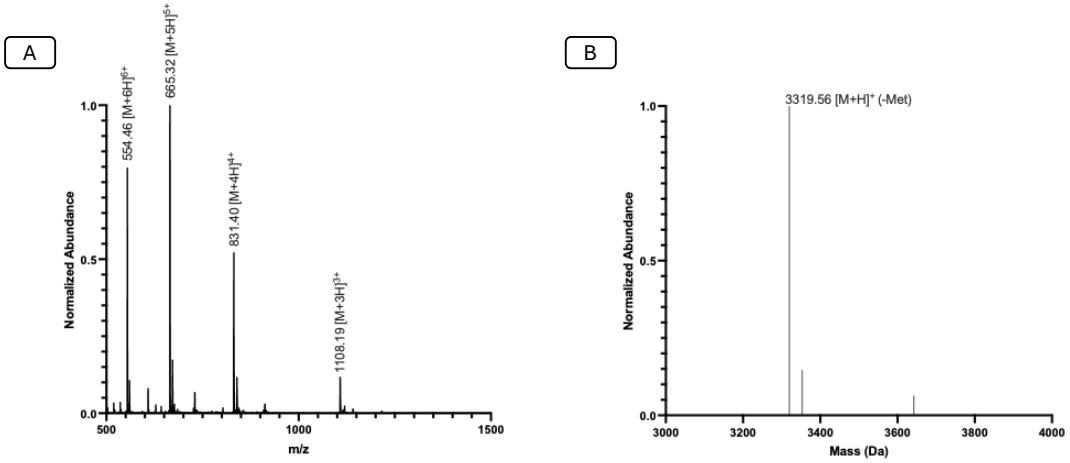


Figure 32. ESI-MS spectrum of purified Nisin-M21V, recombinantly synthesized in *Escherichia coli*, following incubation with NisP. (A) MS chromatogram of Nisin-M21V, showcasing fragmentation pattern for 3319.56 Da peak **(B)** Deconvoluted ESI-MS Spectrum of Nisin-M21V, showcasing the fully modified peptide. calculated masses for Nisin-M21V, was $[M_{calc}+H]^+$ = 3322.10 Da, the observed mass $[M+H]^+$ = 3319.56 Da. **(C)** Observed and calculated masses for Nisin-M21V after the cleavage of leader peptide with Nisin Protease.

The purified core was precipitated and resolubilized in an LC-MS compatible buffer of 80% Water/20% ACN prior to analysis by mass spectrometry. The main observed peak on the deconvoluted spectrum relates to the core peptide of the fully modified Nisin-M21V ($[M_{obs} + H]^+ = 3319.56$) which correlates well to the calculated mass ($[M_{calc} + H]^+ = 3322.1$). Only charge states from z = +3 to +6 are observed with the main peak of 665.32 Da matching the 5-fold charged species $[M+5H]^{5+}$ *(Calc = 665.43 Da)*. A more comprehensive list of the various observed and calculated m/z ions is found in **Table 5**. The calculated masses in this table exhibit a high degree of consistency with the observed masses, with discrepancies noted only in the decimal places. While many other peaks are observed, they do not relate to any calculated mass of the Nisin-M21V core peptides and are impurities that could not be removed through various purification steps.

Table 5. Determination of the molecular masses and charges for Nisin-M21V by ESI-MS.

Species	Calculated Mass (Da)	Observed Mass (Da)
$[M+3H]^{3+}$	1108.37	1108.19
$[M+4H]^{4+}$	831.53	831.40
$[M+5H]^{5+}$	665.43	665.32
$[M+6H]^{6+}$	554.69	554.46

Liquid chromatography-mass spectrometry at the Proteomics Centre was utilized to characterize the modification states of the Nisin(M21V) core peptide. As shown in **Figure 33**, the sample exhibits a heterogeneous distribution of species varying by both mass and elution time. A clear correlation is observed between the extent of dehydration and chromatographic retention time; as the degree of dehydration increases from 5 to 8 (indicated by the color shift from teal to yellow), there is a decrease in molecular mass and a shift toward later elution times (ranging from ~13.5 to 17.5 minutes). Additionally, the substitution of methionine with valine at position 21 is a strategic mutation often employed to enhance the oxidative stability of the peptide, as valine lacks the thioether group susceptible to sulfoxide formation.

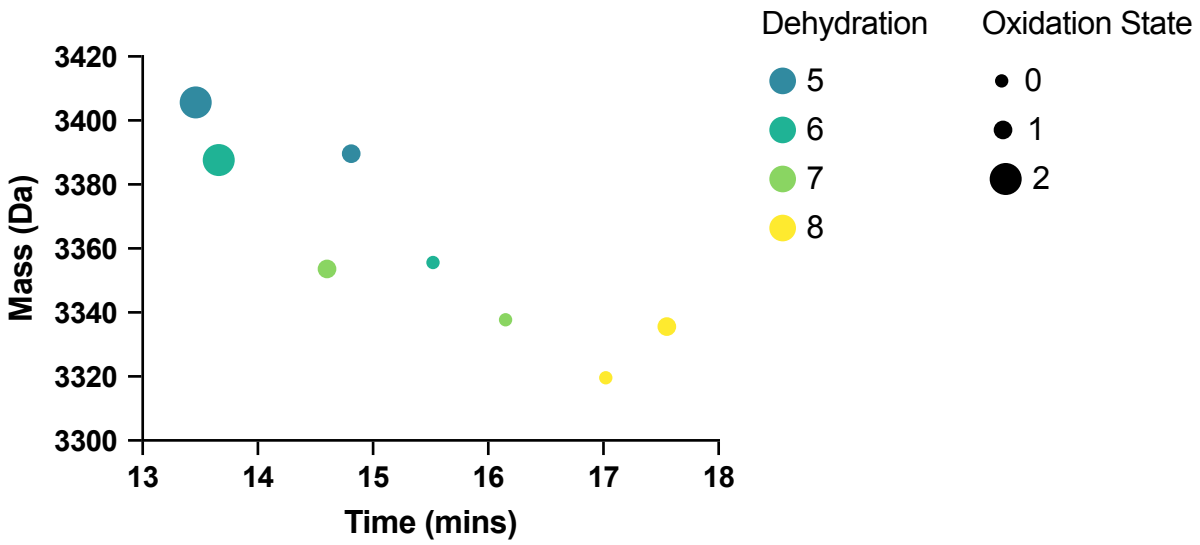


Figure 33. LC-ESI-MS Analysis showcasing separation of varying dehydrated and oxidized species of Nisin-M21V. The colour scale represents the dehydration from 5 (teal) to 8 (yellow). The bubble size represents the oxidation state 0 (no methionine oxidized) and 2 (double oxidization of methionine). The increased dehydration progressively increases the hydrophobic interaction with the column.

3.2.3.3 SPI-based Incorporation of Methionine Analogs in BU14

Mass spectrometry analysis of PreNisin M21V and Nisin M21V variants established baselines for subsequent incorporation studies. Non-canonical amino acids homopropargylglycine (Hpg) and azidohomoalanine (Aha) containing alkyne and azide functionalities, respectively, enable bioorthogonal conjugation of Nisin to target molecules. These residues are incorporated via selective pressure incorporation using methionyl aminoacyl-tRNA synthetase, which substitutes methionine residues with the desired non-canonical amino acids. Consequently, these experiments demand the use of a methionine auxotrophic strain and new minimal media. The laboratory housed a previously developed methionine auxotrophic strain, BU14, which is a derivative of *E. coli BL21* characterized by a knockdown of the *metE* gene. This enzyme is responsible for the methylation of homocysteine to make methionine and thus its knockdown blocks the last step of the

methionine biosynthesis pathway. With the use of minimal media, precise control of nutrients and amino acid concentrations is achieved.

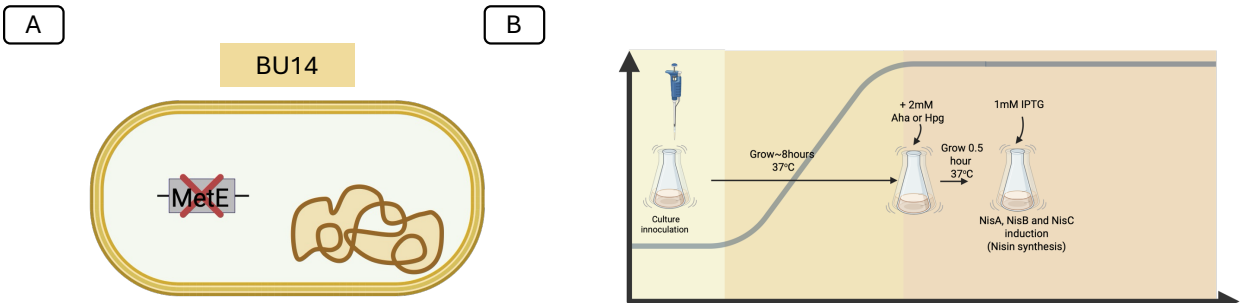


Figure 34. Expression scheme for non-canonical amino acid incorporation into Nisin. (A) The methionine auxotrophic BU14 strain used for incorporation containing a knockdown in metE gene disrupting the last step of the methionine biosynthesis. (B) Expression strategy for ncAA incorporation. The overnight culture is washed with NMM and then inoculation into NMM Media containing a limiting concentration of methionine (35µM) and grown until stagnant growth. The non-canonical amino acid is added at this point and incubated for 30 minutes after which expression of NisA, NisB and NisC is induced. Created with Biorender

Non-canonical amino acid incorporation via SPI was performed using overnight cultures of BU14 harboring pET3a_Nisin(M21V) and pRSFDuet_NisBC expression vectors. Cultures were subjected to washing procedures with either MilliQ water or nutrient-free minimal medium to eliminate residual rich media components, followed by inoculation into fresh minimal medium supplemented with limiting methionine concentrations (35 µM). Bacterial growth proceeded at 37°C until reaching stationary phase, as monitored through optical density measurements. Upon growth cessation, cultures received supplementation with 2 mM concentrations of either methionine (control), Aha, or Hpg, followed by a 30-minute incubation period to facilitate amino acid uptake and metabolic incorporation. Protein expression was subsequently induced using IPTG at 28°C for 16 hours. Normalized aliquots were collected for antimicrobial bioassays to quantify Nisin expression levels based on biological activity. Following optimization of expression parameters, production was scaled up for protein purification purposes. Post-expression, peptides underwent purification and proteolytic cleavage using Nisin protease according to established protocols. Purified peptides were concentrated via trichloroacetic acid (TCA) precipitation, and yields were determined gravimetrically.

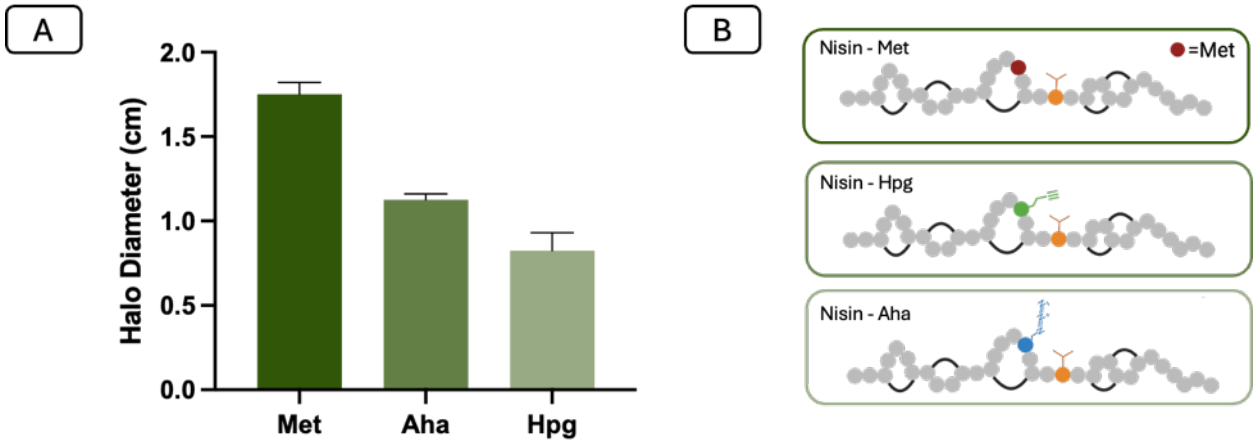


Figure 35. Comparison of Nisin M21V Expression upon Methionine or non-canonical amino acid incorporation in BU14. (A) Antimicrobial assays confirming the expression and functional activity of Nisin M21V labelled with Met, Aha, or Hpg. Cell lysates were prepared by normalizing the bacterial cultures to OD600 = 5.0, and sonicating for cell lysis, followed by centrifugation to remove cellular debris. 40µL of each lysate was loaded into wells on a GM17 agar plate inoculated with the indicator strain *Lactococcus lactis* NZ9000 (pNGNisPT). After overnight incubation at 30°C, the diameters of the resulting antimicrobial inhibition halos were measured and plotted using Prism software. Results demonstrate that strains incubated with Met exhibited the highest expression and activity, followed by Aha, and lastly Hpg, consistent with decreasing incorporation efficiency of the respective ncAA. Comparison of Nisin M21V expression with methionine or methionine analog incorporation (mean ± SD, n=2). **(B)** Schematic illustration depicting the structure of Nisin M21V labeled with Met, Aha, or Hpg. The diagram highlights the M21V mutation site and the specific position of ncAA incorporation within the peptide. Created with Biorender

The control sample with the addition of methionine contains the highest expression of the Nisin-M21V peptide. Methionine supplementation yielded the highest levels of Nisin-M21V expression, consistent with its role as the native substrate. Comparative analysis of non-canonical amino acid variants revealed superior expression levels for Nisin-M21V (Aha) relative to Nisin-M21V (Hpg). Purification yields were 17.5 mg/L and 15 mg/L for Aha and Hpg variants, respectively. Initial expression assessments demonstrated 1.22-fold enhanced production of the Aha variant compared to the Hpg variant. Post-purification analysis confirmed this trend, with Nisin-M21V (Aha) exhibiting 1.16-fold higher yields than Nisin-M21V (Hpg).

The observed expression hierarchy correlates directly with the substrate specificity of methionyl-tRNA synthetase for the respective amino acids. (**Figure 35**) Methionine, as the cognate substrate, exhibits optimal recognition and charging efficiency, accounting for maximal expression levels. Published kinetic analyses of MetRS demonstrate marked

differences in catalytic efficiency (kcat/Km) among substrates: Methionine (5.47×10^{-1} $s^{-1} \cdot \mu M^{-1}$), azidohomoalanine (1.42×10^{-3} $s^{-1} \cdot \mu M^{-1}$) and homopropargylglycine (1.16×10^{-3} $s^{-1} \cdot \mu M^{-1}$)[124]. The marginally superior catalytic efficiency of Aha relative to Hpg provides a mechanistic basis for the observed expression differential. Mass spectrometric data were obtained only for Nisin-M17Aha and Nisin-M21V, not Nisin-M17Hpg. Since the proportion of labelled versus unlabelled species is unknown for M17Hpg, the observed effects cannot be directly attributed to Hpg incorporation. Hpg incorporation is instead inferred from trends consistent with the Aha data. Antimicrobial assays were used semi-quantitatively, which is a limitation: halo size reflects both peptide concentration and intrinsic potency, so a smaller halo cannot be attributed to lower expression alone. Sample diffusion may further confound this comparison. Initial expression assessments and final purification yields showed close agreement ($\Delta = 0.06$ fold, $n = 2$). This supports antimicrobial bioassays as a reasonable proxy for peptide production, though confirmation across more samples is needed.

3.2.4 Enhancement of non-canonical amino acid incorporation with MetG

3.2.4.1 Proof-of Principal Using EGFP

Despite the suboptimal activation kinetics of methionine analogues such as azidohomoalanine by methionyl-tRNA synthetase, protein expression incorporating these non-canonical amino acids remains feasible *in vivo*. However, the incorporation of clickable non-canonical amino acids yields substantially lower peptide production compared to wild-type Nisin expression. The primary limiting factor governing protein yield is the efficiency of amino acid activation by aminoacyl-tRNA synthetases. Extensive research has demonstrated that overexpression of MetRS *in vivo* significantly enhances incorporation efficiency for poorly activated methionine analogues, consequently improving overall protein yields.[125] The CRISPR-associated transposition (CAST) system enables precise integration of donor DNA fragments into specific genomic loci, facilitating the generation of strains with multiple MetRS gene copies under inducible promoter control.

Two MetRS-overexpressing strains were employed: MS51 containing one additional MetRS copy in the initial analysis and MS61 harboring five additional copies, both under L-arabinose promoter control and derived from the methionine auxotrophic strain BU14. Integration sites and copy numbers were confirmed through PCR using integration site-flanking primers and validated by whole-genome sequencing performed by SeqCoast Genomics using Illumina short-read technology. The Breseq computational program was utilized to identify mutations and integrations relative to a reference genome. As depicted in **Figure 36**, MS51 possesses four additional copies of MetG (illustrated in red) distributed across the genome, located downstream of the diverse targeted sites, with the native MetG also represented in green. Furthermore, sequencing has confirmed the presence of five additional copies of MetG in the MS61 strain. The procedure for incorporating non-canonical

amino acids was marginally adjusted to consider the induction of MetG by L-arabinose, as illustrated in **Figure 36**.

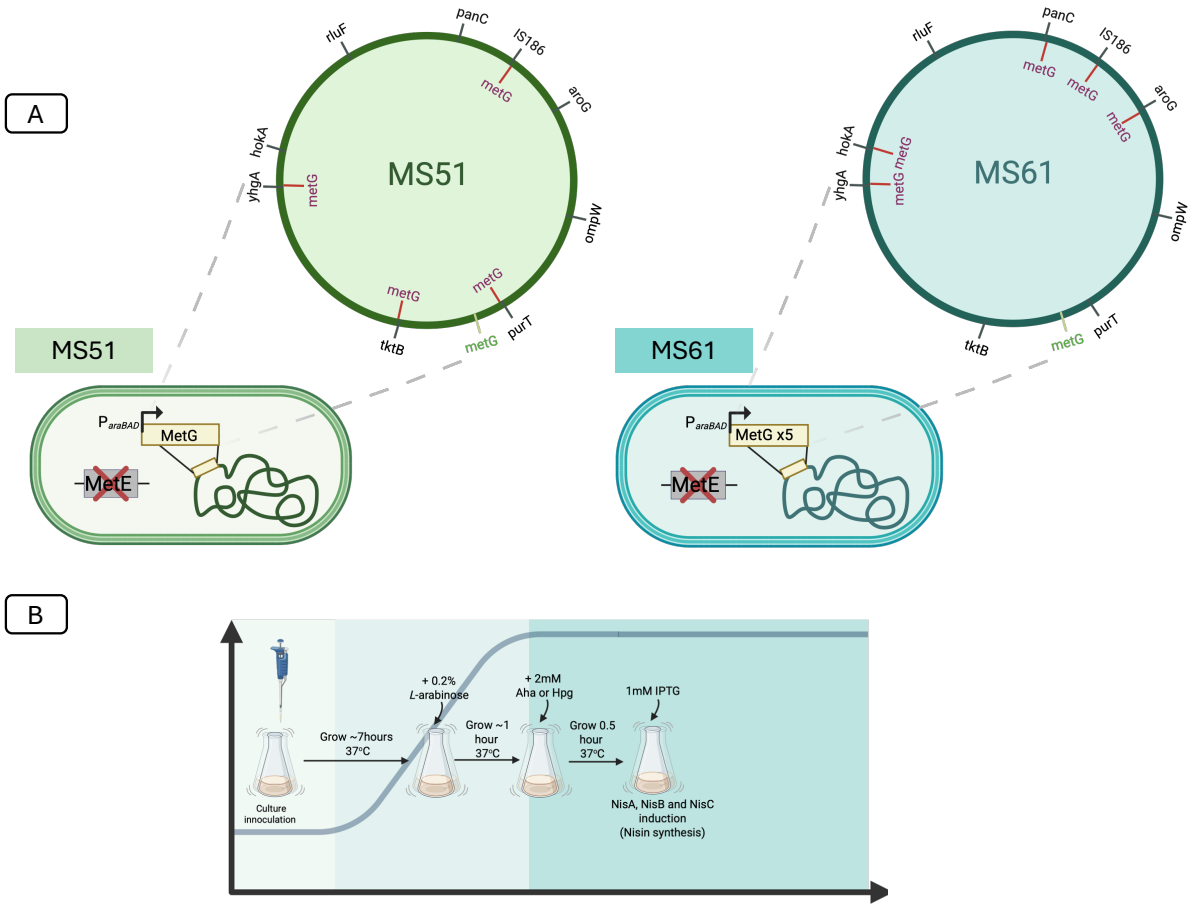


Figure 36. MetRS Overexpression Strains and ncAA Incorporation Protocol. (A) Genomic integration sites of additional MetRS copies in MS51 (4 copies) and MS61 (5 copies), with native *metG* in green and integrated copies in red. **(B)** Expression workflow: growth in limiting methionine (35µM), MetRS induction with L-arabinose at 7h, ncAA addition at growth stagnation, followed by IPTG induction of Nisin genes. Created with Biorender

Initial validation experiments employed the model protein M218-EGFP containing four mutated methionine residues (M79L, M89L, M154T, and M234K). The plasmid pQE80L_EGFP_4M was transformed into control strain BU14 and MetRS-enriched strains MS51 and MS61. Two experimental protocols were implemented: (1) growth in minimal media with limiting methionine (35 µM) followed by MetRS induction with L-arabinose at 7 hours, methionine depletion at 8 hours, azidohomoalanine supplementation, and IPTG induction after 30 minutes; (2) an optimized protocol involving initial growth in LB medium for 3-4 hours, washing with nutrient-free minimal medium, transfer to methionine-free minimal media, MetRS induction, and target protein induction after 1-1.25 hours. Expression

levels were quantified through fluorescence intensity measurements at 495 nm and optical density at 600 nm. Protein incorporation was verified using electrospray ionization mass spectrometry (ESI-MS).

Under the initial minimal media protocol, a single measurement per strain (n = 1) showed a modest increase in fluorescence intensity/OD600 for MS51 relative to BU14, while MS61 showed a slightly lower value. Under the optimized protocol, MS51 and MS61 each showed roughly 2-fold higher fluorescence intensity than BU14 in a single measurement MS61, despite containing the highest number of MetRS copies, did not show a higher value than MS51.

Furthermore, with the use of ESI-MS, the incorporation of azidohomoalanine in M218-EGFP is confirmed. In **Figure 37**, wild-type M218-EGFP ($[M_{calc} +H]^+$ = 27677.14 Da) was not detected in any sample, indicating complete replacement of methionine residues. BU14-expressed Aha-EGFP exhibited $[M_{obs} +H]^+$ = 27663.44 Da (calculated $[M_{calc} +H]^+$ = 27667.17 Da), confirming full azidohomoalanine incorporation at positions Met1 and Met218. MS51 and MS61 strains produced proteins with observed masses of $[M_{obs} +H]^+$ = 27663.14 Da and $[M_{obs} +H]^+$ = 27662.87 Da, respectively, both consistent with complete methionine-to-azidohomoalanine substitution.

As single, unreplicated measurements, these represent preliminary observations, not confirmed trend; however, they provided a general guideline for how to proceed to expression with the Nisin system .One possible explanation for the improvement under the optimized protocol is that initial growth in nutrient-rich medium, followed by controlled amino acid depletion, supports greater metabolic capacity for protein overexpression than minimal medium alone; similarly, the comparable values for MS51 and MS61 may suggest that incorporation efficiency saturates beyond a certain MetRS copy number. Both interpretations require replication to confirm before being treated as established trends.

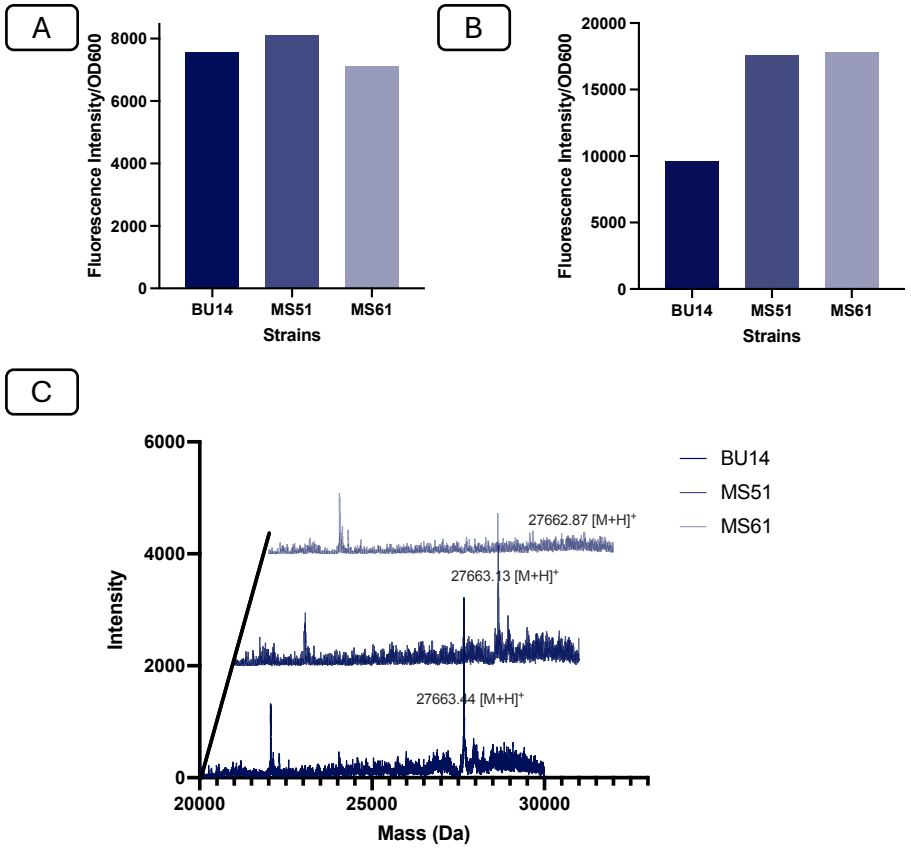


Figure 37. EGFP Expression and Azidohomoalanine Incorporation in MetRS-overexpressing strains. **(A)** Expression levels in minimal media show no differences between BU14, MS51, and MS61 strains. **(B)** LB pre-growth protocol yields 2-fold increased expression in MetRS-enriched strains compared to BU14**. (C)** ESI-MS confirmation of azidohomoalanine incorporation with observed masses of 27663.44 Da (BU14), 27663.13 Da (MS51), and 27662.87 Da (MS61).

The mass spectrometric confirmation of complete non-canonical amino acid incorporation, coupled with enhanced expression levels in MetRS-overexpressing strains, validates this approach as a viable strategy for improving Nisin production with clickable functionalities. These findings demonstrate that MetRS overexpression maintains fidelity of non-canonical amino acid incorporation while significantly enhancing overall protein yields, establishing the foundation for applying this methodology to Nisin expression systems.

3.2.4.1 Application to Nisin A (M21V)

While previous investigations have established the beneficial effects of methionyl-tRNA synthetase co-expression on protein production, the Nisin biosynthetic system presents

additional complexity due to the simultaneous high-level expression of multiple components. The Nisin production pathway requires coordinated expression of three essential proteins: the nisin peptide precursor, the dehydratase (NisB), and the cyclase (NisC), in addition to enhanced MetRS levels. This multi-protein expression system necessitates investigation of whether MetRS overexpression can effectively enhance non-canonical amino acid incorporation under these more demanding cellular conditions, particularly for azidohomoalanine and homopropargylglycine labeling of Nisin.

Plasmids encoding the Nisin peptide sequence (pET3a_NisA_M21V) and its biosynthetic machinery (pRSFDuet_NisBC) were co-transformed into MetRS-enriched strains MS51 and MS61. The experimental protocol followed established procedures (in **Figure 36 and section 3.3)**: bacterial cultures were grown in minimal media containing limiting methionine concentrations (35 μM), with MetRS expression induced using L-arabinose at approximately 7 hours post-inoculation. Following methionine depletion at 8 hours total growth time, cultures received supplementation with either azidohomoalanine, homopropargylglycine, or methionine (control), followed by a 30-minute incubation period. Protein expression was subsequently induced using IPTG and allowed to proceed overnight. Cell pellets were processed for antimicrobial bioassays to quantify PreNisin (M21V) expression levels across all amino acid variants and strains (**Materials and Methods**).

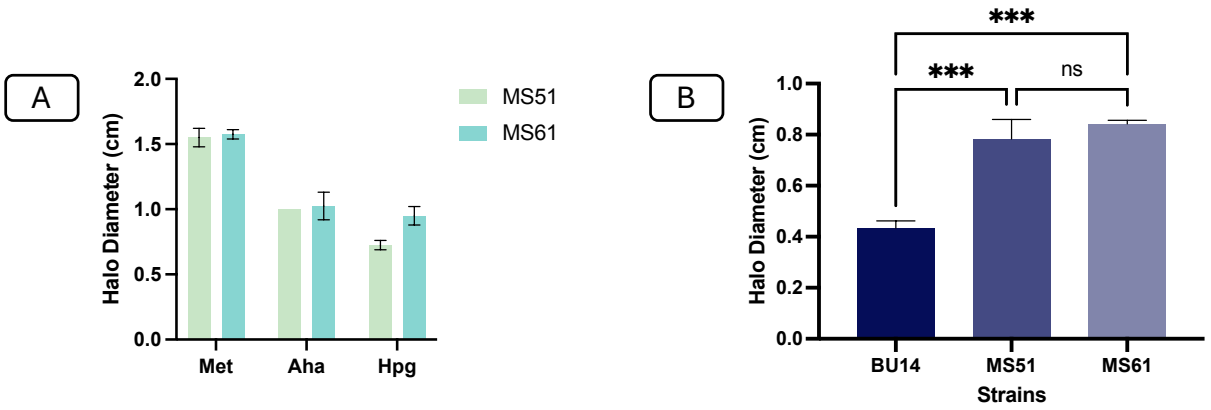


Figure 38. Comparative expression of ncAA-labelled Nisin M21V in MetRS-enriched strains (A) Halo diameters for MS51 and MS61 grown with methionine (Met), azidohomoalanine (Aha), or homopropargylglycine (Hpg) supplementation. As with control strain BU14, methionine yielded the highest expression, followed by Aha, with Hpg lowest; expression did not differ meaningfully between MS51 and MS61. Data represent mean ± SD (n = 2). **(B)** Halo diameters for BU14, MS51, and MS61 following azidohomoalanine (Aha) supplementation in NMM. MetRS-enriched strains showed approximately 2-fold greater antimicrobial activity relative to the BU14 control (ordinary one-way ANOVA with Tukey's multiple comparisons test; BU14 vs. MS51, $p = 0.0003$; BU14 vs. MS61, $p = 0.0001$), with no significant difference between MS51 and MS61 (ns). Data represent mean ± SD (n = 3)

Comparative analysis revealed that methionine incorporation yielded the highest expression levels in both MS51 and MS61 strains, while azidohomoalanine and homopropargylglycine demonstrated comparable expression levels within each strain. (**Figure 38**) Both MetRS-enriched strains (MS51 and MS61) exhibited approximately 2-fold enhanced antimicrobial activity relative to the BU14 control strain across all amino acid incorporation conditions. No significant differences in expression enhancement were observed between the two MetRS-enriched strains, indicating saturation of the beneficial effect beyond the MS51 level of MetRS overexpression.

The observed expression hierarchy directly correlates with the established substrate preferences of methionyl-tRNA synthetase, with methionine demonstrating optimal catalytic efficiency (kcat/Km = 5.47×10^{-1} $s^{-1} \cdot \mu M^{-1}$) compared to the non-canonical amino acids. The consistent 2-fold enhancement observed in MetRS-enriched strains demonstrates that the beneficial effects of MetRS overexpression are maintained even under the increased metabolic burden imposed by the complex Nisin biosynthetic system. The absence of additional improvement in MS61 compared to MS51 suggests that MetRS

expression levels reach a saturation point beyond which further increases do not yield proportional benefits. These findings validate that the positive effects previously observed with the simpler EGFP expression system (**Figure 37**) are reproducible and robust when applied to the more complex multi-protein Nisin biosynthetic pathway, establishing the broader applicability of this approach for enhancing non-canonical amino acid incorporation in demanding expression systems.

Following expression optimization, electrospray ionization mass spectrometry (ESI-MS) analysis was conducted to validate successful azidohomoalanine incorporation in Nisin M21V produced by the MetRS-enriched MS51 strain. (**Figure 39**) The MS51-expressed Aha-Nisin exhibited an observed mass of $[M_{obs} + H]^+ + H_2O$ = 3332.6 Da, confirming complete azidohomoalanine incorporation at methionine position 17. This mass spectrometric evidence demonstrates that the post-translational modification machinery remained functional despite the presence of the non-canonical amino acid, as indicated by successful peptide processing and cleavage of the leader sequence from PreNisin. The observed molecular weight corresponds to a partially modified peptide lacking a single dehydration event, suggesting that azidohomoalanine incorporation does not significantly interfere with the enzymatic activities of the dehydratase (NisB) or cyclase (NisC) components of the biosynthetic pathway.

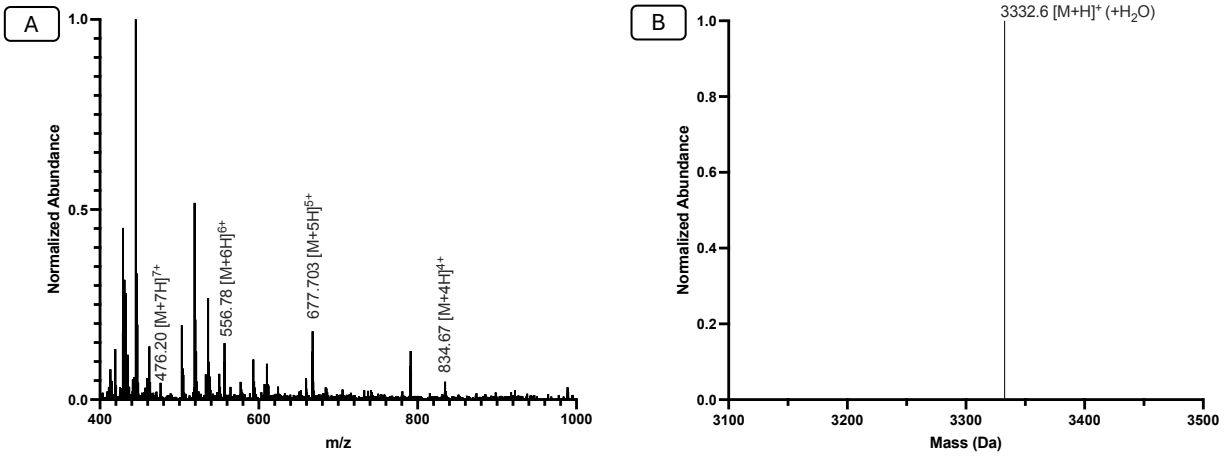


Figure 39. ESI-MS Analysis of Nisin-M21V-Aha produced with MetRS-enriched strain MS51. (A) MS chromatogram of Nisin-M21V-Aha showcasing fragmentation pattern for the 3332.6 Da peak. **(B)** Deconvoluted ESI-MS spectrum of Nisin-M21V-Aha. The incorporation of azidohomoalanine incorporation with observed with the mass of 3332.6 Da, corresponding to partially modified Nisin lacking single dehydration.

Quantitative analysis of incorporation efficiency through mass spectrometry revealed substantial differences between the control and MetRS-enriched strains. (**Appendix Figure 8**) The MS51 strain demonstrated a 2-fold increase in the percentage of PreNisin molecules successfully labeled with azidohomoalanine compared to the BU14 non-enriched control strain. This enhanced incorporation efficiency directly correlates with the increased antimicrobial activity observed in bioassays, providing molecular-level confirmation that MetRS overexpression significantly improves non-canonical amino acid incorporation without compromising the integrity of the complex Nisin biosynthetic machinery or the biological activity of the resulting modified peptide.

3.2.5 Labelling Nisin through *In vivo* azidohomoalanine biosynthesis

3.2.5.1 In vivo Biosynthesis of Azidohomoalanine and in vitro Testing

The preceding data established a positive correlation between the overexpression of the metG gene and an increase in Nisin expression. However, a critical limitation of this engineered system remains its exogenous requirement for azidohomoalanine supplementation. From the large-scale bioproduction perspective, the utilization of Aha presents a significant obstacle to economic feasibility due to high costs associated with this non-canonical amino acid. Thus, the current methodology is impractical for industrial application. A potential strategy to circumvent this economic constraint involves endowing the host organism with the capacity for *de novo* azidohomoalanine synthesis. Prior scientific work has successfully demonstrated the feasibility of engineering an azidohomoalanine biosynthetic pathway. Implementing this approach would negate the need for exogenous supplementation of the amino acid thereby enhancing the overall commercial viability of the Nisin production system.

Prior work has successfully demonstrated the feasibility of generating by Aha by repurposing the trans-sulfuration pathway sourced from *Corynebacterium glutamicum*.[22] This pathway, absent in *E. coli*, initiates with homoserine acetyltransferase (HSAT, encoded by metX) catalyzing L-homoserine activation to yield O-acetyl-L-homoserine (OAHS). The metabolic orthogonality of OAHS in *E. coli* ensures selective channeling toward the engineered pathway, minimizing undesirable side reactions. Subsequently, O-acetylhomoserine sulfhydrylase (MetY), a pyridoxal phosphate-dependent enzyme of the fold-type II subclass, catalyzes the displacement of the acetyl group with azide nucleophiles, producing azidohomoalanine. Notable enzymes within this group include the β-subunit of tryptophan synthase and *O*-acetylserine sulfhydrylase (OASS). OASS plays a crucial role in *L*-cysteine biosynthesis and exhibits substrate promiscuity, accepting various thiols, selenols[126], azides, cyanide, and aromatic five-membered heterocycles with at least two adjacent nitrogen atoms as nucleophiles.[127] The biosynthesis of azidohomoalanine involves the

nucleophilic displacement where the azide displaces the acetyl group from Oahs resulting in the clickable non-canonical amino acid.

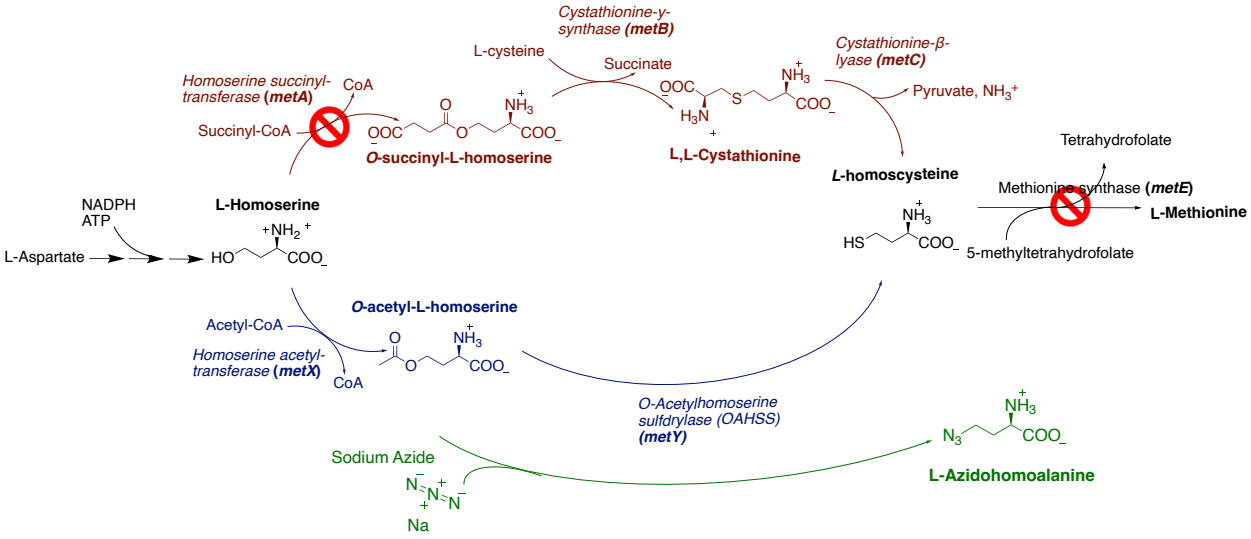


Figure 40. Engineering of direct sulfhydrylation pathway in E. coli methionine metabolism for azidohomoalanine biosynthesis. Scheme representing the potential for Aha biosynthesis where the *metA* and metE are knocked out and direct sulfhydrylation pathway enzymes *cg*HSAT and *cg*OAHSS are introduced. Knockout of *metA* and *metE* results in complete blockage of methionine biosynthesis in *E. coli*. The trans-sulfuration pathway is shown in maroon, direct sulfhydrylation pathway in blue, L-azidohomoalanine production in green.

Prior to *in vivo* biosynthesis validation, *in vitro* characterization of MetY enzyme activity was conducted using purified recombinant protein. The metY gene was amplified from pDo-ColA-RE-rhaB-metY-metX-LE (PM456) and cloned into pQE80L-His-TEV-EcProS (PM519) using Gibson Assembly with the GeneArt™ HiFi Cloning Kit. Successful insertion was confirmed through restriction digest analysis using BamHI and HindIII enzymes, yielding expected fragments of 4700 bp, 1059 bp, and 288 bp, followed by sequence verification. (**Appendix Figure 9**)

For protein expression, overnight cultures were grown in LB medium at 37°C for 4 hours, followed by induction with 0.5 mM IPTG and overnight incubation at 30°C. MetY purification was achieved through sequential affinity chromatography and ion exchange chromatography (**Appendix Figure 10**). *In vitro* enzymatic assays were performed to evaluate O-acetylhomoserine to azidohomoalanine conversion efficiency. Reaction

progress was monitored using thin layer chromatography (TLC) with a mobile phase consisting of butanol:acetic acid:water (12:3:5). **(Materials and Methods)** Amino acid visualization was accomplished using ninhydrin staining, which reacts with primary amino groups to form Ruhemann's purple.[128] Temperature optimization studies were conducted at room temperature, 37°C, and 50°C to determine optimal reaction conditions. (**Figure 41**)

Restriction digest analysis confirmed successful MetY insertion into the pQE80L vector, with observed fragment sizes matching theoretical predictions. Protein purification yielded high-purity MetY enzyme suitable for biochemical characterization. TLC analysis revealed successful conversion of O-acetylhomoserine to azidohomoalanine, with the product exhibiting greater mobility than the substrate. Complete substrate conversion was achieved within 2 hours under optimal conditions. (**Appendix Figure 12).** Temperature optimization studies demonstrated that 37°C yielded the highest conversion efficiency to azidohomoalanine product. At room temperature, the reaction achieved approximately 50% conversion (substrate:product ratio of 50:50), while 50°C also yielded 50% conversion but was associated with amino acid degradation, rendering this temperature suboptimal for practical applications.

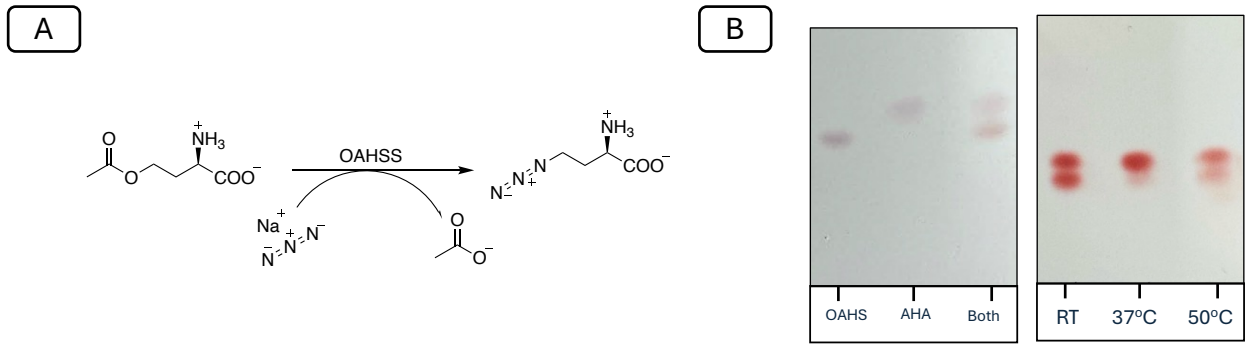


Figure 41. Enzymatic production of L-azidohomoalanine with MetY enzyme (OAHSS) (A) Reaction scheme showcasing enzymatic production of azidohomoalanine with sodium azide precursor. **(B)** Ninhydrin strain thin-layer chromatography of MetY-catalyzed synthesis of Aha. Left image – Controls run with OAHS (lane 1), Aha (lane 3) and co-spot (lane 3), showing compounds can be resolved by TLC. Right image – MetY catalyzed reactions carried out at various temperatures; RT (lane 1), 37°C (lane 2), 50°C (lane 3). The best condition was deemed to be 37°C which resulted in the highest conversion of OAHS to Aha.

Following confirmation of MetY enzyme activity through *in vitro* characterization, the subsequent phase involved validating azidohomoalanine biosynthesis under *in vivo* conditions. Previous research by Schipp *et al.*[21] established a comprehensive system for endogenous azidohomoalanine production through co-expression of MetY and MetX enzymes from *Corynebacterium glutamicum*. Their approach utilized sodium azide supplementation to redirect cellular metabolism toward azidohomoalanine production instead of *L*-homocysteine biosynthesis. The system required engineered double knockouts of *metA* and *metE* genes, which encode enzymes responsible for the initial and terminal steps of E. coli methionine biosynthesis, respectively. These genetic modifications prevent endogenous methionine production while eliminating *L*-homocysteine accumulation through metA deletion.

The original system employed plasmid-based MetXY expression under constitutive glnS' promoter control. Our investigation utilized an alternative approach featuring genomically integrated MetXY genes regulated by an inducible *L*-rhamnose promoter system, designated as strain MS39. (**Figure 42**) This design provides enhanced genetic stability and controllable expression levels compared to plasmid-based systems, potentially offering improved performance for biotechnological applications.

Genomic integration of MetXY was verified through PCR amplification and confirmed by whole-genome sequencing, which identified the integration site downstream of the tktB gene at site 2. (**Appendix Figure 7**) Following established protocols[21], experiments incorporated 0.8 μM sodium azide and 1 mM pantothenic acid supplementation to facilitate continuous azidohomoalanine biosynthesis and cellular accumulation. Unlike the constitutive expression system, MetXY expression was induced using *L*-rhamnose to provide temporal control over pathway activation.

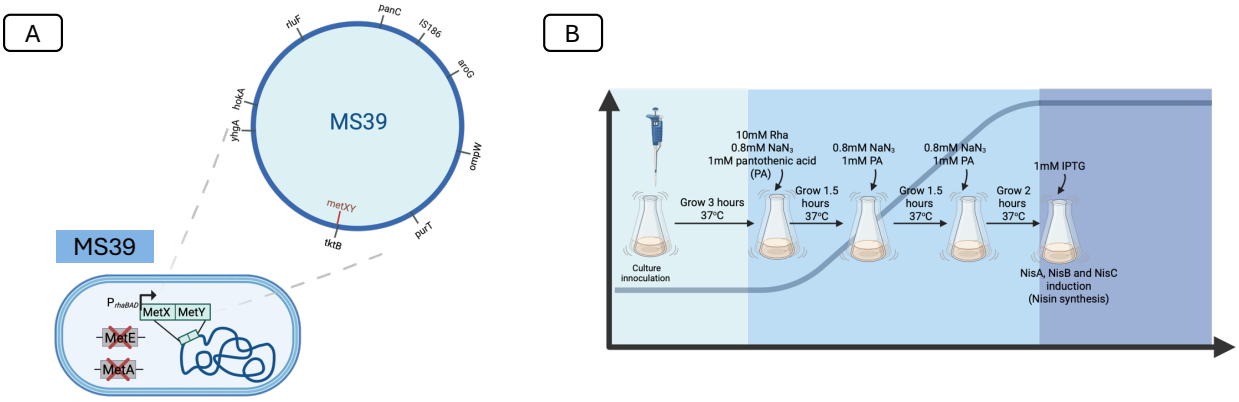


Figure 42. Visualization of Genomic Integrations and Expression Scheme for Azidohomoalanine Biosynthetic Strain (A) Schematic representation of the *E. coli* genome illustrating the integration sites of Met X and MetY in strains MS39**.** Newly integrated copies are highlighted in red. Genomic sequencing confirmed that strain MS39 contained single insertion after gene *tktB*. **(B)** Expression strategy optimized for ncAA incorporation azidohomoalanine biosynthesis strain. The overnight culture is washed with NMM and inoculated into minimal media with a limiting concentration of methionine (35µM). At 3 hours, 10mM *L*-Rha, 0.8mM NaN_3 and 1mM pantothenic acid were added for azidohomoalanine biosynthesis. 2 more addition of the precursors followed 1.5 hours apart resulting in 3 additions of NaN_3 and pantothenic acid. Once stagnant growth is reached, the desired ncAA is added to the culture and incubated for 30 minutes. Subsequently, the expression of Nisin biosynthetic genes (*nisA*, *nisB*, and *nisC*) is induced with 1mM IPTG. Created with Biorender.

Initial validation employed the model protein EGFP using plasmid pQE80L_EGFP_4M transformed into strain MS39. Comparative analysis was conducted using the reference strain BU345 (MDS15A1)[21] co-transformed with pSEVA26'glnS-metY-metX (PM181) to benchmark performance against the established system. The experimental protocol involved MetXY induction followed by triple supplementation with sodium azide and pantothenic acid at 1.5-hour intervals. Following methionine depletion from the culture medium, EGFP expression was induced using IPTG and conducted overnight at 30°C. Expression levels were quantified through fluorescence intensity measurements normalized to optical density at 600 nm using 96-well microplate format. Protein purification was performed according to established protocols, followed by chloroform:methanol precipitation to remove interfering substances prior to mass spectrometric analysis. ESI-MS was employed to determine incorporation efficiency and confirm azidohomoalanine substitution in the expressed proteins.

Comparative expression analysis revealed an approximately 4-fold higher EGFP expression level in strain MS39 compared to the reference BU345 strain in this experiment (n = 1), suggesting the genomically integrated system may support higher protein production, though this observation was not replicated. (**Figure 43**) Mass spectrometric analysis of purified EGFP from MS39 revealed predominately wildtype protein with an observed mass of $[M_{obs} + H]^+ = 27675.31\ Da$, corresponding closely to the calculated wild-type EGFP mass $M_{calc} + H]^+ = 27677.14\ Da$. This indicated minimal azidohomoalanine incorporation despite high expression levels. In contrast, EGFP expression in strain BU345 exhibited partial azidohomoalanine incorporation with an observed mass of $[M_{obs} + H]^+ = 27671.24\ Da$, demonstrating detectable non-canonical amino acid substitution.

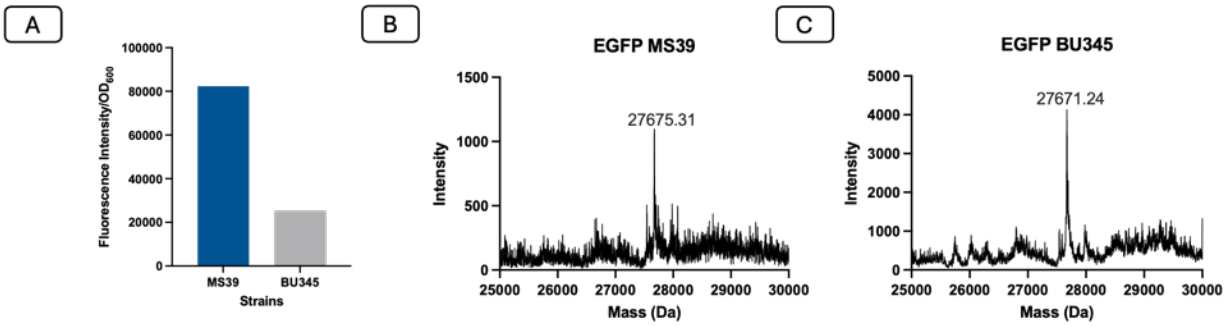


Figure 43. Comparative Expression and Mass Spectrometry Analysis of EGFP with azidohomoalanine biosynthetic strains. **(A)** Quantitative comparison of EGFP expression levels across various *E. coli* strains when expressed in NMM. Expression levels of azidohomoalanine biosynthetic strains were compared. The strain MS39 contained genomic insertions of MetXY while BU456 contains plasmid pSEVA26'glnS-metY-metX for protein expression. Higher expression is seen with genomically integrated strain (n=1). **(B)** ESI-MS analysis of azidohomoalanine labelled EGFP expressed in MS39. The observed [M+H]+ deconvoluted peak mass of 27675.31 Da corresponds to Met labelled EGFP, no Aha labelling occurs. **(C)** ESI-MS analysis of azidohomoalanine labelled EGFP expressed in BU4345. The observed [M+H]+ deconvoluted peak mass of 27671.24 Da corresponds to partial incorporation of Aha into EGFP.

The higher expression levels observed in strain MS39 demonstrate the advantages of genomic integration for stable, high-level protein production. However, the minimal azidohomoalanine incorporation suggests that enhanced expression levels do not necessarily correlate with improved non-canonical amino acid incorporation efficiency. The superior incorporation observed in the reference strain BU345 indicates that the original

plasmid-based constitutive expression system may provide more favorable conditions for azidohomoalanine biosynthesis and incorporation.

Following successful azidohomoalanine biosynthesis demonstration, the system was applied to Nisin production. Strain MS39 was selected over BU345 due to its genomically integrated MetXY genes, providing enhanced stability for extended applications. Plasmids pET3a_NisA_M21V and pRSFDuet_NisBC were transformed into MS39 and compared to BU14 (requiring exogenous azidohomoalanine). MS39 followed protocols (**Materials and Methods)** with sodium azide and pantothenic acid supplementation for endogenous azidohomoalanine biosynthesis.

Expression levels were compared via antimicrobial assays, and purified PreNisin was analyzed by ESI-MS. In this experiment (n = 1), BU14 showed approximately 3–4 fold higher Nisin expression than MS39. ESI-MS analysis revealed multiple peaks corresponding to different modification states. The most abundant peak corresponded to the fully modified methionine-containing M21V-PreNisin ($[M_{obs} + H]^+ = 7267.50$ *Da),* $[M_{calc} + H]^+ = 7268.54$ *Da)*. Additional methionine-containing species included single mis-dehydrated peptides ($[M_{obs} + H]^+ = 7286.45$ *Da*), $[M_{calc} + H]^+ + H_2O = 7286.56$ *Da)* and double mis-dehydrated peptides *(*$[M_{obs} + H]^+ + 2H_2O = 7305.5$ *Da*, $[M_{calc} + H]^+ + 2H_2O) = 7304.57$ *Da*).

Azidohomoalanine-labelled species included a partially modified M21V-PreNisin-Aha lacking four dehydrations *(*$[M_{obs} + H]^+ + 42H_2O = 7335.5$ *Da*), representing 64% intensity of the fully modified methionine peptide. A second azidohomoalanine peak was observed *(*$[M_{obs} + H]^+ + 5H_2O$ = 7253.50 Da), $[M^{calc} + H]^+ + 5H_2O = 7353.61$ *Da)* corresponding to peptides missing five dehydrations. Comprehensive analysis indicated 39% azidohomoalanine incorporation efficiency.

The reduced expression observed in the MS39 strain is consistent with the metabolic burden of simultaneous Nisin and azidohomoalanine biosynthesis, relative to the simpler system in the BU14 strain. The 40% incorporation efficiency demonstrates feasibility of endogenous biosynthesis approaches, establishing proof-of-concept for eliminating expensive exogenous supplementation while maintaining functional peptide production.

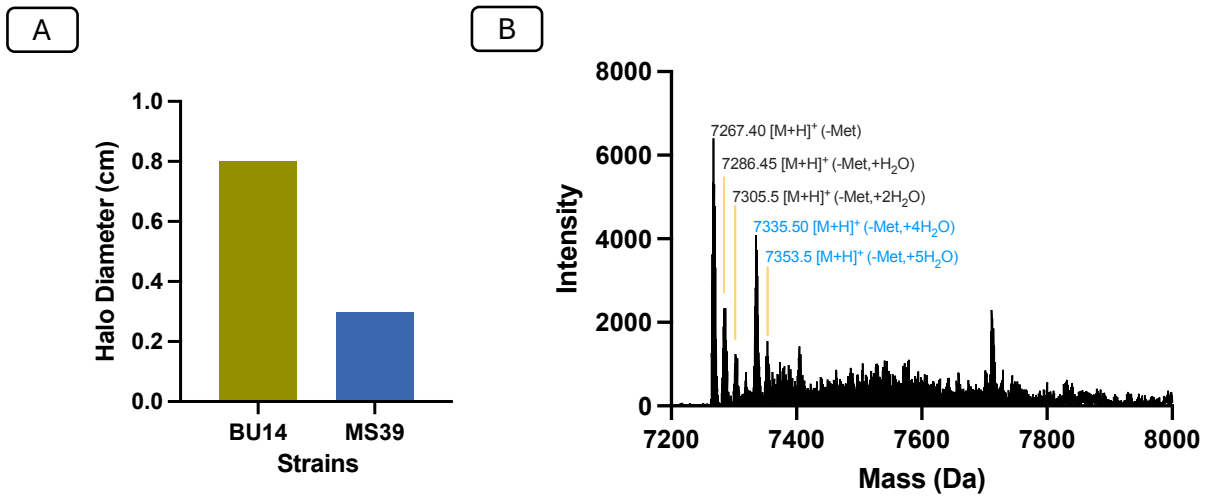


Figure 44. Comparative Expression and Mass Spectrometry Analysis of Nisin M21V with azidohomoalanine biosynthetic strain. (A) Antimicrobial assay halos comparing Nisin M21V expression levels across various *E. coli* strains when expressed in NMM. Expression levels of control strain requiring Aha addition (BU14) and the azidohomoalanine biosynthetic strain (MS39) were compared. Higher expression is seen with the control strain of BU14. (n=1) **(B)** ESI-MS analysis of azidohomoalanine labelled Nisin M21V expressed in MS39. The deconvoluted mass peaks with methionine are shown in black while azidohomoalanine Nisin peaks are shown in blue. Methionine containing Nisin peaks are observed for the fully modified form ($[M+H]^+$ = 7267.40 Da) and partially modified forms($[M+H]^+$ = 7286.45 Da and $[M+H]^+$ = 7305.5 Da). Azidohomoalanine containing Nisin peaks are observed only for the partially modified forms ($[M+H]^+$ = 7335.5 Da and $[M+H]^+$ = 7353.5 Da).

Previous analysis demonstrated that MetG co-expression in strains BU14 and MS51 resulted in doubled expression levels and enhanced azidohomoalanine incorporation efficiency *(Appendix Figure 8)*. Given the established benefits of methionyl-tRNA synthetase co-expression for both protein production and non-canonical amino acid incorporation, rational design dictates integrating MetG into the azidohomoalanine biosynthesis system. The CRISPR-associated transposition (CAST) system enables precise chromosomal integration of MetG into existing strains or sequential integration of MetXY into MetG-containing strains.

The VchCAST system from *Vibrio cholerae* comprises of two functional modules executing RNA-guided transposition. The targeting module (QCascade complex containing Cas6, Cas7, and Cas8-Cas5 fusion protein) utilizes CRISPR RNA to identify complementary chromosomal sites through protospacer adjacent motif recognition. The accessory protein

TniQ associates with this complex to recruit transposition machinery. The transposition module features the TnsA/TnsB complex responsible for precise cargo DNA excision and integration. TniQ initiates the process by recruiting TnsC, establishing the molecular bridge between targeting and transposition complexes. Within the transposition machinery, TnsA mediates initial DNA cleavage while TnsB functions as the primary integrase, catalyzing strand transfer reactions. Integration occurs approximately 50 bp downstream of the TniQ-Cascade R-loop, generating characteristic 4 bp target site duplications (Tsd) flanking the inserted cargo DNA containing Left End (LE) and Right End (RE) sequences.[129]

Three strains were selected for initial integration: MS39 (single *metXY* copy), MS51 (multiple *metG* copies), and MS61 (5 *metG* copies). Donor plasmids containing either the *metG* or *metXY* were co-transformed with pEffector plasmid containing transposition machinery. Overnight cultures grown in LB with kanamycin and spectinomycin were diluted 100-fold and plated on apramycin-containing media for transposition induction at 30°C for two days (**Material and Methods**). Colony PCR was performed using primers flanking intended integration sites to confirm successful integration events. Positive integration was identified by higher molecular weight bands corresponding to insert size and absence of native lower molecular weight bands. Successfully integrated strains underwent plasmid curing using pCutamp transformation followed by sucrose counter-selection to eliminate resistance markers, generating marker-free strains. Strain MS89 required additional *metA* gene knockout to block the transsulfuration pathway and prevent homocysteine accumulation. The *metA* knockout was achieved by inserting premature stop codons, with sequencing confirmation of both *metXY* integration and metA disruption.

Successful integration events were observed only in MS51 and MS61 strains (**Figure 45**). MS51 yielded strain MS88 with three new *metG* integration sites, while MS61 produced strain MS89 with one MetXY integration at site 2. PCR analysis confirmed MS89 exhibited novel insertion characteristics with higher molecular weight consistent with *metXY* integration, supported by sequencing results. MS88 showed bands matching *metG* size rather than the expected 5-6 kb MetXY bands.

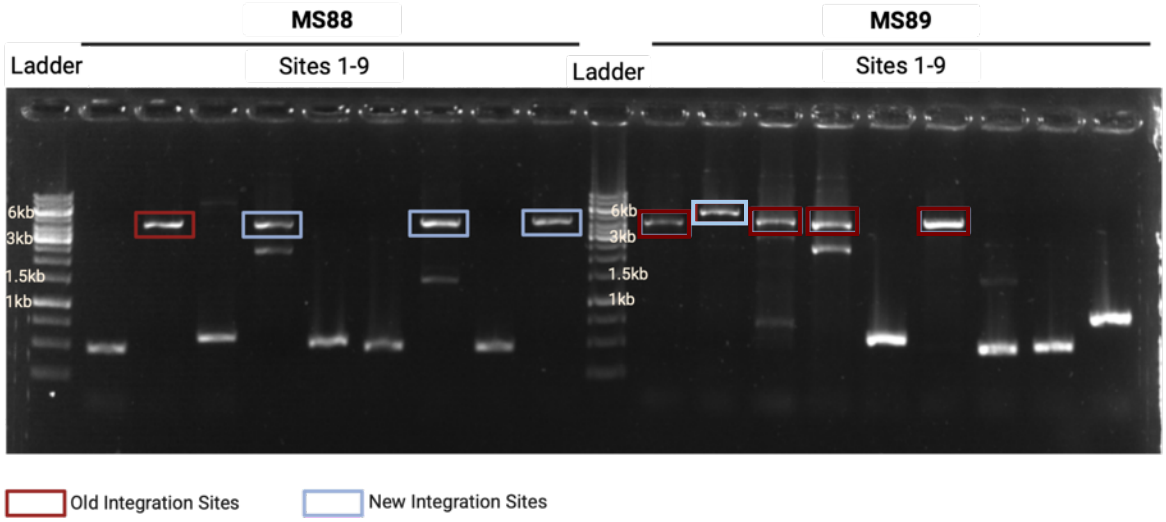


Figure 45. Agarose Gel Verification of Multi-Site Genomic Integration in Strains MS88 and MS89. Colony PCR was used to verify successful site-specific integration of target genes across multiple loci in the *E. coli* genome. 1 kb ladder was used molecular weight marker and primers pairs flanking the 9 insertion sites were utilized for PCR screening. Successful integration is evident by larger molecular weight product (~3.5 to 5 kb) corresponding to genomic region plus the integration cargo DNA. Strain MS88, previously contained integration at site 2 of MetG and new integrations appear at sites 4,7 and 9. The strain MS89 contained 4 previous insertions at sites 1,3,4, and 6 of MetG and a new insertion appears at site 2 at a molecular weight expected of MetXY. In addition, the absence of the native lower molecular weight bands in the positive lanes confirms the successful integrations. Old integration sites are shown in red boxes, and new integration sites are shown in blue boxes.

Plasmid curing was successfully completed, with colonies growing exclusively on sucrose-containing media and showing no growth on selective antibiotics, confirming complete elimination of extraneous plasmids. Sequencing confirmed *metXY* integration at site 2 following the *tktB* gene and successful *metA* knockout in the final strain MS94 (**Appendix Figure 11**).

The successful integration of MetXY into MS61 (creating MS89) demonstrates the feasibility of combining MetG overexpression with azidohomoalanine biosynthetic capability. The failure to achieve MetXY integration in MS88 while maintaining MetG integration suggests potential technical limitations or integration site preferences that warrant further investigation. The requirement for *metA* knockout in MS89 highlights the importance of metabolic pathway control in engineered biosynthetic systems. The resulting strain MS94 (**Figure 46**), containing dual gene knockouts (*metA* and *metE*) and dual gene integrations (*metG* and *metXY*), represents a sophisticated platform combining enhanced

aminoacylation capacity with endogenous azidohomoalanine biosynthesis. This strain design addresses both the incorporation efficiency bottleneck through MetG overexpression and the economic constraints through elimination of exogenous azidohomoalanine supplementation, establishing a foundation for optimized non-canonical amino acid incorporation in biotechnological applications.

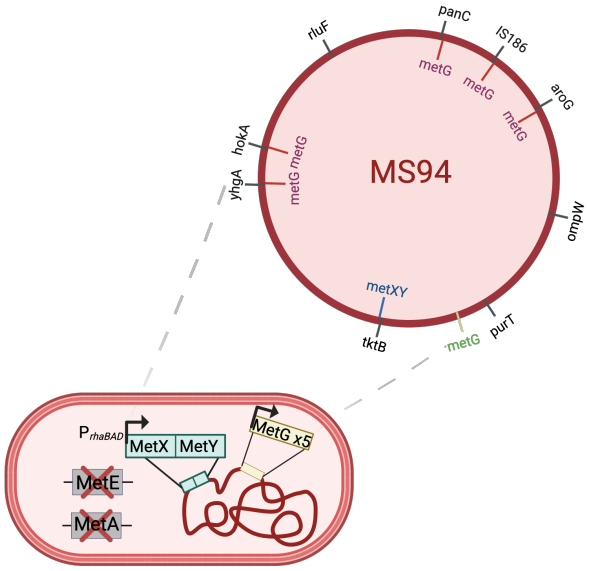


Figure 46. Visualization of Genomic Integrations for multifunctional strain MS94 Schematic representation of the *E. coli* genome illustrating the integration sites of MeXY and MetG in strains MS94**.** Previous strain MS61 was used the base strain, and already present MetG integrations sites are shown in red. Genomic sequencing confirmed the new successful single insertion of *metXY* after gene *tktB* in MS94. Created with Biorender

The complex multiprotein expression system in strain MS94, may exceed the metabolic capacity supported by minimal media, necessitating alternative cultivation approaches. The simultaneous expression of Nisin biosynthetic machinery, azidohomoalanine production enzymes, and MetG overexpression creates substantial cellular burden that requires optimization of nutrient availability and expression timing. Additionally, the post-translational modification machinery (dehydratase and cyclase) contains numerous methionine residues that may be compromised during methionine depletion, potentially affecting proper Nisin modification when azidohomoalanine incorporation occurs.

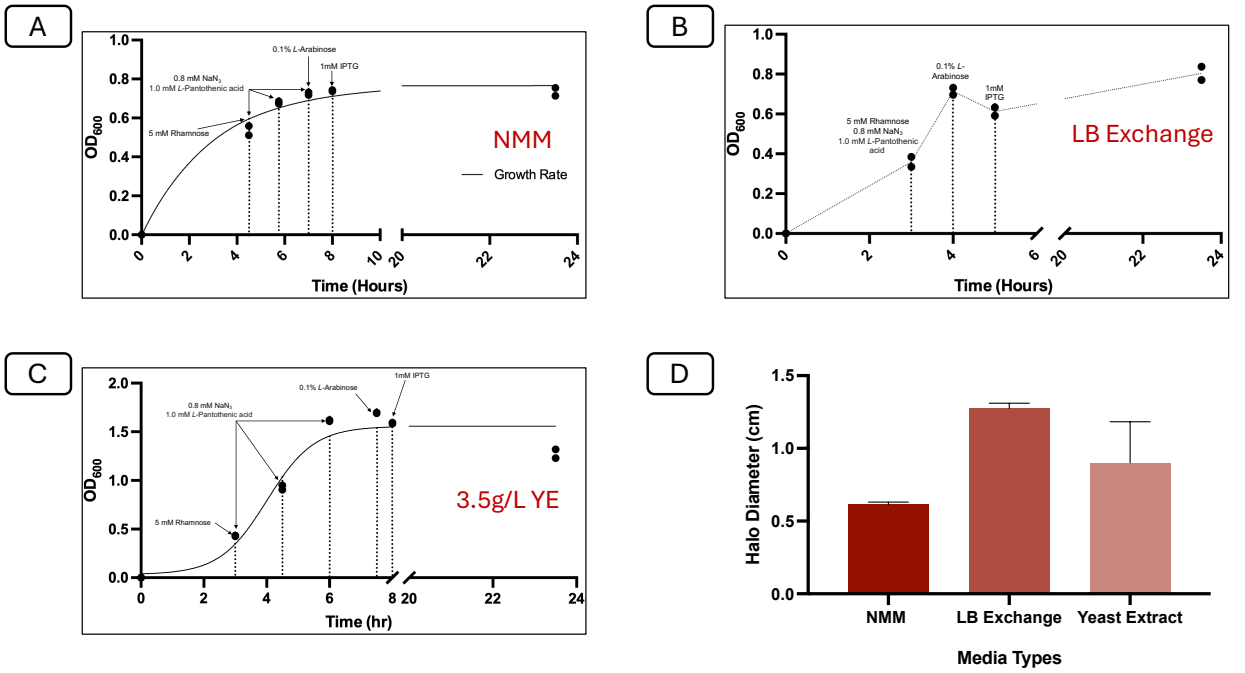


Figure 47. Optimization of Nisin M21V Expression in MS94 Using Various Culture Media. Comparative expression of Nisin-M21V-Aha in strain MS94 across three distinct culture media optimization strategies (A-C) with resulting expression quantified in (D). In all cases, 1mM IPTG was used to induce Nisin expression after stagnant growth was reached. Protein expressed at 28°C overnight with 250 rpm shaking. **(A)**, **(B)** and **(C)** display growth curves and detail the sequential induction protocols, including specific timing and concentrations used for Aha biosynthesis (via *L*-Rha, NaN3, and *L*-pantothenic acid) and MetRS (via *L*-arabinose) under conditions ranging from New Minimal Media (A), a LB-to-NMM transfer (B) and NMM supplemented with 3.5g/L yeast extract (C). (n=2) **(D)** Antimicrobial assays showcasing Nisin-M21V-Aha expression is various expression media. Normalized cell lysates (OD_{600}=5.0) were tested again the indicator strain Lactococcus lactis NZ900 (pNGNisPT) on GM17 agar plates to quantify functional yield of Nisin-M21V-Aha produced under each optimized media condition. Data represent mean ± SD (n = 2)

Three alternative media conditions were evaluated: (1) yeast extract supplementation as methionine source, (2) LB media exchange protocol involving initial azidohomoalanine biosynthesis induction in LB followed by transfer to methionine-free minimal media, and (3) new minimal media (NMM) as control. Growth curves were generated by monitoring OD_{600} at various time points, with protein induction occurring at different intervals for each condition (**Figure 47 A-C**). Following expression optimization, proteins were purified from each condition and subjected to mass spectrometry analysis. A novel plasmid was engineered placing NisBC (dehydratase and cyclase) under constitutive promoter control while maintaining NisA (Nisin peptide) under inducible T7 promoter regulation. This approach

aimed to ensure adequate modification machinery availability prior to methionine depletion and azidohomoalanine incorporation.

Growth analysis revealed maximum optical density of approximately 0.8 in new minimal media, while yeast extract media achieved doubled growth capacity. LB exchange media showed measurement inconsistencies due to the transfer process but yielded the highest Nisin expression levels. Only the LB exchange condition produced sufficient protein quantities for comprehensive mass spectrometry analysis. The precipitated proteins were then dissolved in a solution of 80% water (0.1% formic acid) and acetonitrile and analyzed at the Proteomics Centre.

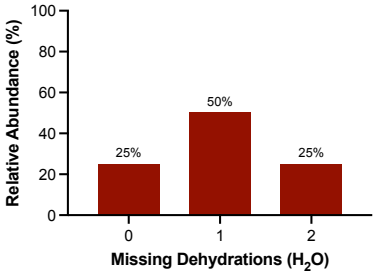
ESI-MS analysis of MS94-produced Nisin revealed distinct methionine and azidohomoalanine-labelled species with varying modification states (**Figure 48**). Methionine-containing peptides showed three prominent peaks: partially modified species lacking two dehydrations *($[M_{obs} + H]^+ + 2H_2O$* = 3355.58 Da, *$[M_{calc} + H]^+ + 2H_2O$* = 3358.11 Da), fully modified peptide *($[M_{obs} + H]^+$* = 3319.57 Da, *$[M_{calc} + H]^+ + 2H_2O$* = 3322.10 Da) and a single mis-dehydrated species *($[M_{obs} + H]^+ + H_2O$* = 3337.57 Da, *$[M_{calc} + H]^+ + H_2O$* = 3340.11 Da). Azidohomoalanine-labeled peptides exhibited predominantly under-modified species, with the most prevalent peak lacking seven dehydrations ($[M_{obs} + H]^+ + 7H_2O$ = 3440.40 Da, $[M_{calc} + H]^+ + 7H_2O$ = 3440.40 Da). Additional species ranged from completely unmodified *($[M_{obs} + H]^+ + 8H_2O$* = 3458.59 Da) to partially modified forms lacking two dehydrations *($[M_{obs} + H]^+ + 2H_2O$* = 3350.59 Da). No fully modified azidohomoalanine-containing peptides were detected, and various dehydrated states were observed and listed the corresponding figure.

Comparative analysis of constitutive versus inducible NisBC expression demonstrated higher overall Nisin expression with inducible promoter control, though constitutive expression may enhance proper modification of azidohomoalanine-labeled peptides (**Appendix Figure 15**).

The superior performance of LB exchange media demonstrates that initial growth in nutrient-rich conditions followed by controlled amino acid depletion provides optimal cellular capacity for complex multi-protein expression systems. The absence of fully modified

azidohomoalanine-labeled Nisin suggests that methionine depletion compromises the post-translational modification machinery, likely due to the methionine-rich composition of NisB and NisC enzymes.

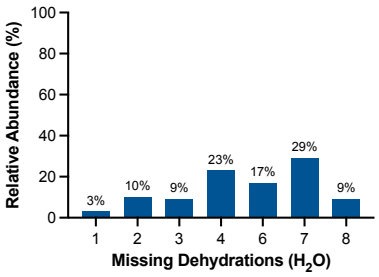
A



B

Missing Dehydrations (H_2O)	Species Description	Expected Mass (Da)	Observed Mass (Da)
0	Fully Modified	3319.568	3319.57
1	Partially Modified (+H_2O)	3337.568	3337.568
2	Partially Modified (+2H_2O)	3355.568	3355.5838

C



D

Missing Dehydrations (H_2O)	Species Description	Expected Mass (Da)	Observed Mass (Da)
1	Partially Modified (+H_2O)	3332.6106	3332.6
2	Partially Modified (+2H_2O)	3350.6211	3350.5908
3	Partially Modified (+3H_2O)	3368.6211	3368.598
4	Partially Modified (+4H_2O)	3386.6211	3386.5843
6	Partially Modified (+6H_2O)	3422.6211	3422.5894
7	Partially Modified (+7H_2O)	3440.6211	3440.604
8	Unmodified (+8H_2O)	3458.6211	3458.591

Figure 48. Analysis of Nisin-M21V Modification Profiles and Extent of Dehydration in Engineered MS94 strain. (A) Relative Met-containing species observed with varying dehydrations from 0-2 **(B)** Relative Aha-containing species observed with varying dehydrations from 1-8 **(C&D)** Tables correlating the expected and observed deconvoluted masses (in Da) for Nisin species identified in (A) and (B) respectively. These tables confirm the molecular masses corresponding to the fully modified, partially modified (with varying degrees of H_2O retention), and unmodified Nisin peptides with presence of either Met (C) or Aha (D).

The predominance of under-modified azidohomoalanine-containing peptides compared to properly modified methionine-containing species indicates a temporal mismatch between modification machinery availability and substrate presentation. The constitutive expression approach for NisBC represents a promising strategy to address this limitation by ensuring adequate enzyme levels prior to methionine depletion and azidohomoalanine incorporation. These findings establish the feasibility of endogenous azidohomoalanine biosynthesis and successful incorporation into Nisin while highlighting critical optimization requirements for achieving proper post-translational modifications. The system demonstrates proof-of-

concept for eliminating exogenous azidohomoalanine supplementation but requires further refinement of expression timing and nutrient availability to achieve fully functional modified peptides comparable to conventional production systems.

3.2.6 “All-in strain: Development of Modified Nisin A producing cell factory

Despite the demonstrated efficacy of the previous expression system, its dependence on extrachromosomal plasmids introduces significant limitations for large-scale production applications. The requirement for antibiotic selection to maintain plasmid stability substantially increases operational costs and renders the system unsuitable for high-volume commercial production. To address these constraints and develop a cost-effective, high-yield process for azidohomoalanine-labeled Nisin, establishing an antibiotic-free production system through stable chromosomal integration of all requisite biosynthetic genes becomes essential. Given that genes for azidohomoalanine biosynthesis (*metXY*) and incorporation enhancement (*metG*) had been previously integrated, the remaining objective involves chromosomal integration of Nisin biosynthetic genes (*nisABC*) to eliminate all antibiotic dependencies.

Utilizing the CAST system, strain MS105 was developed incorporating chromosomally integrated *metG*, *metXY,* and *nisABC* genes. The *nisBC* genes were placed under constitutive promoter control while *nisA* remained under inducible T7 promoter regulation, creating a completely antibiotic-free system. Genomic sequencing was performed to verify integration integrity and identify insertion sites throughout the *E. coli* chromosome. Based on previous optimization studies demonstrating superior performance with LB-to-minimal media transfer protocols, a two-stage expression approach was implemented. Stage one involved azidohomoalanine biosynthesis gene induction in LB media with concurrent sodium azide and *L*-pantothenic acid supplementation, while NisBC modification machinery underwent constitutive expression. Stage two encompassed culture transfer to minimal media, MetG induction, and subsequent NisA induction following complete methionine depletion. Comparative analysis was conducted between the new chromosomally integrated strain (MS105) and the previous plasmid-based system (MS94) to assess the functional consequences of genomic versus plasmid-mediated expression. Antimicrobial bioassays

were employed to quantify Nisin expression levels across both systems and culture conditions.

Genomic sequencing confirmed retention of all previous integrations alongside eight novel nisABC integrations distributed throughout the chromosome (**Figure 49**). Integration sites were identified downstream of genes, *mdlB, nagA, marA, asd,* and *duf*, demonstrating successful incorporation of 14 total genes without genomic instability.

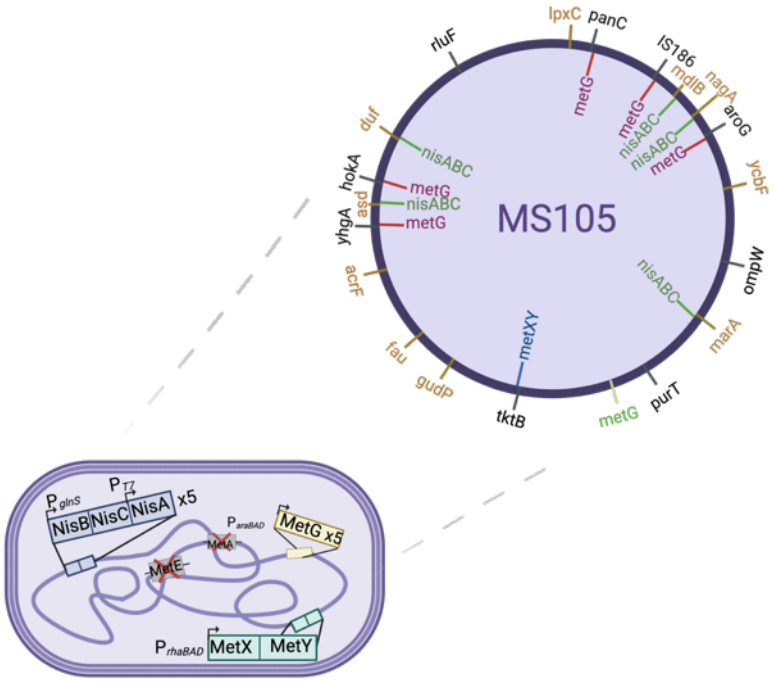


Figure 49. Visualization of Genomic Integrations for 'ALL-IN" strain MS105. Schematic representation of the *E. coli* genome illustrating the integration sites of meXY, *metG* and nisABC in strain MS105. Strain MS94 was used the base strain, previously containing *metG* and *metXY* integrations sites are shown in red and blue respectively. Genomic sequencing confirmed the 5 successful insertions of *nisABC* (shown in green) located scattered across the genome. The black insertion sites shown are targets of PM 452 while *nisABC* was inserted into sites targeted by PM511 (shown in yellow). Created with Biorender

Comparative expression analysis revealed that plasmid-mediated expression (MS94) yielded elevated Nisin production levels compared to chromosomally integrated expression (MS105) across both minimal and LB media conditions (**Figure 50**). Consistent with previous observations, LB media supported superior Nisin production compared to minimal media for both expression systems. While expression levels remained consistent within each

system, the chromosomally integrated strain demonstrated reduced overall productivity compared to its plasmid-based counterpart.

The successful integration of 11 genes into the *E. coli* chromosome without compromising genomic stability demonstrates the robustness of the CAST system for complex multi-gene integration projects. The distributed integration pattern across multiple chromosomal loci suggests effective utilization of available integration sites while maintaining cellular viability.

The reduced expression levels observed in the chromosomally integrated system compared to plasmid-based expression likely reflect differences in gene copy number and transcriptional accessibility. Plasmid-based systems typically provide higher gene dosage due to multiple plasmid copies per cell, whereas chromosomal integration yields single-copy expression that may limit overall productivity. However, the chromosomal system offers superior genetic stability and eliminates costly antibiotic requirements, representing a favorable trade-off for industrial applications where consistency and cost-effectiveness outweigh maximum yield considerations.

The achievement of antibiotic-free azidohomoalanine-labeled Nisin production establishes a foundation for economically viable large-scale biotechnological applications. While further optimization may be required to match plasmid-based expression levels, the system demonstrates proof-of-concept for sustainable, cost-effective production of modified antimicrobial peptides without external dependencies on expensive supplements or selection agents.

The nisin production platform developed in this thesis differs methodologically from prior approaches to introducing non-canonical amino acids into lantibiotics. Bartholomae et al.[130] incorporated Nε-Boc-L-lysine into nisin in both *E. coli* and *L. lactis* using an orthogonal pyrrolysyl-tRNA synthetase/tRNA(Pyl) pair to suppress an amber stop codon at a single defined site, an approach requiring continuous external supplementation of the ncAA and yielding low levels of modified peptide, particularly in *L. lactis*. By contrast, the platform in

this thesis relies on residue-specific incorporation of methionine analogs via an overexpressed MetRS with relaxed substrate specificity, and genomic integration of the azidohomoalanine biosynthesis pathway removes the need for external ncAA supplementation altogether, distinguishing it as an autonomous, self-sufficient production system rather than one dependent on continuous analog dosing.

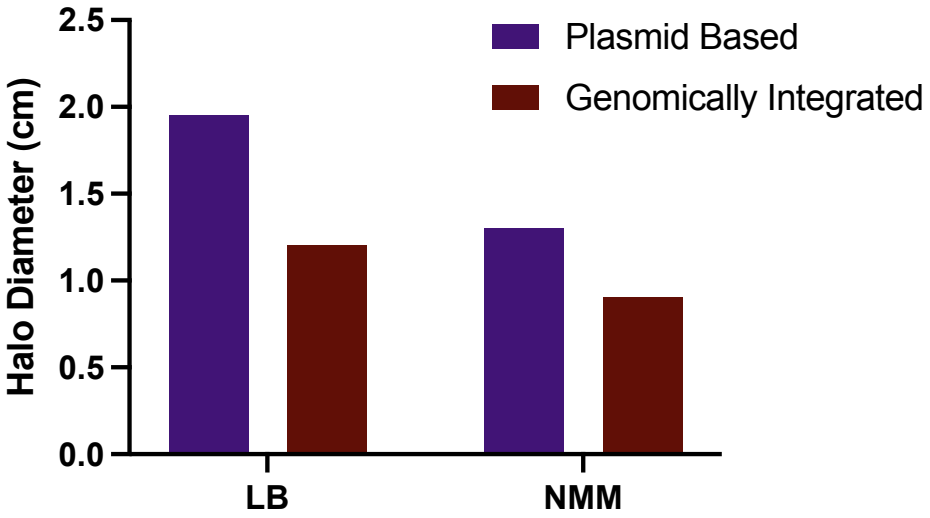


Figure 50. Comparative functional expression of Nisin -M21V-Aha from Plasmid-Based vs Chromosomally Integrated *nisABC* Genes. Antimicrobial assays were used to compare plasmid-based (MS94) and genomically integrated (MS105) *nisABC* genes and their effect on Nisin expression. Cell lysates (normalized OD_{600} = 5.0) were prepared from both strains cultured under two conditions: (1) LB-to-NMM transfer and (2) NMM only. 40µL of each lysate was loaded into wells in GM17 agar inoculated with the indicator strain *Lactococcus lactis* NZ9000 (pNGNisPT) and grown at 30°C overnight. The plasmid-based strain (MS94) consistently exhibits higher Nisin expression yield, which may be attributable to higher gene dosage by the multicopy plasmid. As anticipated, the LB-to-NMM transfer media strategy resulted in higher expression. The initial growth in rich LB medium support robust cell density and synthesis of precursors molecules required for muti-gene expression (n = 1)

3.2.7 Outlook: Toward functional conjugates

3.2.7.1 Readiness of azide/alkyne-labelled Nisin for click chemistry

Through the successful incorporation of non-canonical acids bearing the bioorthogonal functional groups, such as azides or alkynes, establishes Nisin as a versatile scaffold for subsequent chemical functionalization. These functional handles are chemically insert under physiological conditions yet highly reactive in selective ligations reactions, making them ideal for downstream modification without perturbing the native structure or antimicrobial activity of the peptide.

The azide- and alkyne-functionalized Nisin enables the use of copper-catalyzed azide–alkyne cycloaddition. The presence of a single, strategically positioned labelling site, through the substitution of methionine with analogs like azidohomoalanine or homopropargylglycine ensures site-selective conjugation. This design minimizes heterogeneity and preserves the structural integrity of Nisin, which is critical for maintaining its antimicrobial function.

Furthermore, the stability of these bioorthogonal groups throughout peptide biosynthesis, post-translational modification, and purification confirms their compatibility with the Nisin production system. As demonstrated by previous data, the azide-containing amino acid azidohomoalanine can be generated within the cell and subsequently incorporated into Nisin, while remaining stable throughout purification and Nisin cleavage. Notably, similar stability and incorporation efficiency are observed when Aha is supplied exogenously to the system. Importantly, the hinge-region mutant (e.g., M21V) provides an optimal site for incorporation, balancing accessibility for conjugation with retention of biological activity. This strategic placement enhances labeling efficiency while avoiding interference with key lanthionine ring structures involved in membrane interaction and pore formation.

The resulting azide- or alkyne-labelled Nisin is therefore “click-ready,” enabling modular conjugation to a wide range of functional moieties, including fluorophores for imaging, affinity tags for purification, or antimicrobial agents for dual-function therapeutics. This platform expands the chemical diversity and application potential of Nisin beyond its natural

limitations, positioning it as a tunable molecule for both mechanistic studies and therapeutic

3.2.7.2 Transition to dye/probe conjugation and downstream applications

Prior to applying click chemistry to a structural complex molecule such as Nisin, initial experiments were conducted using azidohomoalanine (Aha) as a simplified and well-controlled model substrate. This approach enabled validation and optimization of initial reaction conditions while minimizing potential confounding factors associated with Nisin such as structural constraints and inefficient labelling.

As outlined in **Figure 51**, azidohomoalanine (Aha) was reacted with dansyl-alkyne under standard copper-catalyzed azide–alkyne cycloaddition (CuAAC) conditions. The individual starting materials, Aha (Panel A; RT = 1.06 min) and dansyl-alkyne (Panel B; RT = 13.97 min), were first characterized by HPLC to establish baseline retention times. Initial evidence of reaction progression was obtained using thin-layer chromatography (Panel C), where the appearance of a new fluorescent species in the reaction lane indicates the formation potential of a conjugated product. Although minor impurities are present, this provides rapid qualitative confirmation of azide–alkyne reactivity. Further validation of product formation was achieved through HPLC analysis (Panel D), where a distinct peak corresponding to the putative product is observed alongside residual starting materials. Subsequent ESI-MS analysis (Panel E) confirmed the identity of the conjugated product. The starting materials were detected at the expected masses of 145.1 Da for Aha and 289.1 Da for dansyl-alkyne. Importantly, a peak at 433.2 Da was observed, consistent with the expected mass of the triazole-linked Aha–dansyl conjugate. This signal appears near a peak at 435.2 Da, corresponding to the copper-stabilizing ligand THPTA, further supporting successful cycloaddition under the reaction conditions.

Together, these results demonstrate that the azide functionality of Aha is both chemical accessible and reactive under selected CuAAC conditions, and that the reaction can be reliably monitored and confirmed using complementary analytical techniques. Establishing these conditions in a minimal system provides a critical foundation for subsequent

application to Aha-labelled Nisin, where additional structural complexity may influence reaction efficiency. This stepwise validation ensures that any challenges encountered in downstream systems can be attributed to substrate-specific factors rather than limitations in reaction design or detection methods.

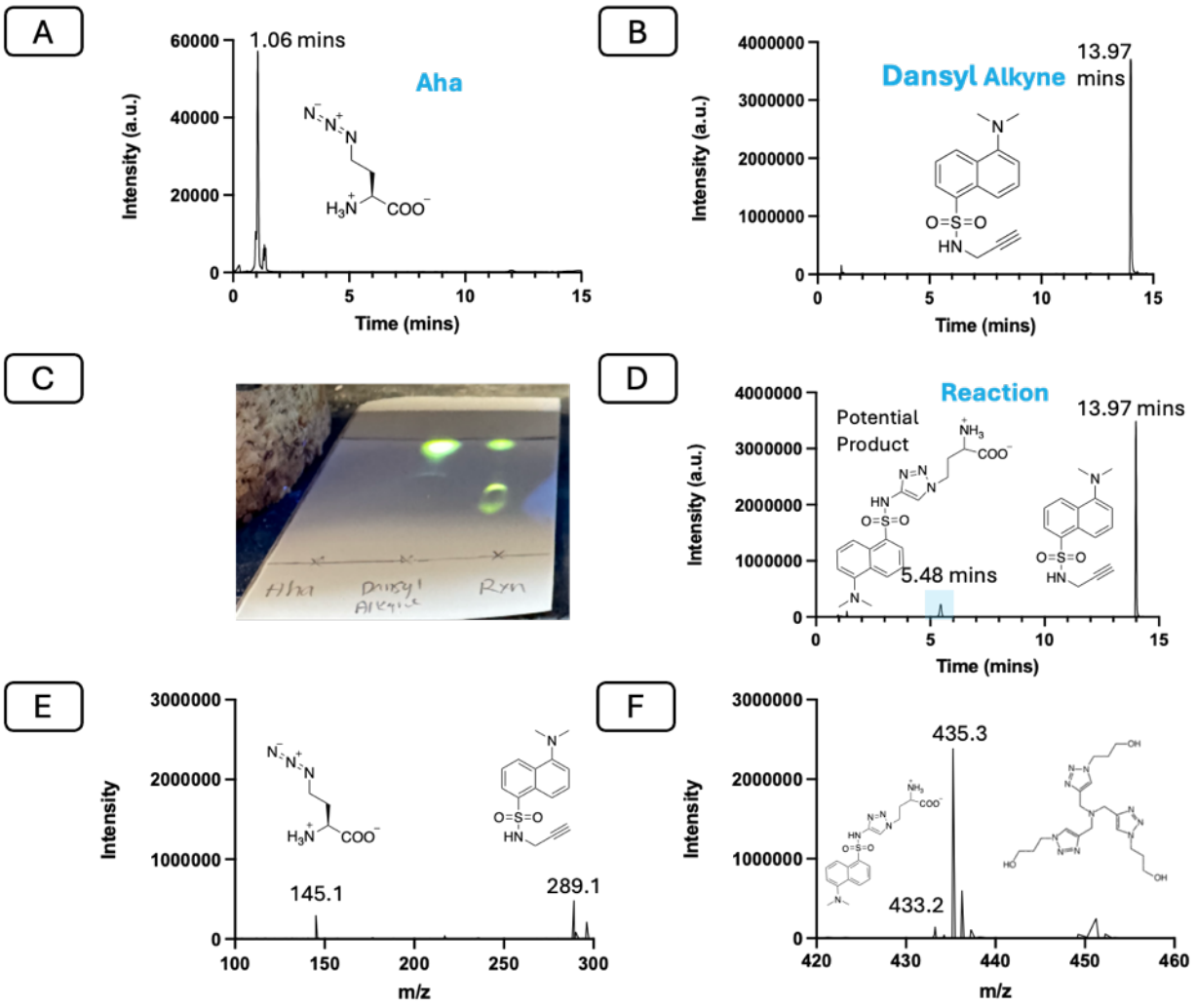


Figure 51. Copper-catalyzed azide-alkyne cycloaddition of Aha and Dansyl Alkyne Dye. A/B – HPLC chromatogram of Azidohomoalanine and Dansyl Alkyne Dye with the appropriate retention times in an H_2O and ACN based mobile phase. **C** – TLC plate of reactants and products under long-wave UV light. In the reaction lane, a new fluorescent spot appears indicating potential product formation. **D** – HPLC chromatogram showing the dansyl dye retained at 13.97 minutes and a new peak at 5.48 minutes which may be product formation. **E** – ESI-MS profile of the reactants: Aha and danysl alkyne dye. The masses correspond to the M+1 of the appropriate reactants. **F** – ESI-MS profile of product. The mass of 433.2 corresponds to M+1 of the clicked product, while 435.3 is the peak corresponding to THPTA.

The successful incorporation of azidohomoalanine into Nisin using previously mentioned methods creates opportunities for post-expression chemical modification via bioorthogonal chemistry. The use of copper-catalyzed azide-alkyne cycloaddition (CuAAC) allows for the creation of nisin derivatives with enhanced properties without compromising the peptide's inherent antimicrobial activity. To validate the functional utility of the azide-modified nisin variants, we employed dansyl alkyne as a model probe to demonstrate successful click chemistry conjugation.

Click chemistry reactions were performed between purified azidohomoalanine-labeled nisin and dansyl alkyne probe using standard CuAAC conditions. Reaction mixtures containing azide-functionalized nisin, dansyl alkyne probe, copper sulfate catalyst, ascorbic acid reducing agent, and THPTA ligand were incubated under mild aqueous conditions to facilitate triazole formation. The conjugation reaction was monitored and confirmed through electrospray ionization mass spectrometry (ESI-MS) analysis, with successful click product formation evidenced by the appearance of characteristic mass shifts corresponding to covalent dansyl attachment.

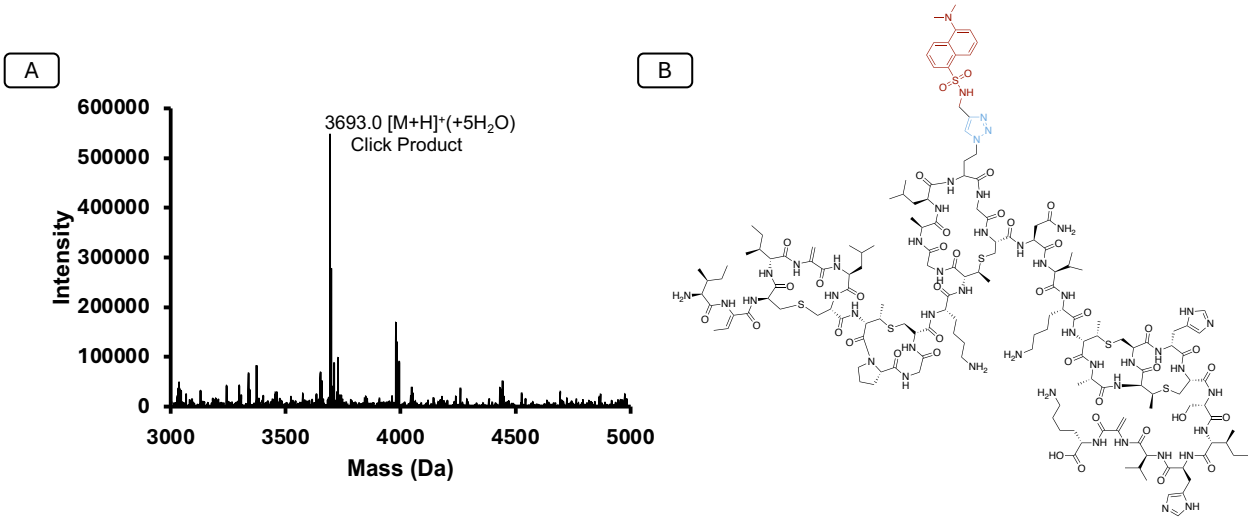


Figure 52. Mass spectrometric Confirmation of Bioorthogonal Click Chemistry Between Azidohomoalanine-labeled Nisin and Dansyl Alkyne. (A) ESI-MS spectrum showing the click product peak at 3693.0 Da ($[M+H]^+$ ($+5H_2O$)), confirming successful copper-catalyzed azide-alkyne cycloaddition. **(B)** Chemical structure of the nisin-dansyl conjugate showing the triazole linkage formed between the azidohomoalanine residue (blue) and dansyl alkyne probe (red).

Mass spectrometric analysis confirmed successful bioorthogonal conjugation between azidohomoalanine-labeled Nisin and dansyl alkyne probe. (**Figure 52**) The ESI-MS spectrum revealed a distinct peak ($[M_{obs}+H]^+ +5H2O$ = 3693.0 Da), corresponding to the expected mass of the click product. This mass represents the covalent attachment of the dansyl probe to the azide-functionalized Nisin through copper-catalyzed azide-alkyne cycloaddition, forming a stable triazole linkage. The presence of additional water molecules indicates the partially modified state of the Nisin peptide, consistent with previous observations of incomplete post-translational modifications in azidohomoalanine-labeled variants.

The successful nisin-dansyl conjugate formation demonstrates that the azide functionality remains intact despite complex post-translational processing. The triazole linkage provides a stable attachment point for functional molecules, enabling development of enhanced nisin derivatives. These preliminary results validate the bioorthogonal approach but reveal incomplete post-translational modifications, as evidenced by additional water molecules in the mass spectrum. Future optimization to achieve fully modified azidohomoalanine-labeled nisin will be essential for comprehensive evaluation of click chemistry efficiency and development of therapeutically relevant conjugates with complete antimicrobial activity.

3.3 Materials and Methods

3.3.1 Media

Name	Composition
ZYP-5052 Media	1% tryptone 0.5% yeast extract 50 mM Na_2HPO_4 50 mM KH_2PO_4 25 mM $(NH_4)_2SO_4$ 0.5% glycerol 0.05% glucose 0.2% α-lactose 2 mM $MgSO_4$ 0.2X trace elements
GM17 Media	0.5% Casien Digest 0.5% Soy Peptone 0.5% Beef Extract 0.25% Yeast Extract 0.05% Vitamin C 1mM $MgSO_4$ 0.019% Disodium-β-glycerophosphate 1% Agar H2O upto desired volume 0.5% (w/v) Glucose 5µg/ml Cm (for NZ9000 +pNGNisPT)
NMM medium	7.5 mM $(NH_4)_2SO_4$ 8.5 mM NaCl 22.5 mM KH_2PO_4 50 mM K_2HPO_4 20 mM glucose 1 mM $MgSO_4$ 50 mg/L amino acids 10 mg/L thiamine 0.01 mg/L trace elements ($CuSO_4$, $ZnCl_2$, $MnCl_2$, MoO_4) 35µM Methionine
Enriched NMM medium	7.5 mM $(NH_4)_2SO_4$ 8.5 mM NaCl 55 mM KH_2PO_4 125 mM K_2HPO_4 20 mM glucose 1 mM $MgSO_4$ 50 mg/L amino acids

	10 mg/L thiamine 0.01 mg/L trace elements ($CuSO_4$, $ZnCl_2$, $MnCl_2$, MoO_4) 3.5g/L Yeast Extract

3.3.2 Buffers

Name	Composition
5x Anode Buffer (check comp)	0.2M Tris-Cl pH 8.9
1x Cathode Buffer	0.1M Tris 0.1M Tricine 0.1% SDS
Separation Gel (15%)	16 ml 38% Glycerol 27 ml acrylamide /bis-acrylamide(37:5:1) 21.4 ml 3M Tris-HCl/SDS (pH 8.45) 600µL 10% SDS 600µL 10% APS 30µL TEMED
Stacking Gel (5%)	21 ml ddH_2O 4.5 ml acrylamide /bis-acrylamide(37:5:1) 4.5 ml 1M Tris-HCl (pH 6.8) 300µL 10% SDS 300µL 10% APS 30µL TEMED
Nisin IMAC Binding Buffer	50mM Phosphate 300 mM NaCl 5M GuHCl pH 8.0
Nisin IMAC Wash Buffer	50mM Phosphate 300 mM NaCl 50mM Imidazole pH 8.0
Nisin IMAC Elution Buffer	50mM Phosphate 300 mM NaCl 250 mM Imidazole pH 7.5
Nisin SEC Buffer	50mM Phosphate 300 mM NaCl 50mM Imidazole pH 7.5
Core Separation IMAC Start Buffer	50mM Phosphate

	300 mM NaCl 0-50mM Imidazole pH 7.5
Core Separation IMAC Elution Buffer	50mM Phosphate 300 mM NaCl 300mM Imidazole pH 7.5
Nisin Protease IMAC Binding Buffer	50mM Phosphate 500mM NaCl pH 7.5
Nisin Protease IMAC Wash Buffer	50mM Phosphate 500 mM NaCl 25mM Imidazole pH 7.5
Nisin Protease IMAC Elution Buffer	50mM Phosphate 500 mM NaCl 250mM Imidazole pH 7.5
Nisin Protease IEX Start Buffer	50mM Phosphate pH 7.5
Nisin Protease IEX Elution Buffer	50mM Phosphate 1 M NaCl pH 7.5
Nisin Cleavage Reaction Buffer	50mM Phosphate 300 mM NaCl pH 7.5

3.3.3 Plasmids

Database Number	Plasmid Name	Resistance	Source
PM 34	pNGNisPT	Cm	From Dr. O.P. Kuipers
PM 104	pET3a-NisA	Amp	From Dr. O.P. Kuipers

PM 108	pRSFDuet_NisBC	Kan	From Dr. O.P. Kuipers
PM 109	pET3a-NisA(M21V)	Amp	From Dr. Budisa MB Plasmid Database
PM 328	pQE80L_NisP	Amp	From Dr. Budisa MB Plasmid Database
PM 452	pTetEffector-array1	Strep	From Dr. Budisa MB Plasmid Database
PM 455	pDo-ColA-RE-araBAD-metG-LE	Kan	From Dr. Budisa MB Plasmid Database
PM 456	pDo-ColA-RE-rhaB-metY-metX-LE	Kan	From Dr. Budisa MB Plasmid Database
PM 511	pTetEffector-array2	Strep	PM348+ TnsABC cassete+(9 sites CRISPR-array)
PM 547	pDo-ColA-pTet-array-RE-Rham-MetY-metX-LE	Kan	From Dr. Budisa MB Plasmid Database
PM 666	pDonor-ColA-glnS-NisC-NisB-T7-NisA (M21V)	Kan	From Dr. Budisa MB Plasmid Database
PM	pQE80L_MetY_6xHis	Amp	This work
PM 191	pSEVA26'glnS-metY-metX	Cm	From Dr. Budisa Berlin Plasmid Database

3.3.4 Strain information

Database Number	Genotype and Notes	Auxotrophy	Source
E. coli BL21 (DE3)	*E. coli B* *F- ompT gal dcm+ lon hsdSB (rBmB-) λ(DE3 [lacI lacUV5-T7p07 ind1sam7 nin5])*	None	From Dr. Nediljko Budisa MB Strain Database
DH5α	F^- endA1 glnV44 thi-1 recA1 relA1 gyrA96 deoR nupG purB20 Φ80dlacZΔM15 Δ(lacZYA-argF)U169, hsdR17(r_K^-, m_K^+), λ	None	From Dr. Nediljko Budisa Manitoba Strain Database
E. coli BL21 (AI)	F- ompT hsdSB (rB-mB-) gal dcm araB::T7RNAP-tetA		
L. lactis NZ9000	Derived from the parent strain: Lactococcus lactis subsp. cremoris strain MG1363		From Dr. O.P. Kuipers
L. lactis NZ9000 (pNGNisPT)	Contains pNGNisPT plasmid		From Dr. O.P. Kuipers
BU14	E. coli B C> F- dcm ompT hsdS(rB- mB-) gal met λ(DE3 [lacI lacUV5-T7 gene 1 ind1 sam7 nin5])	Met	From Dr. Nediljko Budisa Berlin Strain Database
BU456	F ompT hsdSB(rB mB) gal dcm met(ΔE3) ΔmetA	Met	From Dr. Nediljko Budisa Berlin Strain Database
MS39	F- ompT hsdSB(rB- mB-) gal dcm met(ΔE3) ΔmetA tktB::Prha-metXY	Met	From Dr. Nediljko Budisa MB Strain Database

MS51	E. coli B C> F- dcm ompT hsdS(rB- mB-) gal met λ(DE3 [lacI lacUV5-T7 gene 1 ind1 sam7 nin5]) IS186:: ParaB-metG purT::ParaB-metG tktB::ParaB-metG yhgA::ParaB-metG	Met	From Dr. Nediljko Budisa MB Strain Database
MS61	E. coli B C> F- dcm ompT hsdS(rB- mB-) gal met λ(DE3 [lacI lacUV5-T7 gene 1 ind1 sam7 nin5]) panC::ParaB-metG IS186::ParaB-metG aroG::ParaB-metG yhgA::ParaB-metG hokA::ParaB-metG	Met	From Dr. Nediljko Budisa MB Strain Database
MS89	E. coli B C> F- ompT hsdSB(rB- mB-) gal dcm met(ΔE3) ΔmetA panC::ParaB-metG IS186::ParaB-metG aroG::ParaB-metG yhgA::ParaB-metG hokA::ParaB-metG tktB::Prha-metXY	Met	This work
MS94	E. coli B C> F- ompT hsdSB(rB- mB-) gal dcm met(ΔE3) ΔmetA panC::ParaB-metG IS186::ParaB-metG aroG::ParaB-metG yhgA::ParaB-metG hokA::ParaB-metG tktB::Prha-metXY	Met	From Dr. Nediljko Budisa MB Plasmid Database and this work
MS105-5	E. coli B C> F- ompT hsdSB(rB- mB-) gal dcm met(ΔE3) ΔmetA panC::ParaB-metG IS186::ParaB-metG aroG::ParaB-metG yhgA::ParaB-metG hokA::ParaB-	Met	From Dr. Nediljko Budisa MB Plasmid Database and this work

metG tktB::Prha-metXY
mdlB::PglnS-nisBC,PT7-nisA
nagA::PglnS-nisBC,PT7-nisA
marA::PglnS-nisBC,PT7-nisA
asd::PglnS-nisBC,PT7-nisA
duf::PglnS-nisBC,PT7-nisA

3.3.5 Primers Information

Primer Name	**Sequence (5'-> 3')**
pQEGib-F	TAAAAGCTTCGATAATTAGCTGAGCTTGG
pQEGib-R	GGTACCTTGGAAGTACAGGTTCTCG
MetY-F	ATCACGGATCCGAGAACCTGTACTTCCAAGGTACCCCAAAGTACGACAATTCCAATG CTG
MetY-R	AGGAGTCCAAGCTCAGCTAATTATCGAAGCTTTTACTAGATTGCAGCAAAGCCGCCTT CG
452 Integration Set	
panC-F	TCAGGAATTCGCCCAGCGT
panC-R	TCCCGTAACGGTTATCTGAC
tkt-F	TATGTTGGTCTGAAAGGGGC
tkt-R	AAGCGATTGTGGCATTCAGG
aroG-F	TTTGTGCTGACGTTTGCCAG
aroG-R	TGATCATCGCTGCACACGG
yhgA-F	TTCGGGTGAATATTGTCGCG
yhgA-R	ATCTTCGTGCGTTTGTAGGC
ompW-F	ATGGCGCAGTGGTATTTTGG
ompW-R	AATGCCGGTGATACAGCTTC
hokA-F	TCTGCTATCCAGAACGATGG
hokA-R	TGGAAATCAACACAGGAGGC
kdgA-F	ATTGATGGCAGCCGTCGTC
kdgA-R	TGCTGGGTATGGACTACGG
rluF-F	ACCTAAAGCGAAGGCCAAAC
rluF-R	TGCGCATGGTCGCGTATTG
IS186-4R	GGATGCTGCAAATCCCACAG
IS186F	CACTGTAATGATAGGCAATTCAGG
511 Integration Set	
mdlB - F	TTCTGGTGCTTCATCGTGGG
mdlB - R	TTCATAGATCCCCTCCGGTC
ycbF - F	AAGCCAGCGTCAGACAAGCTG

ycbF- R	AAGGGCTTTACGAACGAAGGG
marA-F	TAGCTCATACATAGCTTCCCCC
marA-R	TGGCAAGTAATTAGTTGCAGGGG
lpxT-F	TTTGCCCTGGGTGTTGCTGAC
lpxT-R	TTGATGCGGTCTTGGCGAG
gudP-F	TAGGTCGTTCGCCGAATACGG
gudP-R	TGCCTGGAGTCAAGCGATC
Fau-F	ATGCGCATGATTGTCAGTTGG
Fau-R	AGTCTCAGGGGAGGAGCAATC
agaA-F	TTGCTCCTTTATTGGGCCTTCAC
agaA-R	TGATGAACTTGACGTCGGGC
acrF-F	AGTGGGTATCGGGGTAATGG
acrF-R	AATAGTGAAGGGAGCGGGAAC
asd-F	ATTCATTAAATCTGGGGCGCG
asd-R	ACGTCTCTATCGATACGATCGG
ECD-F	TCATTAACCACGGAAACAGCAC
ECD-R	TGACCACTTCCGGATGGGAG

3.3.6 PreNisin Wildtype and Mutant (M21V) Expression

The wildtype protein was expressed using *E. coli* BL21 (DE3) transformed with pET3a_NisAWT and pRSFDuet_NisBC plasmids. From a glycerol stock, the transformed strain was used for an overnight culture grown in LB media with Kan+Amp (37^{O}C, 250 rpm) From the overnight culture, 1/100 was used to inoculate 500 ml of ZYP-5052 media and culture was grown for 4 hours (37^{O}C, 250 rpm) after which the temperature was decreased to 28^{O}C for overnight expression. After expression overnight, the culture was pelleted via centrifugation (17,000 xg, 15 minutes), pellet was resuspended in 1/10-1/20 volume in Nisin IMAC Binding Buffer and sonicated at 50% amplitude for 20 minutes (15 seconds on/off). The cell debris was centrifuged (20,000 xg, 45 min, 4^{o}C) and pellet was stored at -20^{o}C until purification. The mutant form of Nisin (M21V) was expressed using similar methodology as for the wildtype peptide.

3.3.7 General Nisin Purification Protocol

Protein purification was conducted using a gravity flow column loaded with 3ml of HisPur™ Ni-NTA Resin (Thermo Scientific). The column was equilibrated with Nisin Binding Buffer (50mM Phosphate, 300mM NaCl, 5M Guanidine Hydrochloride, pH 8.0) and the sample was loaded. Any impurities were washed with Nisin Wash Buffer (50mM Phosphate, 300mM NaCl, 250mM Imidazole, pH 8.0) and the peptide was eluted with Nisin Elution Buffer (50mM Phosphate, 300mM NaCl, 300 mM Imidazole, pH 7.5). The protein elution was monitored via Bradford and collected protein was concentrated with a Amicon Ultra-15 Centrifugal Filter 3kDA MWCO (Millipore) about 20x prior to size exclusion chromatography. For SEC analysis, the HiLoad 16/600 Superdex 75pg Column from Cytiva was used with Nisin SEC Buffer (50mM Phosphate, 300mM NaCl, pH 7.5). The column was connected to a BioRAD NGC chromatography system with an NGC fraction collector, and protein elutions were monitored at 230 nm. Post-SEC, fractions were concentrated using an Amicon Ultra-15 Centrifugal Filter (3kDA MWCO, Millipore) in preparation for cleavage.

3.3.8 Nisin Protease Expression and Purification

The protease was expressed using BL21 (DE3) cells transformed with the pQE80_NisP plasmid, containing a truncated soluble form of the protease. Using a glycerol stock, an overnight culture was inoculated into LB media + Ampicillin and grown overnight at 37°C at 250 rpm. Subsequently, 1% of this culture was used to inoculate 500 mL of LB media with ampicillin, and the bacteria were grown at 37°C for 4 hours until an optical density at 600 nm (OD600) of 1.2 was achieved. Protein expression was then induced by adding 0.5 mM IPTG, and the culture was incubated for an additional 4 hours at 37°C. The cells were harvested by centrifugation at 17,000 xg for 15 minutes at 4°C, and the resulting pellet was resuspended in one-tenth of its volume in NisP binding buffer (50 mM phosphate, 500 mM NaCl, pH 7.5). The resuspended pellet was sonicated on ice at 50% amplitude for 15 minutes, with cycles of 15 seconds on and off. After sonication, the cell debris was pelleted via centrifugation (20,000 xg, 45min, 4°C) and the resulting supernatant was passed through a 0.45µm filter

prior to column loading. The protein was purified using a HisTrap™ FF column on a ÄKTA start™ system. After loading onto the column, the impurities were washed with NisP wash buffer (50 mM Phosphate, 500mM NaCl, 25mM Imidazole, pH 7.5) and protein was eluted with NisP Elution Buffer (50 mM Phosphate, 500mM NaCl, 250mM Imidazole, pH 7.5) where protein elution was monitored by measuring absorbance at 280 nm.

The protein was dialyzed into NisP Ion-Exchange start buffer (50mM Phosphate, pH 7.5) and then purified using the Capto™ HiRes Q 5/50 (Cytiva) and it was eluted with NisP IEX Elution Buffer (50mM Phosphate, 1M NaCl, pH 7.5). The elution step involved a 7-column volume (CV) at 10% mobile phase B, followed by a gradient from 10% to 20% B over 30 CV. It was increased to 30% B for 7 minutes, then increased to 50% B over 5 CV, 70% B over 7 CV, and finally 100% B over 3 CV.

3.3.9 Nisin Cleavage and Separation

The purified PreNisin peptides were subjected to cleavage by the purified Nisin Protease for removal of the leader peptide. The protease was incubated with PreNisin samples at a 1/100 ration and incubated at 37°C for cleavage. Subsequently the cleaved product was separated from any remaining uncleaved product and the protease with IMAC chromatography. The sample was loaded onto a HisTrap™ FF affinity column (Cytiva) connected to a BioRAD NGC chromatography system. The core peptides elute with the flow through in the starting buffer (50mM Phosphate, 300mM NaCl, pH 7.5) while the uncleaved or leader peptide and the protease bind the column and only elute in the elution buffer (50mM Phosphate, 300mM NaCl, 250mM Imidazole, pH 7.5). Remaining unprocessed PreNisin is dialyzed to remove imidazole and subject to protease cleavage. The purified core peptide is further processed with trichloroacetic acid precipitation.

3.3.10 Peptide Precipitation with Trichloroacetic acid

Purified core peptide was collected and precipitated with 20% ice-cold TCA overnight at 4°C. The following day, the sample was pelleted via centrifugation (20,000xg, 45 min, 4°C) and the supernatant was carefully removed. Residual TCA and other impurities were washed with ice-cold acetone in 3 wash steps (centrifugation - 20,000xg, 15 minutes, 4°C). After the last step, the acetone was removed, and the pellet was dried. The precipitated pellets were weighed and stored at -20°C until further experimentation. The effect of TCA precipitation on Nisin activity was tested using 96 well plate microdilution assay.

3.3.11 Antimicrobial Assays

To determine the antimicrobial activity, an overnight culture of the nisin sensitive indicator strain *L. lactis NZ9000 (pNZ nisPT)* was incubated in LB media and 5 µg/mL chloramphenicol at 30°C. From this culture, 1 ml was added to 50 ml molten GM17-Agar supplemented with chloramphenicol and poured into a petri dish. Using the wide end of a Pasteur pipette, holes were created in the agar. A similar procedure was followed for assays using the *L. lactis NZ9000* strain (containing no protease). Samples were prepared according to various protocols following expression or purification. For expression samples, 1 ml of the *E. coli* culture was centrifuged (5 minutes, 13000 xg) and resuspended in volume to normalize to OD_{600}=5. The cells were lysed via sonication and cell debris was pelleted via centrifugation (4_oC, 10 minutes, 20000 xg). A 40 µL aliquot of the supernatant was added into holes on the indicator strain plate and incubated at 30°C overnight. For purified and cleaved protein samples, 40 µL was added directly to the plate. For each assay, the buffer of the solution served as the negative control while chloramphenicol at 400 µg/mL as antimicrobial control compound.

3.3.12 Microdilution Assays

Bacterial Prep – OD600 measured and then bacteria OD was normalized to OD_{600} which was $1.0x10^8$ cfu/ml in GM17 media. The normalized bacterial culture was diluted 1:100 and used

for further experimentation. Sterility control was GM17 media without any bacterial inoculation. Bacterial Growth Control: 1:1 ratio of GM17 media and 1:100 dilution of OD_{600} normalized bacteria. Nisin Preparation – The Nisin standard was prepared to a concentration of 22.5 µg/ml. The samples were prepared in buffer and TCA precipitated samples were redissolved in phosphate buffer. Method – The Nisin samples were serially diluted 2x across the wells and 50µL of Normalized bacterial was added to each well. The plate incubated at 30°C overnight and optical density was measured using a Tecan plate reader at 600 nm. The data was plotted using Prism Software.

3.3.13 Tricine Gels

Tricine-SDS-PAGE is used to separate and analyze proteins with smaller molecular weights (<30 kDa). The gel consisted of a 16% acrylamide separation gel and a 4% stacking gel. The samples were mixed with 6x reducing Laemmli SDS sample buffer and incubated at 95°C for 5 minutes. The cathode buffer was loaded unto gel reservoir, and samples were loaded onto the well. The gel was run at 120V for approximately 1.5 to 2 hours until the dye front had reached the bottom of the separating gel. A PageRuler™ Prestained Protein Ladder from Thermo Scientific served as the molecular weight standard. Following electrophoresis, the gels were incubated in a fixing solution (25% isopropanol, 10% acetic acid) at room temperature for 1 hour. Protein visualization was achieved by staining the gels with Coomassie Brilliant Blue staining solution (0.025% Coomassie Brilliant Blue R-250, 30% methanol, 10% acetic acid) in a microwave for 1.5 minutes. The gels were then destained overnight in a solution of 30% methanol and 10% acetic acid. Following destaining, the gels were visualized on a white light box.

3.3.14 Expression in BU14, MS51 and MS61 - ncAA labelling via SPI method

For strains MS39 and MS51, both pET3a_NisA_WT and pRSF_Duet_NisBC plasmids were transformed into each strain. The transformed strain from a glycerol stock was used for an

overnight culture grown in LB media with Kan+Amp at 37 degrees, 250 RPM. The overnight culture was centrifuged (4000xg, 5 minutes, RT) and the LB supernatant was removed. The pellet was washed with water 2x and then inoculated 1/100 into new minimal media with limiting methionine concentration of 35μM. For the MS51 expression, the inoculated bacteria were grown until methionine was depleted from the media (~8 hours) and then supplemented with 2.5mM Azidohomoalanine, 1mM IPTG and 1% *L*-arabinose. Protein expression was conducted at 30°C overnight. For MS39 Expression, the inoculated bacteria were grown for 4.5 hours and then supplemented with 5mM *L*-Rhamnose. At 4, 5.75 and 7 hours, the media was supplemented with 0.8mM NaN_3 and 1mM *D*-pantothenic acid. After full depletion of methionine, the protein expression was induced with 1mM IPTG and protein was expressed at 28 degrees overnight.

3.3.15 *O*-acetylhomoserine sulfhydrylase *in vitro* Assays

The reaction mixture contained 10mM of Oahs substrate (10mM) and 10mM NaN_3 in 20mM sodium HEPES buffer pH 7.2. For the reaction, 5 μM purified *cg*OAHSS was added to reaction to a final volume of 100μL and the reaction for conducted for 1-2 hours at 37 °C. Various reactions were tested at room temperature and 50°C. After completion, 1.5 μL of the samples were analyzed by thin layer chromatography. The mobile phase consisted of 12:3:5 Butanol: Acetic Acid: Water and was run until the mobile reached the top of the TLC plate. The spots of the amino acids were observed following staining with Ninhydrin.

3.3.16 Expression in MS89, MS94 and MS105

For strains MS89 and MS94, both pET3a_NisA_WT and pRSF_Duet_NisBC plasmids were transformed into each strain. The transformed strain from a glycerol stock was used for an overnight culture grown in LB media with Kan+Amp at 37 degrees, 250 RPM. The overnight culture was centrifuged (4000xg, 5 minutes, RT) and the LB supernatant was removed. The pellet was washed with water 2x and then inoculated 1/100 into new minimal media with limiting methionine concentration of 35μM. The inoculated bacteria were grown for 4.5 hours

and then supplemented with 5mM *L*-Rhamnose. At 4, 5.75 and 7 hours, the media was supplemented with 0.8mM NaN_3 and 1mM *D*-pantothenic acid. For expression in 3.5g/L yeast extract, the bacteria were grown for 3 hours and then supplemented with 5mM *L*-Rhamnose. At 3, 4.5 and 6 hours, the media was supplemented with 0.8mM NaN_3 and 1mM *D*-pantothenic acid. In both cases, 1% *L*-arabinose was added around ~7 hours to induce the expression of MetG. For expression in LB media, the overnight culture was inoculated 1/100 into LB media and grown for 3 hours at which point 5mM *L*-Rhamnose, 0.8mM NaN_3 and 1mM *D*-pantothenic acid were added for azidohomoalanine biosynthesis. After 4 hours, the cells were centrifuged (4000xg, 6 minutes, 4°C) and the cell pelleted was washed with water 2x. The washed cells were inoculated into NMM (without methionine) containing 0.8mM NaN_3, 1mM *D*-pantothenic acid and 1% *L*-arabinose. The culture was grown until the stationary phase, after which protein production was induced. For each case, 1mM IPTG was used to induce protein expression and cultured overnight at 28°C and 250 rpm. For the plasmid containing NisBC under constitutive promoter control, only Kan was required as an antibiotic however similar steps were followed for protein expression. For expression in MS105, no transformation of plasmids was required however protein production were like ones previously mentioned.

3.3.17 Construction of MS89 - Transposition

For the construction of the MS88 and MS89 strains, PM452 and PM# was co-transformed into MS51 and MS61 using chemical competent cells. Following heat shock, bacterial were recovered in LB for 90 minutes at 37°C, after which they were spread on LB + Kan + Spect plates and incubated overnight at 37°C. The grown colonies were scrapped and resuspended in sterile MilliQ water. The bacteria were diluted 100x and spread onto LB + Kan + Spect plates containing 1 ng/mL anhydrotetracycline (aTc) as a transposition inducer. This plate was grown overnight at 30°C for 2 days. A few colonies were picked from each plate and cultured overnight in LB+ Kan. The following day, the culture was used to make a glycerol stock and to preform colony PCR using 9 pairs of primers flanking the target insertion sites.

The strains showcasing successful insertion were also sent for genomic sequencing to further confirm integrations.

3.3.18 Plasmid Curing

For plasmid elimination, the pCutamp (PM226) was used which contains a gRNA sequence under the rhamnose-induced promoter system targeting the AmpR promoter in the PM452. This plasmid was transformed into MS88 and MS89, following heat shock, the bacteria were recovered for 1 hr at 37°C. Following this 1-hour incubation, LB media was added up to 1 ml of LB+ 50µg/ml Apr+ 10mM L-Rhamnose and cultured overnight at 37°C. The next day, the culture was diluted (10^4-times dilution) and plated on LB+Apr+5 mM L-Rhamnose plate and incubated overnight. From the plates, a few colonies were picked and cultured in 0.5 ml LB + 10mM sucrose media overnight at 37°C. This culture was diluted (10^6-times dilution) and plated on LB + Sucrose plates to obtain single colonies. This plasmid carries the toxic *sacB* gene which converts sucrose to levan; a highly toxic metabolite to *E. coli*. For testing whether plasmid elimination was successful, the cured strain was tested via spotting single colonies on LB + Kan., LB + Spect., LB + Apr., and LB plates, simultaneously. The colonies which only grew on the LB plate were properly cured and these were grown in LB media for preparation of glycerol stocks.

3.3.19 Colony PCR

Colony PCR was used to verify the site-specific integration of the target genes into the E. coli genome at the intended loci. The PCR master mix was prepared in bulk and fractioned into 105 µL aliquots. Into each aliquot, 0.5 µL of the bacterial template was added which either from a glycerol stock or an overnight culture. This mixture was sub-aliquoted into 9-10 individual PCR tubes as 10 µL reaction fractions, with each tube receiving specific primer pairs flanking one of the intended genomic insertion sites. Following the PCR reaction, as stated below, 2µL of 6x DNA loading dye was added to each sample. The products were analyzed via agarose gel electrophoresis using a 1% gel to confirm correct product sizes after integration.

Step	Cycles	Temperature	Time
Initial denaturation	1	95°C	5 mins
Denaturation		95°C	20 secs
Annealing	30	56°C	30 secs
Extension		72°C	5 mins
Final Extension	1	72°C	7 mins
Hold	1	4°C	hold

3.3.20 Genomic Sequencing

All the strains were analyzed by next-generation whole genome sequencing by SeqCoast Genomics LLC, after culturing of the strain in permissive medium and extraction of the genomic DNA by the PureLink Microbiome DNA Purification Kit (ThermoFisher Scientific). Short-read whole genome sequencing, Illumina, by 400 Mbp/2.7 million reads provides 150 bp paired-end reads for analysis. For analysis of the Breseq computation pipeline was used to find mutations relative to the reference sequences: (CP001509) for the genome and various plasmids for the insertions. The software reported new junctions such as those produced by transposons in an HTML format. The Digital Research Alliance of Canada server was used to this software.

3.3.21 ESI – MS

The purified and cleaved Nisin fragments were prepared using either TCA precipitation or Chloroform/MeOH extraction. These samples were directly infused in the Electrospray ionization time-of-flight mass spectrometry (ESI-TOF-MS) by autosampler with Bruker Elute system at flow rate 0.3 mL/min. The peptides underwent ionization in positive mode with a cone voltage of 40kV and scanning window from 300 to 3000 m/z. The raw fragment data was analyzed using the maximum entropy deconvolution algorithm in Bruker Data Analysis software.

3.3.22 Click Chemistry Conjugation

Click reactions between azidohomoalanine-labeled Nisin and dansyl alkyne were performed using copper-catalyzed azide-alkyne cycloaddition (CuAAC) conditions. Reaction mixtures were prepared in 250 µL total volume containing the following components: 4 µL of 100 mM $CuSO_4$ (1.6 mM final concentration), 20 µL of 1 M ascorbic acid (80 mM final concentration), 40 µL of 50 mM THPTA (8 mM final concentration), 20 µL of 5 mg/mL dansyl alkyne (1.38 mM final concentration), 25 µL of 100 mM phosphate buffer pH 7.4 (10 mM final concentration), and 100 µL of 10 mg/mL Nisin or azidohomoalanine-labeled Nisin (1.28-30 mM final concentration). The reaction volume was adjusted to 250 µL with ultrapure water (41 µL).

Reactions were incubated at 37°C for 1-18 hours with gentle mixing. For reactions involving unprecipitated NisP cleavage products, the same conditions were employed without prior purification steps. Reaction progress was monitored by HPLC analysis, with samples taken at designated time points and analyzed for substrate consumption and product formation based on integrated peak areas at characteristic retention times.

4. Part 3: AC6

4.1 Introduction to Persistent pulmonary hypertension of the newborn and role of AC6

4.1.1 Persistent Pulmonary Hypertension of the Newborn: Clinical Background

Persistent pulmonary hypertension of the newborn (PPHN) is marked by the inability of the pulmonary blood vessels to dilate after birth leading to blood bypassing the lungs and remaining unoxygenated. Further characterized by elevated pulmonary vascular resistance and decreased pulmonary blood flow. While decreased pulmonary blood flow is normal physiological state in the fetus as the placenta is the organ for gas exchange, after birth the lungs must activate and become the main organ for gas exchange which requires the pulmonary blood vessels to dilate and redirect the flow. This effects approximately 25,000 to 30,000 infants and contributes to 1000 deaths annually with a mortality rate ranging from 4% to 33%.[131] The adenylyl cyclase (AC) protein and its product, cyclic adenine monophosphate (cAMP) are crucial for pulmonary vasodilation/cardiac contraction.[132]

4.1.2 cAMP Signaling and Adenylate Cyclases in Vascular Regulation

Adenylate cyclases catalyze the transformation of adenosine triphosphate (ATP) into cyclic adenosine monophosphate (cAMP). These enzymes are categorized into six (I-VI) distinct classes, with prokaryotes having all 6 classes, mammals exclusively encode class III adenylate cyclases. Despite exhibiting significant structural and domain organization differences, the six classes of adenylate cyclase enzymes operate with remarkable functional similarity. In bacteria like *E. coli*, cAMP is crucial for regulating glucose metabolism through the cAMP receptor protein (CRP).[133] Notably, numerous bacterial ACs function as virulence effectors or toxins. For instance, *Bordetella pertussis* (*B. pertussis*) produces the adenylate cyclase toxin, CyaA, which is activated by eukaryotic calmodulin, leading to a significant increase in cAMP levels.[134]

4.1.3 Mammalian Adenylate Cyclase Isoforms and Regulatory Diversity

Mammalian adenylate cyclases comprise of nine membrane-integral isoforms (AC1-9) that are involved in G-protein coupled receptor (GPCR) signalling pathways, along with one soluble isoform (AC10) that is not associated with GPCR signalling. Additionally, these proteins are located on distinctive chromosomal loci. Through the binding of effector molecules, the GCPR activates the G-protein Gαs, a subunit of the heterotrimeric guanine nucleotide protein. The activated G-protein goes onto activate adenylate cyclase thus stimulating the conversion of ATP to cAMP. Furthermore, adenylate cyclase (AC) proteins can be inhibited by the inhibitory alpha subunit, Gαi.[135] Specifically, AC5, AC6, and AC1 are particularly susceptible to inhibition by this protein.[136] The isoforms are localized throughout various tissues, and their product cAMP functions as a crucial second messenger.

4.1.4 Structural Organization and Regulation of AC6

The adenylate cyclase proteins consist of 12 transmembrane (TM) helices and two catalytic domains (C1a and C2a, respectively), which are highly conserved in the class 3 of these enzymes. The C1b and C2b domains are less conserved and may play isoform-specific roles in activity regulation.[133] The Gαs protein binds to the C2 domain and the forskolin and ATP binding sites are located between the two cytosolic domains.[132] While the various isoforms carry out the same function, their expression levels in various locations and response to regulation factors varies. AC1 and AC8 are mainly expressed in the brain and are thought to play roles in memory and learning. The AC3 protein is the most prominent in the olfactory epithelium while the AC2 protein is observed mainly in the heart, brain and skeletal muscle. The AC5 and AC6 isoforms are dominant in the heart and said to be important for cardiac contraction. The isoforms, AC4, AC7 and AC9 are said to be widespread with various or unknown functions. Adenylate cyclase isoforms are categorized into four groups based on their responses to various regulatory factors. The first group includes AC1, AC3, and AC8, which exhibit increased activity in the presence of Ca^{2+} and are inhibited by Gβγ.[136] The second group comprises AC2, AC4, and AC7 which are simulated by Gβγ. The third group consists of AC5 and AC6, which are stimulated by Gβγ and inhibited by $G\alpha i$ and Ca^{2+}. The fourth group includes only AC9, the only isoform unaffected by forskolin.[137] Forskolin (Fsk) is

a diterpene derived from the plant *Coleus forskohlii* root and activates all the membrane-bound AC isoforms expect AC9. This molecule binds between the C1 and C2 domains in an allosteric site which is structurally related to the AC active site and literature suggests that a key residue in AC9 can be mutated in the forskolin binding pocket to restore its forskolin activity. In AC6, the residues T500 and N503 in C1, along with S1035 in C2, interact with forskolin at the allosteric binding site.[138] It is thought that S1035 in C2 interacts with the 7-acetyl group of forskolin. N503 and S1035 are conserved across all AC isoforms except AC9, which may explain why AC9 is not activated by forskolin. While the catalytic core is highly conserved across all isoforms, the N-terminus is highly varied among the isoforms.[138] The AC6 isoform, present in cardiac tissue is highly crucial for cardiac and vascular function. This isoform serves as a principal effector of vasodilator signalling and in regulating potential in vascular myocytes and is increased in neonatal tissues.[132] Overexpression of this isoform has been said to rescue heart function in cardiac injury. This protein experiences several post-translational modifications that help regulate its function. AC6 can be phosphorylated by protein kinase A and C (PKA or PKC) on different threonine or serine residues. Phosphorylation by PKA and PKC inhibits AC6 activity, with potential sites including Ser10, 568, 674, and Thr931.[139] A mutation at Ser10 in AC6 prevents inhibition by PKC phosphorylation. Furthermore, this isoform is regulated by glycosylation, specifically targeting asparagine residues N805 and N890 located on the extracellular loops of TM2 through this post-translational modification. Lastly, nitrosylation, through nitric oxide is crucial for regulating AC6 for various cardiovascular functions.[132] The reactive nitric oxide species can covalently bind to proteins with nitrosylation of cysteine being residue specific.

4.1.5 Systemic Roles of AC6 Beyond the Pulmonary Vasculature

While this thesis focuses on AC6 in the context of pulmonary vasculature and PPHN, this isoform is expressed and functionally important across several other organ systems. In airway and intestinal epithelium, AC6 physically and functionally interacts with the cystic fibrosis transmembrane conductance regulator (CFTR), with severe hypoxia reducing AC6 expression and activity thus impairing CFTR function.[140] This links AC6 dysregulation to

diseases such as cystic fibrosis and this isoform is also involved in regulating ciliary length and function with a AC6 knockout producing cilia that are abnormally long and functionally impaired.[140] Additionally, AC6 contributes to skeletal mechanotransduction, mediating the adaptive response of bone to mechanical loading.[141] Combined with its established role in cardiac contraction and vasodilator signalling, this shows AC6 is important beyond the pulmonary vasculature and is implicated in multiple diseases.

4.1.6 Nitrosylation of AC6 and Gαs in Hypoxia and PPHN

Studies showcase that in PPHN tissues, while the total AC content remain unchanged, the total AC6 content increased. Despite overexpression of this isoform, its catalytic activity decreases upon exposure to hypoxia. Nitrosylation is a protein modification that commonly occurs during hypoxic conditions and may render the protein inactive. S-nitrosylation is a post-translational modification in which NO covalently attaches to the thiol group of cystine (S-NO).[142] Using computational analysis, cysteine residues susceptible to nitric oxide can be predicted.[143] Using site directed mutagenesis, these cysteines residues were mutated to identify ones susceptible to S-nitrosylation. The study demonstrated that the mutation of cysteine 1004 reduced both the basal and stimulated activity of AC6, suggesting its vulnerability to nitrosylation. Additionally, this residue is in the conserved C2 domain, close to the Gαs docking site, and its nitrosylation could potentially influence interactions with Gαs. The study demonstrated that the C1004 mutation enhanced binding to Gαi and reduced binding to Gαs. Gαs binds to C2, increasing the affinity of C1 and C2, which aids catalysis. In contrast, Gαi binds to C1 and inhibits AC by preventing the C1 and C2 domains from achieving a closed conformation. Notably, this effect persists even when forskolin occupies the allosteric site. In addition, a second critical residue is present in Gαs (C174) located near its binding site to AC. These two cysteine residues (C1004 on AC6 and C174 on Gαs) may form the first point of contact between Gαs and AC, essential for AC activation.

These residues are predicted to be ~6Å located at the AC binding cleft and their susceptibility to nitrosylation may result in the lack of AC activation seen in infant hypoxia.[142]

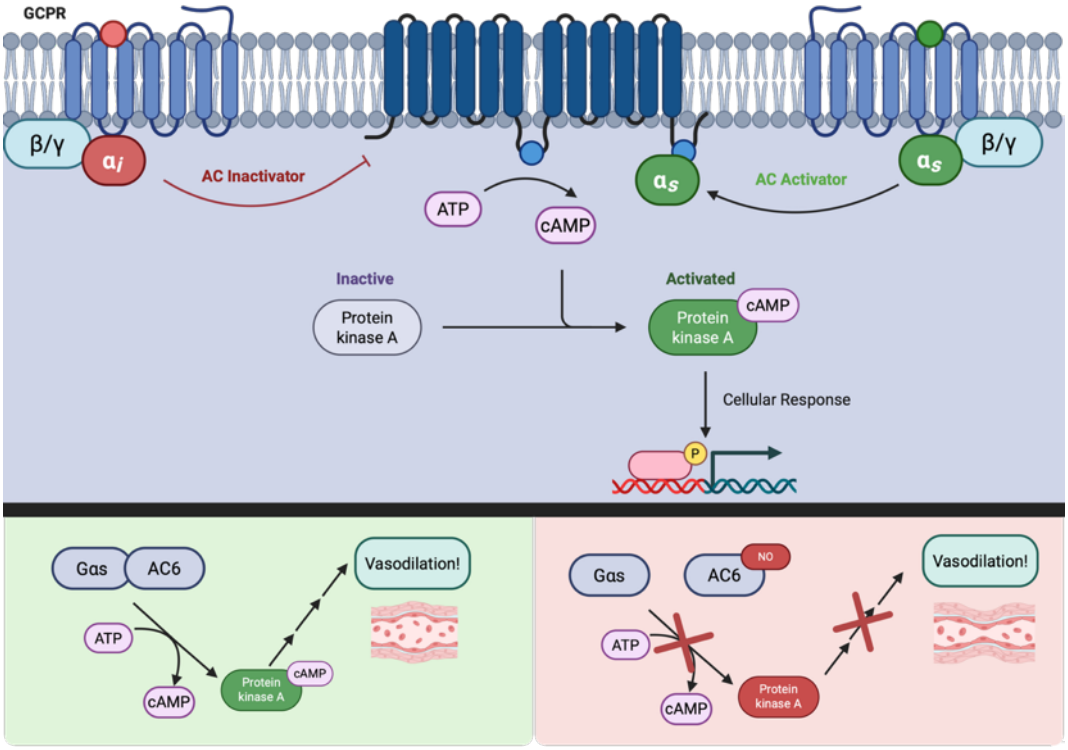


Figure 53. Modulation of cAMP/PKA Signalling Pathway by G-protein Coupled Receptors and Regulation of Vasodilation by Nitric Oxide. Top: Stimulatory (Gαs) and inhibitory (Gαi) GPCR pathways modulate adenylate cyclase activity and cAMP production. **Bottom:** NO-mediated inhibition reduces cAMP/PKA signalling and vasodilation. Created with Biorender

4.1.7 Rationale for Heterologous Expression of AC6 and Gαs

Due to this, the larger project in the Dr. Sorensen lab explores the synthesis of alternative AC6 specific activators (forskolin derivatives) to tackle infant hypoxia. For testing efficiency of the activators, a HPLC method was developed to analyze cAMP turnover in the presence of the AC6 enzyme and various activators. For these tests, functional AC6 and Gαs are required however previous trials in human embryonic kidney (HEK) cells have shown very little protein expression of AC6. Due to these reasons this project explores the heterologous expression of functional AC6 and Gαs in *E. coli*. Despite extensive characterization of AC6 regulation in mammalian systems, the lack of robust recombinant expression platforms has limited both mechanistic and pharmacological studies. While Parts 1 and 2 of this thesis addressed the chemical and translational challenge of introducing non-natural building blocks into proteins, this project addresses a complementary challenge central to

recombinant protein engineering: achieving functional expression of a structurally complex, eukaryotic multi-domain enzyme in a bacterial host. The primary objective of the project was to introduce clickable handles to AC6 and Gαs in *E. coli* by employing the methodologies outlined in Parts 1 and 2, and to utilize click chemistry to achieve full activation of AC6.

4.2 Results and Discussion

4.2.1 Rationale and Design of a Soluble AC6 Expression Construct

To evaluate potential activators of adenylate cyclase 6 using HPLC-based assays, a protein construct amenable to high-yield expression was required. Native expression of AC6 in mammalian systems (e.g., HEK cells) typically results in low protein yields, limiting its utility for biochemical studies. To overcome this, a heterologous expression strategy in *E. coli* was explored, given its well-established capacity for high-level recombinant protein production.

However, full-length AC6 is around 130 kDa with two hydrophobic membrane spanning domains each consisting of six transmembrane helices and two large cytosolic domains C1 and C2 this rendering it difficult for expression in a bacterial system. In bacterial systems, these large transmembrane domains often lead to protein misfolding, aggregation, and accumulation in inclusion bodies, resulting in poor solubility and low recovery of functional protein. To address this limitation, multiple laboratories designed constructs and expressed in bacteria with isolated cytoplasmic domains (C1 and C2) of ACs that showed catalytic activity.[144,145] Following a similar approach, a recombinant construct was designed by the Dr. Chelikani laboratory in which the cytosolic domains of AC6 were retained while the transmembrane regions were omitted to promote solubility. The resulting construct, cloned into the pET30a vector (pET30a_AC6_FlagTAG), included a C-terminal Flag-tag to facilitate downstream purification and detection.

4.2.2 Expression Screening and Solubility of AC6 in *E. coli*

To evaluate expression and solubility, the AC6 construct was transformed into multiple *E. coli* strains, including BL21 (DE3), AI™, and Origami™. These strains were selected to assess different expression environments: BL21 (DE3) as a standard expression host, AI™ for improved tolerance to potentially toxic proteins, and Origami™ to enhance disulfide bond formation.

Following expression, soluble and insoluble fractions were analyzed by SDS-PAGE to assess protein production at the expected molecular weight (~89 kDa). Across all strains, the AC6 construct was predominantly localized to the insoluble fraction (**Figure 54**), indicating limited solubility despite removal of transmembrane domains. In the Origami™ strain, no detectable protein was observed in the soluble fraction, with expression confined to inclusion bodies. In contrast, BL21 (DE3) and AI™ strains showed low levels of expression distributed between soluble and insoluble fractions.

Given the potential toxicity associated with accumulation of misfolded protein, the AI™ strain was selected for further optimization. To improve folding and solubility, expression temperature was reduced to 30°C and 16°C. While overall protein expression increased at both lower temperatures, most of the protein remained insoluble. Notably, expression at 16°C resulted in the highest overall yield and was therefore selected for subsequent experiments.

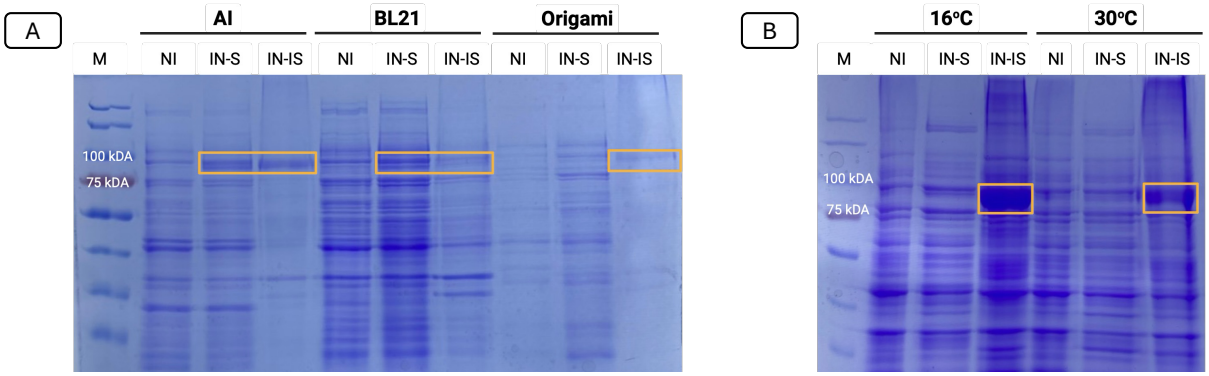


Figure 54. Expression and solubility of truncated AC6 in E. coli strains and at different temperatures (SDS-PAGE). (A) BL21(DE3), AI™, and Origami™; NI, induced soluble (S), and induced insoluble (IS) fractions. **(B)** AI™ expression at 16 °C vs 30 °C. Target band (~89 kDa) indicated

4.2.3 Solubilization, Refolding, and Partial Purification of AC6

Due to the predominantly insoluble nature of the expressed AC6 protein, solubilization and refolding strategies were explored. The protein pellet was solubilized using guanidine hydrochloride or urea, followed by clarification to remove cellular debris. To reduce sample impurities, partial purification was performed using ion exchange chromatography. Samples were dialyzed into the appropriate starting buffer and subjected to both anion and cation exchange chromatography. Fractions corresponding to AC6 were pooled and used for subsequent activity assessment. While complete purification was not achieved, this approach enabled enrichment of AC6 from insoluble material and provided sufficient protein for preliminary functional studies.

4.2.4 Expression and Purification of Gαs for Reconstitution Assays

To assess AC6 activity in the presence of its native activator, the G protein Gαs was expressed and purified for use in reconstitution assays. A recombinant construct encoding a soluble, His-tagged form of Gαs (pET30a_ Gαs _HisTag), previously developed by the Dr. Chelikani laboratory, was used for bacterial expression.

Expression screening was performed across multiple E. coli strains (BL21 (DE3), AI™, and Origami™) to identify optimal production conditions. SDS-PAGE analysis (**Appendix Figure 16**) indicated that BL21 (DE3) and AI™ strains yielded higher expression levels, while Origami™ showed comparatively low expression, consistent with observations for AC6. Based on these results and prior literature precedent, BL21 (DE3) was selected for large-scale expression.

Following expression, cell lysates were fractionated to assess protein solubility. In contrast to AC6, Gαs was predominantly recovered in the soluble fraction, enabling purification via affinity chromatography. SDS-PAGE analysis of elution fractions confirmed successful enrichment of the target protein, although co-purifying impurities were still present. To further improve purity, size exclusion chromatography was employed as a polishing step.

Given the observed instability of Gαs, 10% glycerol was included in the buffer to enhance protein stability during purification. This approach resulted in a substantial increase in purity, as confirmed by SDS-PAGE analysis (**Figure 55**). While minor impurities remained, the final protein preparation was of sufficient quality for use in downstream activity assays.

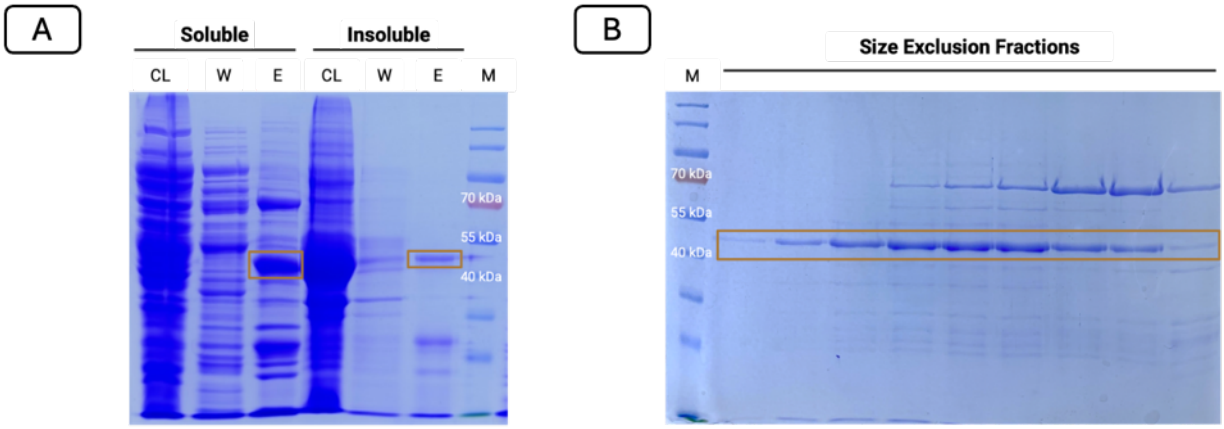


Figure 55. Multi-step Purification of Gαs Analysed by SDS-PAGE. (A) IMAC purification from soluble and insoluble fractions. **(B)** SEC polishing of pooled IMAC elutions. Target band (~43 kDa) indicated.

4.2.5 HPLC Assays Setup and Nucleotide Separation Controls

Following purification of AC6 and Gαs, preliminary activity assays were conducted using an HPLC-based method developed and optimized in collaboration with Alex Pritchard. Prior to enzymatic assays, standards including cAMP, ATP, and ADP were analyzed to establish retention times (**Figure 56**). The method provided clear separation of these species, with

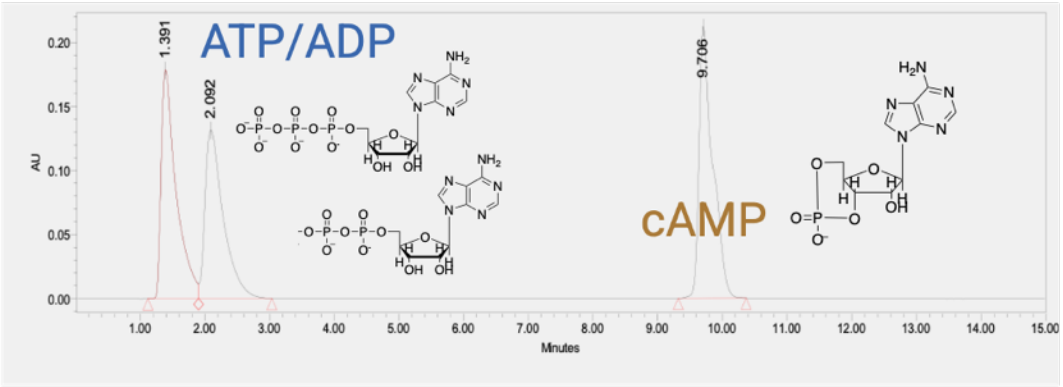


Figure 56. HPLC separation of ATP, ADP, and cAMP standards. ATP and ADP elute early, while cAMP is well resolved at ~9.7 min under the indicated reverse-phase conditions.

cAMP eluting at 9.7 min, and ATP and ADP at 1.4 and 2.1 min, respectively, enabling straightforward resolution of ATP-to-cAMP conversion. An improved separation method was developed later (**Figure 61**)

For activity assays, AC6 fractions obtained from ion exchange chromatography were dialyzed into assay buffer (50 mM Tris, pH 7.4), while Gαs was maintained in size exclusion chromatography buffer to preserve protein stability.

The functional activity of adenylate cyclase variants was evaluated using enzymatic conversion assays as described in **Section 4.3.** Reaction mixtures containing ATP, divalent cofactors, and the activator forskolin were prepared on ice to maintain enzyme stability prior to initiation. Protein concentrations for each fraction were determined by absorbance at 280 nm to ensure consistent loading across samples.

Reactions were initiated by the addition of purified AC6 and incubated at 37°C for 15 minutes before being quenched with 5% (v/v) formic acid. Precipitated protein was removed by centrifugation, and the resulting supernatant was analyzed by HPLC using a phenyl stationary phase column. This approach enabled comparison of enzymatic activity across different protein preparations, including natively soluble fractions and proteins refolded using guanidine hydrochloride or urea. These comparisons were used to assess the extent of functional recovery and to evaluate the influence of denaturant choice on folding efficiency and enzymatic activity.

4.2.6 AC6 Catalytic Activity Depends Strongly on Refolding Conditions

Enzymatic activity assays (**Figure 57**) were performed in duplicate (n = 2), including a negative control lacking enzyme to confirm that no non-enzymatic conversion of ATP to cAMP occurred under assay conditions. Percent conversion was calculated using the relationship: (cAMP peak integration / total peak integration) × 100. Enzymatic activity assays (**Figure 57**) revealed clear differences in catalytic performance depending on protein source

and refolding conditions. In the natively soluble fraction (**Figure 57**A) peaks corresponding to ATP (RT ≈ 1.5 min) and cAMP (RT ≈ 8.8 min) were observed, with ATP remaining the dominant species. Although the soluble protein retained catalytic activity, conversion efficiency was low (~16%), indicating limited substrate turnover under the tested conditions.

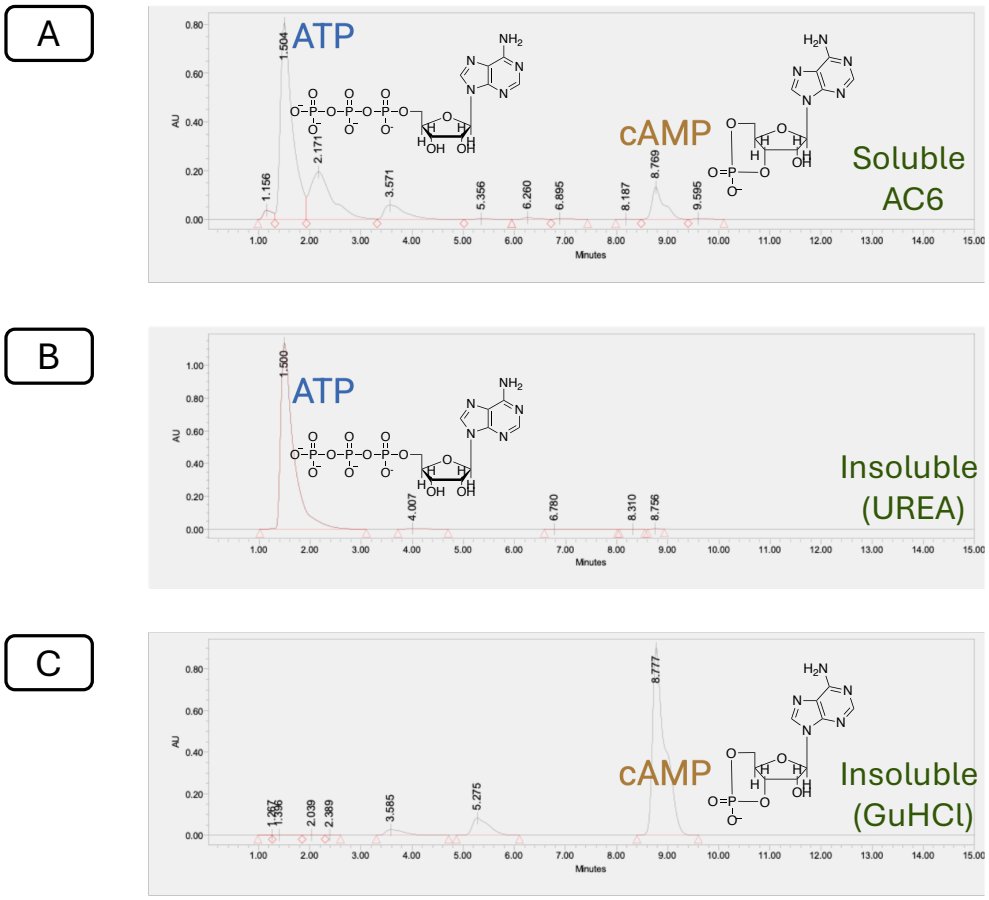


Figure 57. AC6 activity depends on refolding conditions as measured with HPLC. ATP consumption and cAMP formation were monitored for (A) soluble AC6, (B) urea-refolded AC6, and (C) GdnHCl-refolded AC6.

In contrast, significant differences were observed between insoluble fractions refolded using urea or guanidine hydrochloride. The urea-refolded sample (**Figure 57**B) exhibited negligible activity, with ATP largely unconsumed and no detectable cAMP peak at the expected retention time. Minor signals near 8 minutes were observed but did not correspond to cAMP, indicating unsuccessful recovery of functional enzyme. Conversely, the GuHCl-refolded sample (**Figure 57**C) demonstrated substantial catalytic activity, characterized by

near-complete ATP consumption and a prominent cAMP peak at ~8.77 min. These results indicate that, although AC6 is primarily expressed in an insoluble form, functional recovery is highly dependent on the refolding strategy employed. All peak integrations and sample information is provided in **Appendix Figure 17**.

The improved performance of GuHCl-refolded protein likely reflects more complete denaturation and subsequent refolding into a catalytically competent conformation. As a stronger chaotrope, GuHCl disrupts electrostatic and hydrophobic interactions more effectively, promoting uniform unfolding and facilitating proper refolding upon removal. In contrast, urea may stabilize partially folded intermediates, leading to misfolding or aggregation and loss of activity. Overall, these findings demonstrate that GuHCl is more effective than urea for restoring AC6 catalytic function. While measurable activity was observed in both soluble and GuHCl-refolded samples, subsequent studies were directed toward evaluating enzyme performance in the presence of its native activator, Gαs.

4.2.7 Reconstitution Attempts With Activators: Forskolin vs Gαs

For these experiments, the GuHCl-refolded AC6 sample was selected due to its comparatively high catalytic activity observed in prior assays. Basal activity was first assessed in the presence of forskolin alone, serving as a control condition. As shown in **Figure 58**, peaks corresponding to ATP (RT ≈ 2.6 min) and cAMP (RT ≈ 10.6 min) were detected, with ATP remaining the dominant species, indicating limited conversion to cAMP under these conditions.

To evaluate activation by the native regulatory protein, Gαs was used in place of forskolin. Under these conditions, similar ATP and cAMP peaks were observed (RT ≈ 2.6 min and ≈ 10.5 min, respectively), with an approximate twofold increase in cAMP production relative to the forskolin-only condition. This result indicates that Gαs can enhance AC6 activity, although the magnitude of activation differs from expected behavior. The combined effect of both activators was also assessed. In this condition, ATP and cAMP peaks were again observed at comparable retention times; however, cAMP production increased by only ~1.2-fold relative

to forskolin alone. This modest enhancement contrasts with the synergistic activation typically reported for adenylate cyclases in the presence of both Gαs and forskolin. All peak integrations and sample information are provided in **Appendix Figure 18**.

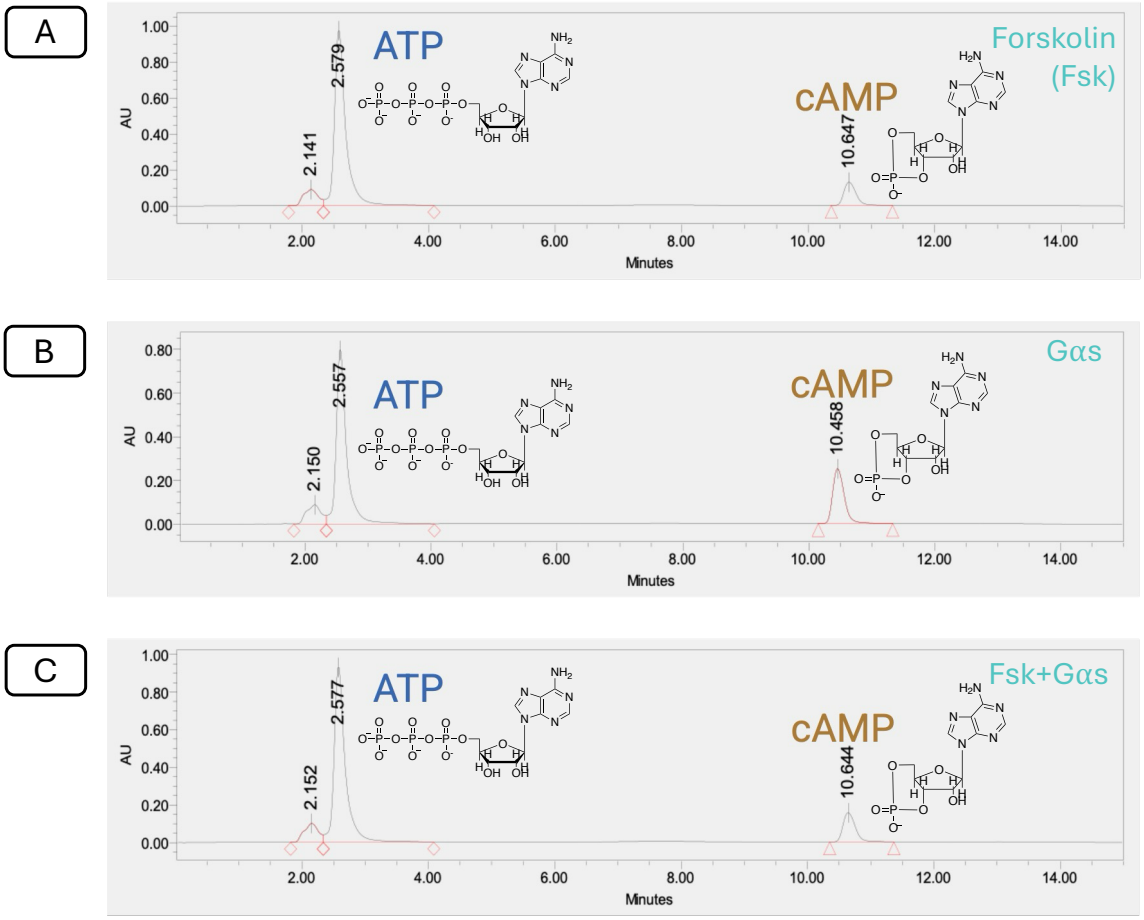


Figure 58. Activation of refolded AC6 by forskolin and Gαs (HPLC). ATP-to-cAMP conversion was measured with **(A)** forskolin, **(B)** Gαs, or **(C)** both activators. Measurements conducted in triplicates (n=3).

The absence of the expected maximal activation suggests that the GuHCl-refolded AC6 may not fully recapitulate native regulatory behavior. One possible explanation is that the refolding process stabilizes the enzyme in a conformation that is partially active but less responsive to allosteric modulation or that simply expressing the cytosolic domains alone might not be sufficient to achieve full AC6 activation, Alternatively, structural perturbations

introduced during refolding may compromise the accessibility or integrity of activator binding sites, despite retention of catalytic function.

Overall, while GuHCl refolding enables recovery of catalytic activity, the altered regulatory response limits the suitability of this protein for detailed functional studies. Additional efforts, including optimization of purification strategies and construct design (e.g., alternative tagging approaches), did not resolve these functional limitations.

4.2.8 Periplasmic Export Strategy to Improve Folding (pelB ± pTUM4)

To address the challenges associated with improper folding and low functional recovery of AC6, an alternative strategy was implemented involving periplasmic expression to promote correct folding and disulfide bond formation. A recombinant construct (pET29a_AC6_pelB) was designed to include an N-terminal pelB signal sequence and a C-terminal His tag, enabling targeting of the protein to the periplasmic space of *E. coli* and facilitating downstream purification. The pelB signal sequence is a 22 residue N-terminal peptide from pectate lyase B (pel) enzyme from the bacterium *Erwinia carotovora* and it is widely used in recombinant protein expression. Similar to other secretory peptides, it contains a positively charged N-terminal region, a central hydrophobic region and a more polar C-terminal region. It plays a role in periplasmic targeting, directing the protein from the cytoplasm across the inner membrane into the periplasm of Gram-negative bacteria like *E. coli*. This peptide utilizes the Sec-dependent translocation pathway, a mechanism that facilitates the transport of proteins across the inner membrane in a predominantly unfolded or loosely folded state. Upon reaching the periplasmic space, the pelB leader sequence is enzymatically processed and removed by a specific signal peptidase. Directing protein translocation to the periplasm offers significant biosynthetic advantages; unlike the cytoplasm which maintains a highly reducing environment that precludes the formation of stable disulfide bonds, the periplasm provides a robust oxidizing environment. This oxidative environment is essential for facilitating proper protein folding and the subsequent establishment of the disulfide bridges required for structural integrity and functional activity

of the enzyme. The protein was transformed into *E. coli* BL21 (DE3), and the colonies were used for an overnight culture. Additionally, BL21 cells transformed with both pet29a_AC6_pelB and the pTUM4 plasmid. The pTUM4 plasmid is a highly specialized co-expression helper vector developed for use within *E. coli*. Its function is to significantly enhance the soluble yield and functional folding of recombinant proteins targeted for secretion into the bacterial periplasmic space. This necessity arises because the native *E. coli* periplasmic machinery is often overwhelmed with the high-level expression of complex proteins requiring proper folding and the formation of multiple disulfide bonds. To overcome such challenges, the pTUM4 vector is engineered to constitutively express four genes that encode essential periplasmic folding proteins. The first set of genes facilitate proper disulfide bond formation: *dsbA* encodes thiol-disulfide oxidoreductase A, which catalyzes the crucial oxidation step leading to disulfide bond formation. Complementing this is *dsbC*, which codes for thiol-disulfide isomerase C that is vital for correcting any incorrectly formed disulfide linkages. The remaining two genes address general folding issues that may arise. The *fkpA* gene encodes peptidyl-prolyl *cis/trans* – isomerase A (PPIase), an enzyme that accelerates the typically rate-limiting *cis-trans* isomerization of peptidyl-prolyl bonds. Finally, the *surA* gene codes for survival protein A which functions as a general chaperone. This protein provides broad folding assistance, aiding in the proper transport and folding of various periplasmic and outer membrane proteins. These four co-expressed factors transform the *E. coli* periplasm into a more robust environment for proper protein folding of recombinantly expressed proteins. Following expression in *E. coli* BL21 (DE3), periplasmic fractions were isolated using an osmotic shock protocol.[146] Briefly, the procedure utilizes a high osmolarity buffer containing sucrose and ETDA to induce rapid cellular swelling and lysis. The high solute concentration in the buffer facilitates the rapid influx of fluid into the cells, causing cell rupture. Concurrently, the inclusion of EDTA chelates divalent metal ions crucial for stabilizing the lipopolysaccharide (LPS) layer of the Gram-negative outer membrane, thereby assisting in membrane permeability and cell disruption.

SDS-PAGE analysis revealed the presence of AC6 in both whole cell and periplasmic fractions, with increased band intensity observed in periplasmic extracts, indicating

successful targeting and extraction. Notably, co-expression with pTUM4 resulted in a marked increase in protein yield compared to expression of AC6 alone, suggesting improved folding and/or stability under these conditions. Periplasmic fractions were subsequently subjected to affinity purification, and elution samples were analyzed by SDS-PAGE, confirming enrichment of the target protein at the expected molecular weight. Protein identity was further validated by Western blot analysis using an anti-His tag antibody.

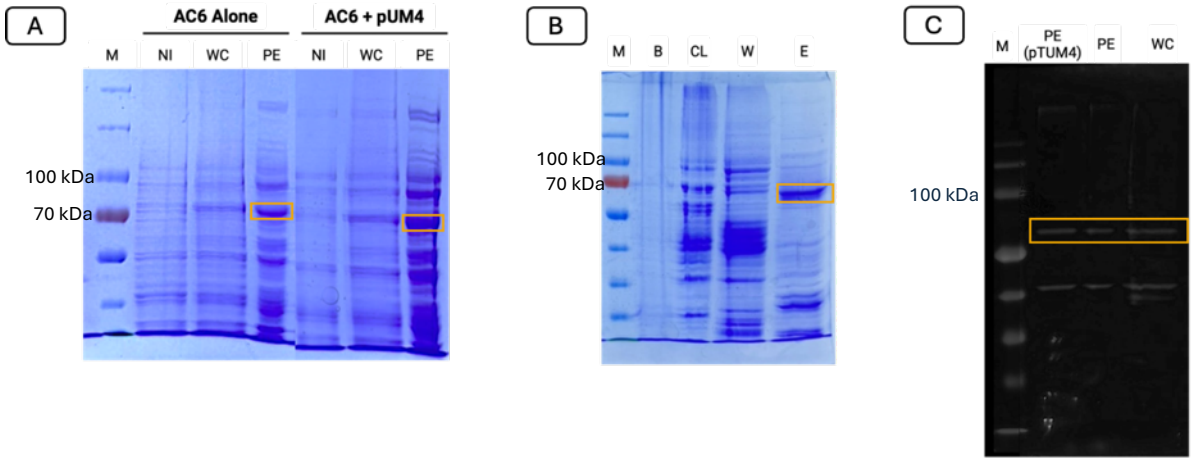


Figure 59. Periplasmic expression of AC6 using pelB signal peptide ± pTUM4 (SDS-PAGE and Western blot) (A) Whole-cell and periplasmic extracts. **(B)** IMAC purification. **(C)** Anti–His-tag Western blot confirming AC6 in periplasmic extracts.

4.2.9 Domain-Based Strategy: Separate C1 and C2 Domains and Activity Tests

Overall, SDS-PAGE analysis (**Figure 59**) confirmed successful expression and periplasmic localization of AC6. Enhanced protein levels were observed upon co-expression with the pTUM4 plasmid, indicating that the presence of periplasmic folding factors improves protein accumulation. However, despite evidence of protein expression, periplasmic production was not consistently reproducible, and further functional characterization of this system was not pursued.

Given the challenges encountered in obtaining soluble, functional AC6, prior literature on heterologous expression of adenylate cyclases was examined. Notably, previous studies

have reported the successful construction of soluble adenylate cyclase variants through fusion of cytosolic domains from different isoforms. In one such approach, the C1a domain of AC1 and the C2a domain of AC2 were linked using flexible peptide linkers of varying lengths. Constructs containing intermediate-length linkers (~14 amino acids) demonstrated higher catalytic activity compared to shorter linkers (~6 amino acids), particularly in the presence of activators such as Gαs and forskolin.[145]

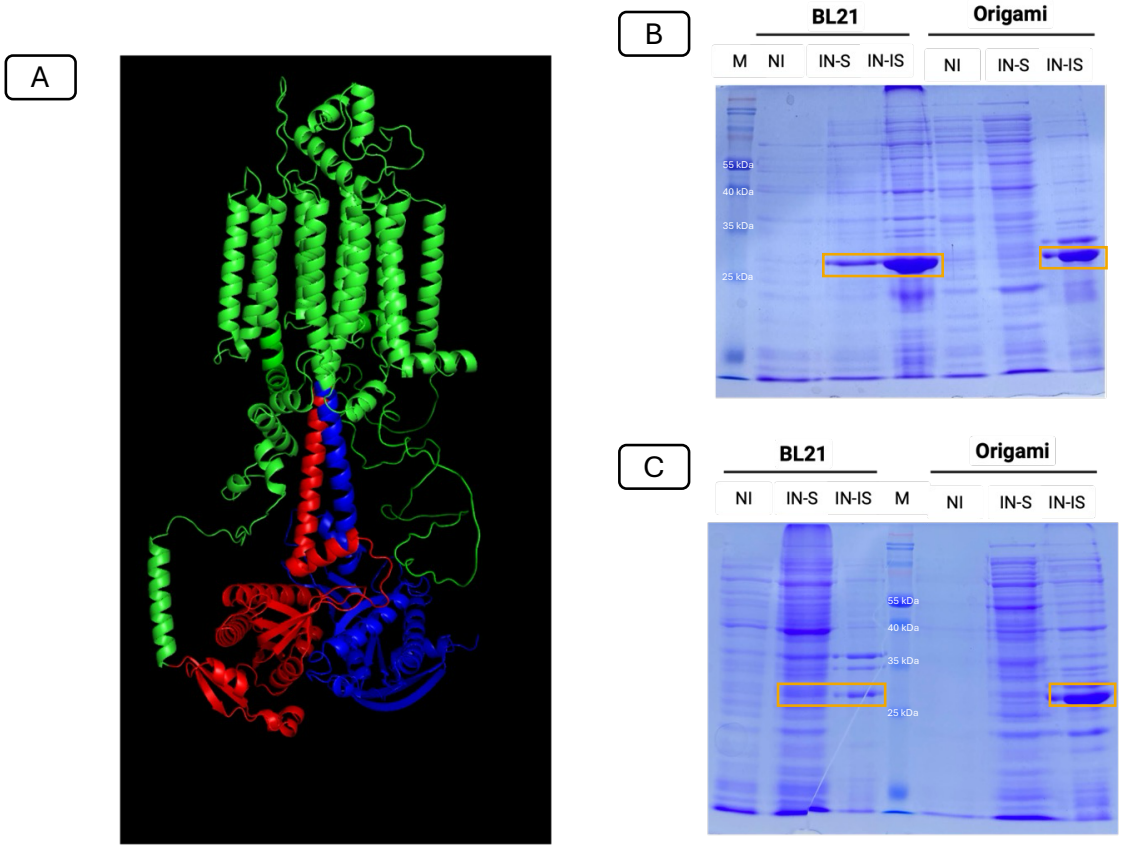


Figure 60. Mapping and expression of AC6 cytosolic domains. (A) AlphaFold model highlighting C1 (blue) and C2 (red) regions. **(B–C)** SDS-PAGE expression of C1 and C2 in BL21(DE3) and Origami™; NI, S, and IS fractions.

These findings informed subsequent design strategies in this work. Unlike the literature approach, where domains were directly fused, initial constructs in this study maintained the domains as separate entities. To guide construct redesign, domain boundaries were identified by aligning the AC6 AlphaFold model with AC1 and AC2 structures, enabling mapping of the corresponding C1a and C2a regions. These domains are highlighted on the

AC6 model, with C1a shown in blue and C2a in red, providing a structural framework for future construct optimization. (**Figure 60**)

Primers were designed to clone the C1 and C2 cytosolic domains into separate pET28b expression vectors. PCR-amplified fragments were assembled using Gibson Assembly, and successful construct formation was confirmed by agarose gel electrophoresis (**Appendix Figure 20**). Verified plasmids were subsequently transformed into *E. coli* BL21 (DE3) and Origami™ strains for expression.

Following optimization of expression conditions, including temperature and induction time, protein production and solubility were assessed by SDS-PAGE (**Figure 60**). Despite removal of transmembrane domains, both constructs remained predominantly insoluble. In the BL21 (DE3) strain, limited protein was observed in both soluble and insoluble fractions, whereas expression in the Origami™ strain resulted primarily in insoluble protein. The persistence of insolubility may be attributed to improper disulfide bond formation within the cytosolic domains, which contain multiple cysteine residues. Mismatched disulfide bonds can promote aggregation and inclusion body formation, consistent with the observed distribution of protein. Soluble fractions obtained from BL21 (DE3) expression were isolated

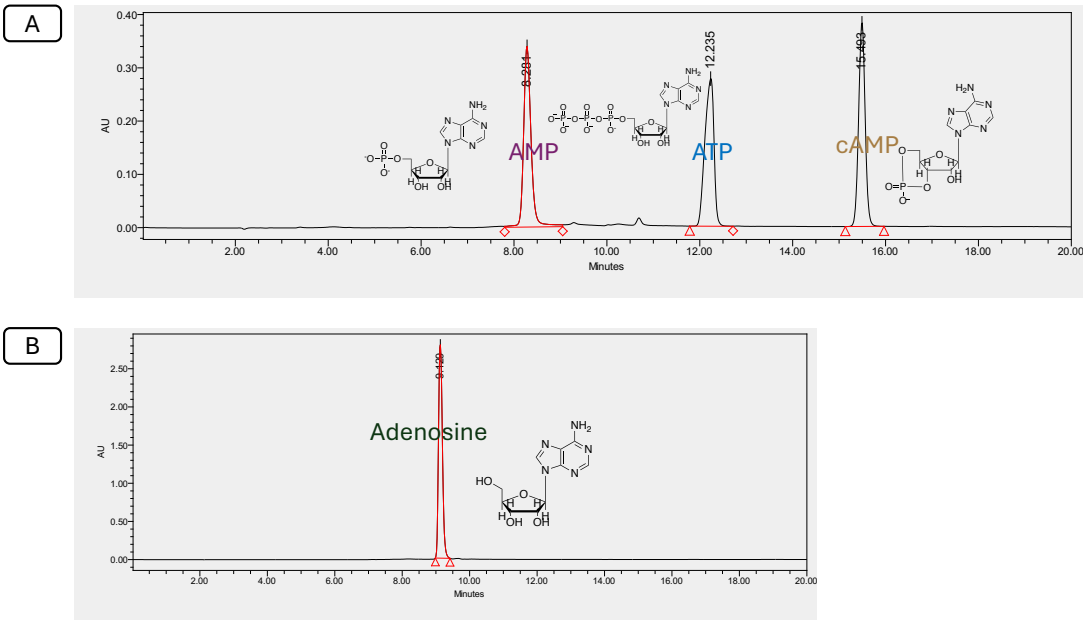


Figure 61. HPLC separation of adenine nucleotides and adenosine standards. AMP, adenosine, ATP, and cAMP were resolved under the indicated reverse-phase conditions.

and purified using nickel affinity chromatography. Purified C1 and C2 domain proteins were subsequently evaluated for activity using the HPLC-based cAMP assay. Prior to conducting the experiments, several control tests were performed utilizing an enhanced method that incorporates ion pairing agents to achieve improved separation of polar molecules during chromatography on a hydrophobic column. (**Figure 61**)

HPLC analysis enabled resolution of key adenine-based molecules, including ATP, ADP, AMP, cAMP, and adenosine, representing an improvement over earlier methods and accounting for observed differences in retention times. Enzymatic assays were performed by combining the C1 and C2 domains in equimolar ratios and incubating under standard conditions.

Following incubation, reactions were quenched with formic acid, clarified by centrifugation, and analyzed by HPLC to assess catalytic activity (**Figure 62**) After 30 minutes, a dominant

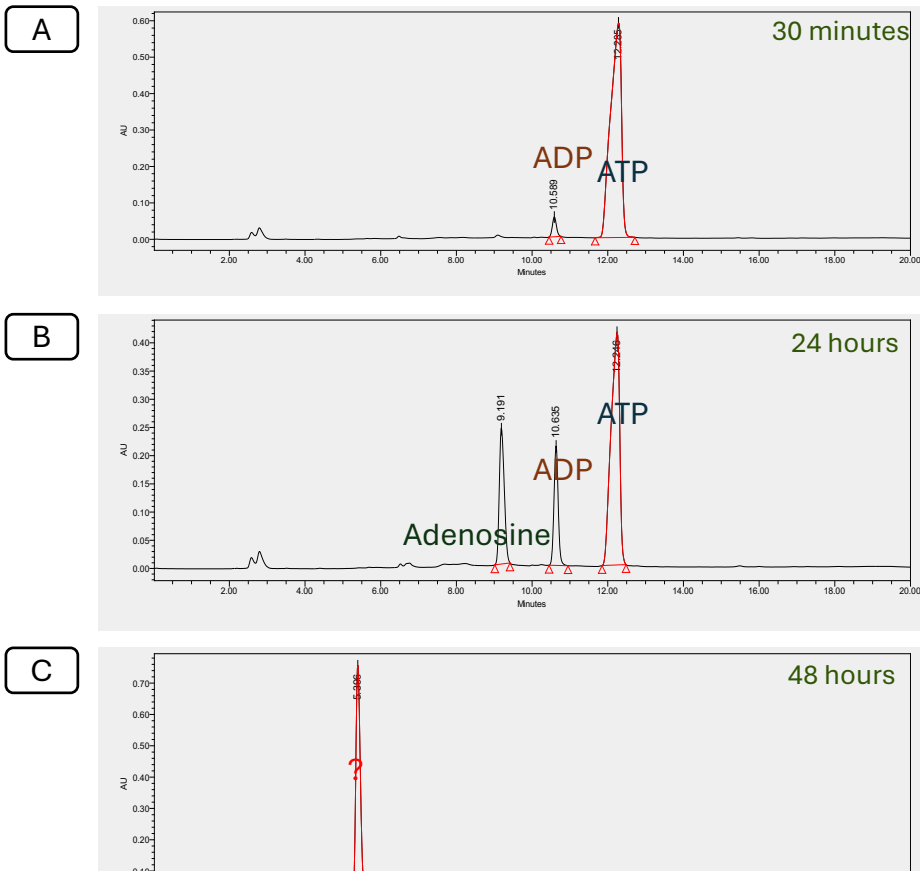


Figure 62. Activity assays of isolated AC6 C1 and C2 domains (HPLC). Chromatograms after **(A)** 30 min, **(B)** 24 h, and (**C)** 48 h incubation show ATP and degradation products, with no detectable cAMP.

ATP peak (RT ≈ 12.3 min) and a smaller ADP peak (RT ≈ 10.6 min) were observed, with no detectable cAMP formation.

After 24 hours, ATP remained the predominant species, accompanied by minor peaks corresponding to ADP and adenosine (RT ≈ 9.2 min), suggesting limited substrate degradation but no cAMP production. Extending the incubation to 48 hours resulted in the loss of discernible ATP and degradation product peaks, with only an unidentified peak observed (RT ≈ 5.4 min), consistent with potential nucleotide degradation pathways (**Appendix Figure 19**). To assess whether cAMP degradation contributed to the absence of detectable product, assays were repeated in the presence of IBMX, a phosphodiesterase inhibitor. However, no cAMP formation was observed under these conditions. Additional control experiments involving spiking cAMP into reaction mixtures prior to HPLC analysis yielded inconsistent results, with variable recovery of cAMP (data not shown).

Collectively, these results indicate that the unlinked C1 and C2 domains do not reconstitute functional catalytic activity under the conditions tested.

4.2.10 Summary and Next Steps

In this work, a comprehensive experimental framework was established to enable the biochemical characterization of adenylate cyclase 6 (AC6) and its regulation by small-molecule and protein activators. A robust HPLC-based assay was successfully developed that allows reliable separation and quantification of ATP, ADP, AMP, and cAMP, providing a direct and sensitive readout for adenylate cyclase activity. This analytical platform represents a key outcome of the study and forms a solid foundation for future functional investigations of AC enzymes and their modulators.

To supply enzymatically active material for these assays, multiple heterologous expression strategies for AC6 were explored in *Escherichia coli*. Truncated constructs lacking the transmembrane domains were designed to enhance solubility; however, across several commonly used expression strains and growth conditions, AC6 was produced predominantly in insoluble inclusion bodies. Lowering expression temperature increased

overall yield but did not substantially improve solubility. Despite these challenges, catalytically active AC6 could be recovered through denaturation and refolding from inclusion bodies. Importantly, the choice of denaturant proved critical: refolding from guanidinium hydrochloride yielded enzyme preparations capable of robust ATP-to-cAMP conversion, whereas urea-refolded protein was catalytically inactive. These results demonstrate that AC6 can adopt a catalytically competent conformation following complete unfolding and refolding, but they also highlight the sensitivity of the enzyme to folding history.

Although guanidinium-refolded AC6 displayed significant catalytic activity, its regulatory behavior differed from that reported for native AC6. Stimulation by Gαs and synergistic activation by forskolin were markedly reduced or inconsistent, suggesting that while the catalytic core was functional, allosteric regulation and protein–protein interaction surfaces were likely compromised during refolding. This limitation renders the refolded enzyme unsuitable for reliable screening of AC6 activators, where correct regulatory responses are essential.

Additional strategies aimed at improving folding fidelity were therefore explored. Periplasmic targeting using a pelB signal sequence, combined with co-expression of folding assistants via the pTUM4 plasmid, increased the apparent accumulation of AC6 in the periplasmic fraction. However, expression and extraction proved variable and insufficiently reproducible to support downstream functional assays. A domain-based approach, inspired by prior studies on chimeric adenylate cyclases, was also investigated by expressing the cytosolic C1 and C2 domains separately. Despite successful cloning and expression, these domains remained largely insoluble and failed to reconstitute detectable cAMP production, even after prolonged incubation and inhibition of phosphodiesterase activity.

Taken together, these findings indicate that while *E. coli* can be used to generate catalytically active AC6 material under certain conditions, obtaining a soluble, reproducible, and properly regulated AC6 preparation remains a significant challenge. The results suggest that correct spatial organization of the C1 and C2 domains is essential not only for catalysis but also for regulatory coupling to Gαs and small-molecule activators. Future efforts should

therefore focus on construct designs that enforce native-like domain geometry, such as single-chain catalytic cores with carefully optimized linker lengths, as well as on folding strategies that preserve allosteric site integrity rather than merely restoring enzymatic activity.

Beyond bacterial expression systems, alternative hosts such as insect or optimized mammalian cells may ultimately be required to achieve fully functional and regulatable AC6 suitable for pharmacological studies. Importantly, the HPLC-based activity assay developed here is independent of the expression platform and can be readily applied to protein produced in other systems. In this sense, the present work establishes both the analytical tools and a clear experimental roadmap for future studies aimed at understanding AC6 regulation and developing novel activators relevant to conditions such as persistent pulmonary hypertension of the newborn.

4.3 Material and Methods

4.3.1 Media

Name	Composition
Enriched Media	2% Tryptone 1% Yeast Extract 0.5% NaCl 0.2% Glycerol 50mM KH_2PO_4

4.3.2 Buffers

Name	Composition
AC6 Refolding Buffer Urea	25mM Tris 300mM NaCl 8M Urea pH 8.0
AC6 Refolding Buffer GuHCl	25mM Tris 300mM NaCl 5M GuHCl pH 8.0
AC6 Cation Start IEX Buffer	50mM TRIS pH 8.0
AC6 Cation Elution IEX Buffer	50mM TRIS 1M NaCl pH 8.0
AC6 Periplasmic Extraction Buffer	500mM Sucrose 1mM EDTA 100mM TRIS-HCl pH 8.0
AC6 Cytosolic IMAC Lysis Buffer	50mM Phosphate 500mM NaCl 5mM Beta-Mercap pH 8.0
AC6 Cytosolic IMAC Wash Buffer	50mM Phosphate 500mM NaCl 5mM Beta-Mercap 20mM Imidazole pH 8.0
AC6 Cytosolic IMAC Elution Buffer	50mM Phosphate

	500mM NaCl 5mM Beta-Mercap 250mM Imidazole pH 8.0
Gas Lysis Buffer insoluble (Soluble version without Urea)	50mM Tris 20mM B-mercap 8M Urea pH 8.0
Gas Wash Buffer insoluble (Soluble version without Urea)	50mM Tris 20mM B-mercap 500mM NaCl 40mM Imidazole 8M Urea pH 8.0
Gas Elution Buffer Insoluble (Soluble version without Urea)	50mM Tris 20mM B-mercap 300mM NaCl 250mM Imidazole 8M Urea 10% Glycerol pH 8.0
Gas Refolding Buffer	20mM Tris pH 8.0 20% Gylcerol 0.1 EDTA 1mM DTT 0.1% CHAPS 100uM GDP
Gas SEC Buffer	20 mM Tris (pH 8.0) 150 mM NaCl 10% glycerol 5 mM $MgCl_2$
HPLC Buffer A	80 mM KH2PO4 pH 6.0 w/ 20% KOH
HPLC Buffer B	MeOH (100%)
HPLC Buffer C	MiliQ water (0.1% FA).

4.3.3 Plasmids

Plasmid Name	Resistance	Source
pET30a_AC6_FlagTag*	Kan	GenScript
pET30a_Gas_HisTag	Kan	GenScript
pET29b_pelB_AC6*	Kan	Twist Bioscience
pET29b_AC6_C1	Kan	This work
pET29b_AC6_C2	Amp	This work

*****Versions of these plasmids without either FlagTag or pelB sequence were created however not used in experimentation

4.3.4 Strain Information

Database Number	Genotype and Notes	Auxotrophy	Source
E. coli BL21 (DE3)	*E. coli B* *F- ompT gal dcm+ lon hsdSB (rBmB-) λ(DE3 [lacI lacUV5-T7p07 ind1sam7 nin5])*	None	From Dr. Nediljko Budisa MB Strain Database
DH5α	F^- endA1 glnV44 thi-1 recA1 relA1 gyrA96 deoR nupG purB20	None	From Dr. Nediljko Budisa Manitoba Strain Database

	Φ80dlacZΔM15 Δ(lacZYA-argF)U169, hsdR17(r_K^-, m_K^+), λ		
E. coli BL21 (AI)	F- ompT hsdSB (rB-mB-) gal dcm araB::T7RNAP-tetA	None	Thermo Fisher
E. coli BL21 (Origami (DE3) pLysS	*Δ(ara-leu)7697 ΔlacX74 ΔphoA PvuII phoR araD139 ahpC galE galK rpsL(Str^R) F'[lac$^+$ lacI^q pro] (DE3) gor522::Tn10 trxB pLysS[T7p20 orip15A](CmR)*		Millipore Sigma Novagen

4.3.5 Primer Information

Primer Name	Sequence (5'-> 3')
FlagTagDel-F	GCTGCTCGGGCCGCCATTC
FlagTagDel-F	GGCGCGGGCCACCACCACCACCACCACTG
pelBDel-F	ATCGCATATGGGAAGTTGGTTTTCCGGG
pelBDel-R	TTCACTCGAGGCTTGACGGGCC
C1-F	AATTTTGTTTAACTTTAAGAAGGAGATATACATATGGCGTTCCAGGAAACCCGTG
C1-R	GTTAGCAGCCGGATCTCAGTGGTGGTGGTGGTGGTGGCTGGCACCCAGTATCAGAA
C2 -F	ATTTTGTTTAACTTTAAGAAGGAGATATACATATGCTCGACTTTCTGTGGAAATTGCA
C2 -R	TTAGCAGCCGGATCTCAGTGGTGGTGGTGGTGGTGGCTTGACGGGCCACC
pET29B -F	CACCACCACCACCACCACT
pET29B -R	CATATGTATATCTCCTTCTTAAAGTTAAACAAAATTATTTCTAGAGGG

4.3.6 AC6 Protein Expression and Purification – Flag-Tag peptide

Various *E. coli* strains such as BL21(DE3), AI™ and Origami™ were transformed with pET30a_AC6_FlagTAg purchased from GenScript. Using an overnight culture, LB media was inoculated and grown at 37 °C until an OD_{600} of 0.6-0.8 was reached. All cultures were induced with 1mM IPTG, with 0.2% L-arabinose required for the Ai™ strain and after induction, the protein was expression at 16°C overnight. Following expression, the cells

pelleted via centrifugation (17,000 xg, 4°C, 15 minutes) and resuspended in various lysis buffers. All buffer contained 25mM Tris, 300mM NaCl and either contained 5mM GuHCl or 8M Urea or no denaturant, and were all adjusted to pH 8.0. The cells were sonicated for 15 minutes for cell lysis, and the cell debris was removed via centrifugation (20,000 xg, 4°C, 45 minutes). Initial assays were conducted with unpurified protein (data not shown).

Initial protein purification attempts using the Flag-Tag were unsuccessful thus ion exchange chromatography was explored as an alternative strategy. The protein following lysis was dialyzed into the IEX start buffer (Tris 20 mM, pH 8.0) and eluted using gradient created with the elution buffer (Tris 20 mM, 1M NaCl, pH 8.0). Proteins were purified using an anionic exchange (Capto HiRes Q 5/50) and cationic exchange (Capto HiRes S 5/50) column. Fractions containing AC6 were grouped to activity assays.

4.3.7 Gas Protein Expression and Purification

The codon-optimized Gas sequence cloned into pET30a was purchases from GenScript and cloned into DH5a for plasmid production. The plasmid pET30a_Gas was transformed into various *E. coli* strains such as BL21(DE3), AI™ and Origami™. From the plates, an overnight culture was made in LB and grown overnight 37 °C. Using the culture, LB media was inoculated and grown at 37 °C until an OD_{600} of 0.6-0.8 was reached. All cultures were induced with 1mM IPTG, with 0.2% L-arabinose required for the Ai™ strain and after induction, the protein was expression at 30°C overnight. Following initial expression tests, BL21(DE3) was chosen as the expression strain and enriched media for better expression. Following expression, the cells were pelleted via centrifugation (17,000 xg, 4°C, 15 minutes) and resuspended in binding buffer (50mM Tris, 20mM B-mercap, pH 8.0). The cells were lysed via sonication for 15 minutes in 15 second pulses and centrifuged to remove cellular debris (20,000 xg, 4°C, 45 minutes). The proteins were purified using metal affinity chromatography using a HisTrap™ FF affinity column (Cytiva) connected to a BioRAD NGC chromatography system. The column was loaded with the sample, impurities were washed with wash buffer (50mM Tris, 20mM B-mercap, 500mM NaCl, 40mM Imidazole, pH 8.0) and

the protein was eluted with the elution buffer (50mM Tris, 20mM B-mercap, 300mM NaCl, 250mM Imidazole, 10% Glycerol, pH 8.0). Following this purification, the sample was dialyzed into SEC buffer (20mM Tris, 150 mM NaCl, 10% Glycerol, 5mM $MgCl_2$, pH 8.0) and purified using a HiLoad 16/600 Superdex 75pg Column (Cytiva) connected to a BioRAD NGC chromatography system. The purified samples were analyzed using SDS-PAGE to confirm protein presence and purity.

4.3.8 General HPLC Separation Method

Prior to the activity assays, the HPLC method was developed by Dr. Pritchard from the Sorensen Lab and method is as follows. For separation of the analytes, the Xbridge Phenyl (5 µm, 3.0 mm x 150 mm) was used, and analysis was carried out using a Waters Alliance 2695 Separations Module with Waters 2996 Photodiode Array Detector. The samples were loaded into Waters total recovery clear glass HPLC vials for assay analysis. The buffers for the method were: Buffer A: 80 mM KH2PO4 (pH 6.0 w/ 20% KOH). Buffer B: MeOH (100%). Buffer C (Wash only): Miliq water (0.1% FA). The separation method was as follows: 0 min, A (100%). 2 min, A (100%). 8 min, A (85%). 13 min, A (85%). 15 min, A (100%). 20 min, (A) 100%. Flow rate: 0.5 mL/minute. The column was equilibrated with potassium phosphate buffer for 15 minutes prior to the run start time and after the run is complete, a wash method is used to return column to 100% MeOH.

4.3.9 Bacterial AC6 Assay

The following materials were prepared to their standard concentrations listed: $MgCl_2$ (100 mM,20 µL), ATP (3.5 mM, 20 µL), Fsk (1mM, 2 µL), AC6 protein (20 µL) tris buffer (50 mM pH 7.4, to 200 µL total volume. Most stock solutions were prepared in Tris Buffer while, Fsk and IBMC were dissolved in DMSO. Following addition of the components, the final stock concentration of reagent in the assay were as follows: 10 mM $MgCl_2$, 0.35mM ATP, 10 µM Fsk, 1mM IBMX. For each assay, the reagents such as $MgCl_2$, ATP, Tris buffer and forskolin were

added to a 1.5 Eppendorf tube on ice. After the AC6 protein was added to the tube and mixed by inverting 5 times. The reaction mixture was placed into a water bath set to 37°C for 15 minutes. After this time, the reaction was halted by adding 50µL of 5% formic acid and the solution was mixed by inverting 5 times. Any insoluble material was removed via centrifugation (14,000 xg, RT, 4 minutes) after which the solution was transferred to the Total Recovery HPLC vials for HPLC analysis.

4.3.10 Improved HPLC Separation Method

The improved HPLC method was developed by Dr. Pritchard from the Sorensen Lab and method is as follows. For separation of the analytes, the Xbridge Phenyl (5 µm, 3.0 mm x 150 mm) was used, and analysis was carried out using a Waters Alliance 2695 Separations Module with Waters 2996 Photodiode Array Detector. The samples were loaded into Waters total recovery clear glass HPLC vials for assay analysis. The buffers for the method were: Buffer A: 65 mM KH_2PO_4 26 mM K_2HPO_4, 39mm TBAHS (tetrabutylammonium hydrogen sulfate) pH 6.0 and Buffer B: 65 mM KH_2PO_4 26 mM K_2HPO_4, MeOH (25%) pH 6.0. The pH was adjusted with phosphoric acid The separation method was as follows: 0 min, A (100%). 3 min, A (70%), 7.5 min A (20%), 15 min A (5%), 16 min A (5%), 18 min A (100%), 20 min A (100%) Flow rate: 0.5 mL/minute. The column was equilibrated with potassium phosphate buffer for 15 minutes prior to the run start time and after the run is complete, a wash method is used to return column to 100% MeOH. A wavelength at 254 nm was recorded for quantification.

4.3.11 Periplasmic Expression of AC6, Extraction and Purification

The codon-optimized sequence of AC6 with a pelB leader peptide was cloned into pET29b was purchased from Twist Bioscience and cloned into DH5a for plasmid amplification. The isolated plasmid (pET29b_AC6_pelB) was transformed into BL21(DE3) and additionally, the pTUM4 plasmid obtained from Dr. Arne Skerra was transformed along with pET29b_AC6_pelB for another experimental set. Overnight cultures were made for each cell

and used to inoculated LB + Kan Media (+Cm for cells with pTUM4). The cultures were grown until OD_{600} = 0.8 to 1.2 at 22°C after which protein expression was induced with 1mM IPTG and expression was carried out at 22°C overnight. The periplasmic extract was prepared according to protocols previously published.[147] The solutions were all chilled to 4°C, and the bacterial pellet were resuspended carefully with ice-cold periplasmic extract buffer. This resuspended pellet was incubated on ice for 30 minutes. To sediment the spheroplasts, the solution was centrifuged (5087 xg, 4°C, 15 minutes). The supernatant was carefully removed (the crude periplasmic cell fraction) and transferred to a fresh falcon tube. It was subjected to additional centrifugation (27,000 xg, 4°C, 15 minutes) to remove any residual debris. The periplasmic fraction was purified using a HisTrap™ FF affinity column (Cytiva) connected to a BioRAD NGC chromatography system. The protein was dialyzed first into the start buffer (50mM Phosphate, 500mM NaCl, pH 8.0) and then loaded onto the column. Impurities were washed with wash buffer (20mM Phosphate, 500mM NaCl, 20mM Imidazole, pH 8.0) and proteins were eluted with elution buffer (20mM Phosphate, 500mM NaCl, 250mM Imidazole, pH 8.0). The protein fractions were analyzed with SDS-PAGE to confirm purity.

4.3.12 Western Blotting of Periplasmic Extracts of AC6

The protein isolates were additionally analyzed using Western Blot to confirm the expression of AC6 within the periplasmic fractions. The proteins were first run on SDS-PAGE gel according to the standard protocols mentioned in **Section 5**. After electrophoresis, the gel was removed from the cast and subjected to the blotting procedure. The Trans-Blot Turbo Mini-size Transfer Stacks (BioRad) and the gel were washed/wetted with Trans-Blot Turbo Transfer Buffer (BioRad). The Immuno-Blot PVDF membrane (BioRad) was activated with 100% MeOH and all components were assembled into the blotting stack. Blotting was preformed using a Trans-Blot Turbo system (BioRad) and run at 1.3A/ 25V/ 7 minutes (the standard preprogrammed procedure). The membrane containing the transferred proteins were washed with TBST Buffer (20mM Tris, 150mM NaCl, 0.1% (w/v) Tween ® 20 Detergent). The blocking step was performed by incubating the membrane in a 5% (w/v) milk powder-

TBST solution for 1 hour. The milk solution was removed, and the membrane was incubated with the primary antibody solution (Novex 6x-His Epitope Tag Antibody (*Invitrogen*) diluted 5000x in 5% (w/v) milk powder-TBST solution). Following the incubation, the membrane was 3x with the TBST buffer for 15 minutes each time. The secondary antibody solution (Goat Anti-Mouse IgG (*EMD Millipore*) diluted 10,000x in 5% (w/v) milk powder-TBS solution) was incubated with the membrane for 1 hour. After this incubation the membrane was washed 3x using the TBST buffer for 15 minutes each time. To visualize the fragments, chemiluminescence was used by applying 1 ml of the Immobilon Forte Western HRP Substrate (*EMD Millipore*) and subsequent visualization with FluorChem Q system (*Cell Biosciences*) in accordance with manufacturer's protocol.

4.3.13 Cloning AC6 C1 and C2

The plasmid pet29a_pelB AC6 served as base of the cloning of the backbone and the cytosolic domain fragments. For isolation of the C1 and C2 domain, the plasmid was digested with Nde1 and Xho1 restriction enzymes. Following digestion, the samples were analyzed via Agarose Gel Electrophoresis, and the bottom band was excised using the gel extraction kit (Invitrogen, Thermo Fisher Scientific). The band was used as the PCR template to amplify the C1 and C2 domains with the primers specified above. The PCR reaction was carried out as listed in Primer Information. For the backbone, the pet29a_pelB AC6 plasmid was digested with Nco1 and Pst1 and following analysis with agarose gel electrophoresis, the appropriate band was excised using the gel extraction kit (Invitrogen, Thermo Fisher Scientific). Following the PCR reactions, correct products were analyzed via gel electrophoresis and excised. The fragments were used to preform Gibson Assembly and transformed into DH5a. The colonies were picked for making overnight cultures and used for plasmid isolation the following day. The isolated plasmid was used to confirm cloning via restriction digestion and analysis with agarose gel electrophoresis.

Table 7. Composition and Conditions for C1 and C1 Domain PCR Reaction.

Composition of PCR Reaction		PCR Conditions			
Component	Volume (µL)	Steps	Temp (°C)	Time	Cycles
MilliQ	35.9	Initial Denaturation	98	2 mins	1
5X HF Buffer	10	Denaturation	98	20 secs	35
dNTPs	1	Annealing	55	20 secs	
F-Primers	1	Extension	72	1 min	
R-Primers	1	Final Extension	72	5 mins	1
Template	1	Hold	10	Infinite	1
Phusion Enzyme	0.1				

Table 6. Composition and Conditions for pET29b Backbone PCR Reaction.

Composition of PCR Reaction		PCR Conditions			
Component	Volume (µL)	Steps	Temp (°C)	Time	Cycles
MilliQ	36.4	Initial Denaturation	98	2 mins	1
5X HF Buffer	10	Denaturation	98	20 secs	35
dNTPs	1	Annealing	55	20 secs	
F-Primers	1	Extension	72	3 mins	
R-Primers	1	Final Extension	72	5 mins	1
Template	0.5	Hold	10	Infinite	1
Phusion Enzyme	0.1				

4.3.14 Expression of C1 and C2 domains

The cloned plasmids pET29b_AC6_C1 and pET29b_AC6_C2 were separately transformed into both *E. coli* BL21(DE3) and Origami™ strains. From an overnight culture, a LB + Kan culture media was inoculated (1/100) and grown at 37°C for 4 hours. Protein production was induced with 1mM IPTG and protein was expressed overnight at 30°C. Following expression, the cell was pelleted via centrifugation (12,000 xg, 4°C, 15 minutes) and resuspended in C1 and 2 lysis buffer (50mM Phosphate, 500mM NaCl, 5mM Beta-Mercap, pH 8.0). The cells were sonicated for 15 minutes for cell lysis and subjected to centrifugation (20,000 xg, 4°C,

45 minutes) to remove any cellular debris. The supernatant was loaded onto a HisTrap™ FF affinity column (Cytiva) connected to an AKTA™ Start system. Any protein impurities were washed with wash buffer (50mM Phosphate, 500mM NaCl, 5mM Beta-Mercap, 25mM Imidazole, pH 8.0) followed by target protein elution with elution buffer (50mM Phosphate, 500mM NaCl, 5mM Beta-Mercap, 250mM Imidazole, pH 8.0). These samples were dialyzed into the AC6 assay buffers and using similar protocols were analyzed for activity.

5. General Materials and Methods

5.1 Materials

5.1.1 Antibiotic Stocks

Name	Stock Concentration
Ampicillin	100 mg/mL
Chloramphenicol	37 mg/mL
Kanamycin	50 mg/mL
Spectinomycin	100 mg/mL
Tetracycline	20 mg/mL

5.1.2 Media

TSB Media

Volume	Material
75 ml	LB Broth (2X)
15 g	PEG-400
1.5 ml	1M MgSO4
1.5 ml	1M MgCl2
7.5 ml	DMSO
upto 150 ml	Distilled Water

5.2 Methods

5.2.1 Preparation of KCM Competent cells

A bacterial overnight culture was inoculated 1:100 into 50 ml of LB media in a 250 ml. The culture was grown at 37°C with shaking at 250 rpm until OD_{600} = 0.3-0.5 was reached. Subsequently, the culture was centrifuged (6000g, 10 mins, 4 °C), the supernatant is discarded, and the pellet is resuspended in 1/10 volume of ice-cold Tryptic soy broth (TSB) media. The resuspended pellet is incubated on ice for 30 minutes after which it is aliquoted

in 100µL portions in pre-chilled 1.5 ml Eppendorf tubes. The tubes are frozen using liquid nitrogen and stored at -80°C.

5.2.2 Transformation

The following mixture is prepared on ice: 25µL of competent bacterial cells, 5µL of 5xKCM buffer, 3µL of plasmid DNA and 17µL of Sterile MilliQ water. Mixture is incubated on ice for 30 minutes, then heat shock at 42°C for 30 seconds (BL21) or 45 seconds (DH5α). Subsequently, the bacteria were chilled on ice for 3 minutes, 250µL of LB media was added and cells recovered (37°C, 1hr, 250 rpm). The cell suspension was plated on agar plates with the appropriate antibiotics and incubated overnight at 37°C.

5.2.3 Standard Gene Expression in *E. coli*

The plasmid containing the gene of interest was transformed into *E. coli BL21(DE3)* expression strain. 10 ml of LB medium with the appropriate antibiotic was inoculated with a frozen cell stock and incubated overnight (37°C, 250 rpm). 1L of fresh LB media with appropriate antibiotics was inoculated with 10ml of overnight culture and cells were grown at 37°C and 250 rpm until OD_{600} = 0.8 -1.2. After reaching the correct optical density, cell culture induced with 1mM isopropyl β-D-1-thiogalactopyranoside (IPTG) and incubated at expression temperature (16°C – 37°C) for 12-16h. Cell are harvested by centrifugation (4°C,12 min, 12,000xg) and pellet stored at -20°C until purification.

5.2.4 Cell Lysis

For cell disruption of E. coli, pellets are resuspended in lysis buffer of choice dependent on protein. The cells were lysed by sonication (Fisherbrand™ Model 50 Sonic Dismembrator, FB4435 probe) at 40% amplitude with pulses of 15s on and 20s off for 15 min on ice. The cell suspension was centrifuged (4°C,45 min, 20,000xg) to pellet cell debris and the supernatant was filtered (0.45µm filter). The filtered lysate was stored on ice until further purification.

5.2.5 Plasmid DNA Isolation

Plasmid isolation was carried out using either the GeneJET Plasmid Mini-prep Kit (Thermo Scientific), PureLink™ Quick Plasmid Miniprep Kit (Thermo Fisher Scientific) or PuroSPIN™ Plasmid Miniprep kit (Luna Nanotech, Canada). The DNA was eluted with preheated elution buffer and stored at -20°C.

5.2.6 DNA Concentration Measurement

The DNA concentration of purified samples was determined by measuring absorbance at 260nm using a NanoDrop™ One Microvolume UV-Vis Spectrophotometer (Thermo Scientific). To evaluate DNA purity, the absorbance was measured at 260 nm and 280nm, with good quality DNA ratio ($A_{260}/A_{280)}$ of 1.8 to 2.0).

5.2.7 Agarose Gel Electrophoresis

Gel electrophoresis was employed to visualize DNA fragments using a 1% agarose gel in 1x TAE buffer supplemented with SYBR™ Safe DNA Gel stain (Thermo Fisher Scientific). DNA samples were either directly loaded onto the gel or combined with 6x DNA Loading Dye (Thermo Scientific) and electrophoresed at 100V for 0.5 to 1 hour. The GeneRuler 1 kb DNA Ladder (Thermo Scientific) served as a molecular weight marker. Visualization of the gel was conducted using the Axygen® Gel Documentation System – BL (Corning Brand) with an EpiBlue light source for 250 seconds. Post-visualization, the gel was either discarded or bands were excised for further analysis.

5.2.8 Sodium Dodecyl Sulfate - Polyacrylamide gel electrophoresis (SDS-PAGE)

Sodium dodecyl sulphate-polyacrylamide gel electrophoresis (SDS-PAGE) was employed for the separation and analysis of proteins exceeding 15 kDa. The gel comprised a separation gel with an acrylamide concentration ranging from 8% to 12%, contingent upon the protein

of interest, and a 5% stacking gel. Protein samples were combined with 6x Laemmli SDS sample buffer (reducing) (Thermo Scientific) and incubated at 95°C for 5 minutes on a heat block. The samples were subsequently loaded into the wells and run for 60 minutes at a constant current of 20 mA. A PageRuler™ Prestained Protein Ladder from Thermo Scientific served as the molecular weight standard. Protein visualization was achieved by staining the gels with Coomassie Brilliant Blue staining solution (0.025% Coomassie Brilliant Blue R-250, 30% methanol, 10% acetic acid) in a microwave for 1.5 minutes. The gels were then destained overnight in a solution of 30% methanol and 10% acetic acid. Following destaining, the gels were visualized on a white light box.

5.2.9 Gibson Assembly – General

The Gibson Assembly protocols were carried out according to protocols listed in the GeneArt™ Gibson Assembly® HiFi Cloning Kits from Invitrogen by Thermo Fisher Scientific. Briefly, after obtaining the gel extracted PCR products, the vector and insert were mixed with 10µL of GeneArt™ Gibson Assembly® HiFi Master Mix on ice. The reaction volume was brought to 20µL with sterile MilliQ water, the reaction was mixed by vortexing and incubated at 50°C for 15 minutes. Following reaction completion, the mixture was diluted 1:5 with sterile water and transformed into DH5α cells.

6. Conclusion and Future Perspectives

This thesis establishes a framework for the incorporation of non-canonical amino acids into functional proteins by integrating chemical design, translational control, and metabolic engineering. Across three distinct systems, it demonstrates that successful non-canonical amino acid incorporation is not governed by chemical compatibility alone, but by the coordinated interaction between amino acid properties, enzymatic specificity, and cellular context.

Using EGFP as a model system, we show that methionine analog incorporation follows predictable principles based on side-chain polarity and local structural environment. These results provide a practical basis for assessing compatibility between non-canonical amino acids and protein stability and function. Importantly, they highlight that even subtle changes in side-chain chemistry can have pronounced effects on folding, fluorescence, and structural integrity.

Building on these principles, we developed a recombinant *E. coli* platform to produce the lantibiotic Nisin and its engineered variants. This system enables residue-specific incorporation of methionine analogs, including azidohomoalanine and homopropargylglycine, into a complex, post-translationally modified peptide. Functional validation confirmed that antimicrobial activity is retained despite chemical modification, demonstrating that site-specific incorporation of clickable groups is compatible with biological function.

A central advance of this work is the transition from external supplementation of non-canonical amino acids to their *in vivo biosynthesis*. Through metabolic pathway engineering and genomic integration, we established strains capable of autonomous azidohomoalanine production, eliminating reliance on costly external inputs. In parallel, overexpression of MetRS improved incorporation efficiency, and chromosomal integration of the nisin biosynthetic machinery increased system stability and reproducibility. The resulting “ALL-

IN" strain represents a genetically encoded and metabolically autonomous platform for producing clickable antimicrobial peptides.

The nisin production platform developed in this thesis differs methodologically from prior approaches to introducing non-canonical amino acids into lantibiotics. Bartholomae et al. incorporated Nε-Boc-L-lysine into nisin in both *E. coli* and *L. lactis* using an orthogonal pyrrolysyl-tRNA synthetase/tRNA(Pyl) pair to suppress an amber stop codon at a single defined site, an approach requiring continuous external supplementation of the ncAA and yielding low levels of modified peptide, particularly in L. lactis. By contrast, the platform in this thesis relies on residue-specific incorporation of methionine analogs via an overexpressed MetRS with relaxed substrate specificity, and genomic integration of the azidohomoalanine biosynthesis pathway removes the need for external ncAA supplementation altogether, distinguishing it as an autonomous, self-sufficient production system rather than one dependent on continuous analog dosing.

Despite these advances, several limitations remain. Incorporation efficiency is incomplete, and post-translational modification of Nisin is not yet fully optimized, resulting in heterogeneous product populations. These constraints reflect the intrinsic complexity of coordinating translation, metabolism, and enzyme-mediated maturation within a single system, particularly the temporal mismatch between amino acid availability and post-translational modification machinery. Addressing these limitations will require further optimization of metabolic flux, enzyme expression levels, and pathway balance.

The work on AC6 highlights additional challenges associated with expressing complex, multi-domain eukaryotic proteins in bacterial systems, particularly with respect to folding, solubility, and functional reconstitution. While partial success was achieved, this system underscores the importance of cellular context and folding environment in determining protein functionality.

Overall, this thesis demonstrates that non-canonical amino acid incorporation is best understood as a *systems-level problem*, in which translational machinery, metabolic state, and protein-specific constraints jointly determine outcome. The developed Nisin platform

provides a scalable route toward the production of chemically programmable antimicrobial peptides, with potential applications in drug development and functional biomaterials.

Future work should focus on improving incorporation efficiency and modification fidelity, expanding the range of non-canonical amino acids that can be biosynthesized in vivo, and applying directed evolution or adaptive strategies to enhance system robustness. In parallel, extending this approach to other ribosomally synthesized and post-translationally modified peptides (RiPPs) could further broaden the scope of chemically functionalized therapeutics.

In conclusion, this work moves the field from simple amino acid substitution toward *genetically encoded and metabolically autonomous systems* for the production of functional, chemically programmable proteins, establishing a foundation for next-generation protein engineering and therapeutic design.

7. References

(1) Devaraj, N. K.; Finn, M. G. Introduction: Click Chemistry. *Chem. Rev.* **2021**, *121* (12), 6697–6698. https://doi.org/10.1021/acs.chemrev.1c00469

(2) Dudchak, R.; Podolak, M.; Holota, S.; Szewczyk-Roszczenko, O.; Roszczenko, P.; Bielawska, A.; Lesyk, R.; Bielawski, K. Click Chemistry in the Synthesis of Antibody-Drug Conjugates. *Bioorganic Chem.* **2024**, *143*, 106982. https://doi.org/10.1016/j.bioorg.2023.106982

(3) Semisch, A.; Ohle, J.; Witt, B.; Hartwig, A. Cytotoxicity and Genotoxicity of Nano - and Microparticulate Copper Oxide: Role of Solubility and Intracellular Bioavailability. *Part. Fibre Toxicol.* **2014**, *11* (1), 10. https://doi.org/10.1186/1743-8977-11-10

(4) Chen, S.-Y.; Liu, S.-T.; Lin, W.-R.; Lin, C.-K.; Huang, S.-M. The Mechanisms Underlying the Cytotoxic Effects of Copper Via Differentiated Embryonic Chondrocyte Gene 1. *Int. J. Mol. Sci.* **2019**, *20* (20), 5225. https://doi.org/10.3390/ijms20205225

(5) Bock, V. D.; Hiemstra, H.; Maarseveen, J. H. van. CuI-Catalyzed Alkyne–Azide "Click" Cycloadditions from a Mechanistic and Synthetic Perspective. *Eur. J. Org. Chem.* **2006**, *2006* (1), 51–68. https://doi.org/10.1002/ejoc.200500483

(6) Besanceney-Webler, C.; Jiang, H.; Zheng, T.; Feng, L.; Soriano del Amo, D.; Wang, W.; Klivansky, L. M.; Marlow, F. L.; Liu, Y.; Wu, P. Increasing the Efficacy of Bioorthogonal Click Reactions for Bioconjugation: A Comparative Study. *Angew. Chem. Int. Ed.* **2011**, *50* (35), 8051–8056. https://doi.org/10.1002/anie.201101817

(7) Benner, S. A.; Sismour, A. M. Synthetic Biology. *Nat. Rev. Genet.* **2005**, *6* (7), 533–543. https://doi.org/10.1038/nrg1637

(8) Ganesh, R. B.; Maerkl, S. J. Biochemistry of Aminoacyl tRNA Synthetase and tRNAs and Their Engineering for Cell-Free and Synthetic Cell Applications. *Front. Bioeng. Biotechnol.* **2022**, *10*. https://doi.org/10.3389/fbioe.2022.918659

(9) Budisa, N. Prolegomena to Future Experimental Efforts on Genetic Code Engineering by Expanding Its Amino Acid Repertoire. *Angew. Chem. Int. Ed.* **2004**, *43* (47), 6426–6463. https://doi.org/10.1002/anie.200300646

(10) Kim, G.; Weiss, S. J.; Levine, R. L. Methionine Oxidation and Reduction in Proteins. *Biochim. Biophys. Acta BBA - Gen. Subj.* **2014**, *1840* (2), 901–905. https://doi.org/10.1016/j.bbagen.2013.04.038

(11) Brosnan, J. T.; Brosnan, M. E.; Bertolo, R. F. P.; Brunton, J. A. Methionine: A Metabolically Unique Amino Acid. *Livest. Sci.* **2007**, *112* (1), 2–7. https://doi.org/10.1016/j.livsci.2007.07.005

(12) Wiltschi, B.; Merkel, L.; Budisa, N. Fine Tuning the N-Terminal Residue Excision with Methionine Analogues. *ChemBioChem* **2009**, *10* (2), 217–220. https://doi.org/10.1002/cbic.200800605

(13) Roje, S. S-Adenosyl-l-Methionine: Beyond the Universal Methyl Group Donor. *Phytochemistry* **2006**, *67* (15), 1686–1698. https://doi.org/10.1016/j.phytochem.2006.04.019

(14) Rosenfeld, M. A.; Yurina, L. V.; Vasilyeva, A. D. Functional Role of Methionine Oxidation in Proteins: Arguments for and Against. *Biol. Bull. Rev.* **2021**, *11* (S1), 1–18. https://doi.org/10.1134/S2079086421070070

(15) Oien, D. B.; Moskovitz, J. Genetic Regulation of Longevity and Age-Associated Diseases through the Methionine Sulfoxide Reductase System. *Biochim. Biophys. Acta BBA - Mol. Basis Dis.* **2019**, *1865* (7), 1756–1762. https://doi.org/10.1016/j.bbadis.2018.11.016

(16) Stadtman, E. R.; Van Remmen, H.; Richardson, A.; Wehr, N. B.; Levine, R. L. Methionine Oxidation and Aging. *Biochim. Biophys. Acta BBA - Proteins Proteomics* **2005**, *1703* (2), 135–140. https://doi.org/10.1016/j.bbapap.2004.08.010

(17) Kiick, K. L.; Tirrell, D. A. Protein Engineering by In Vivo Incorporation of Non-Natural Amino Acids: Control of Incorporation of Methionine Analogues by Methionyl-tRNA Synthetase. *Tetrahedron* **2000**, *56* (48), 9487–9493. https://doi.org/10.1016/S0040-4020(00)00833-4

(18) Bennett, B. D.; Kimball, E. H.; Gao, M.; Osterhout, R.; Van Dien, S. J.; Rabinowitz, J. D. Absolute Metabolite Concentrations and Implied Enzyme Active Site Occupancy in Escherichia Coli. *Nat. Chem. Biol.* **2009**, *5* (8), 593–599. https://doi.org/10.1038/nchembio.186

(19) Lee, H.-S.; Hwang, B.-J. Methionine Biosynthesis and Its Regulation in Corynebacterium Glutamicum : Parallel Pathways of Transsulfuration and Direct Sulfhydrylation. *Appl. Microbiol. Biotechnol.* **2003**, *62* (5–6), 459–467. https://doi.org/10.1007/s00253-003-1306-7

(20) Ferla, M. P.; Patrick, W. M. Bacterial Methionine Biosynthesis. *Microbiology* **2014**, *160* (8), 1571–1584. https://doi.org/10.1099/mic.0.077826-0

(21) Schipp, C. J.; Ma, Y.; Al-Shameri, A.; D'Alessio, F.; Neubauer, P.; Contestabile, R.; Budisa, N.; di Salvo, M. L. An Engineered Escherichia Coli Strain with Synthetic Metabolism for In-Cell Production of Translationally Active Methionine Derivatives. *ChemBioChem* **2020**, *21* (24), 3525–3538. https://doi.org/10.1002/cbic.202000257

(22) Ma, Y.; Biava, H.; Contestabile, R.; Budisa, N.; Di Salvo, M. L. Coupling Bioorthogonal Chemistries with Artificial Metabolism: Intracellular Biosynthesis of Azidohomoalanine and Its Incorporation into Recombinant Proteins. *Molecules* **2014**, *19* (1), 1004–1022. https://doi.org/10.3390/molecules19011004

(23) Nojoumi, S.; Ma, Y.; Schwagerus, S.; Hackenberger, C. P. R.; Budisa, N. In-Cell Synthesis of Bioorthogonal Alkene Tag S-Allyl-Homocysteine and Its Coupling with Reprogrammed Translation. *Int. J. Mol. Sci.* **2019**, *20* (9), 2299. https://doi.org/10.3390/ijms20092299

(24) Kubyshkin, V.; Budisa, N. The Alanine World Model for the Development of the Amino Acid Repertoire in Protein Biosynthesis. *Int. J. Mol. Sci.* **2019**, *20* (21), 5507. https://doi.org/10.3390/ijms20215507

(25) Hartman, H.; Smith, T. F. The Evolution of the Ribosome and the Genetic Code. *Life* **2014**, *4* (2), 227–249. https://doi.org/10.3390/life4020227

(26) Santiveri, C. M.; Jiménez, M. A. Tryptophan Residues: Scarce in Proteins but Strong Stabilizers of β-Hairpin Peptides. *Pept. Sci.* **2010**, *94* (6), 779–790. https://doi.org/10.1002/bip.21436

(27) De Simone, A.; Acevedo-Rocha, C. G.; Georg Hoesl, M.; Budisa, N. Towards Reassignment of the Methionine Codon AUG to Two Different Noncanonical Amino

Acids in Bacterial Translation. *Croat. Chem. Acta* **2016**, *89* (2), 243–253. https://doi.org/10.5562/cca2915

(28) Meinnel, T.; Mechulam, Y.; Blanquet, S. Methionine as Translation Start Signal: A Review of the Enzymes of the Pathway in *Escherichia Coli*. *Biochimie* **1993**, *75* (12), 1061–1075. https://doi.org/10.1016/0300-9084(93)90005-D

(29) Moroder, L.; Budisa, N. Synthetic Biology of Protein Folding. *ChemPhysChem* **2010**, *11* (6), 1181–1187. https://doi.org/10.1002/cphc.201000035

(30) *Engineering the Genetic Code: Expanding the Amino Acid Repertoire for the Design of Novel Proteins | Wiley*. Wiley.com. https://www.wiley.com/en-ca/Engineering+the+Genetic+Code%3A+Expanding+the+Amino+Acid+Repertoire+for+the+Design+of+Novel+Proteins-p-9783527607099 (accessed 2025-09-03)

(31) Valley, C. C.; Cembran, A.; Perlmutter, J. D.; Lewis, A. K.; Labello, N. P.; Gao, J.; Sachs, J. N. The Methionine-Aromatic Motif Plays a Unique Role in Stabilizing Protein Structure *. *J. Biol. Chem.* **2012**, *287* (42), 34979–34991. https://doi.org/10.1074/jbc.M112.374504

(32) Aledo, J. C. Methionine in Proteins: The Cinderella of the Proteinogenic Amino Acids. *Protein Sci.* **2019**, *28* (10), 1785–1796. https://doi.org/10.1002/pro.3698

(33) Cowie, D. B.; Cohen, G. N. Biosynthesis by *Escherichia Coli* of Active Altered Proteins Containing Selenium Instead of Sulfur. *Biochim. Biophys. Acta* **1957**, *26* (2), 252–261. https://doi.org/10.1016/0006-3002(57)90003-3

(34) Munier, R.; Cohen, G. N. Incorporation d'analogues Structuraux d'aminoacides Dans Les Protéines Bactériennes Au Cours de Leur Synthèse *in Vivo*. *Biochim. Biophys. Acta* **1959**, *31* (2), 378–391. https://doi.org/10.1016/0006-3002(59)90011-3

(35) Yoshida, A.; Yamasaki, M. Studies on the Mechanism of Protein Synthesis Incorporation of Ethionine into α-Amylase of *Bacillus Subtilis*. *Biochim. Biophys. Acta* **1959**, *34*, 158–165. https://doi.org/10.1016/0006-3002(59)90243-4

(36) Wolschner, C.; Giese, A.; Kretzschmar, H. A.; Huber, R.; Moroder, L.; Budisa, N. Design of Anti- and pro-Aggregation Variants to Assess the Effects of Methionine Oxidation in Human Prion Protein. *Proc. Natl. Acad. Sci.* **2009**, *106* (19), 7756–7761. https://doi.org/10.1073/pnas.0902688106

(37) van Hest, J. C. M.; Kiick, K. L.; Tirrell, D. A. Efficient Incorporation of Unsaturated Methionine Analogues into Proteins in Vivo. *J. Am. Chem. Soc.* **2000**, *122* (7), 1282–1288. https://doi.org/10.1021/ja992749j

(38) Hoesl, M. G.; Larregola, M.; Cui, H.; Budisa, N. Azatryptophans as Tools to Study Polarity Requirements for Folding of Green Fluorescent Protein. *J. Pept. Sci.* **2010**, *16* (10), 589–595. https://doi.org/10.1002/psc.1263

(39) Pliška, V.; Schmidt, M.; Fauchère, J.-L. Partition Coefficients of Amino Acids and Hydrophobic Parameters π of Their Side-Chains as Measured by Thin-Layer Chromatography. *J. Chromatogr. A* **1981**, *216*, 79–92. https://doi.org/10.1016/S0021-9673(00)82337-7

(40) Charton, M.; Charton, B. I. The Structural Dependence of Amino Acid Hydrophobicity Parameters. *J. Theor. Biol.* **1982**, *99* (4), 629–644. https://doi.org/10.1016/0022-5193(82)90191-6

(41) Kubyshkin, V. Experimental Lipophilicity Scale for Coded and Noncoded Amino Acid Residues. *Org. Biomol. Chem.* **2021**, *19* (32), 7031–7040. https://doi.org/10.1039/D1OB01213D

(42) Octanol-Water Partition Coefficients: Fundamentals and Physical Chemistry: Edited by J Sangster, Volume 2, Wiley Series in Solution Chemistry, John Wiley & Sons, Chichester, 1997, 170 Pp, £ 60,00. *Eur. J. Med. Chem.* **1997**, *32* (11), 842. https://doi.org/10.1016/S0223-5234(97)82764-X

(43) Budisa, N.; Pal, P. P.; Alefelder, S.; Birle, P.; Krywcun, T.; Rubini, M.; Wenger, W.; Bae, J. H.; Steiner, T. Probing the Role of Tryptophans in Aequorea Victoria Green Fluorescent Proteins with an Expanded Genetic Code. **2004**, *385* (2), 191–202. https://doi.org/10.1515/BC.2004.038

(44) To, T. M. T.; Kubyshkin, V.; Schmitt, F.-J.; Budisa, N.; Friedrich, T. Residue-Specific Exchange of Proline by Proline Analogs in Fluorescent Proteins: How "Molecular Surgery" of the Backbone Affects Folding and Stability. *J. Vis. Exp. JoVE* **2022**, No. 180, e63320. https://doi.org/10.3791/63320

(45) Mattheyses, A. L.; Marcus, A. I. Förster Resonance Energy Transfer (FRET) Microscopy for Monitoring Biomolecular Interactions. In *Protein-Protein Interactions: Methods and Applications*; Meyerkord, C. L., Fu, H., Eds.; Springer: New York, NY, 2015; pp 329–339. https://doi.org/10.1007/978-1-4939-2425-7_20

(46) Murray, C. J. L.; Ikuta, K. S.; Sharara, F.; Swetschinski, L.; Aguilar, G. R.; Gray, A.; Han, C.; Bisignano, C.; Rao, P.; Wool, E.; Johnson, S. C.; Browne, A. J.; Chipeta, M. G.; Fell, F.; Hackett, S.; Haines-Woodhouse, G.; Hamadani, B. H. K.; Kumaran, E. A. P.; McManigal, B.; Achalapong, S.; Agarwal, R.; Akech, S.; Albertson, S.; Amuasi, J.; Andrews, J.; Aravkin, A.; Ashley, E.; Babin, F.-X.; Bailey, F.; Baker, S.; Basnyat, B.; Bekker, A.; Bender, R.; Berkley, J. A.; Bethou, A.; Bielicki, J.; Boonkasidecha, S.; Bukosia, J.; Carvalheiro, C.; Castañeda-Orjuela, C.; Chansamouth, V.; Chaurasia, S.; Chiurchiù, S.; Chowdhury, F.; Donatien, R. C.; Cook, A. J.; Cooper, B.; Cressey, T. R.; Criollo-Mora, E.; Cunningham, M.; Darboe, S.; Day, N. P. J.; Luca, M. D.; Dokova, K.; Dramowski, A.; Dunachie, S. J.; Bich, T. D.; Eckmanns, T.; Eibach, D.; Emami, A.; Feasey, N.; Fisher-Pearson, N.; Forrest, K.; Garcia, C.; Garrett, D.; Gastmeier, P.; Giref, A. Z.; Greer, R. C.; Gupta, V.; Haller, S.; Haselbeck, A.; Hay, S. I.; Holm, M.; Hopkins, S.; Hsia, Y.; Iregbu, K. C.; Jacobs, J.; Jarovsky, D.; Javanmardi, F.; Jenney, A. W. J.; Khorana, M.; Khusuwan, S.; Kissoon, N.; Kobeissi, E.; Kostyanev, T.; Krapp, F.; Krumkamp, R.; Kumar, A.; Kyu, H. H.; Lim, C.; Lim, K.; Limmathurotsakul, D.; Loftus, M. J.; Lunn, M.; Ma, J.; Manoharan, A.; Marks, F.; May, J.; Mayxay, M.; Mturi, N.; Munera-Huertas, T.; Musicha, P.; Musila, L. A.; Mussi-Pinhata, M. M.; Naidu, R. N.; Nakamura, T.; Nanavati, R.; Nangia, S.; Newton, P.; Ngoun, C.; Novotney, A.; Nwakanma, D.; Obiero, C. W.; Ochoa, T. J.; Olivas-Martinez, A.; Olliaro, P.; Ooko, E.; Ortiz-Brizuela, E.; Ounchanum, P.; Pak, G. D.; Paredes, J. L.; Peleg, A. Y.; Perrone, C.; Phe, T.; Phommasone, K.; Plakkal, N.; Ponce-de-Leon, A.; Raad, M.; Ramdin, T.; Rattanavong, S.; Riddell, A.; Roberts, T.; Robotham, J. V.; Roca, A.; Rosenthal, V. D.; Rudd, K. E.; Russell, N.; Sader, H. S.; Saengchan, W.; Schnall, J.; Scott, J. A. G.; Seekaew, S.; Sharland, M.; Shivamallappa, M.; Sifuentes-Osornio, J.; Simpson, A. J.; Steenkeste, N.; Stewardson, A. J.; Stoeva, T.; Tasak, N.; Thaiprakong, A.; Thwaites, G.; Tigoi, C.; Turner, C.; Turner, P.; Doorn, H. R. van; Velaphi, S.; Vongpradith, A.;

Vongsouvath, M.; Vu, H.; Walsh, T.; Walson, J. L.; Waner, S.; Wangrangsimakul, T.; Wannapinij, P.; Wozniak, T.; Sharma, T. E. M. W. Y.; Yu, K. C.; Zheng, P.; Sartorius, B.; Lopez, A. D.; Stergachis, A.; Moore, C.; Dolecek, C.; Naghavi, M. Global Burden of Bacterial Antimicrobial Resistance in 2019: A Systematic Analysis. *The Lancet* **2022**, *399* (10325), 629–655. https://doi.org/10.1016/S0140-6736(21)02724-0

(47) Vicente, J., Olga B. ,Irwin, Alec,Berthe, Franck Cesar Jean,Le Gall, Francois G. ,Marquez, Patricio. *Drug-resistant infections : a threat to our economic future (Vol. 2 of 2) : final report*. World Bank. https://documents.worldbank.org/en/publication/documents-reports/documentdetail/en/323311493396993758 (accessed 2025-08-21)

(48) Clancy, C. J.; Nguyen, M. H. Buying Time: The AMR Action Fund and the State of Antibiotic Development in the United States 2020. *Open Forum Infect. Dis.* **2020**, *7* (11), ofaa464. https://doi.org/10.1093/ofid/ofaa464

(49) Plackett, B. Why Big Pharma Has Abandoned Antibiotics. *Nature* **2020**, *586* (7830), S50–S52. https://doi.org/10.1038/d41586-020-02884-3

(50) Irfan, M.; Almotiri, A.; AlZeyadi, Z. A. Antimicrobial Resistance and Its Drivers—A Review. *Antibiotics* **2022**, *11* (10), 1362. https://doi.org/10.3390/antibiotics11101362

(51) Salam, M. A.; Al-Amin, M. Y.; Salam, M. T.; Pawar, J. S.; Akhter, N.; Rabaan, A. A.; Alqumber, M. A. A. Antimicrobial Resistance: A Growing Serious Threat for Global Public Health. *Healthcare* **2023**, *11* (13), 1946. https://doi.org/10.3390/healthcare11131946

(52) Reygaert, W. C. An Overview of the Antimicrobial Resistance Mechanisms of Bacteria. *AIMS Microbiol.* **2018**, *4* (3), 482–501. https://doi.org/10.3934/microbiol.2018.3.482

(53) Munita, J. M.; Arias, C. A. Mechanisms of Antibiotic Resistance. *Microbiol. Spectr.* **2016**, *4* (2), 10.1128/microbiolspec.vmbf-0016–2015. https://doi.org/10.1128/microbiolspec.vmbf-0016-2015

(54) Reygaert, W. Methicillin-Resistant Staphylococcus Aureus (MRSA): Molecular Aspects of Antimicrobial Resistance and Virulence. *Clin. Lab. Sci. J. Am. Soc. Med. Technol.* **2009**, *22* (2), 115–119.

(55) Mazurkiewicz-Pisarek, A.; Baran, J.; Ciach, T. Antimicrobial Peptides: Challenging Journey to the Pharmaceutical, Biomedical, and Cosmeceutical Use. *Int. J. Mol. Sci.* **2023**, *24* (10), 9031. https://doi.org/10.3390/ijms24109031

(56) Kumar, P.; Kizhakkedathu, J. N.; Straus, S. K. Antimicrobial Peptides: Diversity, Mechanism of Action and Strategies to Improve the Activity and Biocompatibility In Vivo. *Biomolecules* **2018**, *8* (1), 4. https://doi.org/10.3390/biom8010004

(57) Lei, J.; Sun, L.; Huang, S.; Zhu, C.; Li, P.; He, J.; Mackey, V.; Coy, D. H.; He, Q. The Antimicrobial Peptides and Their Potential Clinical Applications. *Am. J. Transl. Res.* **2019**, *11* (7), 3919–3931.

(58) Cao, L.; Do, T.; Link, A. J. Mechanisms of Action of Ribosomally Synthesized and Posttranslationally Modified Peptides (RiPPs). *J. Ind. Microbiol. Biotechnol.* **2021**, *48* (3–4), kuab005. https://doi.org/10.1093/jimb/kuab005

(59) McAuliffe, O.; Ross, R. P.; Hill, C. Lantibiotics: Structure, Biosynthesis and Mode of Action. *FEMS Microbiol. Rev.* **2001**, *25* (3), 285–308. https://doi.org/10.1111/j.1574-6976.2001.tb00579.x

(60) Tavares, T. D.; Ribeiro, A. R. M.; Silva, C.; Antunes, J. C.; Felgueiras, H. P. Combinatory Effect of Nisin Antimicrobial Peptide with Bioactive Molecules: A Review. *J. Drug Deliv. Sci. Technol.* **2024**, *91*, 105246. https://doi.org/10.1016/j.jddst.2023.105246

(61) Ortega, M. A.; Hao, Y.; Zhang, Q.; Walker, M. C.; van der Donk, W. A.; Nair, S. K. Structure and Mechanism of the tRNA-Dependent Lantibiotic Dehydratase NisB. *Nature* **2015**, *517* (7535), 509–512. https://doi.org/10.1038/nature13888

(62) Khusainov, R.; van Heel, A. J.; Lubelski, J.; Moll, G. N.; Kuipers, O. P. Identification of Essential Amino Acid Residues in the Nisin Dehydratase NisB. *Front. Microbiol.* **2015**, *6*. https://doi.org/10.3389/fmicb.2015.00102

(63) Li, B.; Yu, J. P. J.; Brunzelle, J. S.; Moll, G. N.; van der Donk, W. A.; Nair, S. K. Structure and Mechanism of the Lantibiotic Cyclase Involved in Nisin Biosynthesis. *Science* **2006**, *311* (5766), 1464–1467. https://doi.org/10.1126/science.1121422

(64) Lubelski, J.; Rink, R.; Khusainov, R.; Moll, G. N.; Kuipers, O. P. Biosynthesis, Immunity, Regulation, Mode of Action and Engineering of the Model Lantibiotic Nisin. *Cell. Mol. Life Sci.* **2008**, *65* (3), 455–476. https://doi.org/10.1007/s00018-007-7171-2

(65) Chen, J.; Heel, A. J. van; Kuipers, O. P. Subcellular Localization and Assembly Process of the Nisin Biosynthesis Machinery in Lactococcus Lactis. *mBio* **2020**. https://doi.org/10.1128/mbio.02825-20

(66) Xu, Y.; Li, X.; Li, R.; Li, S.; Ni, H.; Wang, H.; Xu, H.; Zhou, W.; Saris, P. E. J.; Yang, W.; Qiao, M.; Rao, Z. Structure of the Nisin Leader Peptidase NisP Revealing a C-Terminal Autocleavage Activity. *Acta Crystallogr. D Biol. Crystallogr.* **2014**, *70* (6), 1499–1505. https://doi.org/10.1107/S1399004714004234

(67) Montalbán-López, M.; Deng, J.; van Heel, A. J.; Kuipers, O. P. Specificity and Application of the Lantibiotic Protease NisP. *Front. Microbiol.* **2018**, *9*. https://doi.org/10.3389/fmicb.2018.00160

(68) Cheigh, C.-I.; Pyun, Y.-R. Nisin Biosynthesis and Its Properties. *Biotechnol. Lett.* **2005**, *27* (21), 1641–1648. https://doi.org/10.1007/s10529-005-2721-x

(69) Talapko, J.; Meštrović, T.; Juzbašić, M.; Tomas, M.; Erić, S.; Horvat Aleksijević, L.; Bekić, S.; Schwarz, D.; Matić, S.; Neuberg, M.; Škrlec, I. Antimicrobial Peptides—Mechanisms of Action, Antimicrobial Effects and Clinical Applications. *Antibiotics* **2022**, *11* (10), 1417. https://doi.org/10.3390/antibiotics11101417

(70) Huan, Y.; Kong, Q.; Mou, H.; Yi, H. Antimicrobial Peptides: Classification, Design, Application and Research Progress in Multiple Fields. *Front. Microbiol.* **2020**, *11*. https://doi.org/10.3389/fmicb.2020.582779

(71) Hsu, S.-T. D.; Breukink, E.; Tischenko, E.; Lutters, M. A. G.; de Kruijff, B.; Kaptein, R.; Bonvin, A. M. J. J.; van Nuland, N. A. J. The Nisin–Lipid II Complex Reveals a Pyrophosphate Cage That Provides a Blueprint for Novel Antibiotics. *Nat. Struct. Mol. Biol.* **2004**, *11* (10), 963–967. https://doi.org/10.1038/nsmb830

(72) Kumar, S.; Mollo, A.; Kahne, D.; Ruiz, N. The Bacterial Cell Wall: From Lipid II Flipping to Polymerization. *Chem. Rev.* **2022**, *122* (9), 8884–8910. https://doi.org/10.1021/acs.chemrev.1c00773

(73) 't Hart, P.; Oppedijk, S. F.; Breukink, E.; Martin, N. I. New Insights into Nisin's Antibacterial Mechanism Revealed by Binding Studies with Synthetic Lipid II Analogues. *Biochemistry* **2016**, *55* (1), 232–237. https://doi.org/10.1021/acs.biochem.5b01173

(74) Breukink, E.; Wiedemann, I.; Kraaij, C. van; Kuipers, O. P.; Sahl, H.-G.; de Kruijff, B. Use of the Cell Wall Precursor Lipid II by a Pore-Forming Peptide Antibiotic. *Science* **1999**, *286* (5448), 2361–2364. https://doi.org/10.1126/science.286.5448.2361

(75) Wiedemann, I.; Breukink, E.; Kraaij, C. van; Kuipers, O. P.; Bierbaum, G.; Kruijff, B. de; Sahl, H.-G. Specific Binding of Nisin to the Peptidoglycan Precursor Lipid II Combines Pore Formation and Inhibition of Cell Wall Biosynthesis for Potent Antibiotic Activity *. *J. Biol. Chem.* **2001**, *276* (3), 1772–1779. https://doi.org/10.1074/jbc.M006770200

(76) Prince, A.; Sandhu, P.; Ror, P.; Dash, E.; Sharma, S.; Arakha, M.; Jha, S.; Akhter, Y.; Saleem, M. Lipid-II Independent Antimicrobial Mechanism of Nisin Depends On Its Crowding And Degree Of Oligomerization. *Sci. Rep.* **2016**, *6* (1), 37908. https://doi.org/10.1038/srep37908

(77) Lagedroste, M.; Reiners, J.; Knospe, C. V.; Smits, S. H. J.; Schmitt, L. A Structural View on the Maturation of Lanthipeptides. *Front. Microbiol.* **2020**, *11*. https://doi.org/10.3389/fmicb.2020.01183

(78) Bai, C.; Zhang, Y.; Zhao, X.; Hu, Y.; Xiang, S.; Miao, J.; Lou, C.; Zhang, L. Exploiting a Precise Design of Universal Synthetic Modular Regulatory Elements to Unlock the Microbial Natural Products in Streptomyces. *Proc. Natl. Acad. Sci.* **2015**, *112* (39), 12181–12186. https://doi.org/10.1073/pnas.1511027112

(79) Khosa, S.; Lagedroste, M.; Smits, S. H. J. Protein Defense Systems against the Lantibiotic Nisin: Function of the Immunity Protein NisI and the Resistance Protein NSR. *Front. Microbiol.* **2016**, *7*. https://doi.org/10.3389/fmicb.2016.00504

(80) Clemens, R.; Zaschke-Kriesche, J.; Khosa, S.; Smits, S. H. J. Insight into Two ABC Transporter Families Involved in Lantibiotic Resistance. *Front. Mol. Biosci.* **2018**, *4*. https://doi.org/10.3389/fmolb.2017.00091

(81) AlKhatib, Z.; Lagedroste, M.; Zaschke, J.; Wagner, M.; Abts, A.; Fey, I.; Kleinschrodt, D.; Smits, S. H. J. The C-Terminus of Nisin Is Important for the ABC Transporter NisFEG to Confer Immunity in Lactococcus Lactis. *MicrobiologyOpen* **2014**, *3* (5), 752–763. https://doi.org/10.1002/mbo3.205

(82) Jiang, X.; Geng, Y.; Ren, S.; Yu, T.; Li, Y.; Liu, G.; Wang, H.; Meng, H.; Shi, L. The VirAB-VirSR-AnrAB Multicomponent System Is Involved in Resistance of Listeria Monocytogenes EGD-e to Cephalosporins, Bacitracin, Nisin, Benzalkonium Chloride, and Ethidium Bromide. *Appl. Environ. Microbiol.* **2019**, *85* (20), e01470-19. https://doi.org/10.1128/AEM.01470-19

(83) Verheul, A.; Russell, N. J.; Van'T Hof, R.; Rombouts, F. M.; Abee, T. Modifications of Membrane Phospholipid Composition in Nisin-Resistant Listeria Monocytogenes Scott

A. *Appl. Environ. Microbiol.* **1997**, *63* (9), 3451–3457. https://doi.org/10.1128/aem.63.9.3451-3457.1997

(84) Barbosa, A. A. T.; de Melo, M. R.; da Silva, C. M. R.; Jain, S.; Dolabella, S. S. Nisin Resistance in Gram-Positive Bacteria and Approaches to Circumvent Resistance for Successful Therapeutic Use. *Crit. Rev. Microbiol.* **2021**, *47* (3), 376–385. https://doi.org/10.1080/1040841X.2021.1893264

(85) Mazzotta, A. S.; Montville, T. J. Nisin Induces Changes in Membrane Fatty Acid Composition of Listeria Monocytogenes Nisin-resistant Strains at 10°C and 30°C. *J. Appl. Microbiol.* **1997**, *82* (1), 32–38. https://doi.org/10.1111/j.1365-2672.1997.tb03294.x

(86) Garde, S.; Ávila, M.; Medina, M.; Nuñez, M. Fast Induction of Nisin Resistance in Streptococcus Thermophilus INIA 463 during Growth in Milk. *Int. J. Food Microbiol.* **2004**, *96* (2), 165–172. https://doi.org/10.1016/j.ijfoodmicro.2004.03.023

(87) McBride, S. M.; Sonenshein, A. L. The Dlt Operon Confers Resistance to Cationic Antimicrobial Peptides in Clostridium Difficile. *Microbiology* **2011**, *157* (5), 1457–1465. https://doi.org/10.1099/mic.0.045997-0

(88) Rismondo, J.; Schulz, L. M. Not Just Transporters: Alternative Functions of ABC Transporters in Bacillus Subtilis and Listeria Monocytogenes. *Microorganisms* **2021**, *9* (1), 163. https://doi.org/10.3390/microorganisms9010163

(89) Hiron, A.; Falord, M.; Valle, J.; Débarbouillé, M.; Msadek, T. Bacitracin and Nisin Resistance in Staphylococcus Aureus: A Novel Pathway Involving the BraS/BraR Two-Component System (SA2417/SA2418) and Both the BraD/BraE and VraD/VraE ABC Transporters. *Mol. Microbiol.* **2011**, *81* (3), 602–622. https://doi.org/10.1111/j.1365-2958.2011.07735.x

(90) Gebhard, S.; Mascher, T. Antimicrobial Peptide Sensing and Detoxification Modules: Unravelling the Regulatory Circuitry of Staphylococcus Aureus. *Mol. Microbiol.* **2011**, *81* (3), 581–587. https://doi.org/10.1111/j.1365-2958.2011.07747.x

(91) Randall, C. P.; Gupta, A.; Utley-Drew, B.; Lee, S. Y.; Morrison-Williams, G.; O'Neill, A. J. Acquired Nisin Resistance in Staphylococcus Aureus Involves Constitutive Activation of an Intrinsic Peptide Antibiotic Detoxification Module. *mSphere* **2018**, *3* (6), 10.1128/mspheredirect.00633-18. https://doi.org/10.1128/mspheredirect.00633-18

(92) Field, D.; Blake, T.; Mathur, H.; Connor, P. M. O.; Cotter, P. D.; Ross, R. P.; Hill, C. Bioengineering Nisin to Overcome the Nisin Resistance Protein. *Mol. Microbiol.* **2019**, *111* (3), 717–731. https://doi.org/10.1111/mmi.14183

(93) Xuan, J.; Feng, W.; Wang, J.; Wang, R.; Zhang, B.; Bo, L.; Chen, Z.-S.; Yang, H.; Sun, L. Antimicrobial Peptides for Combating Drug-Resistant Bacterial Infections. *Drug Resist. Updat.* **2023**, *68*, 100954. https://doi.org/10.1016/j.drup.2023.100954

(94) Niemeyer-van der Kolk, T.; Buters, T. P.; Krouwels, L.; Boltjes, J.; de Kam, M. L.; van der Wall, H.; van Alewijk, D. C. J. G.; van den Munckhof, E. H. A.; Becker, M. J.; Feiss, G.; Florencia, E. F.; Prens, E. P.; Moerland, M.; Burggraaf, J.; Rissmann, R.; van Doorn, M. B. A. Topical Antimicrobial Peptide Omiganan Recovers Cutaneous Dysbiosis but Does Not Improve Clinical Symptoms in Patients with Mild to Moderate Atopic Dermatitis in a Phase 2 Randomized Controlled Trial. *J. Am. Acad. Dermatol.* **2022**, *86* (4), 854–862. https://doi.org/10.1016/j.jaad.2020.08.132

(95) Han, Y.; Zhang, M.; Lai, R.; Zhang, Z. Chemical Modifications to Increase the Therapeutic Potential of Antimicrobial Peptides. *Peptides* **2021**, *146*, 170666. https://doi.org/10.1016/j.peptides.2021.170666

(96) Mahlapuu, M.; Håkansson, J.; Ringstad, L.; Björn, C. Antimicrobial Peptides: An Emerging Category of Therapeutic Agents. *Front. Cell. Infect. Microbiol.* **2016**, *6*. https://doi.org/10.3389/fcimb.2016.00194

(97) Wei, D.; Zhang, X. Biosynthesis, Bioactivity, Biotoxicity and Applications of Antimicrobial Peptides for Human Health. *Biosaf. Health* **2022**, *4* (2), 118–134. https://doi.org/10.1016/j.bsheal.2022.02.003

(98) Soares, D. de S.; Reis, A. da F.; Silva Junior, G. B. da; Leite, T. T.; Parente Filho, S. L. A.; Rocha, C. V. de O.; Daher, E. D. F. Polymyxin-B and Vancomycin-Associated Acute Kidney Injury in Critically Ill Patients. *Pathog. Glob. Health* **2017**, *111* (3), 137–142. https://doi.org/10.1080/20477724.2017.1309338

(99) Cresti, L.; Cappello, G.; Pini, A. Antimicrobial Peptides towards Clinical Application—A Long History to Be Concluded. *Int. J. Mol. Sci.* **2024**, *25* (9), 4870. https://doi.org/10.3390/ijms25094870

(100) John, J. F.; Falci, D. R.; Rigatto, M. H.; Oliveira, R. D.; Kremer, T. G.; Zavascki, A. P. Severe Infusion-Related Adverse Events and Renal Failure in Patients Receiving High-Dose Intravenous Polymyxin B. *Antimicrob. Agents Chemother.* **2017**, *62* (1), 10.1128/aac.01617-17. https://doi.org/10.1128/aac.01617-17

(101) Kindrachuk, J.; Scruten, E.; Attah-Poku, S.; Bell, K.; Potter, A.; Babiuk, L. A.; Griebel, P. J.; Napper, S. Stability, Toxicity, and Biological Activity of Host Defense Peptide BMAP28 and Its Inversed and Retro-Inversed Isomers. *Pept. Sci.* **2011**, *96* (1), 14–24. https://doi.org/10.1002/bip.21441

(102) Thakur, A.; Sharma, A.; Alajangi, H. K.; Jaiswal, P. K.; Lim, Y.; Singh, G.; Barnwal, R. P. In Pursuit of Next-Generation Therapeutics: Antimicrobial Peptides against Superbugs, Their Sources, Mechanism of Action, Nanotechnology-Based Delivery, and Clinical Applications. *Int. J. Biol. Macromol.* **2022**, *218*, 135–156. https://doi.org/10.1016/j.ijbiomac.2022.07.103

(103) Kang, S.-J.; Nam, S. H.; Lee, B.-J. Engineering Approaches for the Development of Antimicrobial Peptide-Based Antibiotics. *Antibiotics* **2022**, *11* (10), 1338. https://doi.org/10.3390/antibiotics11101338

(104) Rounds, T.; Straus, S. K. Lipidation of Antimicrobial Peptides as a Design Strategy for Future Alternatives to Antibiotics. *Int. J. Mol. Sci.* **2020**, *21* (24), 9692. https://doi.org/10.3390/ijms21249692

(105) Avinash, D.; Bisht, A.; Kumar, M.; Thakur, S.; Patel, P.; Kurmi, B. D. Empowering Antimicrobial Peptides: Harnessing Nanotechnology and Engineering Strategies to Combat Microbial Resistance. *Pept. Sci.* **2024**, *116* (6), e24376. https://doi.org/10.1002/pep2.24376

(106) Kanchanapally, R.; Nellore, B. P. V.; Sinha, S. S.; Pedraza, F.; Jones, S. J.; Pramanik, A.; Chavva, S. R.; Tchounwou, C.; Shi, Y.; Vangara, A.; Sardar, D.; Ray, P. C. Antimicrobial Peptide-Conjugated Graphene Oxide Membrane for Efficient Removal and Effective Killing of Multiple Drug Resistant Bacteria. *RSC Adv.* **2015**, *5* (24), 18881–18887. https://doi.org/10.1039/C5RA01321F

(107) Taylor, T. M.; Gaysinsky, S.; Davidson, P. M.; Bruce, B. D.; Weiss, J. Characterization of Antimicrobial-Bearing Liposomes by ζ-Potential, Vesicle Size, and Encapsulation Efficiency. *Food Biophys.* **2007**, *2* (1), 1–9. https://doi.org/10.1007/s11483-007-9023-x

(108) Almaaytah, A.; Qaoud, M. T.; Abualhaijaa, A.; Al-Balas, Q.; Alzoubi, K. H. Hybridization and Antibiotic Synergism as a Tool for Reducing the Cytotoxicity of Antimicrobial Peptides. *Infect. Drug Resist.* **2018**, *11*, 835–847. https://doi.org/10.2147/IDR.S166236

(109) Kim, H.; Jang, J. H.; Kim, S. C.; Cho, J. H. Development of a Novel Hybrid Antimicrobial Peptide for Targeted Killing of *Pseudomonas Aeruginosa*. *Eur. J. Med. Chem.* **2020**, *185*, 111814. https://doi.org/10.1016/j.ejmech.2019.111814

(110) Dijksteel, G. S.; Ulrich, M. M. W.; Middelkoop, E.; Boekema, B. K. H. L. Review: Lessons Learned From Clinical Trials Using Antimicrobial Peptides (AMPs). *Front. Microbiol.* **2021**, *12*. https://doi.org/10.3389/fmicb.2021.616979

(111) Field, D.; Fernandez de Ullivarri, M.; Ross, R. P.; Hill, C. After a Century of Nisin Research - Where Are We Now? *FEMS Microbiol. Rev.* **2023**, *47* (3), fuad023. https://doi.org/10.1093/femsre/fuad023

(112) Zheng, Y.; Du, Y.; Qiu, Z.; Liu, Z.; Qiao, J.; Li, Y.; Caiyin, Q. Nisin Variants Generated by Protein Engineering and Their Properties. *Bioengineering* **2022**, *9* (6), 251. https://doi.org/10.3390/bioengineering9060251

(113) Zhou, L.; van Heel, A. J.; Kuipers, O. P. The Length of a Lantibiotic Hinge Region Has Profound Influence on Antimicrobial Activity and Host Specificity. *Front. Microbiol.* **2015**, *6*. https://doi.org/10.3389/fmicb.2015.00011

(114) Khosa, S.; Frieg, B.; Mulnaes, D.; Kleinschrodt, D.; Hoeppner, A.; Gohlke, H.; Smits, S. H. J. Structural Basis of Lantibiotic Recognition by the Nisin Resistance Protein from Streptococcus Agalactiae. *Sci. Rep.* **2016**, *6* (1), 18679. https://doi.org/10.1038/srep18679

(115) Khosa, S.; Lagedroste, M.; Smits, S. H. J. Protein Defense Systems against the Lantibiotic Nisin: Function of the Immunity Protein NisI and the Resistance Protein NSR. *Front. Microbiol.* **2016**, *7*. https://doi.org/10.3389/fmicb.2016.00504

(116) Musiejuk, M.; Kafarski, P. Engineering of Nisin as a Means for Improvement of Its Pharmacological Properties: A Review. *Pharmaceuticals* **2023**, *16* (8), 1058. https://doi.org/10.3390/ph16081058

(117) Bolt, H. L.; Kleijn, L. H. J.; Martin, N. I.; Cobb, S. L. Synthesis of Antibacterial Nisin–Peptoid Hybrids Using Click Methodology. *Molecules* **2018**, *23* (7), 1566. https://doi.org/10.3390/molecules23071566

(118) Karbalaei-Heidari, H. R.; Budisa, N. Combating Antimicrobial Resistance With New-To-Nature Lanthipeptides Created by Genetic Code Expansion. *Front. Microbiol.* **2020**, *11*. https://doi.org/10.3389/fmicb.2020.590522

(119) Baumann, T.; Nickling, J. H.; Bartholomae, M.; Buivydas, A.; Kuipers, O. P.; Budisa, N. Prospects of In Vivo Incorporation of Non-Canonical Amino Acids for the Chemical Diversification of Antimicrobial Peptides. *Front. Microbiol.* **2017**, *8*. https://doi.org/10.3389/fmicb.2017.00124

(120) Abts, A.; Mavaro, A.; Stindt, J.; Bakkes, P. J.; Metzger, S.; Driessen, A. J. M.; Smits, S. H. J.; Schmitt, L. Easy and Rapid Purification of Highly Active Nisin. *Int. J. Pept.* **2011**, *2011* (1), 175145. https://doi.org/10.1155/2011/175145

(121) Donnelly, D. P.; Rawlins, C. M.; DeHart, C. J.; Fornelli, L.; Schachner, L. F.; Lin, Z.; Lippens, J. L.; Aluri, K. C.; Sarin, R.; Chen, B.; Lantz, C.; Jung, W.; Johnson, K. R.; Koller, A.; Wolff, J. J.; Campuzano, I. D. G.; Auclair, J. R.; Ivanov, A. R.; Whitelegge, J. P.; Paša-Tolić, L.; Chamot-Rooke, J.; Danis, P. O.; Smith, L. M.; Tsybin, Y. O.; Loo, J. A.; Ge, Y.; Kelleher, N. L.; Agar, J. N. Best Practices and Benchmarks for Intact Protein Analysis for Top-down Mass Spectrometry. *Nat. Methods* **2019**, *16* (7), 587–594. https://doi.org/10.1038/s41592-019-0457-0

(122) Lubelski, J.; Overkamp, W.; Kluskens, L. D.; Moll, G. N.; Kuipers, O. P. Influence of Shifting Positions of Ser, Thr, and Cys Residues in Prenisin on the Efficiency of Modification Reactions and on the Antimicrobial Activities of the Modified Prepeptides. *Appl. Environ. Microbiol.* **2008**, *74* (15), 4680–4685. https://doi.org/10.1128/AEM.00112-08

(123) Field, D.; Connor, P. M. O.; Cotter, P. D.; Hill, C.; Ross, R. P. The Generation of Nisin Variants with Enhanced Activity against Specific Gram-positive Pathogens. *Mol. Microbiol.* **2008**, *69* (1), 218–230. https://doi.org/10.1111/j.1365-2958.2008.06279.x

(124) Saleh, A. M.; Wilding, K. M.; Calve, S.; Bundy, B. C.; Kinzer-Ursem, T. L. Non-Canonical Amino Acid Labeling in Proteomics and Biotechnology. *J. Biol. Eng.* **2019**, *13* (1), 43. https://doi.org/10.1186/s13036-019-0166-3

(125) Budisa, N. *Engineering the Genetic Code: Expanding the Amino Acid Repertoire for the Design of Novel Proteins*, 1st ed.; Wiley, 2005. https://doi.org/10.1002/3527607188

(126) Chocat, P.; Esaki, N.; Tanaka, H.; Soda, K. Synthesis of Selenocystine and Selenohomocystine with O-Acetylhomoserine Sulfhydrylase. *Agric. Biol. Chem.* **1985**, *49* (4), 1143–1150. https://doi.org/10.1080/00021369.1985.10866849

(127) Maier, T. H. P. Semisynthetic Production of Unnatural L-α-Amino Acids by Metabolic Engineering of the Cysteine-Biosynthetic Pathway. *Nat. Biotechnol.* **2003**, *21* (4), 422–427. https://doi.org/10.1038/nbt807

(128) Stauß, A. C.; Fuchs, C.; Jansen, P.; Repert, S.; Alcock, K.; Ludewig, S.; Rozhon, W. The Ninhydrin Reaction Revisited: Optimisation and Application for Quantification of Free Amino Acids. *Molecules* **2024**, *29* (14), 3262. https://doi.org/10.3390/molecules29143262

(129) Gelsinger, D. R.; Vo, P. L. H.; Klompe, S. E.; Ronda, C.; Wang, H. H.; Sternberg, S. H. Bacterial Genome Engineering Using CRISPR-Associated Transposases. *Nat. Protoc.* **2024**, *19* (3), 752–790. https://doi.org/10.1038/s41596-023-00927-3

(130) Bartholomae, M.; Baumann, T.; Nickling, J. H.; Peterhoff, D.; Wagner, R.; Budisa, N.; Kuipers, O. P. Expanding the Genetic Code of Lactococcus Lactis and Escherichia Coli to Incorporate Non-Canonical Amino Acids for Production of Modified Lantibiotics. *Front. Microbiol.* **2018**, *9*, 657. https://doi.org/10.3389/fmicb.2018.00657

(131) Sikarwar, A. S.; Hinton, M.; Santhosh, K. T.; Dhanaraj, P.; Talabis, M.; Chelikani, P.; Dakshinamurti, S. Hypoxia Inhibits Adenylyl Cyclase Catalytic Activity in a Porcine Model of Persistent Pulmonary Hypertension of the Newborn. *Am. J. Physiol.-Lung Cell. Mol. Physiol.* **2018**. https://doi.org/10.1152/ajplung.00130.2018

(132) Maghsoudi, S.; Shuaib, R.; Van Bastelaere, B.; Dakshinamurti, S. Adenylyl Cyclase Isoforms 5 and 6 in the Cardiovascular System: Complex Regulation and Divergent Roles. *Front. Pharmacol.* **2024**, *15*. https://doi.org/10.3389/fphar.2024.1370506

(133) Khannpnavar, B.; Mehta, V.; Qi, C.; Korkhov, V. Structure and Function of Adenylyl Cyclases, Key Enzymes in Cellular Signaling. *Curr. Opin. Struct. Biol.* **2020**, *63*, 34–41. https://doi.org/10.1016/j.sbi.2020.03.003

(134) Guermonprez, P.; Khelef, N.; Blouin, E.; Rieu, P.; Ricciardi-Castagnoli, P.; Guiso, N.; Ladant, D.; Leclerc, C. The Adenylate Cyclase Toxin of Bordetella Pertussis Binds to Target Cells via the αMβ2 Integrin (Cd11b/Cd18). *J. Exp. Med.* **2001**, *193* (9), 1035–1044. https://doi.org/10.1084/jem.193.9.1035

(135) Taussig, R.; Iñiguez-Lluhi, J. A.; Gilman, A. G. Inhibition of Adenylyl Cyclase by Gαi. *Science* **1993**, *261* (5118), 218–221.

(136) Chandra Jena, B.; Flaherty, D. P.; O'Brien, V. P.; Watts, V. J. Biochemical Pharmacology of Adenylyl Cyclases in Cancer. *Biochem. Pharmacol.* **2024**, *228*, 116160. https://doi.org/10.1016/j.bcp.2024.116160

(137) Ostrom, K. F.; LaVigne, J. E.; Brust, T. F.; Seifert, R.; Dessauer, C. W.; Watts, V. J.; Ostrom, R. S. Physiological Roles of Mammalian Transmembrane Adenylyl Cyclase Isoforms. *Physiol. Rev.* **2022**. https://doi.org/10.1152/physrev.00013.2021

(138) Bhatia, V.; Maghsoudi, S.; Hinton, M.; Bhagirath, A. Y.; Singh, N.; Jaggupilli, A.; Chelikani, P.; Dakshinamurti, S. Characterization of Adenylyl Cyclase Isoform 6 Residues Interacting with Forskolin. *Biology* **2023**, *12* (4). https://doi.org/10.3390/biology12040572

(139) Lin, T.-H.; Lai, H.-L.; Kao, Y.-Y.; Sun, C.-N.; Hwang, M.-J.; Chern, Y. Protein Kinase C Inhibits Type VI Adenylyl Cyclase by Phosphorylating the Regulatory N Domain and Two Catalytic C1 and C2 Domains. *J. Biol. Chem.* **2002**, *277* (18), 15721–15728. https://doi.org/10.1074/jbc.M111537200

(140) Cunnington, R. H.; Singh, N.; Shafizadeh, M.; Hanrahan, J. W.; Dakshinamurti, S.; Chelikani, P. Severe Hypoxia Reduces Adenylyl Cyclase 6 Expression and Function in Bronchial Epithelial Cells. *FASEB BioAdvances* **2026**, *8* (4), e70102. https://doi.org/10.1096/fba.2025-00309

(141) Nguyen, A. M.; Jacobs, C. R. Emerging Role of Primary Cilia as Mechanosensors in Osteocytes. *Bone* **2013**, *54* (2), 196–204. https://doi.org/10.1016/j.bone.2012.11.016

(142) Bhagirath, A. Y.; Bhatia, V.; Medapati, M. R.; Singh, N.; Hinton, M.; Chelikani, P.; Dakshinamurti, S. Critical Cysteines in the Functional Interaction of Adenylyl Cyclase Isoform 6 with Gαs. *FASEB BioAdvances* **2022**, *4* (3), 180–196. https://doi.org/10.1096/fba.2021-00073

(143) Jaggupilli, A.; Dhanaraj, P.; Pritchard, A.; Sorensen, J. L.; Dakshinamurti, S.; Chelikani, P. Study of Adenylyl Cyclase-GαS Interactions and Identification of Novel AC Ligands. *Mol. Cell. Biochem.* **2018**, *446* (1–2), 63–72. https://doi.org/10.1007/s11010-018-3273-4

(144) Hatley, M. E.; Gilman, A. G.; Sunahara, R. K. Expression, Purification, and Assay of Cytosolic (Catalytic) Domains of Membrane-Bound Mammalian Adenylyl Cyclases. In *Methods in Enzymology*; Elsevier, 2002; Vol. 345, pp 127–140. https://doi.org/10.1016/S0076-6879(02)45012-4

(145) Tang, W.-J.; Gilman, A. G. Construction of a Soluble Adenylyl Cyclase Activated by Gas and Forskolin. *Science* **1995**, *268* (5218), 1769–1772.
(146) Schlapschy, M.; Grimm, S.; Skerra, A. A System for Concomitant Overexpression of Four Periplasmic Folding Catalysts to Improve Secretory Protein Production in Escherichia Coli. *Protein Eng. Des. Sel.* **2006**, *19* (8), 385–390. https://doi.org/10.1093/protein/gzl018
(147) Schlapschy, M.; Skerra, A. Periplasmic Chaperones Used to Enhance Functional Secretion of Proteins in E. Coli. In *Heterologous Gene Expression in E.coli*; Evans, T. C., Xu, M.-Q., Eds.; Methods in Molecular Biology; Humana Press: Totowa, NJ, 2011; Vol. 705, pp 211–224. https://doi.org/10.1007/978-1-61737-967-3_12

8. Appendix

Amino Acid Sequences

EGFP

MVSKGEELFTGVVPILVELDGDVNGHKFSVSGEGEGDATYGKLTLKFICTTGKLPVPWPTLVTTLTYG
VQCFSRYPDHMKQHDFFKSAMPEGYVQERTIFFKDDGNYKTRAEVKFEGDTLVNRIELKGIDFKED
GNILGHKLEYNYNSHNVYIMADKQKNGIKVNFKIRHNIEDGSVQLADHYQQNTPIGDGPVLLPDN
HYLSTQSALSKDPNEKRDHMVLLEFVTAAGITLGMDELYKHHHHHH*

EGFP_M219

MVSKGEELFTGVVPILVELDGDVNGHKFSVSGEGEGDATYGKLTLKFICTTGKLPVPWPTLVTTLTYG
VQCFSRYPDHLKQHDFFKSALPEGYVQERTIFFKDDGNYKTRAEVKFEGDTLVNRIELKGIDFKEDG
NILGHKLEYNYNSHNVYITADKQKNGIKVNFKIRHNIEDGSVQLADHYQQNTPIGDGPVLLPDNHY
LSTQSALSKDPNEKRDHMVLLEFVTAAGITLGKDELYKHHHHHH*

NisA

MGSSHHHHHHSQDPMSTKDFNLDLVSVSKKDSGASPRITSISLCTPGCKTGALMGCNMKTATCH
CSIHVSK*

NisA (M21V)

MGSSHHHHHHSQDPMSTKDFNLDLVSVSKKDSGASPRITSISLCTPGCKTGALMGCNVKTATCH
CSIHVSK*

NisB

MIKSSFKAQPFLVRNTILSPNDKRSFTEYTQVIETVSKNKVFLEQLLLANPKLYDVMQKYNAGLLKKK
RVKKLFESIYKYYKRSYLRSTPFGLFSETSIGVFSKSSQYKLMGKTTKGIRLDTQWLIRLVHKMEVDFS
KKLSFTRNNANYKFGDRVFQVYTINSSELEEVNIKYTNVYQIISEFCENDYQKYEDICETVTLCYGDE
YRELSEQYLGSLIVNHYLISNLQKDLLSDFSWNTFLTKVEAIDEDKKYIIPLKKVQKFIQEYSEIEIGEGI
EKLKEIYQEMSQILENDNYIQIDLISDSEINFDVKQKQQLEHLAEFLGNTTKSVRRTYLDDYKDKFIEK
YGVDQEVQITELFDSTFGIGAPYNYNHPRNDFYESEPSTLYYSEEEREKYLSMYVEAVKNHNVINLD

DLESHYQKMDLEKKSELQGLELFLNLAKEYEKDIFILGDIVGNNNLGGASGRFSALSPELTSYHRTIV
DSVERENENKEITSCEIVFLPENIRHANVMHTSIMRRKVLPFFTSTSHNEVLLTNIYIGIDEKEKFYARD
ISTQEVLKFYITSMYNKTLFSNELRFLYEISLDDKFGNLPWELIYRDFDYIPRLVFDEIVISPAKWKIWG
RDVNSKMTIRELIQSKEIPKEFYIVNGDNKVYLSQENPLDMEILESAIKKSSKRKDFIELQEYFEDENII
NKGEKGRVADVVVPFIRTRALGNEGRAFIREKRVSVERREKLPFNEWLYLKLYISINRQNEFLLSYLP
DIQKIVANLGGNLFFLRYTDPKPHIRLRIKCSDLFLAYGSILEILKRSRKNRIMSTFDISIYDQEVERYG
GFDTLELSEAIFCADSKIIPNLLTLIKDTNNDWKVDDVSILVNYLYLKCFFENDNKRILNFLNLVSPKKV
KENVNEKIEHYLKLLKVNNLGDQIFYDKNFKELKHAIKNLFLKMIAQDFELQKVYSIIDSIIHVHNNRL
IGIERDKEKLIYYTLQRLFVSEEYMK*

NisC

MNKKNIKRNVEKIIAQWDERTRKNKENFDFGELTLSTGLPGIILMLAELKNKDNSKIYQKKIDNYIEYI
VSKLSTYGLLTGSLYSGAAGIALSILHLREDDEKYKNLLDSLNRYIEYFVREKIEGFNLENITPPDYDVIE
GLSGILSYLLLINDEQYDDLKILIINFLSNLTKENKGLISLYIKSENQMSQSESEMYPLGCLNMGLAHG
LAGVGCILAYAHIKGYSNEASLSALQKIIFIYEKFELERKKQFLWKDGLVADELKKEKVIREASFIRDAW
CYGGPGISLLYLYGGLALDNDYFVDKAEKILESAMQRKLGIDSYMICHGYSGLIEICSLFKRLLNTKKF
DSYMEEFNVNSEQILEEYGDESGTGFLEGISGCILVLSKFEYSINFTYWRQALLLFDDFLKGGKRK*

NisP

METTNSQQLLSNNINTELINHNSNAILSSTEGSTTDSINLGAQSPAVKSTTRTELDVTGAAKTLLQTSA
VQKEMKVSLQETQVSSEFSKRDSVTNKEAVPVSKDELLEQSEVVVSTSSIQKNKILDNKKKRANFVT
SSPLIKEKPSNSKDASGVIDNSASPLSYRKAKEVVSLRQPLKNQKVEAQPLLISNSSEKKASVYTNSH
DFWDYQWDMKYVTNNGESYALYQPSKKISVGIIDSGIMEEHPDLSNSLGNYFKNLVPKGGFDNEE
PDETGNPSDIVDKMGHGTEVAGQITANGNILGVAPGITVNIYRVFGENLSKSEWVARAIRRAADDG
NKVINISAGQYLMISGSYDDGTNDYQEYLNYKSAINYATAKGSIVVAALGNDSLNIQDNQTMINFLK
RFRSIKVPGKVVDAPSVFEDVIAVGGIDGYGNISDFSNIGADAIYAPAGTTANFKKYGQDKFVSQGYY
LKDWLFTTTNTGWYQYVYGNSFATPKVSGALALVVDKYGIKNPNQLKRFLLMNSPEVNGNRVLNIV
DLLNGKNKAFSLDTPGGGGSGGGGSHHHHHH*

AC6-FlagTag

MSWFSGLLVPKVDERKTAWGERNGQKRSRRRGTRAGGFCTPRYMSCLRDAEPPSPTPAGPPRCP
WQDDAFIRRGGPGKGKELGLRAVALGFEDTEVTTTAGGTAEVAPDAVPRSGRSCWRRLVQVFQSK
QFRSAKLERLYQRYFFQMNQSSTHYPAEVSQRQAFQETRGYIQARLHLQHENRQQERLLLSVLPQ
HVAMEMKEDINTKKEDMMFHKIYIQKHDNVSILFADIEGFTSLASQCTAQELVMTLNELFARFDKLA

AENHCLRIKILGDCYYCVSGLPEARADHAHCCVEMGVDMIEAISLVREVTGVNVNMRVGIHSGRV
HCGVLGLRKWQFDVWSNDVTLANHMEAGGRAGRIHITRATLQYLNGDYEVEPGRGGERNAYLKE
QHIETFLILGASQKRKEEKAMLAKLQRTRANSMEGLMPRWVPDRAFSRTKDSKAFRQMGIDDSSK
DNRGTQDALNPEDEVDEFLSRAIDARSIDQLRKDHVRRFLLTFQREDLEKKYSRKVDPRFGAYVQQ
VESTARLDFLWKLQATGEKEEMEELQAYNRRLLHNILPKDVAAHFLARERRNDELYYQSCECVAVM
FASIANFSEFYVELEANNEGVECLRLLNEIIADFDEIISEERFRQLEKIKTIGSTYMAASGLNASTYDQV
GRSHITALADYAMRLMEQMKHINEHSFNNFQMKIGLNMGPVVAGVIGARKPQYDIWGNTVNVSS
RMDSTGVPDRIQVTTDLYQVLAAKGYQLECRGVVKVKGKGEMTTYFLNGGPSSDYKDDDDK*

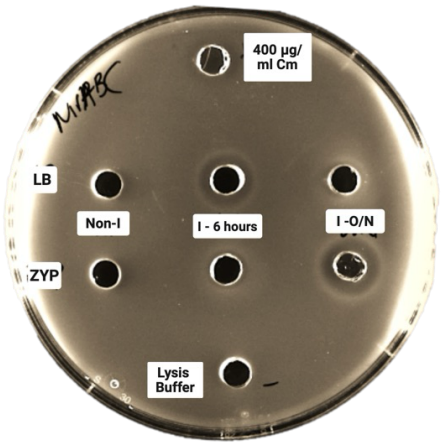
Gas -HisTag

MHHHHHHGCLGNSKTEDQRNEEKAQREANKKIEKQLQKDKQVYRATHRLLLLGAGESGKSTIVK
QMRILHVNGFNGEGGEEDPQAARSNSDGEKATKVQDIKNNLKEAIETIVAAMSNLVPPVELANPE
NQFRVDYILSVMNVPDFDFPPEFYEHAKALWEDEGVRACYERSNEYQLIDCAQYFLDKIDVIKQAD
YVPSDQDLLRCRVLTSGIFETKFQVDKVNFHMFDVGGQRDERRKWIQCFNDVTAIIFVVASSSYNM
VIREDNQTNRLQEALNLFKSIWNNRWLRTISVILFLNKQDLLAEKVLAGKSKIEDYFPEFARYTTPED
ATPEPGEDPRVTRAKYFIRDEFLRISTASGDGRHYCYPHFTCAVDTENIRRVFNDCRDIIQRMHLRQ
YELL*

AC6-pelB-HisTag

MKYLLPTAAAGLLLLAAQPAMAMGSWFSGLLVPKVDERKTAWGERNGQKRSRRRGTRAGGFCTP
RYMSCLRDAEPPSPTPAGPPRCPWQDDAFIRRGGPGKGKELGLRAVALGFEDTEVTTTAGGTAEVA
PDAVPRSGRSCWRRLVQVFQSKQFRSAKLERLYQRYFFQMNQSSTHYPAEVSQRQAFQETRGYIQ
ARLHLQHENRQQERLLLSVLPQHVAMEMKEDINTKKEDMMFHKIYIQKHDNVSILFADIEGFTSLA
SQCTAQELVMTLNELFARFDKLAAENHCLRIKILGDCYYCVSGLPEARADHAHCCVEMGVDMIEAI
SLVREVTGVNVNMRVGIHSGRVHCGVLGLRKWQFDVWSNDVTLANHMEAGGRAGRIHITRATLQ
YLNGDYEVEPGRGGERNAYLKEQHIETFLILGASQKRKEEKAMLAKLQRTRANSMEGLMPRWVPD
RAFSRTKDSKAFRQMGIDDSSKDNRGTQDALNPEDEVDEFLSRAIDARSIDQLRKDHVRRFLLTFQ
REDLEKKYSRKVDPRFGAYVQQVESTARLDFLWKLQATGEKEEMEELQAYNRRLLHNILPKDVAAH
FLARERRNDELYYQSCECVAVMFASIANFSEFYVELEANNEGVECLRLLNEIIADFDEIISEERFRQLE
KIKTIGSTYMAASGLNASTYDQVGRSHITALADYAMRLMEQMKHINEHSFNNFQMKIGLNMGPVV
AGVIGARKPQYDIWGNTVNVSSRMDSTGVPDRIQVTTDLYQVLAAKGYQLECRGVVKVKGKGEMT
TYFLNGGPSSLEHHHHHH*

A

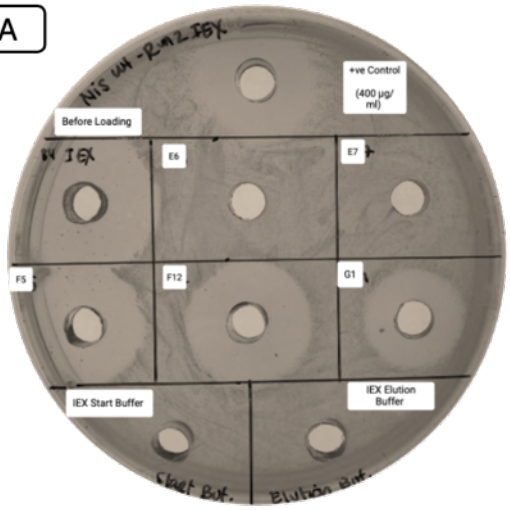


B

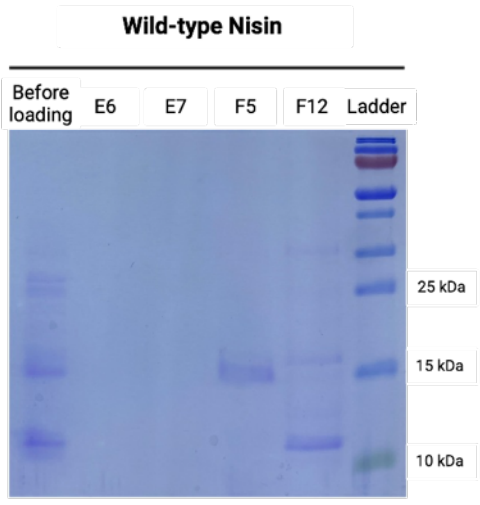
Sample	Halo Diameter (cm)
400µg/l Cm	0.55
LB (I-6 hours)	0.66
ZYP (I – O/N)	0.75

Appendix Figure 1. Agar well diffusion assay of antimicrobial activity under varying induction conditions. LB agar plates were inoculated with bacterial cells and loaded with supernatants from the following conditions: LB (media control), Non-I (non-induced), I–6 h (6-hour induction), I–O/N (overnight induction), ZYP (autoinduction), and lysis buffer (negative control). Chloramphenicol (400 µg/mL) was included where indicated. Zones of inhibition denote antimicrobial activity.

A



B



Appendix Figure 2.IEX purification of nisin. (A) Agar diffusion assay of IEX fractions (E6, E7, F5, F12, G1) with start/elution buffers and a positive control (400 µg/mL); inhibition zones indicate activity. **(B)** SDS-PAGE of corresponding fractions showing nisin enrichment across eluted samples

Time	Mass	Oxidation	Dehydration
15.23	3473.5739	2	3
15.54	3455.5753	2	4
15.23	3437.5713	2	5
15.66	3419.5716	2	6
15.84	3403.5565	1	6
15.84	3439.5739	1	4
16.41	3405.5663	0	5
16.73	3387.5559	0	6
16.96	3369.5469	0	7
17.22	3385.5469	1	7
17.42	3401.5351	2	7
17.87	3367.5353	1	8
18	3383.5285	2	8
18.34	3351.5354	0	8

Appendix Figure 3.Nisin WT LC-MS Analysis at the Proteomics Centre List. This list contains the data presented in **Figure 28**. For each data point, the corresponding time (in minutes) and Mass (in Da) are shown. Additionally, the oxidation state and level of dehydration is shown.

Time	Mass	Oxidation	Dehydration
13.46	3405.607	5	2
13.66	3387.601	6	2
14.6	3353.573	7	1
14.81	3389.591	5	1
15.52	3355.584	6	0
16.15	3337.69	7	0
17.02	3319.564	8	0
17.55	3335.56	8	1

Appendix Figure 4. Nisin M21V LC-MS Analysis at the Proteomics Centre List. This list contains the data presented in **Figure 33**. For each data point, the corresponding time (in minutes) and Mass (in Da) are shown. Additionally, the oxidation state and level of dehydration is shown.

seq id	position	reads (cov)	reads (cov)	score	skew	freq	annotation	gene	product
CP001509	16489 =	NA (NA)					noncoding (1104/1343 nt)	*IS186*	repeat region
PM455-pColA-araB	1404 =	1 (0.000)	106 (0.370)	49/294	0	99.10%	intergenic (–/+215)	*–/araC*	–/L-arabinose regulatory protein
CP001509	16490 =	NA (NA)					noncoding (1105/1343 nt)	*IS186*	repeat region
PM455-pColA-araB	= 5108	0 (0.000)	106 (0.370)	41/294	0	100%	intergenic (+223/–)	*metG/–*	methionine--tRNA ligase/–
CP001509	16492 =	NA (NA)					noncoding (1107/1343 nt)	*IS186*	repeat region
PM455-pColA-araB	= 5109	0 (0.000)	74 (0.260)	41/292	0	100%	intergenic (+224/–)	*metG/–*	methionine--tRNA ligase/–
CP001509	= 16493	NA (NA)					noncoding (1108/1343 nt)	*IS186*	repeat region
PM455-pColA-araB	= 5108	0 (0.000)	100 (0.350)	42/294	0	100%	intergenic (+223/–)	*metG/–*	methionine--tRNA ligase/–
CP001509	= 16494	NA (NA)					noncoding (1109/1343 nt)	*IS186*	repeat region
PM455-pColA-araB	1404 =	1 (0.000)	91 (0.320)	52/294	0	98.90%	intergenic (–/+215)	*–/araC*	–/L-arabinose regulatory protein
CP001509	= 16495	NA (NA)					noncoding (1110/1343 nt)	*IS186*	repeat region
PM455-pColA-araB	1404 =	1 (0.000)	92 (0.320)	43/294	0	98.90%	intergenic (–/+215)	*–/araC*	–/L-arabinose regulatory protein
CP001509	= 546302	0 (0.000)					coding (22/462 nt)	*rzpD*	DLP12 prophage; putative murein endopeptidase
CP001509	551301 =	0 (0.000)	82 (0.930)	48/290	0.1	100%	intergenic (-34/+703)	*ECD_00530/cusS*	hypothetical protein/copper-sensing histidine kinase in two-component regulatory system with CusR
CP001509	549188 =	0 (0.000)					intergenic (+602/-1362)	*nohD/ECD_00513*	DLP12 prophage; DNA packaging protein/hypothetical protein
CP001509	= 1099785	NA (NA)	95 (1.060)	33/294	0.6	100%	intergenic (-56/+346)	*insE-1/serX*	putative transposase-related protein/tRNA-Ser
CP001509	= 550345	0 (0.000)					intergenic (+1759/-205)	*nohD/ECD_00513*	DLP12 prophage; DNA packaging protein/hypothetical protein
CP001509	= 1586961	0 (0.000)	64 (0.730)	27/288	1.1	100%	intergenic (-626/-26)	*stfR/insE-4*	Rac prophage; putative tail fiber protein/putative transposase-related protein
CP001509	691844 =	93 (1.040)					coding (102/1434 nt)	*rhsO*	conserved protein, rhs-like protein
CP001509	= 3628874	0 (0.000)	112 (1.310)	44/282	0.1	71.50%	coding (302/873 nt)	*rhsA*	Rhs protein with putative toxin 55 domain; putative polysaccharide synthesis/export protein; putative neighboring cell growth inhibitor
CP001509	1877802 =	0 (0.000)					intergenic (+19/+37)	*purT/eda*	phosphoribosylglycinamide formyltransferase 2/KHG/KDPG aldolase; 2-dehydro-3-deoxy-phosphogluconate/4-hydroxy-2- oxoglutarate aldolase
PM455-pColA-araB	1407 =	0 (0.000)	62 (0.220)	32/286	0	100%	intergenic (–/+212)	*–/araC*	–/L-arabinose regulatory protein
CP001509	= 1877809	3 (0.030)					intergenic (+26/+30)	*purT/eda*	phosphoribosylglycinamide formyltransferase 2/KHG/KDPG aldolase; 2-dehydro-3-deoxy-phosphogluconate/4-hydroxy-2- oxoglutarate aldolase
PM455-pColA-araB	= 5108	0 (0.000)	62 (0.220)	27/292	0	97.70%	intergenic (+223/–)	*metG/–*	methionine--tRNA ligase/–
CP001509	2446154 =	0 (0.000)					intergenic (+26/+69)	*tktB/ypfG*	transketolase 2, thiamine triphosphate-binding/DUF1176 family protein
PM455-pColA-araB	= 5108	0 (0.000)	83 (0.290)	34/294	0	100%	intergenic (+223/–)	*metG/–*	methionine--tRNA ligase/–
CP001509	= 2446158	3 (0.030)					intergenic (+30/+65)	*tktB/ypfG*	transketolase 2, thiamine triphosphate-binding/DUF1176 family protein
PM455-pColA-araB	1404 =	1 (0.000)	97 (0.340)	41/294	0	98.00%	intergenic (–/+215)	*–/araC*	–/L-arabinose regulatory protein
CP001509	= 2820976	0 (0.000)					intergenic (-512/-48)	*araE/insJ-5*	arabinose transporter/IS150 hypothetical protein
CP001509	2822423 =	0 (0.000)	106 (1.220)	47/286	0.1	100%	intergenic (+30/+593)	*insK-5/kdul*	IS150 putative transposase/hexuronate isomerase
CP001509	3018018 =	0 (0.000)					intergenic (+35/+237)	*yghA/exbD*	putative oxidoreductase/membrane spanning protein in TonB-ExbB-ExbD complex
PM455-pColA-araB	= 5108	0 (0.000)	103 (0.360)	44/292	0	100%	intergenic (+223/–)	*metG/–*	methionine--tRNA ligase/–
CP001509	= 3018022	2 (0.020)					intergenic (+39/+233)	*yghA/exbD*	putative oxidoreductase/membrane spanning protein in TonB-ExbB-ExbD complex
PM455-pColA-araB	1404 =	0 (0.000)	106 (0.370)	42/292	0	99.10%	intergenic (–/+215)	*–/araC*	–/L-arabinose regulatory protein
CP001509	= 3481176	0 (0.000)					coding (205/402 nt)	*nikR*	transcriptional repressor, Ni-binding
CP001509	3485048 =	49 (0.560)	92 (1.040)	51/290	0	79.00%	coding (3473/4236 nt)	*rhsB*	Rhs protein with DUF4329 family putative toxin domain; putative neighboring cell growth inhibitor

Appendix Figure 5. MS51 New Junction Evidence Summary after Breseq Analysis. The short-read next generation sequencing results were compared to E. coli BL21 genome and the donor vector (PM455) sequence. Rows highlighted in teal show positions of insertions within the genome. Insertions were confirmed in 4 locations downstream of various genes such as *IS196, purT, tktB and yghA*. Additionally, positions of junctions at donor DNA in the donor plasmid (PM455) are highlighted.

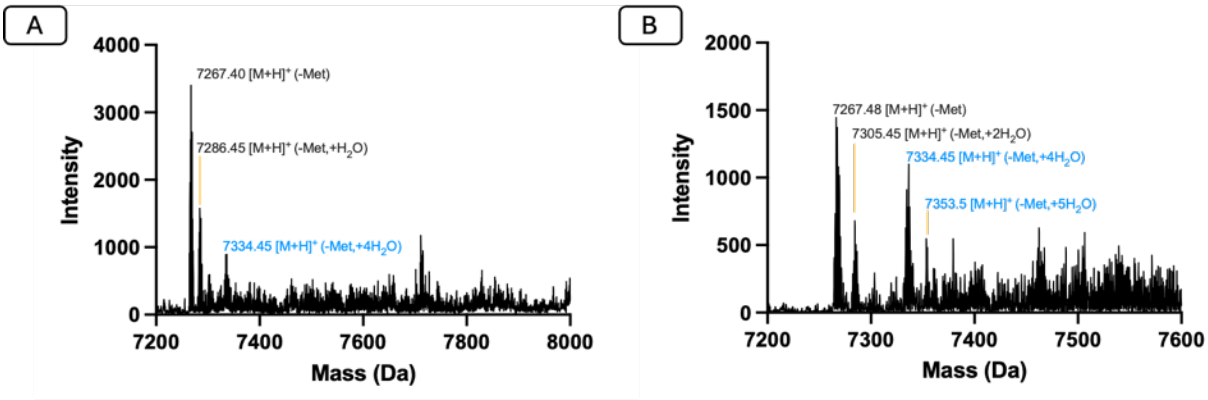
Unassigned new junction evidence

		seq id	position	reads (cov)	reads (cov)	score	skew	freq	annotation	gene	product
*	?	CP001509-E._coli	16492 =	NA (NA)	234 (0.800)	75/292	-0.0	99.6%	noncoding (1107/1343 nt)	*IS186*	repeat region
-	?	PM455-pColA-araB	= 5109	1 (0.000)					intergenic (+224/–)	*metG/–*	methionine--tRNA ligase/–
*	?	CP001509-E._coli	= 16495	NA (NA)	203 (0.690)	68/294	-0.0	100%	noncoding (1110/1343 nt)	*IS186*	repeat region
-	?	PM455-pColA-araB	1404 =	0 (0.000)					intergenic (–/+215)	*–/araC*	–/L-arabinose regulatory protein
*	?	CP001509-E._coli	150721 =	0 (0.000)	91 (0.310)	49/294	0.0	99.5%	intergenic (+47/+27)	*yadD/panC*	transposase_31 family protein/pantothenate synthetase
-	?	PM455-pColA-araB	= 5108	1 (0.000)					intergenic (+223/–)	*metG/–*	methionine--tRNA ligase/–
*	?	CP001509-E._coli	= 150725	10 (0.130)	79 (0.270)	42/290	0.0	94.1%	intergenic (+51/+23)	*yadD/panC*	transposase_31 family protein/pantothenate synthetase
-	?	PM455-pColA-araB	1404 =	0 (0.000)					intergenic (–/+215)	*–/araC*	–/L-arabinose regulatory protein
*	?	CP001509-E._coli	= 546302	0 (0.000)	96 (1.270)	43/290	0.1	100%	coding (22/462 nt)	*rzpD*	DLP12 prophage; putative murein endopeptidase
-	?	CP001509-E._coli	551301 =	0 (0.000)					intergenic (-34/+703)	*ECD_00530/cusS*	hypothetical protein/copper-sensing histidine kinase in two-component regulatory system with CusR
*	?	CP001509-E._coli	549188 =	0 (0.000)	77 (1.000)	31/294	0.5	100%	intergenic (+602/-1362)	*nohD/ECD_00513*	DLP12 prophage; DNA packaging protein/hypothetical protein
-	?	CP001509-E._coli	= 1099785	NA (NA)					intergenic (-56/+346)	*insE-1/serX*	putative transposase-related protein/tRNA-Ser
*	?	CP001509-E._coli	= 550345	0 (0.000)	72 (0.960)	31/288	0.5	100%	intergenic (+1759/-205)	*nohD/ECD_00513*	DLP12 prophage; DNA packaging protein/hypothetical protein
-	?	CP001509-E._coli	= 1586961	0 (0.000)					intergenic (-626/-26)	*stfR/insE-4*	Rac prophage; putative tail fiber protein/putative transposase-related protein
*	?	CP001509-E._coli	691844 =	104 (1.350)	76 (1.030)	39/282	0.1	60.4%	coding (102/1434 nt)	*rhsO*	conserved protein, rhs-like protein
-	?	CP001509-E._coli	= 3628874	0 (0.000)					coding (302/873 nt)	*rhsA*	Rhs protein with putative toxin 55 domain; putative polysaccharide synthesis/export protein; putative neighboring cell growth inhibitor
*	?	CP001509-E._coli	745191 =	8 (0.100)	76 (0.260)	39/294	0.0	94.4%	intergenic (+98/+60)	*aroG/gpmA*	3-deoxy-D-arabino-heptulosonate-7-phosphate synthase, phenylalanine repressible/phosphoglyceromutase 1
-	?	PM455-pColA-araB	= 5108	1 (0.000)					intergenic (+223/–)	*metG/–*	methionine--tRNA ligase/–
*	?	CP001509-E._coli	= 745195	0 (0.000)	69 (0.230)	35/294	0.0	100%	intergenic (+102/+56)	*aroG/gpmA*	3-deoxy-D-arabino-heptulosonate-7-phosphate synthase, phenylalanine repressible/phosphoglyceromutase 1
-	?	PM455-pColA-araB	1404 =	0 (0.000)					intergenic (–/+215)	*–/araC*	–/L-arabinose regulatory protein
*	?	CP001509-E._coli	= 2820976	0 (0.000)	76 (1.020)	40/286	0.1	100%	intergenic (-512/-48)	*araE/insJ-5*	arabinose transporter/IS150 hypothetical protein
-	?	CP001509-E._coli	2822423 =	0 (0.000)					intergenic (+30/+593)	*insK-5/kdul*	IS150 putative transposase/hexuronate isomerase
*	?	CP001509-E._coli	3018018 =	3 (0.040)	82 (0.280)	40/292	0.0	97.6%	intergenic (+35/+237)	*yghA/exbD*	putative oxidoreductase/membrane spanning protein in TonB-ExbB-ExbD complex
-	?	PM455-pColA-araB	= 5108	1 (0.000)					intergenic (+223/–)	*metG/–*	methionine--tRNA ligase/–
*	?	CP001509-E._coli	= 3018022	1 (0.010)	94 (0.320)	45/292	0.0	99.5%	intergenic (+39/+233)	*yghA/exbD*	putative oxidoreductase/membrane spanning protein in TonB-ExbB-ExbD complex
-	?	PM455-pColA-araB	1404 =	0 (0.000)					intergenic (–/+215)	*–/araC*	–/L-arabinose regulatory protein
*	?	CP001509-E._coli	= 3481176	0 (0.000)	92 (1.210)	45/290	0.1	82.1%	coding (205/402 nt)	*nikR*	transcriptional repressor, Ni-binding
-	?	CP001509-E._coli	3485048 =	40 (0.530)					coding (3473/4236 nt)	*rhsB*	Rhs protein with DUF4329 family putative toxin domain; putative neighboring cell growth inhibitor
*	?	CP001509-E._coli	3582495 =	1 (0.010)	93 (0.320)	37/294	0.0	99.5%	intergenic (+80/+107)	*cspA/hokA*	RNA chaperone and antiterminator, cold-inducible/toxic polypeptide, small
-	?	PM455-pColA-araB	1404 =	0 (0.000)					intergenic (–/+215)	*–/araC*	–/L-arabinose regulatory protein
*	?	CP001509-E._coli	= 3582499	9 (0.120)	88 (0.300)	39/294	0.0	94.6%	intergenic (+84/+103)	*cspA/hokA*	RNA chaperone and antiterminator, cold-inducible/toxic polypeptide, small
-	?	PM455-pColA-araB	= 5108	1 (0.000)					intergenic (+223/–)	*metG/–*	methionine--tRNA ligase/–

Appendix Figure 6. MS61 New Junction Evidence Summary after Breseq Analysis. The short-read next generation sequencing results were compared to *E. coli* BL21 genome and the donor vector (PM455) sequence. Rows indicated with metG/araC showcase positions of insertions within the genome. Insertions were confirmed in 5 locations downstream of various genes such as *IS196, panC, aroG, yghA and hokA*. Additionally, positions of junctions at donor DNA in the donor plasmid (PM455) are shown.

seq id	position	reads (cov)	reads (cov)	score	skew	freq	annotation	gene	product
CP001509-E._coli	= 546302	0 (0.000)	130 (1.010)	51/290	0.2	100%	coding (22/462 nt)	*rzpD*	DLP12 prophage; putative murein endopeptidase
CP001509-E._coli	551301 =	0 (0.000)					intergenic (-34/+703)	*ECD_00530/cusS*	hypothetical protein/copper-sensing histidine kinase in two-component regulatory system with CusR
CP001509-E._coli	549188 =	0 (0.000)	145 (1.110)	54/294	0.2	100%	intergenic (+602/-1362)	*nohD/ECD_00513*	DLP12 prophage; DNA packaging protein/hypothetical protein
CP001509-E._coli	= 1099785	NA (NA)					intergenic (-56/+346)	*insE-1/serX*	putative transposase-related protein/tRNA-Ser
CP001509-E._coli	= 550345	0 (0.000)	114 (0.890)	41/288	0.6	100%	intergenic (+1759/-205)	*nohD/ECD_00513*	DLP12 prophage; DNA packaging protein/hypothetical protein
CP001509-E._coli	= 1586961	0 (0.000)					intergenic (-626/-26)	*stfR/insE-4*	Rac prophage; putative tail fiber protein/putative transposase-related protein
CP001509-E._coli	691844 =	109 (0.840)	144 (1.150)	56/282	0.1	73.40%	coding (102/1434 nt)	*rhsO*	conserved protein, rhs-like protein
CP001509-E._coli	= 3628874	0 (0.000)					coding (302/873 nt)	*rhsA*	Rhs protein with putative toxin 55 domain; putative polysaccharide synthesis/export protein; putative neighboring cell growth inhibitor
CP001509-E._coli	2446154 =	0 (0.000)	114 (0.920)	53/294	0	100%	intergenic (+26/+69)	*tktB/ypfG*	transketolase 2, thiamine triphosphate-binding/DUF1176 family protein
PM456-pDonor-Col	1404 =	0 (0.000)					intergenic (–/+198)	*–/E. coli rhaR*	–/transcriptional activator of rhaR and rhaS
CP001509-E._coli	= 2446158	2 (0.020)	131 (1.050)	54/294	0	99.20%	intergenic (+30/+65)	*tktB/ypfG*	transketolase 2, thiamine triphosphate-binding/DUF1176 family protein
PM456-pDonor-Col	= 6449	0 (0.000)					intergenic (-3089/–)	*E. coli rhaS/–*	positive regulator of the rhaB promoter/–
CP001509-E._coli	= 3481176	0 (0.000)	139 (1.080)	64/290	0	74.50%	coding (205/402 nt)	*nikR*	transcriptional repressor, Ni-binding
CP001509-E._coli	3485048 =	95 (0.740)					coding (3473/4236 nt)	*rhsB*	Rhs protein with DUF4329 family putative toxin domain; putative neighboring cell growth inhibitor

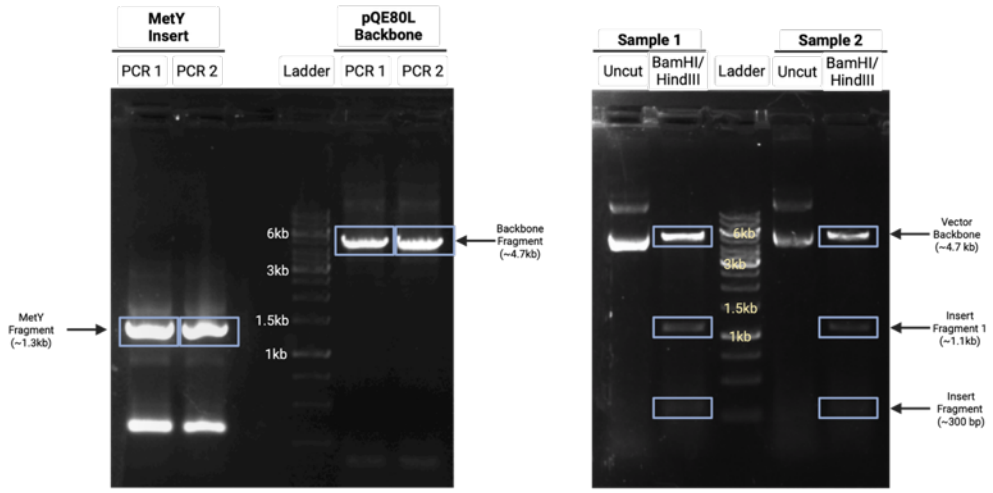
Appendix Figure 7. MS39 New Junction Evidence Summary after Breseq Analysis. The short-read next generation sequencing results were compared to *E. coli* BL21 genome and the donor vector (PM456) sequence. Rows highlighted in blue showcase positions of insertions within the genome. Insertions were confirmed a single location downstream of the *tktB* gene. Additionally, positions of junctions at donor DNA in the donor plasmid (PM456) are shown.



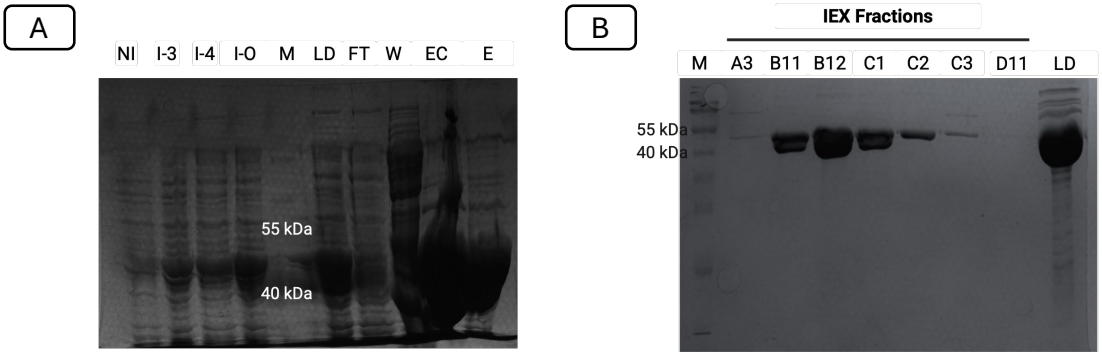
C

Strain	Percent Aha Labelled (%)
BU14	20.8%
MS51	39.9%

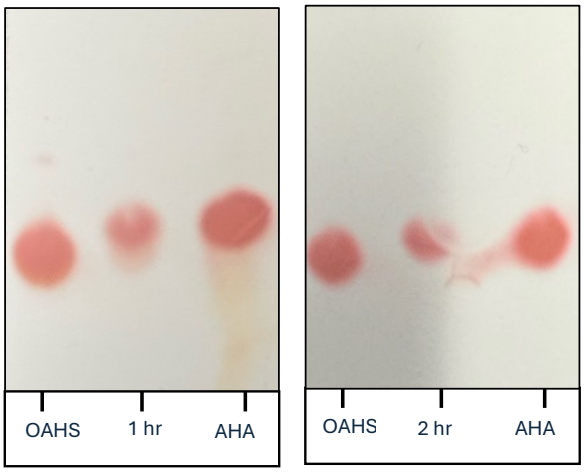
Appendix Figure 8. ESI-MS analysis of azidohomoalanine labelled Nisin M21V expressed in BU14 and MS51. The deconvoluted mass peaks with methionine are shown in black while azidohomoalanine Nisin peaks are shown in blue. **(A)** ESI-MS of Nisin-M21V-Aha expressed in BU14. Methionine containing Nisin peaks are observed for the fully modified form ($[M+H]^+$ = 7267.40 Da) and partially modified forms($[M+H]^+$ = 7286.45 Da Azidohomoalanine containing Nisin peaks are observed only for the partially modified form ($[M+H]^+$ = 7334.45 Da.) **(B)** ESI-MS of Nisin-M21V-Aha expressed in MS51. Methionine containing Nisin peaks are observed for the fully modified form ($[M+H]^+$ = 7267.40 Da) and partially modified forms($[M+H]^+$ = 7305.45 Da Azidohomoalanine containing Nisin peaks are observed only for the partially modified form ($[M+H]^+$ = 7334.45 Da and $[M+H]^+$ = 7353.5 Da) **(C)** Percentage of Aha-labelled peptides expressed in each strain. In the MetRS-enriched strain, doubling in labelling efficiency is seen.



Appendix Figure 9. Cloning of MetY into pQE80L for expression. Left – PCR products observed for insert and backbone. The PCR product for MetY insert observed at expected size (~1.3 kb) and product for vector backbone at expected sizes (~4.7 kb). After extraction of fragments from gel and purification, Gibson assembly was conducted. Right – Restriction digestion of cloned vector for ligation confirmation. The new plasmid was digested with BamHI and HindIII and run on agarose gel. Due to presence of 2 HindIII cut sites in the insert, 3 fragments are expected on the gel. Expected fragments are observed at molecular weights of 300bp, 1.1 kb, and 4.7kb.



Appendix Figure 10. SDS-PAGE analysis of MetY Expression and purification. (A) SDS-PAGE analysis of various expression times and IMAC purification fractions. NI – non-induced, I-3 – induced after 3 hr, I-4 – induction after 4 hr, I-O – induction after O/N, M-marker, LD – column loading, FT – flow-through, W – wash fraction, EC – elution fraction concentrated, E – elution fraction. (B) SDS-PAGE Analysis of ion-exchange chromatography fractions. Fractions (A3 to D11) are shown and protein observed at expected molecular weight with high purity after purification. LD – column loading sample.



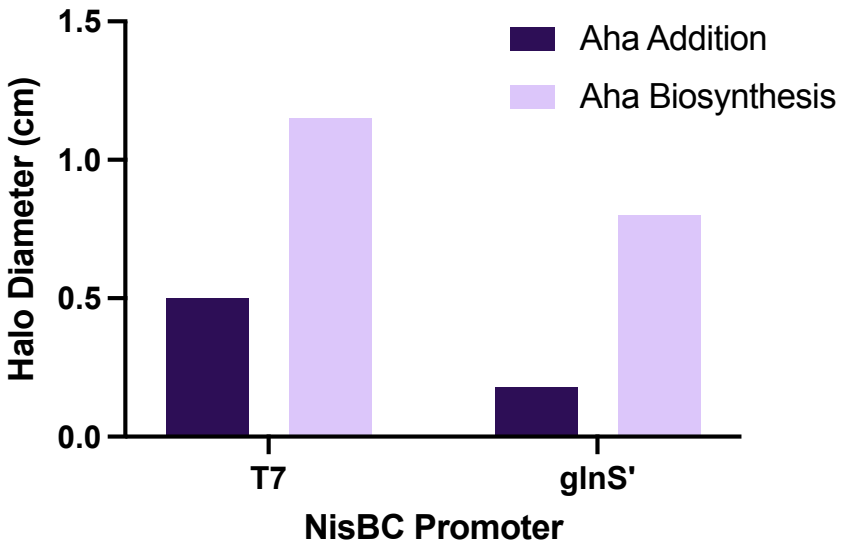
Appendix Figure 12. Ninhydrin strain thin-layer chromatography of MetY-catalyzed synthesis of Aha. Left image –Run with OAHS (lane 1), Aha (lane 3) and reaction after 1 hr incubation at 37°C showcasing partial production formation. Right image – Run with OAHS (lane 1), Aha (lane 3) and reaction after 2 hr incubation at 37°C showcasing partial production formation.

seq id	position	reads (cov)	reads (cov)	score	skew	freq	annotation	gene	product
CP001509-E._coli	16492 =	NA (NA)					noncoding (1107/1343 nt)	*IS186*	repeat region
PM455-pColA-araB	= 5109	0 (0.000)	340 (0.830)	90/294	0	100%	intergenic (+224/–)	*metG/–*	methionine--tRNA ligase/–
CP001509-E._coli	= 16495	NA (NA)					noncoding (1110/1343 nt)	*IS186*	repeat region
PM455-pColA-araB	1404 =	0 (0.000)	306 (0.740)	91/296	0	100%	intergenic (–/+215)	*–/araC*	–/L-arabinose regulatory protein
CP001509-E._coli	150721 =	0 (0.000)					intergenic (+47/+27)	*yadD/panC*	transposase_31 family protein/pantothenate synthetase
PM455-pColA-araB	= 5108	0 (0.000)	83 (0.200)	37/296	0	100%	intergenic (+223/–)	*metG/–*	methionine--tRNA ligase/–
CP001509-E._coli	= 150725	16 (0.150)					intergenic (+51/+23)	*yadD/panC*	transposase_31 family protein/pantothenate synthetase
PM455-pColA-araB	1404 =	0 (0.000)	93 (0.230)	49/292	0	92.20%	intergenic (–/+215)	*–/araC*	–/L-arabinose regulatory protein
CP001509-E._coli	= 546302	0 (0.000)					coding (22/462 nt)	*rzpD*	DLP12 prophage; putative murein endopeptidase
CP001509-E._coli	551301 =	0 (0.000)	97 (0.940)	41/292	0.4	100%	intergenic (-34/+703)	*ECD_00530/cusS*	hypothetical protein/copper-sensing histidine kinase in two-component regulatory system with CusR
CP001509-E._coli	549188 =	0 (0.000)					intergenic (+602/-1362)	*nohD/ECD_00513*	DLP12 prophage; DNA packaging protein/hypothetical protein
CP001509-E._coli	= 1099785	NA (NA)	102 (0.980)	39/296	0.5	100%	intergenic (-56/+346)	*insE-1/serX*	putative transposase-related protein/tRNA-Ser
CP001509-E._coli	= 550345	0 (0.000)					intergenic (+1759/-205)	*nohD/ECD_00513*	DLP12 prophage; DNA packaging protein/hypothetical protein
CP001509-E._coli	= 1586961	0 (0.000)	83 (0.810)	36/290	0.6	100%	intergenic (-626/-26)	*sttR/insE-4*	Rac prophage; putative tail fiber protein/putative transposase-related protein
CP001509-E._coli	691844 =	123 (1.180)					coding (102/1434 nt)	*rhsO*	conserved protein, rhs-like protein
CP001509-E._coli	= 3628874	0 (0.000)	80 (0.800)	34/284	0.7	57.60%	coding (302/873 nt)	*rhsA*	Rhs protein with putative toxin 55 domain; putative polysaccharide synthesis/export protein; putative neighboring cell growth inhibitor
CP001509-E._coli	745191 =	2 (0.020)					intergenic (+98/+60)	*aroG/gpmA*	3-deoxy-D-arabino-heptulosonate-7-phosphate synthase, phenylalanine repressible/phosphoglyceromutase 1
PM455-pColA-araB	= 5108	0 (0.000)	104 (0.250)	43/296	0	99.10%	intergenic (+223/–)	*metG/–*	methionine--tRNA ligase/–
CP001509-E._coli	= 745195	5 (0.050)					intergenic (+102/+56)	*aroG/gpmA*	3-deoxy-D-arabino-heptulosonate-7-phosphate synthase, phenylalanine repressible/phosphoglyceromutase 1
PM455-pColA-araB	1404 =	0 (0.000)	94 (0.230)	42/296	0	97.40%	intergenic (–/+215)	*–/araC*	–/L-arabinose regulatory protein
CP001509-E._coli	2446154 =	2 (0.020)					intergenic (+26/+69)	*tktB/ypfG*	transketolase 2, thiamine triphosphate-binding/DUF1176 family protein
PM456-pDonor-Col	1404 =	0 (0.000)	110 (1.070)	55/296	0	99.10%	intergenic (–/+198)	*–/E. coli rhaR*	–/transcriptional activator of rhaR and rhaS
CP001509-E._coli	= 2446158	2 (0.020)					intergenic (+30/+65)	*tktB/ypfG*	transketolase 2, thiamine triphosphate-binding/DUF1176 family protein
PM456-pDonor-Col	= 6449	0 (0.000)	82 (0.800)	31/296	0.2	98.80%	intergenic (-3089/–)	*E. coli rhaS/–*	positive regulator of the rhaB promoter/–
CP001509-E._coli	= 2820976	0 (0.000)					intergenic (-512/-48)	*araE/insJ-5*	arabinose transporter/IS150 hypothetical protein
CP001509-E._coli	2822423 =	0 (0.000)	92 (0.910)	36/288	0.6	100%	intergenic (+30/+593)	*insK-5/kduI*	IS150 putative transposase/hexuronate isomerase
CP001509-E._coli	3018018 =	5 (0.050)					intergenic (+35/+237)	*yghA/exbD*	putative oxidoreductase/membrane spanning protein in TonB-ExbB-ExbD complex
PM455-pColA-araB	= 5108	0 (0.000)	134 (0.330)	50/294	0	98.20%	intergenic (+223/–)	*metG/–*	methionine--tRNA ligase/–
CP001509-E._coli	= 3018022	3 (0.030)					intergenic (+39/+233)	*yghA/exbD*	putative oxidoreductase/membrane spanning protein in TonB-ExbB-ExbD complex
PM455-pColA-araB	1404 =	0 (0.000)	129 (0.320)	58/294	0	98.90%	intergenic (–/+215)	*–/araC*	–/L-arabinose regulatory protein
CP001509-E._coli	= 3481176	0 (0.000)					coding (205/402 nt)	*nikR*	transcriptional repressor, Ni-binding
CP001509-E._coli	3485048 =	52 (0.510)	137 (1.330)	55/292	0	84.00%	coding (3473/4236 nt)	*rhsB*	Rhs protein with DUF4329 family putative toxin domain; putative neighboring cell growth inhibitor
CP001509-E._coli	3582495 =	1 (0.010)					intergenic (+80/+107)	*cspA/hokA*	RNA chaperone and antiterminator, cold-inducible/toxic polypeptide, small
PM455-pColA-araB	1404 =	0 (0.000)	117 (0.280)	48/296	0	99.60%	intergenic (–/+215)	*–/araC*	–/L-arabinose regulatory protein
CP001509-E._coli	= 3582499	13 (0.120)					intergenic (+84/+103)	*cspA/hokA*	RNA chaperone and antiterminator, cold-inducible/toxic polypeptide, small
PM455-pColA-araB	= 5108	0 (0.000)	116 (0.280)	49/296	0	94.70%	intergenic (+223/–)	*metG/–*	methionine--tRNA ligase/–

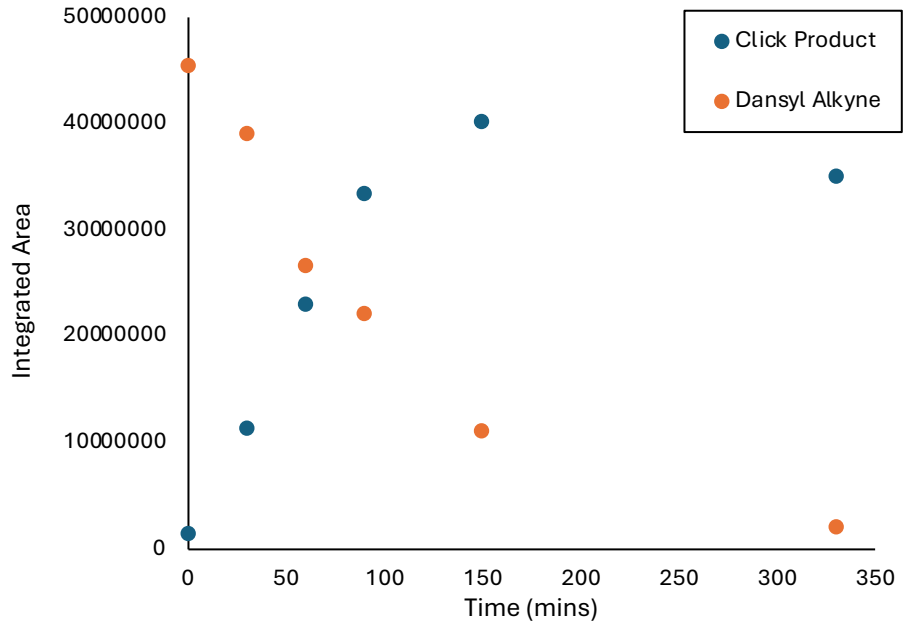
Appendix Figure 11. MS94 New Junction Evidence Summary after Breseq Analysis. The short-read next generation sequencing results were compared to *E. coli* BL21 genome and the donor vectors (PM455 and PM456) sequence. Rows indicated highlighted in teal showcase positions of previous insertions of *metG* within the genome. Insertions were confirmed in 5 locations downstream of various genes such as *IS196, panC, aroG, yghA and hokA*. A new insertion of *metXY* confirmed to be located downstream of *tktB* gene. Additionally, positions of junctions at donor DNA in the donor plasmids (PM455 and PM456) are shown.

seq id	position	reads (cov)	reads (cov)	score	skew	freq	annotation	gene	product
CP001509-E._coli	16492 =	NA (NA)	402 (0.750)	93/294	0	100%	noncoding (1107/1343 nt)	*IS186*	repeat region
PM455-pColA-araB	= 5109	0 (0.000)					intergenic (+224/–)	*metG*/–	methionine--tRNA ligase/–
CP001509-E._coli	= 16495	NA (NA)	375 (0.690)	86/296	0	99.70%	noncoding (1110/1343 nt)	*IS186*	repeat region
PM455-pColA-araB	1404 =	1 (0.000)					intergenic (–/+215)	–/*araC*	–/L-arabinose regulatory protein
CP001509-E._coli	150721 =	0 (0.000)	123 (0.230)	51/296	0	100%	intergenic (+47/+27)	*yadD*/*panC*	transposase_31 family protein/pantothenate synthetase
PM455-pColA-araB	= 5108	0 (0.000)					intergenic (+223/–)	*metG*/–	methionine--tRNA ligase/–
CP001509-E._coli	= 150725	9 (0.060)	156 (0.290)	62/292	0	97.20%	intergenic (+51/+23)	*yadD*/*panC*	transposase_31 family protein/pantothenate synthetase
PM455-pColA-araB	1404 =	0 (0.000)					intergenic (–/+215)	–/*araC*	–/L-arabinose regulatory protein
CP001509-E._coli	441508 =	14 (0.100)	184 (0.470)	54/296	0.2	96.30%	intergenic (+45/-136)	*mdlB*/*glnK*	putative multidrug ABC transporter ATPase/nitrogen assimilation regulatory protein for GlnL, GlnE, and AmtB
PM666-475_NisCB-	= 6512	0 (0.000)					intergenic (+271/–)	*NisA*/–	–/–
CP001509-E._coli	= 441512	28 (0.190)	173 (0.440)	56/294	0.2	92.60%	intergenic (+49/-132)	*mdlB*/*glnK*	putative multidrug ABC transporter ATPase/nitrogen assimilation regulatory protein for GlnL, GlnE, and AmtB
PM666-475_NisCB-	1404 =	0 (0.000)					intergenic (–/-241)	–/*nisC*	–//modified_by=User
CP001509-E._coli	= 546302	0 (0.000)	140 (0.970)	51/292	0.3	100%	coding (22/462 nt)	*rzpD*	DLP12 prophage; putative murein endopeptidase
CP001509-E._coli	551301 =	0 (0.000)					intergenic (-34/+703)	*ECD_00530*/*cusS*	hypothetical protein/copper-sensing histidine kinase in two-component regulatory system with CusR
CP001509-E._coli	549188 =	0 (0.000)	149 (1.010)	54/296	0.2	100%	intergenic (+602/-1362)	*nohD*/*ECD_00513*	DLP12 prophage; DNA packaging protein/hypothetical protein
CP001509-E._coli	= 1099785	NA (NA)					intergenic (-56/+346)	*insE-1*/*serX*	putative transposase-related protein/tRNA-Ser
CP001509-E._coli	= 550345	0 (0.000)	149 (1.030)	48/290	0.4	100%	intergenic (+1759/-205)	*nohD*/*ECD_00513*	DLP12 prophage; DNA packaging protein/hypothetical protein
CP001509-E._coli	= 1586961	0 (0.000)					intergenic (-626/-26)	*stfR*/*insE-4*	Rac prophage; putative tail fiber protein/putative transposase-related protein
CP001509-E._coli	691844 =	187 (1.270)	135 (0.960)	50/284	0.3	60.10%	coding (102/1434 nt)	*rhsO*	conserved protein, rhs-like protein
CP001509-E._coli	= 3628874	0 (0.000)					coding (302/873 nt)	*rhsA*	Rhs protein with putative toxin 55 domain; putative polysaccharide synthesis/export protein; putative neighboring cell growth inhibitor
CP001509-E._coli	745191 =	3 (0.020)	134 (0.250)	45/296	0	98.90%	intergenic (+98/+60)	*aroG*/*gpmA*	3-deoxy-D-arabino-heptulosonate-7-phosphate synthase, phenylalanine repressible/phosphoglyceromutase 1
PM455-pColA-araB	= 5108	0 (0.000)					intergenic (+223/–)	*metG*/–	methionine--tRNA ligase/–
CP001509-E._coli	= 745195	2 (0.010)	145 (0.270)	53/296	0	99.00%	intergenic (+102/+56)	*aroG*/*gpmA*	3-deoxy-D-arabino-heptulosonate-7-phosphate synthase, phenylalanine repressible/phosphoglyceromutase 1
PM455-pColA-araB	1404 =	1 (0.000)					intergenic (–/+215)	–/*araC*	–/L-arabinose regulatory protein
CP001509-E._coli	1568342 =	4 (0.030)	128 (0.330)	47/292	0.5	98.50%	intergenic (-146/-74)	*ECD_01488*/*marR*	putative phage protein/transcriptional repressor of multiple antibiotic resistance
PM666-475_NisCB-	= 6511	0 (0.000)					intergenic (+270/–)	*NisA*/–	–/–
CP001509-E._coli	= 1568348	2 (0.010)	98 (0.250)	38/294	1.1	99.00%	intergenic (-152/-68)	*ECD_01488*/*marR*	putative phage protein/transcriptional repressor of multiple antibiotic resistance
PM666-475_NisCB-	1405 =	0 (0.000)					intergenic (–/-240)	–/*nisC*	–//modified_by=User
CP001509-E._coli	2446154 =	2 (0.010)	142 (0.960)	50/296	0	99.30%	intergenic (+26/+69)	*tktB*/*ypfG*	transketolase 2, thiamine triphosphate-binding/DUF1176 family protein
PM499-pDonor-Col	1404 =	0 (0.000)					intergenic (–/+198)	–/*E. coli rhaR*	–/transcriptional activator of rhaR and rhaS
CP001509-E._coli	= 2446158	8 (0.050)	107 (0.730)	43/296	0	96.40%	intergenic (+30/+65)	*tktB*/*ypfG*	transketolase 2, thiamine triphosphate-binding/DUF1176 family protein
PM499-pDonor-Col	= 6449	0 (0.000)					intergenic (+1485/–)	*metY (O-acetyl homoerine sulfhydrylase)*/–	–/–
CP001509-E._coli	= 2820976	0 (0.000)	140 (0.980)	50/288	0.3	100%	intergenic (-512/-48)	*araE*/*insJ-5*	arabinose transporter/IS150 hypothetical protein
CP001509-E._coli	2822423 =	0 (0.000)					intergenic (+30/+593)	*insK-5*/*kdul*	IS150 putative transposase/hexuronate isomerase
CP001509-E._coli	3018018 =	5 (0.030)	158 (0.290)	61/294	0	98.50%	intergenic (+35/+237)	*yghA*/*exbD*	putative oxidoreductase/membrane spanning protein in TonB-ExbB-ExbD complex
PM455-pColA-araB	= 5108	0 (0.000)					intergenic (+223/–)	*metG*/–	methionine--tRNA ligase/–
CP001509-E._coli	= 3018022	3 (0.020)	151 (0.280)	57/294	0	99.00%	intergenic (+39/+233)	*yghA*/*exbD*	putative oxidoreductase/membrane spanning protein in TonB-ExbB-ExbD complex
PM455-pColA-araB	1404 =	0 (0.000)					intergenic (–/+215)	–/*araC*	–/L-arabinose regulatory protein
CP001509-E._coli	3150308 =	4 (0.030)	156 (0.400)	48/296	0.4	98.70%	intergenic (+185/-166)	*agaA*/*agaS*	N-acetylgalactosamine-6-phosphate deacetylase/tagatose-6-phosphate ketose/aldose isomerase
PM666-475_NisCB-	= 6512	0 (0.000)					intergenic (+271/–)	*NisA*/–	–/–
CP001509-E._coli	= 3150312	12 (0.080)	146 (0.370)	51/296	0.3	96.00%	intergenic (+189/-162)	*agaA*/*agaS*	N-acetylgalactosamine-6-phosphate deacetylase/tagatose-6-phosphate ketose/aldose isomerase
PM666-475_NisCB-	1404 =	0 (0.000)					intergenic (–/-241)	–/*nisC*	–//modified_by=User
CP001509-E._coli	3436761 =	0 (0.000)	156 (0.400)	57/296	0.1	100%	intergenic (-109/+164)	*glgB*/*asd*	1,4-alpha-glucan branching enzyme/aspartate-semialdehyde dehydrogenase, NAD(P)-binding
PM666-475_NisCB-	1404 =	0 (0.000)					intergenic (–/-241)	–/*nisC*	–//modified_by=User
CP001509-E._coli	= 3436765	0 (0.000)	171 (0.440)	52/296	0.3	100%	intergenic (-113/+160)	*glgB*/*asd*	1,4-alpha-glucan branching enzyme/aspartate-semialdehyde dehydrogenase, NAD(P)-binding
PM666-475_NisCB-	= 6512	0 (0.000)					intergenic (+271/–)	*NisA*/–	–/–
CP001509-E._coli	= 3481176	0 (0.000)	150 (1.030)	59/292	0.1	77.30%	coding (205/402 nt)	*nikR*	transcriptional repressor, Ni-binding
CP001509-E._coli	3485048 =	88 (0.610)					coding (3473/4236 nt)	*rhsB*	Rhs protein with DUF4329 family putative toxin domain; putative neighboring cell growth inhibitor
CP001509-E._coli	3582495 =	3 (0.020)	139 (0.260)	44/296	0	98.60%	intergenic (+80/+107)	*cspA*/*hokA*	RNA chaperone and antiterminator, cold-inducible/toxic polypeptide, small
PM455-pColA-araB	1404 =	1 (0.000)					intergenic (–/+215)	–/*araC*	–/L-arabinose regulatory protein
CP001509-E._coli	= 3582499	9 (0.060)	140 (0.260)	55/296	0	96.90%	intergenic (+84/+103)	*cspA*/*hokA*	RNA chaperone and antiterminator, cold-inducible/toxic polypeptide, small
PM455-pColA-araB	= 5108	0 (0.000)					intergenic (+223/–)	*metG*/–	methionine--tRNA ligase/–
CP001509-E._coli	3723659 =	0 (0.000)	162 (0.410)	64/296	0	100%	intergenic (+59/-26)	*ECD_03539*/*ECD_03540*	Aec78/hypothetical protein
PM666-475_NisCB-	= 6512	0 (0.000)					intergenic (+271/–)	*NisA*/–	–/–
CP001509-E._coli	= 3723663	8 (0.050)	175 (0.450)	54/292	0.2	97.80%	intergenic (+63/-22)	*ECD_03539*/*ECD_03540*	Aec78/hypothetical protein
PM666-475_NisCB-	1404 =	0 (0.000)					intergenic (–/-241)	–/*nisC*	–//modified_by=User

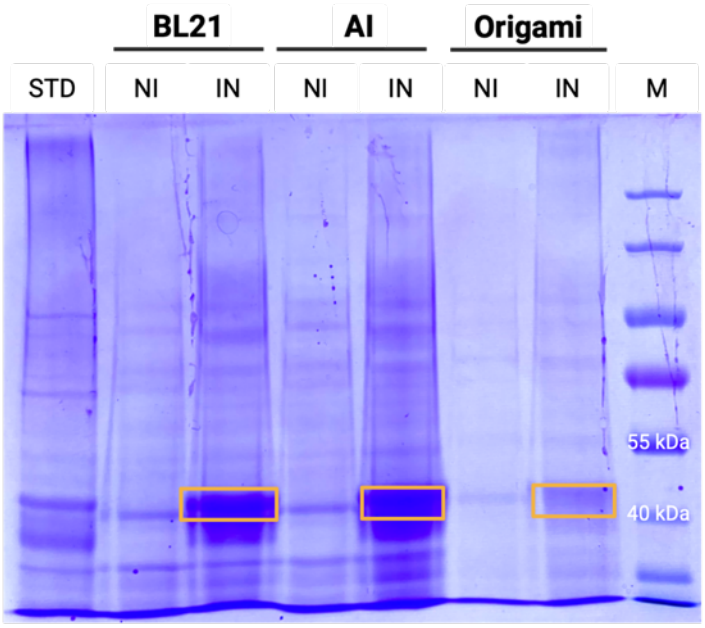
Appendix Figure 13. MS105 New Junction Evidence Summary after Breseq Analysis. The short-read next generation sequencing results were compared to *E. coli BL21* genome and the donor vectors (PM 108, PM109, PM455, PM456) sequence. Rows indicated highlighted in teal showcase positions of insertions of *metG* within the genome while blue highlighted row indicates insertion of *metXY* gene. Insertions were confirmed in 5 locations downstream of various genes such as *asd, marR, mdlB, duf, nagA*. These new Nisin gene insertions are highlighted in purple. Additionally, positions of junctions at donor DNA in the donor plasmids (PM 108, PM109, PM455, PM456) are shown.



Appendix Figure 15. Effect of Promoter Architecture of *nisBC* Genes on the Yield of Functionally Modified Nisin as Measured by Antimicrobial Activity. Normalized cell lysates (OD_{600}=5.0) were tested again the indicator strain Lactococcus lactis NZ900 (pNGNisPT) on GM17 agar plates to quantify functional yield of Nisin-M21V-Aha production through external addition or biosynthesis. Higher yields observed through Aha biosynthesis in both promoter cases. Overall, higher expression seen when modification machinery genes are under the control of inducible promoter.



Appendix Figure 14. HPLC-monitored click reaction kinetics between azidohomoalanine and dansyl alkyne. Time course showing consumption of dansyl alkyne (retention time 11.84 min, orange) and formation of click product (retention time 6.93 min, blue) based on integrated HPLC peak areas. Reaction demonstrates successful bioorthogonal conjugation of azidohomoalanine with alkyne probe.



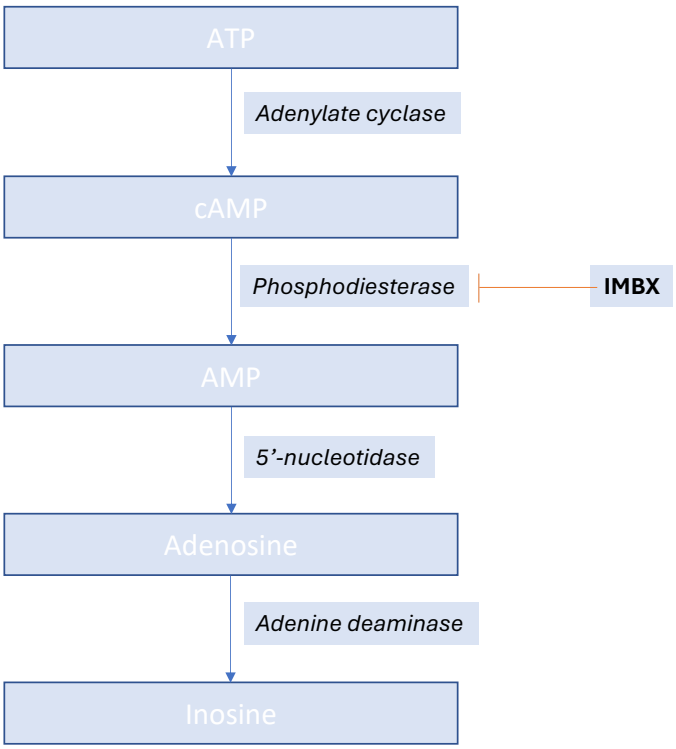
Appendix Figure 16. Gαs expression trials in various E. coli strains. Expression in various *E. coli* strains such as BL21(DE3), AI™ and Origami ™ was tested. The expression standard from Genscript (STD) served as the expression control. For each strain, the non-induced (NI) and induced (I) samples were tested and a PAGE ruler served as a marker (M). Expression is seen in all strains around a molecular weight of ~43 Da, with higher expressed observed in the BL21 and AI™ strains.

Sample #	Sample Information	Replicate	ATP integration	cAMP Intergration	Total Integration	% Conversion	Average (%)
Sample 1	Insoluble anion IEX (B12 to C12) - Urea	Replicate 1	19064304	476660	19540964.00	2.44	2.61
		Replicate 2	19060289	545802	19606091.00	2.78	
Sample 2	Soluble anionic IEX (G1-G12) - Urea	Replicate 1	19141181	926701	20067882.00	4.62	4.71
		Replicate 2	16934359	854899	17789258.00	4.81	
Sample 3	Soluble anionic IEX (H1-H12) - Urea	Replicate 1	19733299	13477	19746776.00	0.07	0.07
		Replicate 2	19674310	15725	19690035.00	0.08	
Sample 4	Soluble cationic IEX (E6 - E12/F1-6)	Replicate 1	13208510	2123946	15332456.00	13.85	13.95
		Replicate 2	13140172	2149262	15289434.00	14.06	
Sample 5	Insoluble cationic IEX (A2-A7) - GuHCl	Replicate 1	37113	15340771	15377884.00	99.76	99.75
		Replicate 2	40375	15532984	15573359.00	99.74	
Sample 7	Soluble cationic IEX (G8-G12)	Replicate 1	19319641	91089	19410730.00	0.47	0.46
		Replicate 2	19283633	87198	19370831.00	0.45	
Sample 8	Soluble cationic IEX (H1-H5)	Replicate 1	19343662	25919	19369581.00	0.13	0.13
		Replicate 2	19359086	24557	19383643.00	0.13	
Sample 9	Soluble cationic IEX (H6-H7)	Replicate 1	19466878	50475	19517353.00	0.26	0.53
		Replicate 2	7233915	57813	7291728.00	0.79	

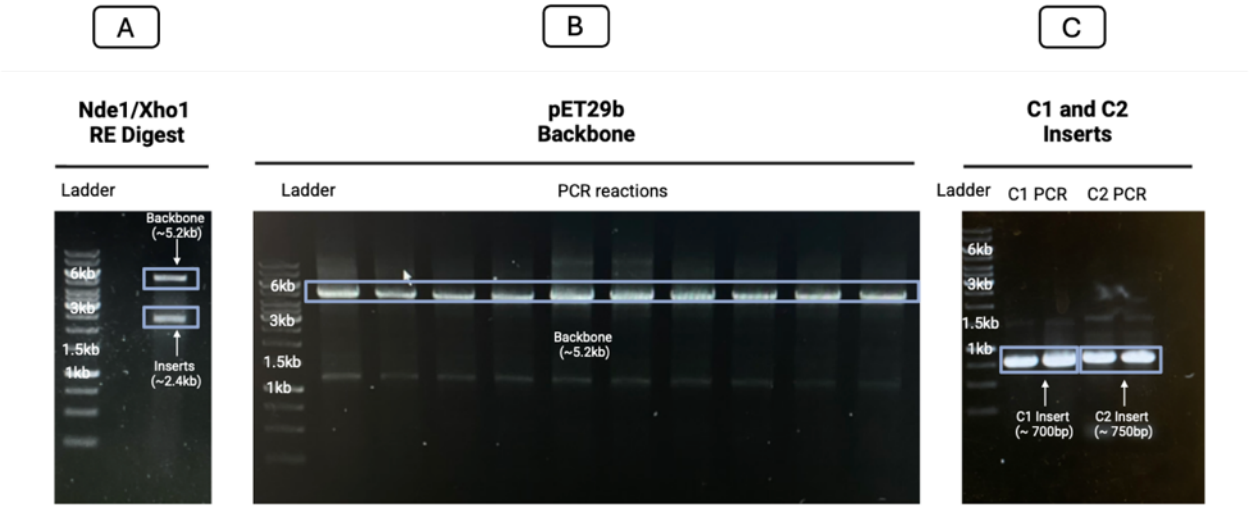
Appendix Figure 17. HPLC Peak Integration data for AC6 Assays Following Protein Refolding. The origin of the samples is provided in the sample information column. The peaks were integrated using the Waters Empower Software which measured the area under the curves. The % conversion was calculated by following the equation: (cAMP integration/total integration) x100. The averages from the replicates for each sample are also reported.

Sample	Replicate	ATP integration	cAMP Intergration	Total	Conversion %	Average (%)
Standard Sample	Triplicate 1	7490893	41770	7532663	0.55	0.56
	Triplicate 2	7265668	32834	7298502	0.45	
	Triplicate 3	7106229	48841	7155070	0.68	
GProtein	Triplicate 1	7518482	54111	7572593	0.71	0.80
	Triplicate 2	7448300	61577	7509877	0.82	
	Triplicate 3	7415919	64609	7480528	0.86	
Gprotein + Fsk	Triplicate 1	7200059	50475	7250534	0.70	0.67
	Triplicate 2	7233915	54284	7288199	0.74	
	Triplicate 3	7553330	42452	7595782	0.56	

Appendix Figure 18. HPLC Peak Integration data for AC6 Assays with Various Activators. The source of the AC6 protein was the GuHCl refolded sample. The peaks were integrated using the Waters Empower Software which measured the area under the curves. The % conversion was calculated by following the equation: (cAMP integration/total integration) x100. The averages from the replicates for each sample are also reported.



Appendix Figure 19. Metabolic Pathway for the Enzymatic Breakdown of ATP to Inosine. The pathway initiates with the conversion of ATP to cAMP by adenylate cyclase and this product subsequently degrades into AMP mediated by phosphodiesterase. This enzyme can be inhibited with IMBX to stabilize cAMP levels when necessary. The pathway continues with the dephosphorylation of AMP to adenosine by 5'-nulceotidase, followed by the final conversion of adenosine to inosine by adenine deaminase.



Appendix Figure 20. Cloning of C1a and C1b Domains into pET29b for Expression. (A) Restriction Digest of pET29b_AC6_pelB following incubation with Nde1 and XhoI. Two fragments observed for the backbones and full length AC6 insert. **(B)** PCR of the pET29b backbone with primers for Gibson Assembly. Lanes represent different annealing temperature that were tested. **(C)** PCR amplification of the C1 and C2 inserts. Successful PCR inserts observed at appropriate expected sizes for each fragment as shown.